# DEVELOPMENT AND TESTING OF A METHODOLOGY FOR ATTRIBUTING SOURCES OF AIRBORNE POLLUTANTS TO THEIR RECEPTORS

Youjun Qin

A thesis submitted in partial fulfilment of the requirements
of the University of Abertay Dundee for the
Degree of Doctor of Philosophy

This research programme was carried out in collaboration
with Dundee City Council

June 2002

I certify that this thesis is the true and accurate version of the thesis approved by the examiners.

Signe[redacted]
(Director of Studies)

Date June 18, 2002

# Acknowledgements

This studentship has been supported by **the University of Abertay Dundee**. The following persons or departments are be dutifully acknowledged for their role and for supporting this research project.

**Dr. K. Oduyemi** is gratefully acknowledged for his dedication, support and supervision throughout the project.

**Dr. D. Lill** is gratefully acknowledged for his support and supervision of the project.

**Planning and Transportation Department, Dundee City Council** is thankfully acknowledged for granting access to road traffic flow data.

Acknowledgements are also made to **Mr. B. Davidson** formerly of the Department of Consumer & Environmental Protection, Dundee City Council, for his help in accessing data about airborne pollutant emission sources.

On a personal note, I would like to extend my deepest gratitude to my wife, Zhenfeng Liu, and to all of my family and friends for their support and understanding throughout my research.

# Abstract

Identification of airborne pollutant sources and estimation of source contributions to air quality 'hot spots' are very important in ambient air quality management. Social, economical, political and legal constraints on air quality management demand a convenient and accurate method for attributing air pollution sources to the 'hot spots'. In this PhD research degree project, an automatic air pollution monitoring station was set up on the library roof at the University of Abertay Dundee to monitor urban background air quality in Dundee. Concentrations of the particulate with aerodynamic diameter less than 10 μm ($PM_{10}$), the total suspended particulate (TSP), nitric oxide (NO), nitrogen dioxide ($NO_2$) and nitrogen oxides (NOx) as well as wind speed, wind direction, ambient temperature and total rainfall were measured continuously for one year. The chemical components of $PM_{10}$ and TSP, calcium ($Ca^{2+}$), magnesium ($Mg^{2+}$), copper (Cu), lead (Pb), nickel (Ni), zinc (Zn), sulphate ($SO_4^{2-}$), nitrate ($NO_3^-$), chloride ($Cl^-$), ammonium ($NH_4^+$), sodium ($Na^+$) and potassium ($K^+$) were analysed in the laboratory. Additionally, the inventories of atmospheric emission sources in Dundee were investigated in detail in order to satisfy the needs of air dispersion model. A new software package for the atmospheric dispersion models was also developed by the author using Microsoft Visual C++. In contrast to other available software packages, this package offers a choice of different atmospheric models. The user may select a model according to the situation prevailing and the available parameters. The package for the atmospheric dispersion models was used to simulate transport of airborne pollutants in Dundee. Performance of the models was evaluated using the data gathered at the monitoring station and atmospheric emission inventories. The contributions of various air pollution sources of NOx and $PM_{10}$ measured at the station were estimated. The receptor model was used to discriminate airborne pollutant emission sources and quantitatively apportion $PM_{10}$ measured at the station to these sources. The results from the atmospheric dispersion model and the receptor model were compared and used in a complementary manner. A new methodology that combines the features of the receptor oriented and source oriented models, and supplements and corrects the two modelling approaches has been developed. The applicability of the methodology has been tested against the gathered air quality and source emission data in Dundee. The following outputs from the research work are completely novel:

- A comprehensive database that consists of concentrations of gaseous pollutants and particulates, chemical compositions of particulates, weather conditions and atmospheric emission inventories.
- A new software package for modelling atmospheric dispersion. This was programmed using Microsoft Visual C++. In contrast to other available commercial packages, the models embedded in the package include a modified hybrid plume dispersion model and a ground level release dispersion model that incorporate recent advances in the understanding of planetary boundary layer and atmospheric dispersion. They also include the conventional Gaussian plume dispersion model that is still generally used. The user may select different models according to the prevailing situation and the available parameters when applying the package.
- The use of error estimate in 'weighting' the data of element matrix and complementary use of subjective information in receptor model trials.
- A new methodology that complements atmospheric dispersion and receptor models to attribute sources of airborne pollutants to their receptors.

# CONTENTS

# List of Figures

# List of Tables

# List of abbreviations and variables

| | |
|---|---|
| CMB | chemical mass balance model |
| FA | factor analysis |
| PCA | principal component analysis |
| PMF | positive matrix factorization model |
| HPDM | hybrid plume dispersion model |
| | |
| TEOM | tapered element oscillating microbalance |
| AAS | atomic absorption spectrophotometry |
| HPLC | high performance liquid chromatography |
| XRF | x-ray fluorescence |
| PIXE | particle induced x-ray emission |
| INAA | instrumental neutron activation analysis |
| | |
| EPA | Environmental Protect Agency, America |
| EPAQS | expert panel on air quality |
| | |
| $PM_{10}$ | particulate with aerodynamic diameter less than 10 μm |
| TSP | total suspended particulate |
| NO | nitric oxide |
| $NO_2$ | nitrogen dioxide |
| NOx | nitrogen oxides |
| $Ca^{2+}$ | calcium |
| $Mg^{2+}$ | magnesium |
| Cu | copper |
| Pb | lead |
| Ni | nickel |
| Zn | zinc |
| $Cl^-$ | chloride |
| $Na^+$ | sodium |
| $K^+$ | potassium |
| $SO_4^{2-}$ | sulphate |
| $NO_3^{-1}$ | nitrate |
| $NH_4^+$ | ammonium |
| | |
| $T$ | temperature |
| $L$ | Monin-Obukhov length |
| $z_i$ | mixing height |
| $u_*$ | friction velocity |
| $w_*$ | convective velocity scale |
| $z_0$ | surface roughness |
| $H$ | surface heat flux |
| $d\theta/dz$ | gradient of potential temperature |
| $\sigma_v$ | lateral turbulent component |
| $\sigma_w$ | vertical turbulent component |

# Chapter 1 Introduction

## 1.1 Background

Combating air pollution is a high priority in the UK. Progress on legislation for air quality, fuel quality, vehicle emissions and the control of airborne heavy metals and persistent organic pollutants has been made. The Clean Air Act of 1956 was the first legislative document for the management of urban air quality. A second Clean Air Act in 1968 changed the manner in which homes and buildings are heated. Gas, electrical and central heating technology were introduced to replace coal. The Environment Act (1995) established the legal frame for local authorities to manage the air quality within their areas. Improving air quality has been included in sustainable development policy in the UK in order to find a balance between protecting human health and the environment, and imposing unacceptable economic and social costs. Although extreme air pollution ($SO_2$ / particulates (smog) pollution) is a thing of the past, there are still problems on congested streets (vehicle emission pollution) and in some industrial and inner city areas in the UK.

The UK National Air Quality Strategy, the first of its kind in Europe, was published in March 1997. It was reviewed in January 1999 (Department of the Environment, Transport and the Regions, 1999). According to this, local authorities are required to undertake a review and assessment of local air quality. Where air quality objectives will not, or are unlikely to be met by the year 2005 (achievement date is one year early for some objectives), the authorities will be required to designate an Air Quality Management Area and draw up an Action Plan to remedy the situation. A minimum of two air quality reviews is recommended in order to assess compliance with air quality objectives. One is to assess air quality at the outset of the National Air Quality Strategy and a second is to be carried out near to the objective achievement date. Scientific, precise and convenient tools are needed when local authorities conduct air quality reviews and draw up the action plan to remedy the situation.

Existing air quality standards ((Department of the Environment, Transport and the Regions, 1999) have been published in the UK. The objectives to be achieved by 2005 have been suggested by an Expert Panel on Air Quality (EPAQS) for eight airborne pollutants: benzene, 1,3-butadiene, carbon monoxide (CO), lead (Pb), nitrogen dioxide

($NO_2$), ozone ($O_3$), particles ($PM_{10}$, the particulate with aerodynamic diameter less than 10 μm), and sulphur dioxide ($SO_2$).

For monitoring and assessing air quality, air quality automatic monitoring networks have been set up in the UK since 1972 (AEA, 1995). The networks consist of three sub networks of urban, rural and hydrocarbon. In 1997, there were 54, 17, and 12 automatic monitoring stations in the three sub-networks, respectively (The Secretary of State for the Environment, 1997). Most of the automatic monitoring stations in the urban network are located in large cities to monitor urban background air quality. A few of them are set up at 'hot spots' such as the urban kerbside and the vicinity of industrial sources. $O_3$, $NO_2$, CO, $SO_2$ and $PM_{10}$ are typical airborne pollutants monitored in the urban network monitoring stations. Most of the monitoring stations in the rural network are located in remote or rural areas. Only $O_3$ is monitored in most of these stations. Dundee and many other small cities in the UK do not have permanent air quality automatic monitoring stations.

Some surveys on ambient air quality have been conducted in Dundee (Collett, Oduyemi and Davidson, 1997; Oduyemi and Davidson, 1998). Diffusion tube measurement of $NO_2$ in Dundee has been performed since the beginning of the National $NO_2$ Survey. The sites for placing diffusion tubes were increased in number, so as to try to determine the 'hot spots' in Dundee. Dundee City Council, in the meantime, purchased a mobile air quality monitoring station in 1999 and has been using the equipment since then. The concentrations of NO, $NO_2$, $NO_x$, CO, $SO_2$ and $PM_{10}$ were monitored for three months at two roadside sites. Now, Dundee City Council is conducting a review and assessment of the air quality in urban areas. Nonetheless, the available air quality data especially the data that can show urban background air quality is minimal in Dundee. There is therefore the scope for increasing the air quality database in Dundee.

The small airborne particulate pollution is causing concern in the UK (The Quality of Urban Air Review Group, 1996). It is believed that these particulates can adversely affect health. Some important messages about the sources of airborne pollutants could be derived from the chemical composition of the airborne particulates. Research investigations have been conducted on the chemical composition of the airborne particulates in East England, Birmingham, Plymouth and the UK mainland coastal rim of the NE Irish sea (Kitto and Harrison, 1992; Harrison and Jones, 1995; Dye et al, 2000; Chester et al., 2000). Only mass concentration of $PM_{10}$ is measured in the automatic urban monitoring network, except for the five multi-element monitoring stations. For the

particulate sample obtained at the five multi-element monitoring stations, eight types of heavy metal content of airborne particulates, cadmium (Cd), chromium (Cr), copper (Cu), iron (Fe), manganese (Mn), nickel (Ni), lead (Pb) and zinc (Zn) are analysed. Some important chemical components of $PM_{10}$ such as $SO_4^{2-}$, $NO_3^-$, $NH_4^-$, $Cl^-$, $Na^+$ are not analysed.

Emission sources of airborne pollutants have generally been investigated in the UK. The United Kingdom National Atmospheric Emissions Inventory (NAEI) and The United Kingdom Emissions Factors Database (UK EFD) are available (Department of the Environment, Transport and the Regions, 1998a). Vehicle emissions are the largest air pollution source in the UK. In Greater London, road traffic contributes approximately 75% of total $NO_x$ (Barratt et al., 1997). Some detailed surveys about the emissions of various types of petrol and diesel vehicle were conducted (Farrow et al., 1993a, 1993b and 1993c). The impact studies of vehicle emissions on urban air quality were carried out as well (The Quality of Urban Air Review Group, 1993; Oduyemi and Davidson, 1998). However, the inventory of airborne emission sources is usually a list of emission quantities of various air pollution sources such as vehicle, industrial, commercial and domestic. The inventory has not been able to properly show the air pollution source type and its spatial distribution and temporal variation in detail. Thus, it can not fully satisfy the requirement for the application of an atmospheric dispersion model. Supplementary investigations are needed to define the spatial distribution and temporal variation in the domain in which the review and assessment of air quality are conducted.

Atmospheric dispersion modelling has been used generally to simulate the transport and dispersion of airborne pollutants. It is a useful tool to assess the impact of airborne pollutant emission sources on ambient air quality (Pasquill and Smith, 1983). Various types of theories and models have been used to develop these models, with the differences being in the physics and mathematics. Department of the Environment, Transport and the Regions, UK (1998b) recommended a series of atmospheric dispersion models as a guide to potential users. Some software packages for atmospheric dispersion models have been developed as well. In the past twenty years, new developments in theories, numerical simulation methodologies and computing techniques have been added to improve the atmospheric dispersion models and software packages to try to get the results that can represent the real situation. The interfaces of the software package have also been improved. However, atmospheric dispersion is a random phenomenon. The model error

and natural variability, such as turbulence fluctuations and temporal variations of emission sources, may allow the results of the atmospheric dispersion model to depart from real concentration distribution. Atmospheric modelling is source-oriented, the precision of which depends directly on the precision of the sources. The precise source profile is difficult to obtain, except for some huge emission sources. Sometimes, source profiles investigated previously can not accurately describe present source emissions.

In contrast to the approaches of atmospheric dispersion models, the receptor model is a receptor-oriented model. It has been used generally to identify airborne pollutant emission sources and their contributions to air pollution 'hot spots' (Hopke, 1991a, b). In cases where the source profiles are not reasonably defined, the receptor model provides a useful tool for identifying an air pollution source. Several approaches and software packages for receptor model analysis have been developed. Most of them are based on multivariate data analysis. Receptor models analyse the behaviour of airborne pollutants, especially chemical components of airborne particulates at the point of impact. It is believed that this behaviour contains the information of source composition. However, this behaviour may sometimes be the result of the mutual effects of meteorology and coincident source location. The source profiles derived from a receptor model may on occasion be misleading.

The atmospheric dispersion model and receptor model are two different types of models. They both have their advantages and shortcomings. In previous research work on air pollution, it was usually only one kind of model that was used. In this case, the errors caused by the model's shortcomings are difficult to identify and remedy. Seigneur et al. (1999) suggested in their 24-hour time average modelling assessment on particulate matters, that two models should be used to complement each other. Chow et al. (1999) tried to use both models to estimate middle and neighbourhood scale variations of $PM_{10}$ source contributions in Las Vegas, Nevada. However, they analysed the model results separately and did not attempt to run a combined analysis of the two sets of results.

## 1.2 Objectives of the research project

Identification of airborne pollutant emission sources and estimation of source contributions to air quality 'hot spots' are very important in ambient air quality management. Social, economical, political and legal constraints on air quality management

demand a convenient and accurate method for attributing air pollution sources to the air quality 'hot spots'. In this research project, a new methodology that combines an atmospheric dispersion model and a receptor model to attribute sources of airborne pollutants to their receptors is developed and tested. This methodology will provide a scientifically accurate way for environmental scientists to model airborne pollutants. It may also be used by local authorities to manage their local air quality.

The research project consists of five parts and they are described briefly below:

1. Urban background air quality in Dundee is monitored using an automatic air pollution monitoring station set up on the roof of the library of the University of Abertay Dundee. Concentrations of $PM_{10}$, TSP (total suspended particulate), NO, $NO_2$ and NOx as well as wind speed, wind direction, ambient temperature and the amount of rainfall are measured continuously for one year. The chemical components of $PM_{10}$ and TSP ($Ca^{2+}$, $Mg^{2+}$, Zn, Ni, Pb, Cu, $SO_4^{2-}$, $NO_3^-$, $NH_4^+$, $Cl^-$, $Na^+$, $K^+$) are analysed using wet chemical analysis. The data gathered at this station further enhances the urban background air quality database in Dundee. It increases the existing knowledge about air pollution throughout the UK as well.
2. The airborne emission sources in Dundee are investigated and characterised as point, line and area type. The spatial distribution and temporal variations of various sources are surveyed in detail. The main focus is vehicle emissions on the road networks. The atmospheric emission inventories for Dundee are created in order to satisfy the requirements of the atmospheric dispersion model. These atmospheric emission inventories improve the information available to the local authority for air quality management. These atmospheric emission inventories and the air quality and weather condition data measured by the author at the monitoring station provide a comprehensive database to develop and test the methodology for attributing sources of airborne pollutants to their receptors.
3. A new software package for the application of atmospheric dispersion models is developed. The models embedded in the package include a modified hybrid plume dispersion model and a ground level release dispersion model that incorporates recent advances in the understanding of planetary boundary layer and atmospheric dispersion. They include the conventional Gaussian plume dispersion model as well. Users can select a suitable model, according to the prevailing situation and available parameters. This software is evaluated using the air quality and emission

inventories databases. It is used to simulate the transport of airborne pollutants over the Dundee urban area. The contributions of various airborne pollutant emission sources, such as point, line and area sources to air quality are assessed.

4. Analysis is carried out on the air quality databases, using a receptor model, which consists of a positive matrix factorisation model. This will be used quantitatively to apportion airborne pollutants to their sources as well. The various airborne pollutant emission sources and their contributions to air pollution in Dundee are estimated.
5. The results derived from the atmospheric dispersion model and the receptor model are analysed and compared. The difference between the two approaches and the causes of the differences are analysed. A new methodology that combines the advantages of the atmospheric dispersion model and the receptor model to overcome shortcomings of the two models is developed to attribute sources of airborne pollutant to their receptors.

The following four contributions of the research project are completely novel:

1. A comprehensive database that consists of concentrations of gaseous pollutants and particulates, chemical compositions of particulates, weather conditions and atmospheric emission inventories has been established. This database further enhances the information needed by Dundee City Council in the management of local air quality. It advances the existing knowledge about the air pollution in the UK. This database can be used to evaluate available atmospheric dispersion models and receptor models. It can also be used to develop a new methodology for air quality management.
2. A new software package for atmospheric dispersion models has been programmed using C++. Compared with other available software packages, the new package allows different models to be chosen. The user may select a different model according to the prevailing situation and available parameters. The atmospheric dispersion models that have been used in the software package include a modified hybrid plume dispersion model and a ground-level release dispersion model that represents recent advances in the understanding of planetary boundary layer and atmospheric dispersion, and a conventional Gaussian plume model. A function ($P$) that represents the probability that a receptor is under the influence of the plume is added to the modified hybrid plume dispersion model. This function is important when distance between source and receptor is large or wind speed is low. The

software package provides a scientific and convenient tool for local authorities in the management of air quality. It can also be used as an educational software package for students on environmental science, engineering or related programmes of study in universities.

3. The weighting of the data of element matrix using error estimates and the complementary use of subjective information in the receptor model trial.
4. A new methodology that combines an atmospheric dispersion model and a receptor model to attribute sources of airborne pollutants to their receptors.

# Chapter 2 Literature Review

In this research project, sampling of airborne particulates and analysing their chemical composition are two major tasks in field monitoring and laboratory analysis respectively. The atmospheric dispersion models and receptor models are two basic approaches used to simulate the transport of airborne pollutants, identify air pollution sources and estimate the source contributions. Thus, the literature review focuses on four areas:

- Sampling and analysis methods of airborne particulates.
- Chemical composition of airborne particulates.
- Atmospheric dispersion theories and models.
- Development and application of receptor models.

## 2.1 Sampling and analysis methods for airborne particulates

### 2.1.1 Sampling methods for airborne particulates

Manual sampling and automatic sampling are two types of methods used to sample airborne particulates in the field of air quality monitoring. A special sample inlet provides the means for particulate size cutting point (for example 10 or 2.5 μm). The airborne particulates can be separated and sampled according to their size range.

In the manual method, the airborne particulates are collected on a special filter using an air sampler. The filter is removed to a laboratory for mass and chemical composition analysis (EPA, 1994). There are two popular types of air samplers, the so-called High Volume and Mini Volume. A 203.2 mm x 254.0 mm filter is used in the High Volume sampler. The sampling flow rate that passes the filter is very high (over 1000 L $min^{-1}$) in the High Volume sampler. Relatively large mass of particulates can be collected in a 24 hour standard sample time. A filter with a diameter of 47 mm is used for the Mini Volume sampler. The sampling flow rate for the Mini Volume is low (about 16.7 L $min^{-1}$). Relatively less mass of particulates can be collected in the standard sample time. The manual method is generally adopted as the standard method for particulate sampling in USA and continental Europe. The advantage of manual sampling method is that the chemical composition of airborne particulates can be analysed using various approaches after the mass is measured by gravimetric method. The shortcoming of this method is that

twenty-four hours or more sample time is usually needed to get enough particulate mass. Thus, the short-term temporal variation of airborne particulate matter is rarely observed by this method. The cost and manpower for adopting a manual method when sampling particulate matters are high.

Tapered Element Oscillating MicroBalance (TEOM) is usually adopted for automatic sampling (Patashnich and Rupprecht, 1991). This automatic sampling method measures the mass accumulation of airborne particulates on a heated filter attached to the tip of a hollow, tapered, oscillating glass rod. The change in the oscillation frequency is used to make a direct measurement of the particulate mass accumulation on the filter over time. TEOM is a cost-effective method for the measurement of airborne particulate concentration. This method is favoured in the UK, because of the advantage of being able to observe temporal variation of particulate concentration. The shortcoming of this method is that the chemical composition of airborne particulates can not be analysed.

The difference in the measured mass of airborne particulates between the manual method and TEOM has caused concern. A substantial fraction of airborne particulates may be semi-volatile, especially in urban areas. The presence of these inorganic semi-volatile materials such as hygroscopic material (particle-bound water), ammonium nitrate and ammonia, and organic semi-volatile materials in the particulate phase introduces a degree of difficulty and uncertainty in measurement of airborne particulates. The amount of particulate-phase semi-volatile material relates to ambient temperature, relative humidity and its gas-phase concentration. The TEOM collects particulates on an oscillating filter heated to 50 °C. The higher the sample temperature is, the higher the loss of semi-volatile material. The observed results by TEOM are generally lower than that observed by the manual method, especially for fine particulate matters.

Allen et al. (1997) conducted a comparative study between TEOM sample results and manual sample results in various urban areas in America and Mexico. They found that the entire difference between TEOM and manual method could be attributed to the particulate ammonium nitrate that was lost via volatilisation, upon the collection of the particulate on the TEOM filter. The mass difference between TEOM and manual sample varied widely with sites and seasons. For some areas, the difference is less in summer and large in winter. The ratio of TEOM results to manual results varies between 0.62 and 1.06 for $PM_{10}$ (the particulate fraction with aerodynamic diameter less than 10 μm) and between 0.64~0.89 for $PM_{2.5}$ (the particulate fraction with aerodynamic diameter less than 2.5 μm).

Brook et al. (1999) have also compared the mass difference between TEOM sample results and manual sample results, measured in Canada. They found the difference between TEOM sample results and manual sample results was relatively small in the warmer months, averaging about 12%. During the colder months the difference between TEOM sample results and manual sample results averages about 23%, but could be as large as 50%.

### 2.1.2 Analysis methods for airborne particulates

The airborne particulate samples collected using a manual method can be moved to a laboratory for mass, elements, water-soluble ions and organics measurement or analysis. Gravimetric measurement, physical analysis, wet chemical analysis and organic analysis may be conducted on the samples to elicit various information on the samples.

#### 2.1.2.1 Mass measurement

Gravimetric analysis is generally used for mass measurement of airborne particulates. It is a technique for measuring the net mass on a filter paper by weighing the filter paper before and after sampling, within a temperature and relative humidity controlled environment. The filter papers should be equilibrated for 24 hours at a constant relative humidity between 20% and 40% (within ±5%) and at a constant temperature of between 15 and 30°C (within ±3°C). The aims of equilibration are to remove the particle-bound water and minimise the loss of semi-volatile species. Nominal values of 30% relative humidity and 15°C to 20°C best conserve the particulate deposits during sample weighting (Watson and Chow, 1993).

The balance used for mass measurement must have equivalent sensitivity (EPA, 1994). The balance used to weigh the filter paper mounted in the High Volume sampler must have a sensitivity of at least 100 μg. The balance that is used to weigh the filter paper mounted on the Minimum Volume sampler should have a sensitivity of at least 10 μg. Balance calibration should be established before and after each weighing session. Approximately one out of ten filters should be re-weighed by a different person at a later time. These re-weighed values should be used to calculate the precision of the measurements.

### 2.1.2.2 Physical analysis

Physical analysis provides a convenient means for many elements' analysis with non-destructive multi-element capabilities, relatively low cost and high detection limits. X-ray fluorescence, particle induced x-ray emission, instrumental neutron activation analysis and microscopy are four of the various types of instruments that are usually used in physical analysis for airborne particulates. They are described briefly below.

#### X-ray fluorescence

In x-ray fluorescence (XRF), the filter deposit is irradiated by high energy x-rays which eject inner shell electrons from the atoms of each element in the sample (EPA, 1994). When a higher energy electron drops into the vacant lower energy orbital, a fluorescent x-ray photon is released. The energy of this photon is unique to each element, and the number of photons is proportional to the concentration of the element. Concentrations are quantified by comparing photon counts for a sample with those obtained from thin-film standards of known concentration.

XRF methods may be broadly divided into two categories: wavelength dispersive x-ray fluorescence (WDXRF), which utilises crystal diffraction for observation of fluorescent x-rays, and energy dispersive x-ray fluorescence (EDXRF), which uses a silicon semiconductor detector. The WDXRF methods are characterised by high spectral resolution, which minimises peak overlaps. It requires high power excitation to overcome low sensitivity, resulting in excessive sample heating and potential degradation. Conversely, EDXRF features high sensitivity but less spectral resolution, requiring complex spectral de-convolution procedures.

XRF analysis of airborne particulate samples has had widest application to samples collected on membrane-type filters such as Teflon- or polycarbonate-membrane filter substrates. These membrane filters collect the deposit on their surfaces, which eliminates biases due to absorption of x-ray by the filter material. These filters also have a low area density which minimises the scatter of incident x-rays, and their inherent trace element content is very low. XRF analysis is not suitable for the airborne particulate samples collected on glass- and quartz-fiber filters

Larger particulates collected during airborne particulate sampling have sufficient size to cause absorption of x-rays within the particulates. Attenuation factors for fine particulates ($PM_{2.5}$) are generally negligible, even for the lightest elements, but attenuation

can be significant for coarse fraction particulates (the particulate with aerodynamic diameter from 2.5 to 10 μm). It is therefore necessary to apply correction factors for XRF to coarse particulate measurements.

**Particle Induced X-Ray Emission**

Particle induced x-ray emission (PIXE) is another form of elemental analysis based on the characteristics of x-rays and the nature of x-ray detection (EPA, 1994). PIXE uses beams of energetic ions, consisting of protons at an energy level of 2 to 5 MeV, to create inner electron shell vacancies. As inner electron shell atomic vacancies are filled by outer electrons, the emitted characteristics of x-rays can be detected by wavelength dispersion or energy dispersion. The development of focusing energetic proton beams has expanded the application of PIXE from environmental and biological sciences to geology and material sciences. PIXE analysis is often used for impactor samples or small filter substrates, since proton beams can be focused on a small area with no loss of sensitivity.

Very thick filters or thick particle deposits on filter substrates scatter the excitation protons and lower the signal-to-noise ratio for PIXE. PIXE, like XRF, requires particulate size diameter corrections (for low atomic number targets) associated with a spherical particle of a given diameter (typical particulate with aerodynamic diameter > 2.5 μm) and compositions typical in ambient airborne particulates studies. These analysis also require correction for ample loadings that reflect the passage of x-rays through a uniform deposit layer.

PIXE analysis can provide information on one of the widest range of elements in a single analysis, since x-ray results require two or three separate anodes. However, attempts to improve sensitivity of PIXE analysis may result in damage to Teflon-membrane filters. Recent developments using PIXE analysis at moderate sensitivity plus single anode XRF analysis at high sensitivity for transition/heavy metals have achieved the minimum detectable limits of less than 0.01 ng $m^{-3}$. With the addition of hydrogen analysis (a surrogate for organic matter), almost all gravimetric mass concentrations can be explained.

**Instrumental Neutron Activation Analysis**

Instrumental neutron activation analysis (INAA) basically involves irradiation of a thin membrane filter sample in the core of a nuclear reactor for periods ranging from a few minutes to several hours (EPA, 1994). Bombardment of the sample with neutrons induces

a nuclear reaction of the stable isotopes in the sample. The energies of the gamma rays emitted by the decay of this induced radioactivity are used to identify them, and therefore, their parents. With the use of prepared standard sample, the amount of parent element in the sample can be determined since the intensity of these gamma rays are proportional to their number.

The gamma-ray spectra of radioactive species are usually collected with a high resolution germanium detector utilising commercially available amplifiers and multi-channel analysers. In order to obtain a full suite of elemental analysis results (often over 40 elements), multiple counting periods and irradiations are performed on the same sample (e. g. two irradiations would produce elements separated into short- and long-lived decay products).

The power of INAA is that it is not generally subject to interference like XRF or PIXE due to a much better ratio of gamma ray peak widths to total spectral width, by a factor of about 20. INAA does not quantify some of the abundant species in airborne particulates such as silicon, nickel, tin, cadmium, mercury, and lead. While INAA is technically nondestructive, sample preparation involves folding the samples tightly and sealing it in plastic, and the irradiation process makes the filter membrane brittle and radioactive. These factors limit the use of the sample for subsequent analysis by other methods. The technique also suffers from the fact that a nuclear reactor is usually used as a source of neutrons. However, since the advent of high-resolution gamma–ray detectors, individual samples can be analysed for numerous elements simultaneously, most at remarkably trace levels without the need for chemical separation. This greatly diminishes the danger of contamination due to excessive sample handling and introduction of chemical reagents used for separation procedures.

**Microscopy analysis of particle size, shape, and composition**

Optical microscopy and scanning electron microscopy have been applied to examine the fine particulate size, shape and composition (EPA, 1994). The optical microscopy may provide particulate size information regarding the morphology of microscopic features. The practical resolution of optical microscopes is limited by the wavelengths associated with light of the visible spectrum. It is typically 1 to 2 μm. Scanning electron microscopy, using accelerated electrons can magnify images and

increase depth of field. It provides the resolution of a few angstroms ($10^{-4}$ μm). Electron microscopy has now evolved to include:

- The transmission electron microscope (TEM).
- The scanning electron microscope (SEM).
- The scanning transmission electron microscope (STEM).

The SEM and STEM use accelerated electrons to strike the sample. As the electron beam strikes the samples, various signals are generated. These signals can be collected to provide highly detailed information on a point-by-point basis. The secondary electron signal yields a sample image with three-dimensional prospective, high depth of field, and illuminated appearance. Back scattered electron images are used to separate phases containing elements of different atomic number.

The information obtained from optics and scanning microscopy analyses is usually considered to be qualitative, due to the limited number of particulates counted. To achieve a quantitative analysis, a sufficient number of particles must be properly sized and identified by morphology and/or chemistry to represent the entire sample. Selection of filter media, optimal particulate loadings, and sample handling methods are also of importance. Microscopic analysis requires a high degree of skill and extensive quality assurance to provide quantitative information. The techniques are complex and expensive. The evolution of computer technology has allowed for quantitative analysis of particulate samples of an entire population of features. With advanced pattern recognition methods, data from individual particle features can be sorted and summarised by size and composition, permitting improved quantitative source apportionment.

Recent development of the SEM/XRF allows analysis of elemental composition and morphological information on small quantities of material. Coupled with statistical data analysis, computer controlled scanning electron microscopy shows great promise for identifying and quantifying complex pollution sources in the field of receptor modelling of source apportionment.

### 2.1.2.3 Wet chemical analysis

The water soluble ions and water soluble or strong solvent soluble trace elements of airborne particulates can be analysed by wet chemical analysis instruments. High performance liquid chromatography, ion chromatography, atomic absorption spectrophotometry, and inductive coupled plasma atomic emission spectrophotometry are

four of the various types of instruments that are usually used in wet chemical analysis for airborne particulates.

**High Performance Liquid Chromatography and Ion Chromatography**

High performance liquid chromatography (HPLC) and ion chromatography (IC) with separate columns are usually used for both water soluble anions (fluoride, chloride, nitrite, bromide, nitrate, phosphate, sulphate) and cations (soluble potassium, ammonium, soluble sodium). All ion analysis methods require filters to be extracted in deionised water and then filtered to remove the insoluble residue. The extraction volume needs to be as small as possible, in case the solution becomes too dilute to detect the desired constituents. In HPLC and IC, the sample extract passes through an ion-exchange column that separates the ions in time for individual quantification, usually by an electroconductivity detector. The ions are identified by their elution/retention times and are quantified by the conductivity peak area or peak height. HPLC and IC are especially desirable for particulate samples because they provide results for several ions with a single analysis and they use a small portion of the filter extract with low detection limits.

**Atomic Absorption Spectrophotometry and Inductive Coupled Plasma Atomic Emission Spectrophotometry**

Atomic absorption spectrophotometry (AAS) and inductive coupled plasma atomic emission spectrophotometry (ICP/AES) are two methods for analysing strong solvent soluble simple ions and trace elements. In AAS analysis, the sample is first extracted in a strong solvent to dissolve the solid material. Then, the extract is introduced into a flame where the elements are vaporised. Most elements absorb light at certain wavelengths in the visible spectrum, and light beam with wavelengths specific to the elements being measured is directed through the flame to be detected by a monochrometer. The light absorbed by the flame containing the extract is compared with the absorption from known standards to quantify the elemental concentrations. AAS requires an individual analysis for each element, and a large filter or several filters are needed to obtain concentrations for a large number of the elements. AAS is a useful complement to other methods, such as XRF and PIXE, for species that can not be easily quantified by XRF and PIXE. Airborne particulates are chemically complex and do not dissolve easily into complete solution, regardless of the

strength of the solvent. There is always the possibility that insoluble residues are left behind or soluble species may co-precipitate them on container walls.

In ICP/AES, the dissolved sample is introduced into an atmosphere of argon gas seeded with free electrons induced by high voltage from a surrounding Tesla coil. The high temperatures in the induced plasma raise valence electrons above their normal stable states. When these electrons return to their stable states, a photon of light is emitted which is unique to the element which was excited. This light is detected at specified wavelengths to identify the elements in the sample. ICP/AES requires a large number of elemental concentrations using small sample volumes with acceptable detection limits for atmospheric samples. As with AAS, this method requires complete extraction and destruction of the sample.

#### 2.1.2.4 Analysis of Organic and Elemental Carbon

Carbon is one of the major components of airborne particulates. It can be analysed in particulates collected on a quartz-fiber filter. Carbon in airborne particulate is usually divided into two classes: organic carbon (or non-light absorbing carbon) and elemental carbon (or light-absorbing carbon). Many methods have been applied to the separation of organic and elemental carbon in airborne particulate samples. The definitions of organic and elemental carbon are operational and reflect the method and purpose of measurement. Comparisons among the results analysed by different methods show that they yield comparable quantities of total carbon in airborne particulate samples, but distinctions between organic and elemental carbon are quite different.

Thermal/optical reflectance (TOR) and thermal manganese oxidation (TMO) are two methods that are most commonly applied in airborne particulate studies in the USA (EPA, 1994). In the TOR method, a quartz-fiber filter is subjected to volatilisation at temperatures ranging from ambient to 550°C in a pure helium atmosphere, then to combustion at temperatures of 550 to 800°C in a 2% oxygen and 98% helium atmosphere with several temperature ramping steps. The carbon that evolves at each temperature is converted to methane and quantified with a flame ionisation detector. The reflectance from the deposit side of the filter punch is monitored throughout the analysis. This reflectance usually decreases during volatilisation in the helium atmosphere owing to the pyrolysis of organic material. When oxygen is added, the reflectance increases as the light-absorbing carbon is combusted and removed. Organic carbon is defined as that which evolves prior to

re-attainment of the original reflectance, and elemental carbon is defined as that which evolves after the original reflectance has been re-attained. By this definition, 'organic carbon' is actually organic carbon that does not absorb light at the wavelength (632.8 nm) used, and 'elemental carbon' is light-absorbing carbon.

The TMO method uses manganese dioxide ($MnO_2$), present and in contact with the sample throughout the analysis, as the oxidising agent, and temperature is relied upon to distinguish between organic and elemental carbon. Carbon evolving at 525 °C is classified as organic carbon, and carbon evolving at 850°C is classified as elemental carbon.

## 2.2 Chemical compositions of airborne particulates around the world

### 2.2.1 Collection of Databases for chemical composition of airborne particulates

Many monitoring programs for airborne particulates have been conducted around the world in the past thirty years. Some of these programs have been reported in the literature, in particular the analysis results of chemical compositions of airborne particulate. Most of this literature reports the chemical compositions of airborne particulates in North America and Europe. Some of them report the analysis results in Asia. The literature which reports the chemical compositions of airborne particulates measured in Africa, South America and Australia is fragmented.

In North America, Polissar et al. (1998) reported the spatial and seasonal variation of 15 chemical components of $PM_{2.5}$ measured in six national parks in Alaska, USA in the period 1987-1995. All these monitoring sites are in remote areas. Chow et al. (1993) conducted a monitoring program in California' San Joaquin valley, USA during 1988-1989. Six monitoring sites located in different areas such as urban, industry, rural and remote were set up. The investigation analysed mass and forty three chemical components for both $PM_{2.5}$ and $PM_{10}$. Pryor et al. (1997) reported the characteristics of fine aerosols measured in the Lower Fraser valley, Canada in 1993. Concentrations of 14 chemical components measured in four rural sites were presented in detail. Xie et al (1999) quoted an 11-year database of $PM_{10}$ measured at an arctic site in Canada. The concentrations of 24 species were shown in their paper.

In Europe, Lee et al. (1994) reviewed the atmospheric concentration of trace elements measured at 7 sites located in urban, industry and rural areas in the UK between 1970 and 1989. The concentrations of 18 trace elements of $PM_{10}$ have been described. The

Quality of Urban Air Review Group, the UK (1996) reported the chemical compositions of airborne particulate in central London, Haverah Park and Leeds. The concentrations of 10 trace elements of $PM_{10}$ for Central London during 1992 to1993 were presented while only 4 chemical components of both $PM_{2.5}$ and $PM_{10}$ for Haverah Park and Leeds in 1982 were shown. Pintor et al. (1996) reported a monitoring result both for $PM_{2.5}$ and $PM_{10}$ conducted in the Czech Republic in the period 1992-1994. Mass and 18 trace elements as well as some other chemical components were analysed. Kubilay and Daydamm (1995) measured the chemical compositions of TSP at a rural site located on the Turkish coast of the Northeastern Mediterranean Sea in the period 1991-1992. Thirteen trace elements had been analysed in their research.

In Asia, Kaneyasu et al. (1995) observed the seasonal variation of chemical composition of $PM_{10}$ in Sapporo, Japan in the period 1987-1988. The mass and 11 chemical components were described. Mukai et al. (1990) conducted a long-term monitoring project from 1983 to 1988 at a remote site located in Oki Island in the Sea of Japan. Long-term variations of 24 chemical components for $PM_{10}$ were described in detail. The monitoring results of aerosol chemical composition at a remote site located in Cheju Island, Korea between 1992 and 1995 had been reported. The concentrations of mass and 8 chemical components for TSP were discussed by Carmichael et al. (1997) while the concentrations of mass and 10 chemical components for $PM_{2.5}$ were analysed by Kim et al. (1998). Qin et al. (1998) reviewed the seasonal and spatial variations of chemical composition for both $PM_{10}$ and TSP in Hong Kong in the period 1992-1994. Mass and 19 chemical components were described in detail. Fang et al. (1999) had measured the airborne particulates in central Taiwan in 1998. Both $PM_{2.5}$ and $PM_{10}$ were sampled in their project. Mass and the 10 chemical components were analysed. Orlic et al. (1999) reviewed a two-year monitoring program for airborne particulates at two sites in Singapore between 1996 and 1997. Concentrations of 18 metal elements for both $PM_{2.5}$ and $PM_{10}$ and their seasonal variation were reported. Kulshrestha et al. (1995) sampled TSP at an urban site near the Taj Mahal, India in the period 1991-1992. Mass and 18 chemical components were analysed. Pandey et al. (1999) conducted another TSP monitoring project at an urban site located in central-east India in the period 1995-1996. 16 chemical components were analysed.

In Africa, South America and Australia, Maenhaut et al. (1996) had studied the impact of biomass burning on atmospheric aerosol composition in a remote area of the

eastern Transvaal, South Africa in 1992. Mass and 48 chemical components were analysed for both $PM_{2.5}$ and $PM_{10}$. Morales et al. (1998) monitored the TSP at 2 remote sites located in the western Venezuelan savannah region in the period 1988-1989. 7 trace elements were analysed in their project. Chan et al. reported the characterisation of chemical species of $PM_{2.5}$ and $PM_{10}$ measured in Brisbane, Australia between 1993 and 1994. The concentrations of mass and 20 chemical species of airborne particulates were reported. The databases of airborne particulate quoted in here are shown in detail in Table 2.1. The geographical locations of all the sampling sites mentioned here are shown in Figure 2.1.

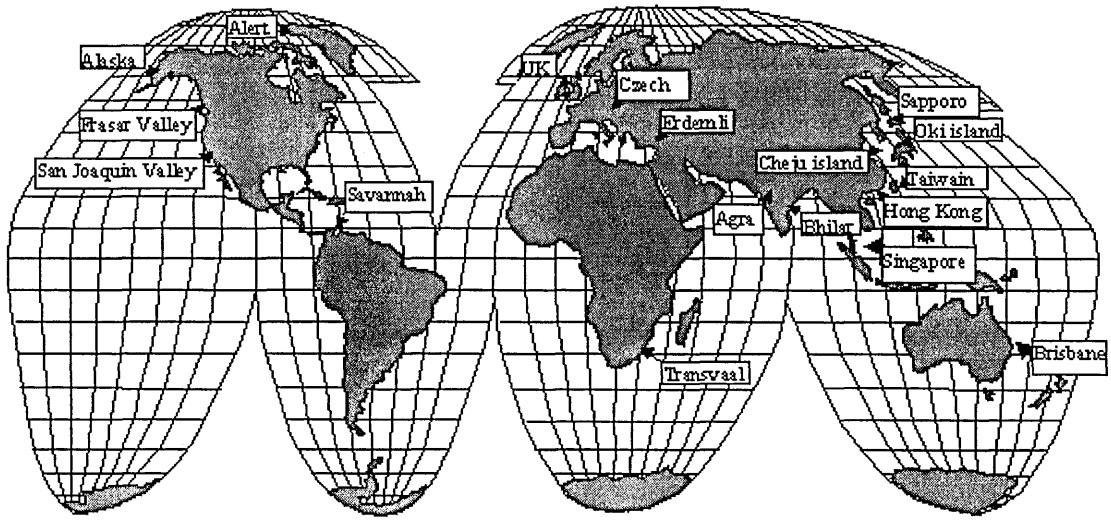


Figure 2.1 Geographical locations of aerosol databases

The databases of chemical compositions of airborne particulates quoted here are very different in sample method, time, analysis items, etc. Different sampling and analysis methods are used in different monitoring programs. $PM_{2.5}$, $PM_{10}$ and TSP, three different types of airborne particulates are sampled. The type of airborne particulate depends on the sampler used in the program. The regions in which monitoring programs were conducted covered six different continents. The times that the monitoring programs began vary from 1970 to 1997. The duration of the monitoring programs are from the shortest of a few months to the longest of nearly two decades. The number of samples for one type of particulate varies from 10 in Venezuela to the largest of 2463 in Hong Kong. The items analysed ranged from only 4 species in Haverah Park and Leeds, the UK, to 48 species in

the eastern Transvaal, South Africa. The monitoring sites are located in various areas, comprising of, for example, urban, industrial to rural, remote and even arctic. The airborne particulates measured in urban and industrial sites show characteristics of air quality 'hot spots'. The airborne particulates measured in rural, remote and arctic sites show their background characteristics and the effects of long distance transport and transformation. For comparing different databases and to discuss the characteristics of airborne particulates around the world, mass and 22 chemical components appearing frequently in the different databases ($SO_4^{2-}$, $NO_3^-$, $NH_4^+$, Al, Si, $Ca^{2+}$, Fe, $K^+$, Mn, $Na^+$, $Cl^-$, Pb, $Br^-$, V, Ni, Se, As, Zn, Cd, Cu, Ti, Cr) are selected here.

Table 2.1 Databases of chemical compositions of airborne particulates

| Site | Area | Sampling time | Sample Items and Numbers* | Reference |
|---|---|---|---|---|
| Alaska, USA | | | | Polissar et al., 1998 |
| Bering Land Bridge National Presurve | Remote | 1987-1992 | $PM_{2.5}$ (340) | |
| Denali National Park | Remote | 1988-1995 | $PM_{2.5}$ (711) | |
| Gates of the Arctic National Park | Remote | 1987-1992 | $PM_{2.5}$ (384) | |
| Katmai National Park | Remote | 1987-1993 | $PM_{2.5}$ (296) | |
| Northwest Alaska Area National Park | Remote | 1986-1992 | $PM_{2.5}$ (491) | |
| Wrangell St. Wlias National Park | Remote | 1987-1992 | $PM_{2.5}$ (347) | |
| Yukon Charley National Preserve | Remote | 1986-1992 | $PM_{2.5}$ (514) | |
| San Joaquin Valley, USA | | | | Chow et al., 1993 |
| Bakersfield | Urban | 1988-1989 | $PM_{2.5}$, $PM_{10}$ | |
| Crows Landing | Rural | 1988-1989 | $PM_{2.5}$, $PM_{10}$ | |
| Fellows | Industry | 1988-1989 | $PM_{2.5}$, $PM_{10}$ | |
| Fresno | Urban | 1988-1989 | $PM_{2.5}$, $PM_{10}$ | |
| Kern | Remote | 1988-1989 | $PM_{2.5}$, $PM_{10}$ | |
| Stockton | Urban | 1988-1989 | $PM_{2.5}$, $PM_{10}$ | |
| The Lower Fraser Valley, Canada | | | | Pryor et al., 1997 |
| CHIL | Rural | 1993 | $PM_{2.5}$(27) | |
| CLBR | Rural | 1993 | $PM_{2.5}$(26) | |
| ISEA | Rural | 1993 | $PM_{2.5}$(22) | |
| PIME | Rural | 1993 | $PM_{2.5}$(25) | |
| Alert, Canada | Arctic | 1980-1991 | $PM_{10}$(532) | Xie et al., 1999 |
| UK | | | | |
| Altrincham | Urban | 1978-1989 | $PM_{10}$ | Lee et al., 1994 |
| Manchester | Urban | 1975-1989 | $PM_{10}$ | |
| Brent | Urban | 1975-1989 | $PM_{10}$ | |
| Chilton | Rural | 1971-1989 | $PM_{10}$ | |
| Flixton | Urban | 1975-1989 | $PM_{10}$ | |
| Walsall | Industry | 1976-1989 | $PM_{10}$ | |
| Windermere | Rural | 1970-1989 | $PM_{10}$ | |
| Central London | Urban | 1992/3 | $PM_{10}$ | The Quality of Urban Air Review Group, 1996 |
| Haverah Park | Rural | 1982 | $PM_{2.5}$, $PM_{10}$ | |

Table 2.1 (Continue)

| Site | Area | Sampling time | Sample Items and Numbers* | Reference |
|---|---|---|---|---|
| Leeds | Urban | 1982 | $PM_{2.5}$, $PM_{10}$ | |
| The Czech Republic | | | | Pinto et al., 1998 |
| Prachatice | Rural | 1993 | $PM_{2.5}$, $PM_{10}$ | |
| Teplice | Industry | 1992-1994 | $PM_{2.5}$, $PM_{10}$ | |
| Erdemli, Turkey | Rural | 1991-1992 | TSP(339) | Kubilay and Daydamm, 1995 |
| Sapporo, Japan | Urban | 1987-1988 | $PM_{10}$(61) | Kaneyasu et al., 1995 |
| Oki island, Japan | Remote | 1983-1988 | $PM_{10}$(54) | Mukai et al., 1990 |
| Cheju Island, Korea | Remote | 1992-1995 | TSP(600) | Carmichael et al., 1997 |
| | | 1994 | $PM_{2.5}$ | Kim et al., 1998 |
| Hong Kong | Urban | 1992-1994 | $PM_{10}$(2400), TSP(2463) | Qin et al., 1998 |
| Central Taiwan | | | | Fang et al, 1999 |
| HKIT | Rural | 1998 | $PM_{2.5}$ (10), $PM_{10}$(10) | |
| THU | Suburban | 1998 | $PM_{2.5}$ (10), $PM_{10}$(10) | |
| Singapore | | | | Orilc et al, 1999 |
| CSC | Urban | 1996-1997 | $PM_{2.5}$ | |
| AJC | Urban | 1996-1997 | $PM_{2.5}$, $PM_{10}$ | |
| Agra, India | Urban | 1991-1992 | TSP | Kulshrestha et al., 1995 |
| Bhilai, India | Urban | 1995-1996 | TSP(105) | Pandey et al., 1998 |
| The eastern Transvaal, South Africa | | | | Maenhaut et al., 1996 |
| Palmer | Remote | 1992 | $PM_{2.5}$(42), $PM_{10}$(42) | |
| Pretoriuskop | Remote | 1992 | $PM_{2.5}$(40), $PM_{10}$(40) | |
| Skukuza | Remote | 1992 | $PM_{2.5}$(41), $PM_{10}$(41) | |
| Savannah region, Venezuela | | | | Morales et al., 1996 |
| La Esperanza | Remote | 1988-1989 | TSP(12) | |
| Catatumbo | Remote | 1988-1989 | TSP(10) | |
| Brisbane, Australia | Urban | 1993-1994 | $PM_{2.5}$(261), $PM_{10}$(379) | Chan et al., 1997 |

*The number in the parentheses is total number of samples

### 2.2.2 Chemical composition of $PM_{2.5}$

The concentrations of mass and 22 chemical components for the $PM_{2.5}$ databases collected in this study are shown in Table 2.2. The mass concentration of $PM_{2.5}$ ranges from 5925 ng $m^{-3}$ to 61260 ng $m^{-3}$. The lowest concentration appears in ISEA, a site located in the rural area of the lower Fraser valley, Canada. The highest concentration appears in Teplice, a site located in an industrial area, Czech Republic.

$SO_4^{2-}$, $NO_3^-$ and $NH_4^+$ are the three major chemical components of $PM_{2.5}$. They represent about 32.4% to 87.4% of $PM_{2.5}$ mass. It is believed that significant quantities of $SO_4^{2-}$, $NO_3^-$ and $NH_4^+$ in atmospheric aerosols may be of a secondary origin. They are formed from gaseous $SO_2$, $NO_x$ and $NH_3$. The concentration of $SO_4^{2-}$ is lower in North America and higher in other continents. The lowest value of 1406 ng $m^{-3}$ is in ISEA,

Canada, which represents about 23.7% of $PM_{2.5}$ mass. The highest value of 17695 ng $m^{-3}$ is in HKIT, a site located in a rural area in central Taiwan, represents about 69.0% of $PM_{2.5}$ mass. The concentration of $NO_3^-$ is significantly high in San Joaquin valley, USA. The highest value of 10820 ng $m^{-3}$ is in Bakersfield, an urban site, which represents about 27.5% of $PM_{2.5}$ mass. The lowest concentration of $NO_3^-$ is 320 ng $m^{-3}$ in ISEA, which only represents about 5.4% of $PM_{2.5}$ mass. The concentration of $NH_4^+$ is also relatively high in San Joaquin valley. The highest value of 4860 ng $m^{-3}$ appears at the same site as $NO_3^-$, which represents about 12.2% of $PM_{2.5}$ mass. The concentration of $NH_4^+$ is 196 ng $m^{-3}$ in ISEA, which only represents about 3.3% of $PM_{2.5}$ mass.

Al, Si, $Ca^{2+}$, Fe, $K^+$ and Mn are usually considered as crustal elements that come from soil. They are important chemical components of $PM_{2.5}$ that represent about 1.1% to 6.9% of the mass. The crustal element concentrations are low in the $PM_{2.5}$ sampled in Alaska. The concentration of Al varies between 4.1 and 258.0 ng $m^{-3}$. The highest value is in Teplice, a Czech site located in an industrial area. The concentration of Si varies between 29.8 and 820.0 ng $m^{-3}$. The highest value is in Fellows, a San Joaquin valley site located in an industrial area. The concentrations of $Ca^{2+}$ and Fe vary between 6.3 and 270.0 ng $m^{-3}$ and 51 and 1300 ng $m^{-3}$ respectively. The highest values for $Ca^{2+}$ and Fe are in THU, a central Taiwan site located in suburban area. The concentration of $K^+$ varies between 9.2 and 340 ng $m^{-3}$. The highest value is in Palmer, a South African site located in a remote area. The concentration of Mn varies between 0.4 and 25.0 ng $m^{-3}$. The highest value is in HKIT, a central Taiwan site located in a rural area.

$Na^+$ and $Cl^-$ are major components of marine aerosol. They are important chemical components of the airborne particulates sampled in coastal areas and represent about 0.0% to 7.7% of $PM_{2.5}$ mass. The concentration of $Na^+$ varies between 12 and 540 ng $m^{-3}$, while the concentration of $Cl^-$ varies between 1.1 and 1500 ng $m^{-3}$. The highest values for both $Na^+$ and $Cl^-$ are in Cheju island, Korea.

The concentrations of the remaining chemical components of aerosol are low and usually considered as trace elements. Pb, $Br^-$, V, Ni, Se and As may be used as traces for some special airborne pollutants emission sources. It is believed that Pb and $Br^-$ mainly come from petrol vehicular emission. V and Ni are related to fuel oil burning emission. Se and As are related to coal burning emission. The concentrations of these 6 trace elements are generally higher in industrial and urban areas and lower in remote areas. The concentration of Pb varies between 0.5 and 75.2 ng $m^{-3}$. The highest value is in Teplice, a

Table 2.2 Chemical compositions of $PM_{2.5}$ (ng $m^{-3}$)

| Site | Mass | $SO_4^{2-}$ | $NO_3^-$ | $NH_4^+$ | Al | Si | $Ca^{2+}$ | Fe | $K^+$ | Mn | $Na^+$ | $Cl^-$ | Pb | $Br^-$ | V | Ni | Se | As | Zn | Cd | Cu | Ti | Cr |
|---|---|---|---|---|---|---|---|---|---|---|---|---|---|---|---|---|---|---|---|---|---|---|---|
| Alaska, USA | | | | | | | | | | | | | | | | | | | | | | | |
| Bering Land Bridge National Preserve | | | | | 18.8 | 61.3 | 47.4 | | 23.6 | 1.0 | 69.0 | 7.6 | 3.8 | 1.8 | 0.5 | | 0.2 | 0.2 | 2.3 | 2.8 | | 2.2 | |
| Denali National Park | | | | | 6.7 | 33.0 | 9.0 | | 9.3 | 0.4 | 18.9 | 1.9 | 0.5 | 0.4 | 0.4 | | 0.1 | 0.1 | 0.9 | 2.8 | | 1.3 | |
| Gates of the Arctic National Park | | | | | 5.4 | 29.9 | 6.4 | | 9.8 | 0.5 | 13.5 | 1.2 | 1.2 | 0.7 | 0.6 | | 0.1 | 0.1 | 0.9 | 3.4 | | 1.4 | |
| Katmai National Park | | | | | 8.7 | 37.6 | 12.5 | | 10.0 | 0.6 | 44.7 | 9.3 | 3.8 | 1.5 | 0.5 | | 0.1 | 0.1 | 0.8 | 2.9 | | 1.8 | |
| Northwest Alaska Area National Park | | | | | 4.1 | 29.8 | 18.6 | | 10.6 | 0.5 | 41.7 | 4.6 | 1.6 | 1.1 | 0.5 | | 0.2 | 0.2 | 1.4 | 3.0 | | 1.1 | |
| Wrangell St. Wlias National Park | | | | | 7.1 | 40.1 | 11.8 | | 9.3 | 0.5 | 12.0 | 1.1 | 0.8 | 0.4 | 0.4 | | 0.1 | 0.1 | 0.9 | 2.7 | | 1.6 | |
| Yukon Charley National Preserve | | | | | 5.2 | 40.7 | 10.6 | | 13.0 | 0.5 | 12.6 | 1.1 | 0.9 | 0.5 | 0.5 | | 0.1 | 0.1 | 1.2 | 2.8 | | 1.6 | |
| San Joaquin Valley, USA | | | | | | | | | | | | | | | | | | | | | | | |
| Bakersfield | 39800 | 3910 | 10820 | 4860 | 140.0 | 390.0 | 120.0 | 200.0 | 220.0 | 6.9 | | 16.0 | 43.0 | 12.0 | 9.7 | 15.0 | 0.8 | | 110.0 | | 140.0 | 15.0 | 5.6 |
| Crows Landing | 20040 | 1970 | 6280 | 2630 | 150.0 | 400.0 | 51.0 | 150.0 | 110.0 | 4.2 | | 31.0 | 18.0 | 4.9 | 3.8 | 2.7 | 1.1 | | 59.0 | | 77.0 | 15.0 | 2.2 |
| Fellows | 27530 | 4620 | 7520 | 3590 | 220.0 | 820.0 | 150.0 | 220.0 | 110.0 | 4.8 | | 38.0 | 12.0 | 6.9 | 5.9 | 63.0 | 1.5 | | 62.0 | | 75.0 | 21.0 | 2.9 |
| Fresno | 39220 | 2750 | 9420 | 4040 | 150.0 | 380.0 | 72.0 | 170.0 | 250.0 | 7.3 | | 170.0 | 51.0 | 17.0 | 3.4 | 2.3 | 1.6 | | 69.0 | | 69.0 | 16.0 | 1.6 |
| Kern | 23290 | 2500 | 8520 | 3600 | 110.0 | 330.0 | 81.0 | 110.0 | 110.0 | 2.7 | | 33.0 | 10.0 | 7.2 | 6.8 | 6.0 | 1.3 | | 57.0 | | 77.0 | 13.0 | 1.4 |
| Stockton | 29450 | 2270 | 6420 | 2850 | 140.0 | 440.0 | 100.0 | 230.0 | 140.0 | 9.4 | | 130.0 | 41.0 | 10.0 | 4.5 | 4.2 | 1.0 | | 110.0 | | 140.0 | 20.0 | 5.2 |
| The Lower Fraser Valley, Canada | | | | | | | | | | | | | | | | | | | | | | | |
| CHIL | 9912 | 1797 | 2201 | 1060 | 38.7 | 70.6 | 16.4 | | | | 89.8 | | 2.5 | 2.2 | | | | | 7.5 | | | | |
| CLBR | 11156 | 2000 | 2238 | 1150 | 41.6 | 61.9 | 17.5 | | | 2.0 | 115.0 | | 3.1 | 2.1 | 1.1 | | | | 6.2 | | | | |
| ISEA | 5925 | 1406 | 320 | 196 | 25.8 | 48.1 | 13.4 | | | 1.7 | 172.6 | | 1.2 | 1.7 | 0.9 | | | | 2.2 | | | | |
| PIME | 7796 | 1790 | 763 | 467 | 44.3 | 60.0 | 27.6 | | | 3.4 | 117.7 | | 2.0 | 1.9 | 1.5 | | | | 4.5 | | | | |
| UK | | | | | | | | | | | | | | | | | | | | | | | |
| Haverah Park | | 5300 | 1700 | 2300 | | | | | | | | 200.0 | | | | | | | | | | | |
| Leeds | | 5800 | 1900 | 2200 | | | | | | | | 400.0 | | | | | | | | | | | |
| Czech | | | | | | | | | | | | | | | | | | | | | | | |
| Prachatice | 30950 | 5891 | | | 101.0 | 227.5 | 62.0 | 101.5 | 163.5 | 4.4 | | 110.0 | 38.5 | 7.6 | 2.8 | 2.0 | 1.3 | 16.0 | 52.0 | | 19.0 | 13.4 | 0.7 |
| Teplice | 61260 | 10575 | | | 258.0 | 496.0 | 102.4 | 230.0 | 194.8 | 11.2 | | 276.6 | 75.2 | 12.2 | 4.8 | 41.6 | 3.7 | 15.2 | 94.6 | | 10.1 | 27.6 | 2.7 |
| Cheju Island, Korea | 20610 | 8400 | 890 | 2810 | | | 70.0 | | 240.0 | | 540.0 | 1040.0 | | | | | | | | | | | |

Table 2.2 (Continue)

| Site | Mass | $SO_4^{2-}$ | $NO_3^-$ | $NH_4^+$ | Al | Si | $Ca^{2+}$ | Fe | $K^+$ | Mn | $Na^+$ | $Cl^-$ | Pb | $Br^-$ | V | Ni | Se | As | Zn | Cd | Cu | Ti | Cr |
|---|---|---|---|---|---|---|---|---|---|---|---|---|---|---|---|---|---|---|---|---|---|---|---|
| Central Taiwan | | | | | | | | | | | | | | | | | | | | | | | |
| HKIT | 25650 | 17695 | 4725 | | | | 265.0 | 330.0 | | 25.0 | | 1550.0 | 18.5 | | | | | | 85.0 | | 21.5 | | 50.0 |
| THU | 25900 | 13065 | 2100 | | | | 270.0 | 1300.0 | | 14.0 | | 1185.0 | 53.5 | | | | | | 121.0 | | 21.5 | | 190.0 |
| Singapore (Pre-Haxe) | | | | | | | | | | | | | | | | | | | | | | | |
| CSC | | | | | 84.0 | 173.0 | 116.0 | 105.0 | 332.0 | 7.2 | 212.0 | 116.0 | 29.0 | 15.0 | 18.5 | 5.0 | | | 43.0 | | 52.0 | 7.6 | |
| AJC | | | | | 231.0 | 278.0 | 82.0 | 115.0 | 315.0 | 5.2 | 207.0 | 105.0 | 42.0 | 17.0 | 8.5 | 7.1 | | | 41.0 | | 26.6 | 4.4 | |
| Brisbane, Australia | 7300 | 788 | 190 | | 29.0 | 80.0 | 29.0 | 51.0 | 55.0 | 4.0 | 227.0 | 197.0 | 48.2 | 16.8 | | | | | 26.3 | | | 5.1 | |
| The eastern Transvaal, South Africa | | | | | | | | | | | | | | | | | | | | | | | |
| Palmer | 18000 | | | | 250.0 | 440.0 | 38.0 | 167.0 | 340.0 | 4.0 | 184.0 | 22.0 | 6.0 | 10.9 | 0.6 | | | 0.2 | 5.2 | | 0.8 | 15.6 | |
| Pretoriuskop | 12300 | | | | 138.0 | 300.0 | 35.0 | 85.0 | 220.0 | 2.4 | 430.0 | 42.0 | 4.5 | 8.6 | 0.5 | | 0.3 | 0.1 | 2.9 | | 0.7 | 10.7 | |
| Skukuza | 9400 | | | | 75.0 | 157.0 | 34.0 | 51.0 | 220.0 | 1.3 | 540.0 | 52.0 | 3.4 | 8.2 | 0.4 | | 0.6 | 0.1 | 2.1 | | 0.4 | 5.7 | |

Czech industrial site. The concentration of $Br^-$ varies between 0.4 and 17.0 ng $m^{-3}$. The highest value is in Fresno and AJC, the urban sites in San Joaquin valley and Singapore. The concentration of V varies between 0.4 and 19.5 ng $m^{-3}$. The highest value is in CSC, another urban site in Singapore. The concentration of Ni varies between 2.0 and 63.0 ng $m^{-3}$. The highest value is in Fellow, an industrial site in San Joaquin valley. The concentration of Se varies between 0.1 and 3.7 ng $m^{-3}$. The highest value is also in Teplice. The concentration of As varies between 0.1 and 16.0 ng $m^{-3}$. The highest value is in Prachatice, a rural site in the Czech Republic.

The sources of Zn, Cd, Cu, Ti and Cr are complex. The concentration of Zn varies between 0.8 and 121.0 ng $m^{-3}$. The highest value is in THU, a suburban site in central Taiwan. Cd was only analysed in the $PM_{2.5}$ sampled in Alaska. Its concentration varies between 2.7 and 3.4 ng $m^{-3}$. The concentration of Cu varies between 0.4 and 140.0 ng $m^{-3}$. The highest value occurred in Bakersfield, an urban site in San Joaquin valley. The concentration of Ti varies between 1.1 and 27.6 ng $m^{-3}$. The highest value is in Teplice, a Czech industrial site. The concentration of Cr varies between 0.7 and 190.0 ng $m^{-3}$. The highest value occurred also in THU.

In general, the chemical compositions of $PM_{2.5}$ can be grouped according to geographical region. The chemical compositions of $PM_{2.5}$ measured at Cheju, THU and HKIT, three near-the-coast sites located at remote, suburban and rural areas in eastern Asia, are very similar. They show the characteristics of the coal burning emission pollution and marine aerosol, with high concentrations of $SO_4^{2-}$ and $Cl^-$. The chemical compositions of $PM_{2.5}$ measured at Pretoriuskop, Skukuza and Palmer, three remote sites in South Africa, are similar and significantly different to those measured at other sites. They show the impact of biomass burning with high concentrations for $K^+$ and $Na^+$ and low concentration for $Cl^-$. The chemical compositions of $PM_{2.5}$ measured at seven sites located in remote areas in Alaska's national parks or national preserves approach ambient background composition of $PM_{2.5}$ with low concentrations for all chemical components. The chemical compositions of $PM_{2.5}$ measured at other sites vary with location. They show the obvious impact of local anthropogenic airborne pollutant emission sources with the very high concentrations for mass and most of the chemical components.

### 2.2.3 Chemical composition of $PM_{10}$

The concentrations of mass and 22 chemical components for $PM_{10}$ databases collected in this study are shown in Table 2.3. The concentration of $PM_{10}$ ranges from 12200 ng $m^{-3}$ to 82900 ng $m^{-3}$. The lowest concentration of $PM_{10}$ should be at Alert, an arctic site in Canada because all chemical components, except $Cl^-$ measured there have lowest concentrations. However, no mass concentration is reported for Alert's database. The lowest concentration instead appeared at a remote site located in Oki island, Japan. The highest concentration appeared at Bakersfield, an urban site in San Joaquin valley.

$SO_4^{2-}$, $NH_4^+$ and $NO_3^-$ are the three major chemical components of $PM_{10}$, in a similar manner to $PM_{2.5}$. Compared with $PM_{2.5}$, the percentage that these three chemical components represent relative to mass is lower for $PM_{10}$, with the values ranging from 14.8% to 73.7%. The highest concentration of $SO_4^{2-}$ with the value of 20600 ng $m^{-3}$, occurred at HKIT, the same site that represented maximum $SO_4^{2-}$ for $PM_{2.5}$. It represents about 53.90% of $PM_{10}$ mass. The concentrations of $NO_3^-$ and $NH_4^+$ for $PM_{10}$ are also relatively high in San Joaquin valley as well. The highest concentrations of $NO_3^-$ and $NH_4^+$, 13840 and 5520 ng $m^{-3}$ respectively, occurred at Bakersfield, an urban site. They represent about 16.3% and 6.7% of $PM_{10}$ mass respectively.

The percentage of the crustal elements relative to mass is much higher for $PM_{10}$ than that for $PM_{2.5}$. This percentage for the $PM_{10}$ varies between 2.9% and 24.9%. The concentration of Al varies between 65 and 4900 ng $m^{-3}$. The concentration of Si varies between 973 and 8710 ng $m^{-3}$. The highest values of Al and Si were at urban and industrial areas, San Joaquin valley. The concentration of $Ca^{2+}$ varies between 70 and 2225 ng $m^{-3}$. The concentration of Fe varies between 150 and 349500 ng $m^{-3}$. The highest values of $Ca^{2+}$ and Fe for $PM_{10}$ occurred also in THU. The concentration of K varies between 7.3 and 548.9 ng $m^{-3}$. The highest value is in Hong Kong, a metropolis. The concentration of Mn varies between 0.8 and 39.0 ng $m^{-3}$. The highest value is in Stockton, an urban site located in San Joaquin valley.

The percentage of $Na^+$ and $Cl^-$ relative to the mass is much higher for $PM_{10}$ than that for $PM_{2.5}$. They represent about 0.3% to 14.1% of $PM_{10}$ mass. The concentration of $Na^+$ varies between 100 and 1890 ng $m^{-3}$. The highest value is at Skukuza, a remote site in South Africa. The concentration of $Cl^-$ varies between 45 and 6216 ng $m^{-3}$. The highest value is at Walsall, an industrial site in UK. The lowest value for $Cl^-$ is at Oki island.

Table 2.3 Chemical compositions of $PM_{10}$ (ng $m^{-3}$)

| Site | Mass | $SO_4^{2-}$ | $NO_3^-$ | $NH_4^+$ | Al | Si | $Ca^{2+}$ | Fe | $K^+$ | Mn | $Na^+$ | $Cl^-$ | Pb | $Br^-$ | V | Ni | Se | As | Zn | Cd | Cu | Ti | Cr |
|---|---|---|---|---|---|---|---|---|---|---|---|---|---|---|---|---|---|---|---|---|---|---|---|
| San Joaquin Valley, USA | | | | | | | | | | | | | | | | | | | | | | | |
| Bakersfield | 82900 | 5000 | 13480 | 5520 | 4990 | 8210 | 1350 | 1790 | 350.0 | 36.0 | | 420 | 58 | 16.0 | 19.0 | 17.0 | 1.2 | | 100 | | 93.0 | 150.0 | 9.4 |
| Crows Landing | 51080 | 2410 | 7450 | 2690 | 2870 | 7100 | 580 | 1370 | 210.0 | 29.0 | | 320 | 17 | 6.5 | 11.0 | 5.5 | 1.2 | | 95 | | 14.0 | 13.0 | 8.0 |
| Fellows | 55940 | 5330 | 8050 | 3700 | 2530 | 8710 | 1140 | 1310 | 200.0 | 25.0 | | 300 | 20 | 11.0 | 71.0 | 70.0 | 1.7 | | 87 | | 55.0 | 110.0 | 11.0 |
| Fresno | 75640 | 3200 | 10260 | 4060 | 2940 | 7490 | 850 | 1480 | 360.0 | 35.0 | | 340 | 67 | 17.0 | 10.0 | 5.1 | 1.9 | | 87 | | 77.0 | 14.0 | 8.1 |
| Kern | 48340 | 2790 | 9480 | 3660 | 1850 | 5180 | 810 | 900 | 190.0 | 17.0 | | 250 | 14 | 8.9 | 11.0 | 8.1 | 1.4 | | 43 | | 48.0 | 85.0 | 5.2 |
| Stockton | 63620 | 2660 | 7900 | 2880 | 2780 | 8410 | 960 | 1630 | 240.0 | 39.0 | | 700 | 57 | 13.0 | 12.0 | 7.2 | 1.1 | | 95 | | 91.0 | 15.0 | 12.0 |
| Alert, Canada | | 490 | 45 | 57 | 65 | | 70 | | 7.3 | 0.8 | 100 | 63 | 1 | 2.6 | 0.3 | | | 0.1 | 2 | | | 5.0 | |
| UK | | | | | | | | | | | | | | | | | | | | | | | |
| Altrincham | | | | | 563 | | | 737 | | | 1310 | 4478 | 267 | 108.0 | 15.4 | 17.2 | 2.6 | 4.7 | 113 | 3.6 | | | 17.2 |
| Mancheester | | | | | 581 | | | 840 | | | 1300 | 5009 | 360 | 122.5 | 29.5 | 13.2 | 2.8 | 7.1 | 237 | 6.2 | | | 7.0 |
| Brent | | | | | 489 | | | 938 | | | 1223 | 3401 | 670 | 232.0 | 26.5 | 11.9 | 2.3 | 6.1 | 126 | 9.2 | | | 4.4 |
| Chilton | | | | | 222 | | | 242 | | | 730 | 1939 | 100 | 32.0 | 9.0 | | 1.3 | 2.7 | 76 | 3.1 | | | 2.2 |
| Flixtton | | | | | 694 | | | 737 | | | 1398 | 4554 | 427 | 177.0 | 20.9 | 9.8 | 2.8 | 7.1 | 115 | 4.8 | | | 6.0 |
| Walsall | | | | | 838 | | | 1687 | | | 1447 | 6216 | 1316 | 155.0 | 21.2 | 31.2 | 16.7 | 93.9 | 2634 | 28.3 | | | 24.9 |
| Windermere | | | | | 142 | | | 156 | | | 928 | 2178 | 53 | 23.0 | 5.5 | 3.1 | 0.9 | 1.8 | 39 | 2.0 | | | 1.5 |
| Central London | | | | | | | | 891 | | 21.0 | | | 78 | | 12.0 | 5.2 | | | 59 | 0.4 | 13.0 | | 5.4 |
| Haverah Park | | 6200 | 2800 | 2600 | | | | | | | | 1100 | | | | | | | | | | | |
| Leeds | | 6800 | 2800 | 2400 | | | | | | | | 1500 | | | | | | | | | | | |
| Czech | | | | | | | | | | | | | | | | | | | | | | | |
| Prachatice | 37800 | 6436 | | | 486 | 973 | 285 | 307 | 246.5 | 9.0 | | 117 | 43 | 9.8 | 3.3 | 2.1 | 1.4 | 18.3 | 60 | | 25.0 | 54.9 | 1.0 |
| Teplice | 77060 | 11375 | | | 1342 | 2456 | 562 | 820 | 335.8 | 22.1 | | 357 | 82 | 16.8 | 6.0 | 42.6 | 4.0 | 17.3 | 109 | | 17.5 | 116.0 | 3.6 |
| Sapporo, Japan | 24750 | 3898 | 898 | 815 | 810 | | 1025 | | 253.3 | | 669 | 849 | | | | | | | | | | | |
| Oki island, Japan | 12200 | 3590 | 114 | 510 | 228 | | 151 | 150 | 130.0 | 5.6 | 430 | 45 | 12 | | 1.6 | 0.9 | | 3.3 | 15 | 0.3 | 1.7 | 12.4 | |
| Hong Kong | 57477 | 9535 | 1624 | 2319 | 307 | | 804 | | 548.9 | 18.9 | 1480 | 1160 | 71 | 12.4 | 13.1 | 4.2 | | | 111 | 1.2 | 123.8 | | |
| Central Taiwan | | | | | | | | | | | | | | | | | | | | | | | |
| HKIT | 38250 | 20600 | 7580 | | | | 1050 | 2970 | | 28.5 | | 2490 | 23 | | | | | | 115 | | 27.5 | | 61.5 |
| THU | 38050 | 17480 | 4420 | | | | 2225 | 3495 | | 15.5 | | 1915 | 67 | | | | | | 126 | | 24.5 | | 328.0 |
| AJC, Singapore (Pre-Haze) | | | | | 917 | 1495 | 847 | 606 | 584.0 | | 746 | 1068 | 69 | 60.0 | 11.9 | 11.8 | | | 80 | | 54.6 | 41.4 | |
| The eastern Transvaal, South Africa | | | | | | | | | | | | | | | | | | | | | | | |
| Palmer | 33200 | | | | 1310 | 2340 | 238 | 827 | 539.0 | 21.2 | 484 | 73 | 8 | 12.9 | 2.7 | 1.3 | | 0.3 | 8 | | 2.1 | 78.6 | 5.8 |
| Pretoriuskop | 31700 | | | | 1088 | 2300 | 295 | 605 | 500.0 | 19.0 | 1590 | 1342 | 21 | 12.7 | 1.9 | 0.8 | 0.3 | 0.1 | 6 | | 2.4 | 80.7 | 2.7 |
| Skukuza | 25600 | | | | 705 | 1367 | 221 | 421 | 402.0 | 10.7 | 1890 | 1722 | 5 | 11.6 | 1.4 | | 0.6 | 0.2 | 4 | | 1.3 | 49.7 | 1.8 |
| Brisbane, Australia | 26600 | | | | 585 | 1197 | 745 | 452 | 159.6 | 10.9 | 878 | 1330 | 106 | | | | | | 24 | | | 12.8 | 7.2 |

The concentration of Pb varies between 1 and 1316 ng $m^{-3}$. The highest value is also at Walsall. The concentration of $Br^-$ varies between 2.6 and 232.0 ng $m^{-3}$. The highest value is at Brent, an urban site in UK. The concentration of V varies between 0.3 and 71.0 ng $m^{-3}$ while the concentration of Ni varies between 0.8 and 70.0 ng $m^{-3}$. The highest values for these two elements appeared at Fellow, an industrial site in San Joaquin valley. The concentration of Se varies between 0.3 and 16.7 ng $m^{-3}$ while the concentration of As varies between 0.1 and 93.9 ng $m^{-3}$. The highest values for these two elements appeared also at Walsall.

The concentration of Zn varies between 2.3 and 2634.0 ng $m^{-3}$ while the concentration of Cd varies between 0.3 and 28.3 ng $m^{-3}$. The highest values for these two elements appear at Walsall. The concentration of Cu varies between 1.3 and 123.8 ng $m^{-3}$. The highest value is at Hong Kong. The concentration of Ti varies between 5.0 and 150.0 ng $m^{-3}$. The highest value is at Bakersfield, San Joaquin valley. The concentration of Cr varies between 1.0 and 328.0 ng $m^{-3}$. The highest value is at THU, central Taiwan.

The chemical compositions of $PM_{10}$ collected here can be generally grouped according to geographical region as well. The impact of marine aerosol on $PM_{10}$ in the UK is very obvious. The concentrations of $Na^+$ and $Cl^-$ of $PM_{10}$ sampled at Manchester, Flixton, Brent and Altrincham, four urban sites in the UK are very high, especially for $Cl^-$. They are relatively high at Haverah Park, Leeds, Chilton and Windermere, another four sites in the UK. $PM_{10}$ measured at six sites located in San Joaquin valley in USA has significantly high concentrations for mass and most of the chemical components. $PM_{10}$ sampled in Alert, an arctic site in Canada, is very different to those sampled in other sites for its extremely low concentration for all chemical components. $PM_{10}$ sampled in Walsall, an industrial site in the UK shows obvious regional characteristic with very high concentrations for $Cl^-$, Pb and Zn. $PM_{10}$ measured in Oki island should have shown the characteristics of the coal burning emission pollution and marine aerosol because Oki island is located in eastern Asia. However, the concentrations of $SO_4^{2-}$, $Na^+$ and $Cl^-$ in $PM_{10}$ are low at this site.

### 2.2.4 Chemical composition of TSP

The concentrations of mass and 22 chemical components for TSP databases are shown in Table 2.4. Few TSP databases have been reported. The databases show the regional characteristics. It is difficult to conduct a system analysis because there is a few

Table 2.4 Chemical compositions of TSP (ng $m^{-3}$)

| Site | Mass | $SO_4^{2-}$ | $NO_3^-$ | $NH_4^+$ | Al | Si | $Ca^{2+}$ | Fe | $K^+$ | Mn | $Na^+$ | $Cl^-$ | Pb | $Br^-$ | V | Ni | Se | As | Zn | Cd | Cu | Ti | Cr |
|---|---|---|---|---|---|---|---|---|---|---|---|---|---|---|---|---|---|---|---|---|---|---|---|
| Erdemli, Turkey | | | | | 685 | | 3140 | 685 | | 13 | 1900 | | 30 | | 7.7 | 5.6 | | | 19 | 0.2 | | | 8.6 |
| Cheju Island, Korea | | 7160 | 1160 | 1270 | | | 470 | | 390 | | 1660 | 1880 | | | | | | | | | | | |
| Hong Kong | 88347 | 12871 | 3548 | 1565 | 665 | | 2299 | | 514 | 33 | 4269 | 4123 | 75 | 22 | 14.4 | 6.8 | | | 140 | 1.6 | 183.9 | | |
| Agra, India | 368520 | 14140 | 7630 | | 1230 | | 1580 | 14520 | 1030 | 360 | 15820 | 6150 | 850 | | | 150.0 | | | 930 | 40.0 | 710.0 | | 10.0 |
| Bhilai, India | | 5292 | 3468 | | | | | 5264 | | 154 | | 2469 | 690 | | 7.1 | 24.0 | | 7.9 | 6263 | 0.5 | 771.4 | 58.8 | 16.7 |
| Savannah region, Venezuela | | | | | | | | | | | | | | | | | | | | | | | |
| La Esperanza | | | | | | | 480 | 195 | 440 | | 1155 | | | | | | | | 10 | | 240.0 | | |
| Catatumbo | | | | | | | 220 | 195 | 300 | | 645 | | | | | | | | 21 | | 205.0 | | |

database collected. $SO_4^{2-}$, $NO_3^-$ and $NH_4^+$ represent about 20.48% of TSP mass in Hong Kong while $SO_4^{2-}$, $NO_3^-$ represent about 5.9% of TSP mass in Agra, an urban site in India. The concentrations for some special elements measured in Indian cities were very high such as Fe and $Na^+$ in Agra and Zn in Bhilai.

## 2.3 The atmospheric dispersion model

There are different kinds of turbulence with different scales in the atmosphere, everywhere and at any time. Randomness is the major characteristic of turbulence. The velocity components of turbulence flow at any location vary randomly with time. Their exact values can never be predicted precisely. It is only possible to determine some convenient statistical properties of velocity components. The random fluctuations in the velocities exist in the turbulent field. As a result of these random fluctuations in the velocities, different parts of the fluid may be mixed or exchanged intensively. Turbulent transport will occur when there are some inhomogeneities in spatial distributions of heat, vapour, chemical species etc. A high concentration zone will be generated in the atmosphere when airborne pollutants are emitted from pollution sources. Then, the airborne pollutant will be transported from the high concentration zone to a low concentration zone by turbulent mixing. The rate of turbulent mixing is several orders of magnitude larger than molecular motion mixing. Atmospheric dispersion is a turbulent dispersion. The atmospheric advection and convection also transport airborne pollutants from the high concentration zone to a low concentration zone.

The atmospheric dispersion model has been generally used to simulate the transport and dispersion of airborne pollutant and assess the impact of an air pollution source on ambient air quality (Pasquill and Smith, 1983). Various theories and models of atmospheric dispersion have been developed. They have been used in abatement and control of air pollution in urban areas. They may also be used in assessment of impact of global air pollution on climate as well. Atmospheric dispersion models are particularly useful as analytical tools in the following topics:

- Establishment of emission control legislation.
- Evaluation of proposed emission control techniques and strategies.
- Planning the location of future sources of air contaminants.
- Planning for the control of air pollution episodes.

- Assessment of responsibility of existing level of air pollution.

As well as the velocity components of turbulent flow, one can never predict with certainty the distribution of concentration of marked particles emitted from a source because of the inherent random character of atmospheric turbulent motion. Although the basic equations for describing turbulent dispersion are available, there does not exist a single mathematical model that can be used as a practical means of computing atmospheric concentration over all ranges of conditions. Previously, Weil et al. (1992) carried out a performance evaluation of various air quality models. Recently, Collett and Oduyemi (1997) conducted a technical review of mathematical approaches used for air quality modelling. These publications are important starting points for understanding the characteristics of the various air quality models.

### 2.3.1 Atmospheric dispersion approaches and theories

#### 2.3.1.1 Eulerian approach

There are two basic ways of considering the problem of turbulent dispersion (Seinfeld and Pandis, 1997). They are the Eulerian approach and the Lagrangian approach. In the Eulerian approach, the behaviour of airborne pollutants is described relative to a fixed coordinate system. The material balance is carried out over an infinitesimal region fixed in space. The Eulerian description is the common way of treating heat and mass transfer phenomena. The Eulerian methods attempt to formulate the concentration statistics in terms of the statistical properties of the Eulerian fluid velocities, that is the velocities measured at fixed points in the fluid. A formulation of this type is very useful not only because the recordings of the wind Eulerian statistics are readily measurable (as determined from continuous time recordings of the wind velocities by a fixed network of anemometers) but also because the mathematical expressions are directly applicable to situations in which chemical reactions are taking place. It is convenient to express concentration and wind velocity components in turbulence as $\bar{c}+c'$ and $\bar{u}_i+u_i'$, $i$ = 1, 2, 3, where $\bar{c}$ and $\bar{u}_i$ represent the mean concentration and mean velocity components that can be determined. $c'$ and $u_i'$ represent fluctuating concentration and fluctuating velocity components, The governing equation for an Eulerian approach is (Seinfeld and Pandis, 1997):

$$\frac{\partial \bar{c}}{\partial t}+\frac{\partial}{\partial x_i}\left(\bar{u}_i \bar{c}\right)+\frac{\partial}{\partial x_i}\left(\overline{u_i' c'}\right)=D_i \frac{\partial^2 \bar{c}}{\partial x_i \partial x_i}+R+S \tag{2.1}$$

where $D_i$ is molecular diffusivity, $R$ represents chemical reactions, S represents airborne pollutant emission sources. Equation 2.1 contains dependent variables $\bar{c}$ and $\overline{u_i' c'}$, $i$=1,2,3. There are more dependent variables than equations. The Eulerian approach leads to a serious mathematical obstacle known as the closure problem, for which no generally valid solution has yet been found. The most common means to ensure equation (2.1) is closed is so called K-theories that relates $\overline{u_i' c'}$ to $\bar{c}$ (see section 2.3.1.4).

### 2.3.1.2 Lagrangian approach

In the Lagrangian approach, the behaviour of airborne pollutants is described relative to the moving fluid. The meandering of marked fluid particles in the flow is considered. The Lagrangian techniques attempt to describe the concentration statistics in terms of the statistical properties of the displacements of particles released in the fluid. Lamb and Neiburger (1971) developed a general Lagrangian statistical expression for use in air quality modelling. The ensemble mean pollutant concentration at location $\vec{r}$ and time $t$ can be calculated by integrating initial pollutant concentrations and continuing source emissions over all possible starting locations, weighted by the probability densities of displacement from starting location $\vec{r}'$ to the location of interest, $\vec{r}$, for all times, giving:

$$\langle c(\vec{r},t)\rangle = \int_{-\infty}^{\infty}\int_{-\infty}^{\infty}\int_{-\infty}^{\infty} P(\vec{r},t|\vec{r}_0,t_0)\langle c(\vec{r}_0,t_0)\rangle d\vec{r}_0 + \int_{-\infty}^{\infty}\int_{-\infty}^{\infty}\int_{-\infty}^{\infty}\int_{t_0}^{t} P(\vec{r},t|\vec{r}',t')S(\vec{r}',t')dt'd\vec{r}' \tag{2.2}$$

where $P(\vec{r}, t \mid \vec{r}', t')$ is the transition probability density that a fluid particle existing at location $\vec{r}'$ at time $t'$ will undergo a displacement to location $\vec{r}$ at time t; $S(\vec{r}', t')$ is the spatial and temporal distribution of emissions evaluated at location $\vec{r}'$ at time $t'$; $\vec{r}_0$ and $t_0$ are the initial conditions for location and time.

The mathematics for the Lagrangian approach is more tractable than that of the Eulerian approach, in that no closure problem is encountered. However, there are two substantial problems with equation 2.2. First, it holds only when the particles are not undergoing chemical reactions. Second, such complete knowledge of the turbulence properties as would be needed to know $P$ is generally unavailable except in the simplest of circumstances.

The Eulerian and Lagrangian approaches yield different types of mathematical relationships for the species concentrations that can ultimately be related. Each approach is a valid description of turbulent dispersion. The choice of which approach to adopt in a given situation will be seen to depend on the specific features of the situation. Each approach can be shown to have certain inherent difficulties that render impossible an exact solution for the mean concentration of species in a turbulent flow. For the purposes of practical computation, several approximate theories have been developed for calculating the mean concentration of species in turbulence. Two popularly used theories are statistical theory and *K*-theory.

### 2.3.1.3 Atmospheric dispersion statistical theory

Statistical theory has been applied to study turbulent dispersion because of the association of turbulence with random motion. The probability density function ($P(x, y, z)$) is used to describe the motion of a particle in a turbulence field. If the probability density function was available, the distribution of concentration for a point emission source with emission rate $Q$ could be described as:

$$c(x,y,z) = Q \cdot P(x,y,z) \tag{2.3}$$

Dispersion rate is the most important parameter used in describing turbulent dispersion. There are different methods used for representing the dispersion rate, based on different theories and experiments. In statistical theory, standard deviations of airborne pollutant distribution ($\sigma_x$, $\sigma_y$, $\sigma_z$) are parameters used to represent the turbulent dispersion rate. The wider the airborne pollutant distribution is, the faster the turbulent dispersion. The standard deviations of pollutant in a puff emitted from a point source can be calculated by using the following formulae:

$$\sigma_x^2 = \frac{\int_{-\infty}^{\infty} c \cdot x^2 dx}{\int_{-\infty}^{\infty} c \cdot dx} \qquad \sigma_y^2 = \frac{\int_{-\infty}^{\infty} c \cdot y^2 dy}{\int_{-\infty}^{\infty} c \cdot dy} \qquad \sigma_z^2 = \frac{\int_{-\infty}^{\infty} c \cdot z^2 dz}{\int_{-\infty}^{\infty} c \cdot dz} \tag{2.4}$$

It is obvious that $\sigma_x$, $\sigma_y$ and $\sigma_z$ are functions of dispersion time or distance. They have a length dimension and increase with dispersion distance. The values of $\sigma_x$, $\sigma_y$, $\sigma_z$ vary with meteorological and surface conditions. $\sigma_x$, $\sigma_y$, $\sigma_z$ are also called dispersion parameters because they are a measure of the dispersion rate.

In statistical theory, the dispersion parameters can be linked to $P$(x, y, z) using:

$$\sigma_x^2 = \frac{\int_{-\infty}^{\infty} x^2 \cdot P(x,y,z)dx}{\int_{-\infty}^{\infty} P(x,y,z)dx} \qquad \sigma_y^2 = \frac{\int_{-\infty}^{\infty} y^2 \cdot P(x,y,z)dy}{\int_{-\infty}^{\infty} P(x,y,z)dy} \qquad \sigma_z^2 = \frac{\int_{-\infty}^{\infty} z^2 \cdot P(x,y,z)dz}{\int_{-\infty}^{\infty} P(x,y,z)dz} \tag{2.5}$$

The appropriate description of a probability density function is a major research field in turbulent dispersion statistical theory. Taylor (1921) first described the dispersion parameter with statistical characteristics in turbulent fluctuating field and derived the classical Taylor formula:

$$\sigma_y^2 = 2\overline{v'^2} \int_0^T \int_0^t R_L(\zeta) d\zeta dt \tag{2.6}$$

where $v'$ is a turbulent fluctuating speed in the y direction, $R_L(\zeta)$ the Lagrangian correlation coefficient. $R_L(\zeta)$ approaches one when $T$ is very small and zero when $T$ is very large. Equation 2.6 can be used to show that the variation of the mean concentration distribution varies with time, that is,

$$\sigma_y \approx t \qquad \text{as } t \to 0 \tag{2.7}$$

$$\sigma_y \approx t^{1/2} \qquad \text{as } t \to \infty. \tag{2.8}$$

The Lagrangian correlation coefficient can not be parameterised in terms of readily measured Eulerian quantities. In an effort to overcome the practical difficulties associated with equation 2.6, Pasquill (1971) suggested an alternative definition that retained the essential features of Taylor's statistical theory but which is more amenable to parameterisation in terms of readily measured Eulerian quantities. As adopted by Draxler (1976), American Meteorological Society (1977), and Irwin (1979), the Pasquill representation leads to

$$\sigma_y = \sigma_v \, t \, F_y \tag{2.9}$$

$$\sigma_z = \sigma_w \, t \, F_z \tag{2.10}$$

where $\sigma_v$ and $\sigma_w$ are the standard deviations of the wind velocity fluctuations in the y- and z-direction respectively, $F_y$ and $F_z$ are universal functions of a set of parameters that specify the characteristics of the atmospheric boundary layer and transport time to the receptor point. The exact forms of $F_y$ and $F_z$ are to be determined from monitoring data.

$F_y$ and $F_z$ are assumed to depend on the friction velocity $u_*$, the Monin-Obukhov length $L$, the Coriolis parameter $f$, the mixing layer height $z_i$, the convective velocity scale $w_*$, the surface roughness $z_0$, and the height of pollutant release above the ground $h_*$.

The variances, $\sigma_y^2$ and $\sigma_z^2$, are therefore treated as empirical dispersion coefficients, the functional forms of which are determined by matching the Gaussian equation's solution to data. In that way, $\sigma_y$ and $\sigma_z$ actually compensate for deviations from stationary, homogeneous conditions that are inherent in the assumed Gaussian distribution. Of the two standard deviations, $\sigma_y$ and $\sigma_z$, more is known about $\sigma_y$. First, most of the experiments from which $\sigma_y$ and $\sigma_z$ values are inferred involve ground level measurements. Such measurements provide an adequate indication of $\sigma_y$, where vertical concentration distributions are needed to determine $\sigma_z$. Also, the Guassian expression for vertical concentration distribution is known not to be obeyed for ground-level releases (Seinfeld and Pandis, 1997), so the fitting of a measured vertical distribution to a Gaussian form is considerably more difficult than that for the horizontal distribution where lateral symmetry and an approximate Gaussian form are good assumptions.

For lateral dispersion, Irwin (1979) developed expressions for $\sigma_v$ based on the work of Deardorff and Willis (1975), Draxler (1976) and Nieuwstadt and Van Duuren (1979),

$$\sigma_v = 1.78u_*\left[1 + 0.059(-z_i / L)\right]^{1/3} \qquad z_i/L < 0 \qquad (2.11)$$

and

$$\sigma_v = 1.78u_* \qquad z_i/L \geq 0 \qquad (2.12)$$

He proposed the following form for $F_y$

$$F_y = \left[1 + (t/T_i)^{1/2}\right]^{-1};\ T_i^{-1} = \frac{2.5u_*}{z_i}\left[1 + 0.0013(z_i / L)\right]^{1/3} \qquad z_i/L \leq 0 \qquad (2.13)$$

and

$$F_y = \left[1 + 0.9(t/T_0)\right]^{-1};\ T_0^{-1} = 1.001 \qquad z_i/L > 0 \qquad (2.14)$$

A wide range of field and laboratory measurements on vertical wind velocity fluctuations under unstable conditions can be represented by (Irwin, 1979) :

$$\sigma_w = w_* G(z/z_i) \qquad (2.15)$$

with

$$G(z/z_i) = 1.342(z/z_i)^{0.333} \qquad z/z_i < 0.03 \qquad (2.16)$$

and

$$G(z/z_i) = 0.763(z/z_i)^{0.175} \qquad 0.03 < z/z_i < 0.40 \qquad (2.17)$$

and

$$G(z/z_i) = 0.722(1 - z/z_i)^{0.207} \qquad 0.40 < z/z_i < 0.96 \qquad (2.18)$$

and

$$G(z/z_i) = 0.37 \qquad z/z_i > 0.96 \qquad (2.19)$$

Under neutral and stable conditions, $\sigma_w$ can be represented by (Binkowski, 1979)

$$\sigma_w = u_* \left[ \frac{\phi_m(z/L) - z/L}{3kf_m} \right]^{1/3} \qquad z/L \geq 0 \qquad (2.20)$$

where

$$\phi_m(z/L) = 1 + 4.7z/L \qquad (2.21)$$

and

$$f_m = 0.4\left[1 + 3.9z/L - 0.25(z/L)^2\right] \qquad z/L \leq 2 \qquad (2.22)$$

and

$$f_m = 0.4\left[6.78 + 2.39(z/L - 2)\right] \qquad z/L > 2 \qquad (2.23)$$

Under neutral and stable conditions, $F_z$ may be represented by (Draxler, 1976)

$$F_z = \left[1 + 0.9(t/T_0)^{1/2}\right]^{-1} \qquad z < 50 \text{ m} \qquad (2.24)$$

and

$$F_z = \left[1 + 0.945(t/T_0)^{0.8}\right]^{-1} \qquad z \geq 50 \text{ m} \qquad (2.25)$$

Equations 2.9 –2.25 represent the application of atmospheric dispersion research results in the 1970's for parameterisations of $\sigma_y$ and $\sigma_z$ in planetary boundary layer. There is no direct expression for $\sigma_z$ in unstable conditions because the vertical distribution is significantly non-Gaussian.

Carruthers et al. (2000) summarised the atmospheric dispersion research results in the 1980's and the experiments undertaken in the UK. They derived a set of formulae to calculate $\sigma_y$ and $\sigma_z$ in ADMS (Atmospheric Dispersion Model System).

For stable and neutral conditions, the lateral dispersion is given by

$$\sigma_y^2 = \sigma_{y_t}^2 + \sigma_{y_w}^2 \qquad (2.26)$$

with

$$\sigma_{y_t} = \sigma_v t(1 + 25u_* tL/z_i^2)^{-1/2} \qquad \text{if } z_i/L > 1 \qquad (2.27)$$

and

$$\sigma_{y_t} = \sigma_v t(1 + 25u_* t/z_i^2)^{-1/2} \qquad \text{otherwise} \qquad (2.28)$$

and

$$\sigma_{y_w} = \sigma_\theta x \qquad \text{if } \sigma_\theta \text{ is specified by a user} \qquad (2.29)$$

and

$$\sigma_{y_w} = 0.065x\sqrt{7T/u_{10}} \qquad \text{otherwise} \qquad (2..30)$$

where $T$ is the sampling time in hours, $u_{10}$ is ground wind speed.

The vertical dispersion (Carruthers et al., 2000)

$$\sigma_z = \sigma_w t\left(\frac{1}{b^2} + \frac{N^2t^2}{1+2Nt}\right)^{-1/2} \qquad (2.31)$$

where $N$ is the buoyancy frequency and

$$b = \frac{1+0.4u_*t/h_e}{1+u_*t/h_e} \qquad \text{if } h_e/z_i \le 0.05 \qquad (2.32)$$

where $h_e$ is effective emission height, and

$$b = \left[1-(z-0.05)/0.1\right]\left(\frac{1+0.4u_*t/h_e}{1+u_*t/h_e}\right) + (z-0.05)/0.1 \qquad \text{if } 0.05 < h_e/z_i \le 0.15 \qquad (2.33)$$

and

$$b = 1 \qquad \text{if } h_e/z_i > 0.15 \qquad (2.34)$$

In unstable conditions, the lateral dispersion is also calculated from two parts. The first for dispersion due to convection $\sigma_{y_c}$, the second due to mechanically driven turbulence $\sigma_{y_n}$

$$\sigma_{y_c} = \sigma_{v_c} t\left(1+0.91\frac{t}{z_i}w_*\right)^{-1/2} \qquad (2.35)$$

$$\sigma_{y_n} = \sigma_{v_{nc}} t\left(1+2.5\frac{t}{z_i}w_*\right)^{-1/2} \qquad (2.36)$$

Venkatram (1996) examined the Pasquill-Gifford-Turner dispersion scheme and derived the effective vertical dispersions that can be used in Gaussian formulation even for unstable condition.

$$\sigma_z = \sqrt{\frac{2}{\pi}}\frac{u_*Lx}{u|L|} \qquad \text{for } \frac{x}{|L|} \le 1.4 \qquad (2.37)$$

and

$$\sigma_z = \sqrt{\frac{2}{\pi}}\frac{u_*L}{u}1.12\left(\frac{x}{|L|}\right)^{2/3} \qquad \text{for } \frac{x}{|L|} > 1.4, L > 0 \text{ (stable conditin)} \qquad (2.38)$$

and

$$\sigma_z = \sqrt{\frac{2}{\pi}} \frac{u_* x}{u\left(1+0.006\left(x/|L|\right)^2\right)^{1/2}} \qquad \text{for } L<0 \text{ (unstable condition)} \qquad (2.39)$$

Venkatram (1996) thought these three formulae represent current understanding of vertical dispersion observed in the Prairie Grass experiment in terms of governing micrometeorological variables. However, these formulae are only suitable for describing the vertical dispersion from ground level emission sources because they are based on the data collected in the Prairie Grass experiment, a ground source emission atmospheric dispersion experiment.

The parameterisation of atmospheric dispersion using similarity theory can describe the atmosphere, using the latest observed and research results in boundary layer characteristics and structure (Carruthers et al., 2000). However, the knowledge of atmospheric boundary layer characteristics and structure such as friction velocity $u_*$, the Monin-Obukhov length $L$, the mixing layer depth $z_i$, the convective velocity scale $w_*$ and the surface roughness $z_0$. These are not available from normal meteorological observations. Various empirical formulae and supposition have to be used if one wants to estimate these atmospheric parameters using routine meteorological observation data. In that case, one needs correlations for $\sigma_y$ and $\sigma_z$ based on readily available ambient data. The Pasquill stability categories *A* to *F* (Table 2.5) provide a basis for such correlations.

The most widely used $\sigma_y$ and $\sigma_z$ correlations based on the Pasquill stability classes are those developed by Gifford (1961). The correlations commonly referred to as the Pasquill-Gifford curves are shown in Figures 2.2 and 2.2.

Table 2.5 Estimates of Pasquill stability classes*

| Surface Wind speed at 10 m ($m\ s^{-1}$) | Solar Radiation | | | Night time Cloud Cover Fraction | |
|---|---|---|---|---|---|
| | Strong | Moderate | Slight | ≥ 4/8 | ≤ 3/8 |
| < 2 | *A* | *A-B* | *B* | | |
| 2-3 | *A-B* | *B* | *C* | *E* | *F* |
| 3-5 | *B* | *B-C* | *C* | *D* | *E* |
| 5-6 | *C* | *C-D* | *D* | *D* | *D* |
| >6 | *C* | *D* | *D* | *D* | *D* |

*A*: extremely unstable; *B*: moderately unstable; *C*: Slightly unstable;
*D*: neutral; *D*: slightly stable; *F*: moderately stable.

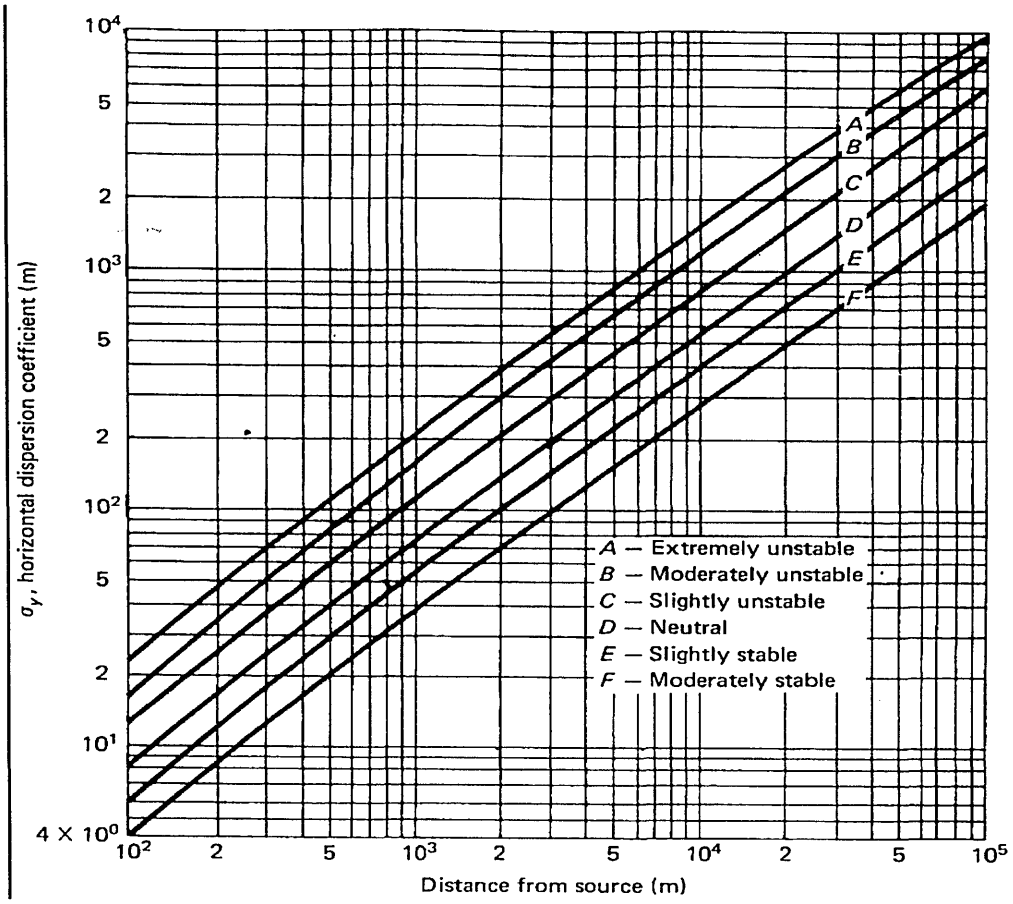


Figure 2.2 Pasquill-Gifford curves for $\sigma_y$ (Seinfeld and Pandis, 1997)

For use in dispersion formulae, it is convenient to have analytical expressions for $\sigma_y$ and $\sigma_z$ as functions of dispersion distance, $x$. Many of the empirically determined forms can be represented by the power-law expressions:

$$\sigma_y = ax^b \tag{2.40}$$

$$\sigma_z = cx^d \tag{2.41}$$

The values of coefficients a, b, c and d depend on the atmospheric stability class and the averaging time. The values recommended by the American Society of Mechanical Engineers (ASME, 1973) and Klug (1969) are shown in Table 2.6.

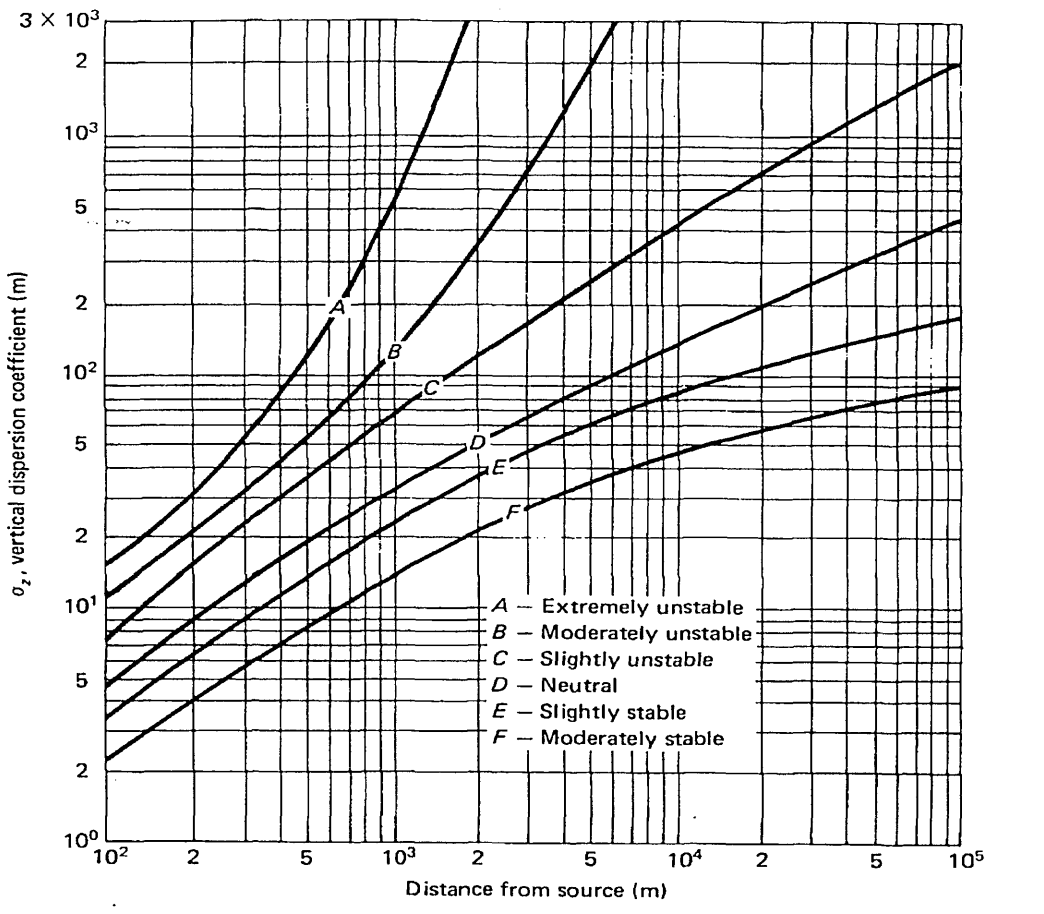


Figure 2.3 Pasquill-Gifford curves for $\sigma_z$ (Seinfeld and Pandis, 1997)

Table 2.6 The values of coefficients a, b, c and d

| | Average time | Coefficient | Stability Class | | | | | |
|---|---|---|---|---|---|---|---|---|
| | (min) | | A | B | C | D | E | F |
| ASME | 60 | *a* | 0.40 | 0.36 | | 0.32 | | 0.31 |
| | | *b* | 0.91 | 0.86 | | 0.78 | | 0.71 |
| | | *c* | 0.40 | 0.33 | | 0.22 | | 0.06 |
| | | *d* | 0.91 | 0.86 | | 0.78 | | 0.71 |
| Klug | 10 | *a* | 0.469 | 0.306 | 0.230 | 0.219 | 0.237 | 0.273 |
| | | *b* | 0.903 | 0.885 | 0.855 | 0.764 | 0.691 | 0.594 |
| | | *c* | 0.017 | 0.072 | 0.076 | 0.140 | 0.217 | 0.262 |
| | | *d* | 1.380 | 1.021 | 0.879 | 0.727 | 0.610 | 0.500 |

The statistical theory is concerned with the actual velocity of individual particles in stationary, homogeneous turbulence. Under this assumption, the statistics of the motion of one typical particle provides a statistical estimate of the behaviour of all particles. In the atmosphere one may expect the cross-wind component ($v$) of turbulence to be nearly

homogeneous since the variations in the scale and intensity of $v$ with height are often small. On the other hand, the vertical velocity component ($w$) is decidedly inhomogeneous, since characteristically $w$ increases with height above the ground. Thus, the $\sigma_y$ and $\sigma_z$ correlations based on the Pasquill stability classes should be suitable for describing the spread of a plume in the cross-wind direction regardless of the height, but, for vertical spread only in the early stage of travel from a source considerably elevated far above the ground. The $\sigma_y$ and $\sigma_z$ based on similarity theory are more suitable for describing vertical dispersion that varies with height.

### 2.3.1.4 Atmospheric dispersion *K*-theory

As discussed in section 2.3.1.1, the Eulerian approach leads to the so-called closure problem (equation 2.1) with new dependent variables $\overline{u_i'c'}$, $i = 1, 2, 3$. The turbulent fluxes $\overline{u_i'c'}$ should be related to $\bar{c}$ if we do not wish to introduce additional differential equations. The most common means of relating $\overline{u_i'c'}$ to $\bar{c}$ is based on the mixing-length model. In the mixing-length model, the turbulent fluid is envisioned as comprising lumps of fluid which, for a short time, retain their integrity before being destroyed. These lumps or eddies transfer momentum, heat, and material from one location to another, conceptually in much the same way as molecular motion is responsible for transport in gases. Thus, it is possible to imagine an eddy, originally at one level in the fluid, breaking away and conserving some or all of its momentum until it mixes with the mean flow at another level.

In turbulent dispersion *K*-theory, it is assumed that

$$\overline{u_i'c'} = -K_{ik}\frac{\partial \bar{c}}{\partial x_k} \qquad i = 1, 2, 3 \tag{2.42}$$

where $K_{ik}$ is called the eddy diffusivity. Since equation 2.42 is only a definition of the $K_{jk}$, which are in general functions of location and time, the three unknowns $\overline{u_i'c'}$, $i = 1, 2, 3$ in equation 2.1 can be replaced with six unknowns $K_{ik}$, $i, k = 1, 2, 3$ ($K_{ik} = K_{ki}$). If the coordinate axes coincide with the principal axes of the eddy diffusivity tensor $\{K_{ik}\}$, then only three diagonal elements $K_{11}$, $K_{22}$ and $K_{33}$ are non-zero. Equation 2.42 becomes

$$\overline{u_i'c'} = -K_{ii}\frac{\partial \bar{c}}{\partial x_i} \qquad i = 1, 2, 3 \tag{2.43}$$

This equation indicates that the transport rate for a species caused by turbulent mixing depends on the extent of the species unbalanced distribution (mean concentration gradient)

and the dispersion ability of the turbulence field (eddy diffusivity). In the Eulerian approach, two other assumptions are usually invoked:

- Molecular diffusion is negligibly smaller than the turbulent diffusion.
- The atmosphere is incompressible.

In a more general form, Equation 2.1 becomes

$$\frac{\partial \bar{c}}{\partial t}+\bar{u}\frac{\partial \bar{c}}{\partial x}+\bar{v}\frac{\partial \bar{c}}{\partial y}+\bar{w}\frac{\partial \bar{c}}{\partial z}=\frac{\partial}{\partial x}\left(K_{xx}\frac{\partial \bar{c}}{\partial x}\right)+\frac{\partial}{\partial y}\left(K_{yy}\frac{\partial \bar{c}}{\partial y}\right)+\frac{\partial}{\partial z}\left(K_{zz}\frac{\partial \bar{c}}{\partial z}\right)+R+S \quad (2.44)$$

This equation is the basic equation for the Eulerian approach. It is termed the atmospheric dispersion equation. The key problem in the use of Equation 2.44 is the choice of the functional forms of the mean wind speeds, $\bar{u}$, $\bar{v}$ and $\bar{w}$, and the eddy diffusivities, $K_{xx}$, $K_{yy}$ and $K_{zz}$. The mean wind speed field may be simulated numerically using an atmospheric dynamic model. The expressions available for $K_{zz}$ are based on Monin-Obukhov similarity theory coupled with observational or computationally-generated data. It is best to organise the expressions according to the type of atmospheric stability.

In the 50 – 100 m above ground surface layer (shear stress and heat flux constant; wind determined by nature of surface and vertical temperature gradient), $K_{zz}$ can be expressed as (Seinfeld and Pandis, 1997)

$$K_{zz}=\frac{\kappa u_* z}{\phi(z/L)} \quad (2.45)$$

Where $\kappa$ =0.4 is the so called Karman's constant, $u_*$ is the friction velocity, $L$ is the Monin-Obukhov length, $\phi(z/L)$, which is given by

$$\phi(z/L) = 1 + 4.7z/L \qquad z/L > 0 \qquad \text{stable} \quad (2.46)$$

and

$$\phi(z/L) = 1 \qquad z/L = 0 \qquad \text{neutral} \quad (2.47)$$

and

$$\phi(z/L) = [1 - 15z/L] \qquad z/L < 0 \qquad \text{unstable} \quad (2.48)$$

In the 300 – 500 m above ground layer ( wind determined by surface drag, temperature gradient, and Coriolis force), Lamb and Duran (1977) derived an empirical expression for $K_{zz}$ under unstable conditions

$$\frac{K_{zz}}{w_* z_i}=2.5\left(\kappa\frac{z}{z_i}\right)^{4/3}[1-15(z/L)]^{1/4} \qquad 0 \le z/z_i < 0.05 \quad (2.49)$$

and

$$\frac{K_{zz}}{w_* z_i} = 0.021 + 0.408\left(\frac{z}{z_i}\right) + 1.351\left(\frac{z}{z_i}\right)^2 - 4.096\left(\frac{z}{z_i}\right)^3 + 2.560\left(\frac{z}{z_i}\right)^4 \qquad 0.05 \le z/z_i \le 0.6 \qquad (2.50)$$

and

$$\frac{K_{zz}}{w_* z_i} = 0.2\exp\left[6 - 10\left(\frac{z}{z_i}\right)\right] \qquad 0.6 < z/z_i \le 1.1 \qquad (2.51)$$

and

$$\frac{K_{zz}}{w_* z_i} = 0.0013 \qquad z/z_i > 1.1 \qquad (2.52)$$

where $z_i$ is the mixed layer height, $u_*$ is the convective velocity scale.

Lamb et al. (1975) derived an empirical expression for $K_{zz}$ under neutral conditions for the Ekman layer

$$K_{zz} = \frac{u_*^2}{f}\left[7.396\times10^{-4} + 6.082\times10^{-2}\left(\frac{zf}{u_*}\right) + 2.532\left(\frac{zf}{u_*}\right)^2 - 12.72\left(\frac{zf}{u_*}\right)^3 + 15.17\left(\frac{zf}{u_*}\right)^4\right] \qquad 0 \le zf/u_* \le 0.45 \qquad (2.53)$$

and

$$K_{zz} \cong 0 \qquad zf/u_* \ge 0.45 \qquad (2.54)$$

where $f$ is the Coriolis parameter. In Equations 2.34 and 2.35, $u_*/f$ instead of $L$ (Monin-Obukhov length ) is used as vertical length scale because $L = \infty$ in neutral conditions.

Under stable conditions, Businger and Arya (1974) proposed that $K_{zz}$ in the Ekman layer could be described as

$$K_{zz} = \frac{\kappa u_* z}{0.74 + 4.7(z/L)}\exp\left(-\frac{8fz}{u_*}\right) \qquad (2.55)$$

For typical meteorological conditions, the maximum value of $K_{zz}$ under stable conditions is in the range 0.5 to 5 $m^2 s^{-1}$.

For horizontal eddy diffusion coefficients $K_{xx}$ and $K_{yy}$, Seinfeld (1986) proposed

$$K_{yy} \cong 0.1 z_i^{3/4}(-\kappa L)^{-1/3} u_* \qquad (2.56)$$

$$K_{xx} = K_{yy} \qquad (2.57)$$

The important issues of interest with respect to the $K$-theory are:

- Under what conditions of source configuration and turbulence field can this theory be applied?

- To what extent can the eddy dispersion be specified in a prior manner from measured properties of the turbulence?

In summary, the spatial and temporal scales of turbulence should be small in comparison with the corresponding scales of the concentration field.

### 2.3.2 Atmospheric dispersion physical models

These models use physical means to simulate atmospheric dispersion in the laboratory or field. The use of a wind tunnel is a major physical means for simulating atmospheric dispersion in a laboratory. A scaled terrain model for the domain to be simulated is put into the wind tunnel. Similar conditions of wind and dispersion in the planetary boundary layer are produced in the tunnel. A trace gas is released from an imaginary source. The characteristics of atmospheric dispersion can be shown by concentration distribution of the trace gas. Hoydysh and Dabberdt (1988, 1991) successfully simulated the dispersion of vehicular emission in different street canyons. A wind tunnel is a huge, complex and expensive piece of equipment. It is rarely available to environmental scientists. The planetary boundary layer conditions are too complex to be simulated completely, especially for large regions. Some ideal simplifications are used in the experiment. The ideal atmospheric dispersion conditions produced in the tunnel may deviate from the real field data.

In the field, it is usually the practice to use a released trace gas when observing atmospheric dispersion. DePaul and Sheih (1985) had observed the atmospheric dispersion in a street canyon by releasing $SF_6$ trace gas. However, the field physical methods need huge human and financial resources. It is only suitable for a small domain. The observed results just show the characteristics of air diffusion in the specified area. Furthermore, the trace gas released in the environment may cause some nuisances. Thus, physical methods (both in the laboratory and field) are used only in some special circumstances.

### 2.3.3 Atmospheric dispersion empirical model

This model is a kind of simple atmospheric dispersion model. It is derived from the field observations of atmospheric dispersion. Jahnson (1973) developed a famous empirical model that could simulate dispersion of airborne pollutant emitted by vehicles in a street canyon. A vortex may exist in the street canyon when prevailing wind at the canyon top is perpendicular to the street. As a result, the concentration in the leeward side

of the canyon may be higher than that in the windward side. In the leeward side, the concentration of vehicular emitting pollutant is predicted by:

$$c_l = \frac{KQ}{(u+0.5)[(x^2+z^2)^{1/2}+2]} \tag{2.58}$$

In the windward side, the concentration of vehicular emitting pollutant is predicted by:

$$c_w = \frac{KQ}{W(u+0.5)} \tag{2.59}$$

where $Q$ is the vehicular emission rate, $u$ the wind speed on the top of street canyon, $x$ the lateral distance from the receptor to street central line, $z$ the height of the receptor, $W$ the width of the street and $K$ an empirical constant. The value of $K$ approaches 7 in a street canyon in San Jose, USA.

Although the empirical model is simple, it may perform as well as other complex models in a small scale domain with complex atmospheric dispersion conditions such as a street canyon. Qin and Kot (1993) developed an empirical model and applied the model successfully in simulating dispersion of vehicular emitting pollutants in a street canyon in Guangzhou, China. The empirical constants in the empirical model are usually derived from a special domain and atmospheric dispersion condition. The constants in the empirical model need to be adjusted to fit local conditions if one wants to use the model to simulate atmospheric dispersion.

### 2.3.4 Gaussian model

This model can be derived from both statistical theory and $K$-theory. As described above, the difficulty of the statistical theory is how to describe the probability density function ($P(x,y,z)$) appropriately. Under the condition of stationary, homogeneous turbulence, the probability density distribution has a Gaussian form. The Gaussian form of concentration distribution of airborne pollutants can be derived from the Gaussian form of probability density. Assuming constant turbulent dispersion coefficients $K_{xx}$, $K_{yy}$, and $K_{zz}$, the solution of the atmospheric dispersion model has a Gaussian form as well. There are various kinds of forms for the Guassian model. One that is used frequently is the so called 'conventional' Gaussian plume model. In windy conditions, the concentration of airborne pollutant emitted from a point source at a receptor with a 'downwind distance' $x$, 'crosswind distance' $y$ and height $z$ can be calculated from (Seinfeld and Pandis, 1997):

$$C(x,y,z)=\frac{Q}{2\pi u_s \sigma_y \sigma_z}\exp\left[-0.5\left(\frac{y}{\sigma_y}\right)^2\right]\left\{\exp\left[-0.5\left(\frac{z-h_e}{\sigma_z}\right)^2\right]+\exp\left[-0.5\left(\frac{z+h_e}{\sigma_z}\right)^2\right]\right\} \quad (2.60)$$

where $Q$ is airborne pollutant emission rate for the point source; $u_s$ is wind speed at stack height; $\sigma_y$ and $\sigma_z$ are lateral and vertical atmospheric dispersion parameters; $h_e$ ($h_e = h_s + \Delta h$) is effective emission height; $h_s$ is stack or release height and $\Delta h$ is plume rise height.

The Gaussian model is one of the most popular models used in environmental research and management because it is easy to use. It is also an important model listed in "Selection and use of dispersion models" published by Department of the Environment, Transport and the Regions, the UK (Department of the Environment, 1998). Many software packages have been developed for the Gaussian model. The Gaussian model and the package have been improved continually during the past twenty years. In the 1980s, the conventional Gaussian plume model with $\sigma_y$ and $\sigma_z$ correlations based on the Pasquill stability classes was used as the basis for some famous packages such as R-91 (Clarke, 1979) in the UK, ISC (EPA, 1995) and CALINE4 (Benson, 1984) in USA etc. As discussed above, $\sigma_y$ and $\sigma_z$ correlations based on the Pasquill stability classes are built up on the assumption of stationary and homogeneous turbulence. In the atmospheric environment, one may expect the cross-wind component ($v$) of turbulence to be nearly homogeneous since the variations in the scale and intensity of $v$ with height are often small. On the other hand, the vertical velocity component ($w$) is decidedly inhomogeneous, since characteristically $w$ increases with height above the ground. Thus, the conventional Gaussian plume model, with $\sigma_y$ and $\sigma_z$ correlations based on the Pasquill stability classes should be suitable for describing the spread of a plume in the cross-wind direction regardless of height but for vertical spread only in the early stage of travel from a source considerably elevated far above the ground. In the 1990s, the so-called new generation Gaussian models such as ADMS and ADMS-Urban (McHugh et al., 1997) in the UK and SPPAM (Wang et al., 1999) in USA were developed. In the so called new generation Gaussian models, the concentration profiles are assumed to be skewed-Gaussian for convective conditions, to allow for the skewness of the vertical velocity within the boundary layer. The correlations for $\sigma_y$ and $\sigma_z$ are based on the similarity theory that are used in these models. In SPPAM, the effect of finite time of plume transport from source to receptor is also considered. These effects can be very significant when the distance between the source and receptor is large or in light-wind conditions.

### 2.3.5 Atmospheric dispersion equation

The atmospheric eddy dispersion equation (2.44) is a basic model for the Eulerian approach. In the atmospheric eddy dispersion equation $u\frac{-\partial\bar{c}}{\partial x}, v\frac{-\partial\bar{c}}{\partial y}, w\frac{-\partial\bar{c}}{\partial z}$ are the so called advection terms, they describe the mass transport caused by an average wind field; $\frac{\partial}{\partial x}(K_{xx}\frac{\partial\bar{c}}{\partial x}), \frac{\partial}{\partial y}(K_{yy}\frac{\partial\bar{c}}{\partial y}), \frac{\partial}{\partial z}(K_{zz}\frac{\partial\bar{c}}{\partial z})$ are the so-called dispersion terms, which describe the mass transport caused by the turbulent field.

The atmospheric dispersion equation provides a more general approach to simulate transport and transformation of airborne pollutants. The processes of atmospheric dispersion and atmospheric chemistry can be simulated by digitally solving the atmospheric dispersion equation. Many complex factors such as wind shear, rugged surface topography, the various reaction mechanisms of atmospheric chemistry and deposition may be considered in solving the equation. Thus, the atmospheric eddy dispersion equation may be used to study complex atmospheric environmental phenomena such as aerosol formation and transformation and chemical smog. Olendrzynski et al. (2000) developed the EMEP Eulerian model in 50 km x 50 km grids to simulate acid deposition over Europe. Wexler at al. (1994) developed a very complex Eulerian model to simulate the urban and regional aerosols. Various processes that may influence the aerosol size and composition such as emission, deposition, advection, turbulent dispersion, condensation, evaporation, coagulation, nucleation, settling and heterogeneous chemical reactions have been included in their general dynamic equation that describes the composition of an internally mixed aerosol over time:

$$\frac{\partial q_i(m,\vec{r},t)}{\partial t} + (\vec{V}(\vec{r},t) - V_s(m)\vec{k})\cdot\nabla q_i(m,\vec{r},t) = H_i(m,\vec{r},t)q(m,\vec{r},t) - \frac{\partial(mq_iH)}{\partial m}$$

$$+ \int_0^m \Gamma(m', m-m', \vec{r}, t) q_i(m', \vec{r}, t)\frac{q(m-m', \vec{r}, t)}{m-m'}dm' - q_i(m,\vec{r},t)\int \Gamma(m', m, \vec{r}, t)\frac{q(m', \vec{r}, t)}{m'}dm'.$$

$$\nabla\cdot(\vec{K}(\vec{r},t)\nabla q_i(m,\vec{r},t)) + E_i(m,\vec{r},t) + R_i(m,\vec{r},t) + N_i(m,\vec{r},t) \qquad (2.61)$$

Where $q(m,\vec{r},t)$ is the total mass distribution, such that $q_i(m,\vec{r},t)dm$ is the mass concentration of species $i(i=1,2,\ldots s)$ in the mass range $[m, m+dm]$ and $q = \sum_{i=1}^{s} q_i$ ; $m_i$ is the mass of species $i$ in an individual particle and total mass $m = \sum_{i=1}^{s} m_i$ ;

$H_i = (1/m)dm_i/dt$ is the inverse of the characteristic time for particle growth due to condensation or evaporation of species $i$ and $H = \sum_{i=1}^{s} H_i$; $\Gamma(m',m) = \Gamma(m,m')$ is the binary coagulation coefficient; $\vec{r}$ is the spatial coordinate vector; $t$ is time; $\vec{V}$ is the wind velocity vector; $V_s$ is the settling velocity; $\vec{k}$ is the unit vector in the vertical direction; $\vec{K}(\vec{r},t)$ is the turbulent dispersion coefficient; and $E_i$, $R_i$ and $N_i$ are, respectively, the emission, reaction, and nucleation rates of species $i$ in the mass range $m$ to $m+dm$.

In equation 2.61, $\frac{\partial q_i(m,\vec{r},t)}{\partial t}$ describes the local change rate for species $i$; $(\vec{V}(\vec{r},t) - V_s(m)\vec{k}) \cdot \nabla q_i(m,\vec{r},t)$ describes the spatial advection and gravitational settling rate; $H_i(m,\vec{r},t)q(m,\vec{r},t) - \frac{\partial(mq_iH)}{\partial m}$ describes the condensation and evaporation rate; $\int_0^m \Gamma(m',m-m',\vec{r},t)q_i(m',\vec{r},t)\frac{q(m-m',\vec{r},t)}{m-m'}dm' - q_i(m,\vec{r},t)\int \Gamma(m',m,\vec{r},t)\frac{q(m',\vec{r},t)}{m'}dm'$ describes the coagulation rate; $\nabla \cdot (\vec{K}(\vec{r},t)\nabla q_i(m,\vec{r},t)$ describes the spatial dispersion rate; and, $E_i(m,\vec{r},t), R_i(m,\vec{r},t), N_i(m,\vec{r},t)$ describe the emissions, reaction, and nucleation rates respectively. Lurmann et al. (1997) applied this model to predict the size-resolved concentration of all major primary and secondary components of atmospheric particulates in California's south coast air basin.

In contrast to convenient Gaussian plume model with $\sigma_y$ and $\sigma_z$ correlations based on the Pasquill stability classes that performs well in a small domain, the atmospheric dispersion equation, based on turbulence dispersion $K$-theory can perform reasonably well in a large region. As discussed in 2.3.1.4, the spatial and temporal scales of the turbulence should be small in comparison with the corresponding scales of the concentration field. Lamb (1973) suggested that gradient-transport theory was only applicable when $t_e/T_c \ll 1$, where $t_e$ is the maximum time over which the turbulent eddy maintains its integrity and $T_c$ is the time scale associated with the mean flow field. This condition may be satisfied in simulating atmospheric dispersion in a large region. The transport caused by turbulent eddy dispersion is much smaller than that caused by advection of average flow field when this condition is satisfied.

### 2.3.6 Lagrangian model

Lagrangian approach uses a moving frame of reference to describe atmospheric dispersion. It has been used to simulate long distance transport of an air parcel and the chemical transformation, dry and wet deposition of airborne pollutants in the air parcel. Many kinds of Lagrangian models such as the air parcel trajectory model have been developed. Most of them are based on atmospheric dispersion statistical theory. However, the atmospheric dispersion $K$-theory may also be formulated in the Lagrangian frame of reference.

In the Lagrangian statistical model, the air parcel can be represented by hypothetical mass points, the trajectories of which are computed from a stochastic solution to the atmospheric dispersion equation. Pollutant concentrations are determined by the probability that an air parcel exists at a location and time (Gray and Cass, 1998). Equation 2.2 is a general Lagrangian statistical expression for use in air quality modelling.

Recently, Gray and Cass (1998) used a Lagrangian particle in cell air quality model to attribute source contributions to atmospheric fine carbon particles in the Los Angeles area. The long time average form of Equation 2.2 was used in their model. Bergin et al. (1999) analysed the formal uncertainty of a Lagrangian photochemical air pollution model.

A problem that has to be solved when using a Lagrangian statistical model is the comparison of model results with field monitoring data. Most of the meteorological factors and the concentrations of pollutants are measured at fixed stations. This means that most of the field monitor data are based on an Eulerian frame of reference. The theoretical relationship between the Eulerian and Lagrangian approaches was discussed by Lamb and Seinfeld (1973).

On the other hand, the atmospheric dispersion equation in the Lagrangian form has been used to simulate long distance transport and transformation of airborne pollutants. Liousse et al. (1996) simulated the global distribution of carbonaceous aerosols using the Grantour model (a global three dimensions Lagrangian model of transport, transformation, and removal which uses the wind and precipitation fields of the Community Climate Model (CCM1)). Metcalfe et al. (1995) estimated the sulphur deposition across the UK and its likely source attribution using the Hull Acid Rain Model (HARM). In HARM, the change rate of trace constituent concentration in the air parcel is calculated using:

$$\frac{d[c_i]}{dt} = \frac{E_i}{h} + P_i - L_i[c_i] - \frac{V_i}{h}[c_i] - S_i[c_i] \tag{2.62}$$

where $[c_i]$ is the concentration of the trace constituent species, $i$; $E_i$ is the instantaneous emission rate of the species, $i$; $h$ is height of atmospheric boundary layer; $P_i$ is the instantaneous production rate of the species, $i$; $L_i$ is the instantaneous loss coefficient for the species, $i$; $V_i$ is the spatially dependent and species dependent dry deposition velocity; and, $S_i$ is the spatially dependent and species dependent wet scavenging coefficient. 24 trace constituent species had been included in their work.

Eldering and Cass (1996) studied air pollutant effects on visibility in the South Coast Air Basin of California using a mathematical model with a Lagrangian formulation of the atmospheric dispersion equation. The equation for aerosol phase species $i$ of size $k$ is:

$$\frac{\partial c_{ik}}{\partial t} - \frac{\partial}{\partial z}(K_{zz}\frac{\partial c_{ik}}{\partial z}) + L_{ik}(C,T,RH) \qquad i=1,2,\ldots,n, \quad k=1,2,\ldots,m \qquad (2.63)$$

The equation for gas phase species $i$ is:

$$\frac{\partial c_i}{\partial t} - \frac{\partial}{\partial z}(K_{zz}\frac{\partial c_i}{\partial z}) + R_k(c_1,c_2,\mathrm{K},c_n,T) - \sum L_{ik}(C,T,RH) \quad i=1,2,\ldots,n \qquad (2.64)$$

where $c_{ik}$ is the aerosol phase concentration of species i of size $k$; $L_{ik}(C, T, RH)$ is the rate of gain or loss of the aerosol material due to dispersion movement between the gas and the aerosol phase, which is a function of the aerosol species concentrations and gas phase concentrations (denoted by $C$), temperature ($T$) and relative humidity ($RH$). $R_i(c_1, c_2, \ldots, T)$ is the rate of production or loss of species $i$ at temperature $T$ due to gas phase chemical reaction.

The above model is suited to an internally mixed aerosol. The internally mixed aerosol is defined as one in which all particles of the same size have exactly the same chemical composition. Kleeman and Cass (1997, 1998, 1999) had expanded the above model to represent the ambient aerosol either as internally mixed or as a source-oriented that is externally mixed. An item, $M_{ik}(c_k, T, RH)$, that describes the production rate of species $i$ within particles of size $k$ due to aqueous phase chemical reaction had been added to aerosol phase equation 2.63. They had applied their model to attribute the source contributions to the size and composition distribution of urban particulate airborne pollutants in California. Like equation 2.61, equations 2.63 and 2.64 provide a means to simulate the aerosol formation, transformation and deposition. However, application of this equation group is limited by our knowledge of the mechanisms of aerosol formation, transformation and deposition.

## 2.4 Receptor models

The atmospheric dispersion model is a source-oriented model. It focuses on the processes of transport, dilution and transformations of airborne pollutant that begin at the source. The precision of the atmospheric dispersion model depends directly on the precision of the emission source. However, the precise source profiles are only available for some special sources. In addition to these special emission sources, there are many fugitive and small sources with widely varying compositions. The precise source profiles for these sources are very difficult to obtain. Sometimes, the source profiles may have changed since they were last investigated. An alternative method, receptor modelling, has been developed to identify airborne pollutant sources and their contributions to air pollution, particularly for cases where the source profiles are not comprehensive. In contrast to atmospheric dispersion model, the receptor model focuses on the behaviour of the ambient environment at the point of impact. These methods require that samples be obtained at locations of interest, the receptors, and that samples be analysed for the properties that are characteristic of the pollutant sources.

Various approaches for receptor model analysis have been developed. Most of receptor models such as chemical mass balance and factor analysis are based on multivariate data analysis. Henry (1997) has reviewed the history and fundamentals of multivariate air quality receptor models. The scanning electron microscopy and air parcel backward trajectory provide two other approaches for receptor modelling. Rahn (1999) used a graphical technique to determine major components in the mixed airborne particulates. Recently, Seigneur et al. (1999) grouped the types of receptor models into three major categories:

- Models that apportion primary airborne pollutants using source information.
- Models that apportion primary airborne pollutants without using source information.
- Models that apportion both primary and secondary airborne pollutants.

### 2.4.1 The chemical mass balance model (CMB)

The chemical mass balance model (CMB) is a fundamental receptor model. It is a model that apportions airborne pollutant using source information. CMB is based on the assumption of mass conservation and the use of a mass balance analysis. The chemical

mass balance model uses the chemical and physical characteristics of gaseous and particulate pollutants measured at the source and receptor locations to both identify the presence of source and quantify source contributions to the pollutants measured at the receptor. Watson and Chow (1991) have described CMB modelling procedures and an application and validation protocol. The CMB model consists of a least squares solution to a set of linear equations which expresses each receptor concentration of a chemical species as a linear sum of products of source composition and source contribution:

$$c_{ij} = \sum_{k=1}^{p} S_{ik} f_{kj} \qquad i=1,\ldots, m; \qquad j=1,\ldots, n. \tag{2.65}$$

where $c_{ij}$ is the $i$th chemical species concentration measured in the $j$th sample at the receptor. $S_{ik}$ is the composition of the $i$th chemical species in the $k$th source. $f_{kj}$ is the contribution of $k$th source to $j$th sample. The input data for the CMB model are source compositions and the receptor concentration. The output of the model is the amount contributed by each source to each chemical species.

A commonly used software package for CMB model is CMB7 (EPA, 1989). Watson et al. (1991) developed this software package and applied it to apportion $PM_{10}$ sources in California's South Coast Air Basin (SoCAB). A total of 27 source profiles that were grouped into four types: geological material, vehicular emissions, marine aerosol and secondary aerosol. Most of the source profiles for geological material and vehicular emissions come from these source emission samples. Most of the profiles for marine aerosol and secondary aerosol are ideal profiles. Chow et al. (1992) further applied the CMB7 model to apportion $PM_{10}$ sources in California's San Joaquin Valley, for which 8 source profiles were selected. Recently, Chen et al. (1997) used this model to assess the source contributions to ambient aerosol in central Taiwan. Eight and seven source profiles were used for fine and coarse particles, respectively. A few of the source profiles adopted the figures proposed by the EPA because locally measured data were unavailable. Vega et al. (1997) applied this model to respirable particulate matter in Mexico City. Most of the 11 used source profiles adopted the figures proposed by the EPA. Only three source profiles were derived from local samples. Motallebi (1999) used this model to apportion wintertime airborne particlate sources at Sacramento, California. 7 source profiles were used in his work.

The CMB model is based on a series of assumptions:

- Compositions of source emission are constant over the period of sampling at the receptor locations.
- The chemical species do not react with each other in the period between the sources and the receptor.
- All potential sources with a significant contribution to the receptor have been identified and characterised,
- The source compositions are linearly independent of each other.
- The number of sources is less than or equal to the number of chemical species.
- Measurement of uncertainties are random, uncorrelated, and normally distributed.

These assumptions are fairly restrictive and can never be totally complied with in practice (Henry, 1991). Although the CMB model can tolerate deviations from these assumptions, the uncertainties of the source contribution estimates would increase with the deviations. Like the atmospheric dispersion model, the error in estimating source contributions due to biases in all of the elements of source profile is directly in proportion to the magnitude of the biases. When one tries to apply the CMB model, the number and the types of the potential sources are not easy to identify. The precise and stable source profiles are difficult to obtain. Sometimes, some source profiles applied in foreign countries or even another continents had to be adopted because locally measured profiles are unavailable. These quoted source profiles may not match with the same types of local source emissions.

### 2.4.2 The factor analysis (FA) or the principal component analysis (PCA) model

The factor analysis (FA) or the principal component analysis (PCA) model is developed from the CMB model. FA or PCA is a multivariate statistical model that apportions primary airborne pollutant without using source information. Henry (1991) described the multivariate receptor models in detail. FA or PCA is based on the idea that the components from the same source will be correlated and these correlations can be used to estimate the source composition. The principal method of FA or PCA model is the singular value decomposition. The basic equation for FA or PCA is:

$$X = GF \tag{2.66}$$

where $X$ is an airborne pollutant concentrations matrix with dimensions of $n \times m$. $n$ represents the sample number measured at the receptor. $m$ represents the chemical species number analysed for each sample. FA or PCA model divides airborne pollutant

concentrations matrix $\boldsymbol{X}$ into two new matrices $\boldsymbol{G}$ and $\boldsymbol{F}$ with dimensions of $n \times p$ and $p \times m$ in such a way that $\boldsymbol{GF}$ explains the variation in $\boldsymbol{X}$ as well as possible. $p$ is the rank of factorisation. $\boldsymbol{G}$ the factor score matrix and $\boldsymbol{F}$ is the factor loading matrix. Eigenvector analysis is the principal approach applied in analysing airborne pollutant concentration data. Eigenvector analysis tries to simplify the description of a system by determining the minimum number of new variables necessary to reproduce the measured attributes of the system.

Some famous statistical software such as SPSS and MINITAB provide the tools for both FA and PCA. Recently, Veltkamp et al. (1996) applied SPSS to conduct a principal component analysis for summer time organic aerosols at Niwot Ridge, Colorado. Huang et al. (1999) assessed the performance of the PCA method using aerosol data measured at Narragansett, Rhode Island. Artaxo et al. (1999) applied an absolute principal factor analysis model that could provide a quantitative elemental source profile instead of a qualitative factor loading to apportion aerosols to their sources in Santiago de Chile.

The basic ideas of FA or PCA are that the components from the same source will be correlated and these correlations can be used to estimate the source composition. However, observed correlations between chemical species at the receptor, which are assumed to bear source composition information may be the result of the mutual effects of meteorology and coincident source location. The source profiles derived by FA or PCA may be misleading, because a singular value decomposition is a non-unique solution problem. Some additional constraints, physical or mathematical, usually have to be applied to models in order to make the solution to be mathematically determinate. Sometimes, negative values may appear in the factor loading matrix. The results of FA or PCA with negative factor loading are ambiguous and difficult to interpret.

### 2.4.3 The positive matrix factorisation (PMF) model and multilinear engine

A new variant of factor analysis, Positive Matrix Factorisation (PMF) and the corresponding software package were developed by Paatero and Tapper (1994). The PMF model is causing general interest because it can produce strictly non-negative loading factors, optimally based on error estimates of data values, with almost no rotational ambiguity. The PMF model has been described in detail by Paatero et al. (1994, 1997). There are two types, namely two-way and three-way PMF models. Two-way PMF is a two-dimensional principal component analysis model. A two-dimensional matrix is used as

input database. Three-way PMF is a straightforward generalisation of two-way PMF. It is a tri-linear factor analysis model. A three-dimensional matrix is used as input database.

The two-way PMF model can be written as

$$X_{ij} = \sum_{h=1}^{p} G_{ih} F_{hj} + E_{ij} \qquad (i=1,\ldots,n; j=1,\ldots,m) \tag{2.67}$$

where $E_{ij} = X_{ij} - \sum_{h=1}^{p} G_{ih} F_{hj}$ is a matrix of residuals. The principle of the two-way PMF model can be presented as

$$\text{minimize} Q = \sum_{i=1}^{n} \sum_{j=1}^{m} \left( \frac{E_{ij}}{S_{ij}} \right)^2 \quad \text{with } G_{ih} \geq 0, F_{hj} \geq 0 \tag{2.68}$$

where $S_{ij}$ is the point-by-point error estimate of $X_{ij}$ and $E_{ij}/S_{ij}$ is the scaled residual.

Three-way PMF model be written as

$$X_{ijk} = \sum_{h=1}^{p} A_{ih} B_{jh} C_{kh} + E_{ijk} \qquad (i=1,\ldots, n; j=1,\ldots,m; k=1,\ldots,o) \tag{2.69}$$

where $E_{ijk} = X_{ijk} - \sum_{h=1}^{p} A_{ih} B_{jh} C_{kh}$ is a matrix of residuals. The principle of the three dimensional PMF model can be presented as

$$\text{minimize} Q = \sum_{i=1}^{n} \sum_{j=1}^{m} \sum_{k=1}^{o} \left( \frac{E_{ijk}}{S_{ijk}} \right)^2 \qquad \text{with } A_{ih} \geq 0, B_{jh} \geq 0, C_{kh} \geq 0 \tag{2.70}$$

where $S_{ijk}$ is the point-by-point error estimate of $X_{ikj}$ and $E_{ijk}/S_{ijk}$ is the scaled residual.

In recent years, the PMF model has been a popular receptor model applied to identify atmospheric aerosol sources. Huang et al. (1999) have tested and optimized FA and PMF on a set of aerosol data. They found that the PMF model could utilize information more efficiently and separate sources up to an order of magnitude better than FA although it was harder to use than FA. The research group headed by Dr. Hopke has made a good progress in PMF model applications (Polissar et al., 1996; Alexandr et al., 1998; Xie et al., 1998, 1999a, 1999b; Hope et al., 1998; Ramadan, 2000). Source characterizations and seasonal variations of airborne particulate sampled in the Arctic region and fine airborne particulate sampled over Alaska have been identified.

One of the major advantages of a PMF model is that it can handle various elements with different variation ranges and uncertainties, by use of error estimates. The error estimates used for the individual data point values in a PMF model are utilized as point-by-

point weight by a $\boldsymbol{S}$ matrix (standard deviation array) for $\mathbf{X}$ matrix (elements array). Chemical components measured in the ambient environment vary widely, especially for some trace elements in aerosols. Huang et al. (1999) divided aerosol chemical components into five classes:

- Those from specific sources that are measured precisely.
- Those from specific sources but are measured less precisely.
- Those from multiple sources that are measured well.
- Those from multiple sources but are occasionally with analytical problems.
- Those which could not serve as source markers and are measured poorly.

They thought that the choice of elements might affect the results of factor analysis because some elements could degrade the resolution of factor analysis by varying randomly in response to analytical uncertainties or by being below detection limits. The problem could be resolved by using the PMF model and selecting a relatively large value in the error estimate for these elements with large analytical uncertainties.

The PMF model has recently been extended to 'multilinear engine', a new concept for solving a variety of multilinear problems (Paatero, 1998) Xie et al. (1999c) applied the 'multilinear engine' to identify the source nature and seasonal variations of an Arctic aerosol. The multilinear model can be written in the sum-of-products form as:

$$x_i = y_i + e_i = \sum_{k=1}^{K_i} \prod_{j \in \xi_{ik}} f_j + e_i \quad (i=1,\ldots,M) \tag{2.71}$$

The principle of the multilinear model can be presented as

$$\text{minimize}\, Q(x,f) = \sum_{i=1}^{M} \left( \frac{e_i}{s_i} \right)^2 = \sum_{i=1}^{M} \left( \frac{x_i - \sum_{k=1}^{k_i} \prod_{j \in \xi_{ik}} f_j}{s_i} \right)^2 \qquad f_j \geq 0 \ (j \in 1,\ldots,N) \tag{2.72}$$

where $s_i$ are uncertainties connected with the measurement.

### 2.4.4 Scanning electron microscopy

With the development of the energy dispersive detector for x-ray analysis, the scanning electron microscopy (SEM) has been revolutionised from an instrument that could only produce images of small portions of matter (micrographs) to an extremely versatile analytical instrument (Hopke, 1991b). The ability of the SEM/XRF (x-ray fluorescence) system to perform elemental analysis of extremely small volumes of materials provides a powerful tool for the characterisation of individual particles and the

subsequent identification and quantitative mass apportionment of those particles to sources. Individual particles can be analysed for their elemental constituents as well as morphological information that aids in determining the processes by which the particles are formed.

VanMalderen et al. (1996) used electron probe x-ray analysis (EPXMA) to analyse the chemical and morphological characteristics of micron-sized particles. More than 20,000 individual aerosol particles (400 per sample) sampled over the total area of Lake Baikal, Russia were analysed. The result of the cluster analysis of data indicated 11 major particle types; among which soil dust, Fe-rich, Ca-rich, organic, biogenic, S-rich particles and gypsum were most abundant. Ganor et al. (1998) analysed 6170 individual aerosol particles, sampled above the Israeli Mediterranean coast by SEM, using an energy-disperse x-ray micro-analyser (EDS). 10 types of particles, nitrate and sulphate aerosols were identified in their research. Most of these particles can be classified into four groups; dominated by gypsum, aluminosilicate and quartz, salt mixed sulphate and sulphate respectively. Dye et al. (2000) used transmission electron microscopy (TEM) to analyse the quantitative morphology of roadside and background urban airborne particulates in Plymouth, UK.

The information obtained from SEM analyses is usually considered to be qualitative, due to the limited number of particulates counted. SEM is laborious and expensive if full quantitative analysis is conducted. With the improvement of computer technology, the computer controlled scanning electron microscopy (CCSEM) coupled with advanced pattern recognition methods permits scanning and image analysis to be done in close to real time. The size, shape and elemental composition can be obtained for a large number of particles in a reasonable length of time. CCSEM is a powerful tool for the identification and classification of particles.

### 2.4.5 The air parcel backward trajectories model

The receptor models described above can identify the possible sources in terms of their chemical composition. However, they can not determine the specific locations of sources and their preferred pathways. The air parcel backward trajectories model provides a means to identify the air pollution source locations. In rural or remote sites there is usually no local emission source, airborne pollutants come from the transboundary effect or long distance transport. The location of airborne pollutant source may be traced

backwards on the air parcel travelling path. The air parcel backward trajectories models have been generally used to identify the source of air pollutants related to long distance transportation (Pio et al., 1991; Yaaqub et al., 1991; Wakamatsu, 1996).

Various kinds of three-dimensional trajectory models, based on different weather observation networks have been developed and applied. Maenhaut et al. (1996) calculated the air parcel trajectories using the model of McGrath at the European Centre of Medium-range Weather Forecasts (ECMWF). The 5 days or 10 days backward trajectories of the air parcel that arrived at the central Arctic Ocean had been calculated with 1000 hPa or surface pressure as arrival pressure. Harris et al. (1994) developed and applied the isentropic transport model at the Climate Monitoring and Diagnostics Laboratory (CMDL) to calculate 10 days backward trajectories of air parcel that arrived at Barrow, Alaska, twice daily at the 500 m elevation above sea level. Input to the model is in the form of 2.5° latitude-longitude gridded meteorological parameters and topography furnished by the ECMWF or US National Centres for Environmental Prediction. Xie at al. (1999b) applied a three-dimensional AES trajectory model (Olson et al., 1978) to calculate the 5 days backward trajectories of the air parcel that arrived at Alert, an arctic site, four times daily at 925 hPa and 850 hPa levels. Input to the model used three-dimensional objectively analysed wind field data at four pressure levels: 1000, 850, 700, and 500 hPa. The information was collected from Canadian Meteorological Centre. Charron et al. (2000) used the air parcel backward trajectories model (Martin et al., 1987) to study the source-receptor relationships influencing the acidity of precipitation collected at a rural site in France. They found that highest acidities and concentrations of sulphate and nitrate in the precipitation were associated with the transport from the high emission areas of central Europe. Alkaline events were associated with air masses originating from the Mediterranean basin or northern Africa.

The air parcel backward trajectories only show potential source distribution qualitatively. The potential source contribution function (PSCF) should be constructed to describe potential source distribution quantitatively (Polissar et al., 1999). The probability that represents the potential for transport of material from a cell of address ($i$, $j$) to the receptor site can be defined as:

$$P[A_{ij}] = \frac{n_{ij}}{N} \tag{2.73}$$

where $N$ is the total number of backward trajectories from the receptor. $n_{ij}$ is the number of the backward trajectories whose endpoints lie at the cell of address $(i, j)$. Among the $n_{ij}$ counts, there will be $m_{ij}$ points for which the measured air pollution parameters exceed the criterion values selected for these parameters (e. g. ambient air quality criteria or arithmetic average values). The probability that cell $(i, j)$ is related to the observed high concentrations, $B_{ij}$, can be defined as:

$$P[B_{ij}] = \frac{m_{ij}}{N} \tag{2.74}$$

The potential source contribution function (PSCF), a form of conditional probability, can then be defined as:

$$PSCF_{ij} = P[B_{ij} | A_{ij}] = \frac{m_{ij}}{n_{ij}} \tag{2.75}$$

*PSCF* can be interpreted as a conditional probability describing the spatial distribution of a possible geographical source. Cells related to the high values of *PSCF* are the potential source areas. The grid size chosen for the PSCF computations should be sufficiently large to assimilate the uncertainty of a trajectory endpoint. A scale of about 500 km may be a suitable choice.

The air parcel backward trajectories model is subjected to uncertainty arising from interpolation of sparse meteorological data, assumptions regarding vertical transport, observational errors, sub-grid-scale phenomenon, turbulence, convection, evaporation, and condensation. Some studies to assess the performance of the trajectory model have been conducted. It is estimated that the average horizontal trajectory errors may be 800-1000 km for 5 days backward trajectory (Kahl et al., 1989). The uncertainty is higher for 10 days backward trajectory. Any trajectory calculated by the model should be considered to represent the large-scale circulation. It may be used to estimate potential source regions. However, it does not imply that a particular air parcel sampled at the trajectory destination exactly followed this path.

# Chapter 3 Airborne pollutant emission sources in Dundee

Atmospheric emission inventories that can show geographical distribution and temporal variations of airborne pollutant sources are the primary information needed in air quality management. They are very useful in land use planning for identifying parts of the region that are likely to be subject to high levels of pollution and the location of pollution sources in relation to sensitive areas. They can be used in estimating the cost of introducing controls, identifying who should bear those costs and designing monitoring networks to assess which areas are the most representative. Furthermore, inventories provide the basic data for atmospheric dispersion modelling in order to predict pollutant concentrations and assess future air quality trends.

As part of the UK government's continuing programme of air pollution studies, the former Warren Spring Laboratory maintained and developed a national inventory of air pollution sources and the type and quantity of the pollutants they emit on behalf of the Department of the Environment, Transport and the Regions, UK (London-Research Centre, 2000). This is the so called National Atmospheric Emission Inventory and has been compiled on the basis of a 10 x 10 kilometres grid (Figure 3.1). 9 pollutants are covered in this inventory. They are carbon dioxide ($CO_2$), sulphur dioxide ($SO_2$), nitrogen oxides (NOx), non-methane volatile organic compounds (NMVOC), carbon monoxide (CO), black smoke, benzene, 1,3-butadiene, particulate matters with aerodynamic diameter less than 10 μm ($PM_{10}$). Some heavy metals and halogens are being considered for future inclusion in the inventory. The purposes of the National Atmospheric Emission Inventory stated by the inventory compilers are:

- As an input to discussion with various international bodies.
- As an input to the UK policy-making with respect to pollution abatement and control.
- To assist in judging the effectiveness of existing policies.
- As an aid to the interpretation of air quality measurements.
- As an input to atmospheric dispersion models.
- For general public information.

However, a 10 x 10 kilometres grid is too large for urban air quality management, certainly for medium and small sized cities. It can not show the spatial distribution and

temporal variations of air pollution sources in the detail required for model accuracy. Thus, the National Atmospheric Emission Inventory does not satisfy the needs of input into atmospheric dispersion models to simulate transport of airborne pollutants in Dundee. For this thesis, the data on airborne pollutant source emissions in Dundee had to be gathered to create local atmospheric emission inventories. NOx and $PM_{10}$ are two of the important airborne pollutants attracting public attention in the UK (AEA Technology, 1995). They are the two major airborne pollutants studied in this project. The data gathering for airborne pollutant emission sources focuses on these two pollutants from industrial or commercial processes and traffic emission. The inventories were compiled according to source types (point, line or area emission).

Figure 3.1 The 10 x 10 kilometre grid used in the National Atmospheric Emissions Inventory, the UK

### 3.1 Industrial and commercial process emission sources

The Environmental Protection Act 1990 introduced in the UK a single system of control over "prescribed processes", in industry and commerce, which are likely to result in the release of pollutants to the environment. A common system of authorisation,

enforcement and public access to information applies to the Environment Agencies and local authorities. The Environment Agencies are responsible for the control of about 2,200 processes that are most likely to cause serious pollution, which are referred to as "Part A processes", and local authorities control more than 12,000 less threatening processes, referred as "Part B processes". The Environmental Protection (Prescribed Processes and Substances) Regulations 1991, lists both the processes and substances coming under the Environment Agency control and those under local authority control.

There was no Part A process that was registered in Scottish Environment Protection Agency East Region, Dundee Area. 56 Part B processes, industrial or commercial processes, were registered in the Scottish Environment Protection Agency East Region, Dundee Area. Airborne pollutant emission data are available for four processes. The names of the companies holding these four processes are Michelin Tyre plc Dundee, Halley Stevensons Ltd., Nynas UK Oil Refinery and Dundee Energy Recycling Limited. The locations of Michelin Tyre plc Dundee and Dundee Energy Recycling Limited are shown in Figure 3.2.

Michelin Tyre plc Dundee is located on Baldovie industrial estate (Figure 3.2). According to its emission report in 1997. $SO_2$ and $NO_2$ are the two major airborne pollutants emitted from the company's premises in Dundee. The monthly emissions of $NO_2$ are shown in Table 3.1. The zero emission in October and November may mean that factory stops production for maintenance.

Table 3.1 Monthly emission of $NO_2$ from Michelin Tyre Plc Dundee (Tonnes)

| JAN | FEB | MAR | APR | MAY | JUN |
|---|---|---|---|---|---|
| 2.03 | 2.36 | 2.20 | 4.72 | 2.20 | 2.20 |
| JUL | AUG | SET | OCT | NOV | DEC |
| 1.74 | 0.27 | 0.42 | 0.00 | 0.00 | n/a |

Baltic Works, Halley Stevensons Ltd. is located in Annfield Road. Ammonia is a major airborne pollutant emitted from the works.

There are three important airborne pollutant emission sources (vacuum heater, boiler and Beverly heater) at Nynas UK Oil Refinery. CO, $SO_2$, $NO_2$ and particulate matter are the four major pollutants emitted from these sources. However, the emission data for $NO_2$ and particulate matter are unavailable for these sources.

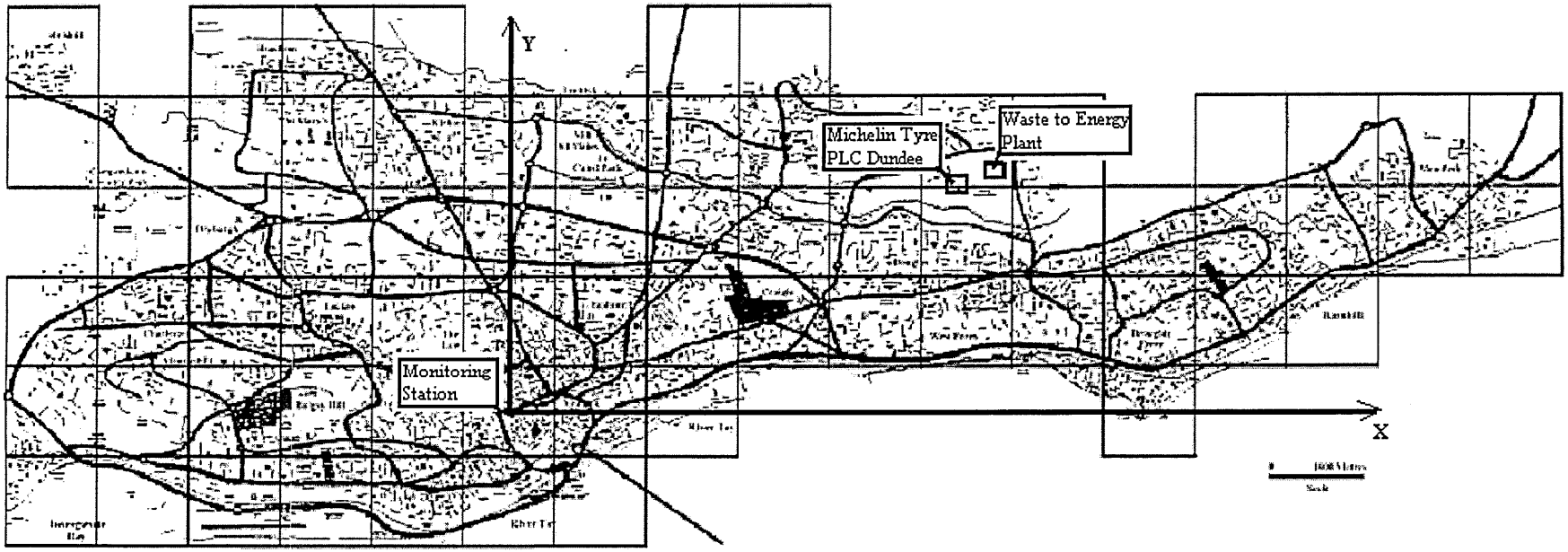


Figure 3.2 Location of point emission sources and the geographical coordinate system and 1 x 1 km grids

Baldovie Waste to Energy Plant (WTE), which is known as Dundee Energy Recycling Limited, is located in the Baldovie Industrial Estate next to Michelin Tyre Plc Dundee (Figure 3.2). There are two 7 tonnes/hour municipal incinerators and a 500 kg/week animal carcass crematorium incinerator at the plant. The main emission point is a 70 m high stack shared by the two municipal incinerators. Emission from this stack is released at a temperature of approximately 300 ± 5°C with an associated efflux velocity of between 15 to 20 m $s^{-1}$. Total particulates, HCl, HF, $SO_2$, NOx and CO are the major airborne pollutants emitted continuously from the stack. The emission rates for total particulates and NOx are shown in Table 3.2.

Table 3.2 The emission rates of total particulates and NOx from WTE

| | Predicted level | | Guaranteed level | |
|---|---|---|---|---|
| | Concentration ($mg\ m^{-3}$) | Release rate ($g\ s^{-1}$) | Concentration ($mg\ m^{-3}$) | Release rate ($g\ s^{-1}$) |
| Total suspended particulates | 5 | 0.109 | 30 | 0.654 |
| NOx | <240 | 5.232 | 350 | 7.6304 |

## 3.2 Vehicle emission sources

Road vehicle emission is the largest airborne pollutant emission source in the UK, particularly in urban areas (Barratt et al., 1997). It is a major air pollution source in Dundee. Vehicle emission is a very complex process. It depends on various factors such as vehicle type, fuel type, mileage, speed, driving mode, ambient temperature etc. Emission factors are usually used to describe the average emission of a type of vehicle in a certain driving mode. The total road vehicle emission can be estimated by using vehicle emission factors, traffic volume, composition of road vehicle fleet and road length if measured data is unavailable.

### 3.2.1 Vehicular emission factors

Road vehicles in the UK are classified into 8 different types in atmospheric emission inventories (London-Research Centre, 2000). These are petrol cars, petrol LGVs (light goods vehicles), diesel cars, diesel LGVs, rigid HGVs (Heavy goods vehicles), articulated HGVs, buses and coaches, and motorcycles. Emission factors for these 8 types

of vehicles, when operating at various speeds, are available in the atmospheric emission inventories (for 1997, 1999, and 2005).

The emission factors of NOx for eight types of vehicle at various speeds in 1999 are shown in Table 3.3. The emission factors of NOx for petrol cars and petrol LGVs increase with vehicle speed. The emission factors of NOx for diesel cars, diesel LGVs, rigid HGVs, articulated HGVs, buses and coaches are different from those of petrol cars and petrol LGVs. Their values are largest at lower speeds. When speed increases, they decrease to low values and then increase again. The vehicular speed in which lowest emission occurs varies with the vehicle type. The emission factor of NOx for motorcycles does not vary with vehicle speed.

Table 3.3 Emission factors for 8 types of vehicle at various speeds in 1999 (NOx, g $km^{-1}$)

| Speed ($km\ h^{-1}$) | Petrol cars | Petrol LGVs | Diesel cars | Diesel LGVs | Rigid HGVs | Articulated HGVs | Buses and coaches | Motorcycles |
|---|---|---|---|---|---|---|---|---|
| 10 | 0.75 | 1.20 | 0.70 | 1.17 | 8.39 | 16.14 | 13.93 | 0.12 |
| 20 | 0.75 | 1.20 | 0.58 | 1.00 | 7.52 | 14.43 | 11.97 | 0.12 |
| 30 | 0.77 | 1.22 | 0.48 | 0.85 | 6.81 | 12.91 | 10.30 | 0.12 |
| 40 | 0.81 | 1.27 | 0.40 | 0.73 | 6.26 | 11.57 | 8.91 | 0.12 |
| 50 | 0.87 | 1.34 | 0.33 | 0.65 | 5.87 | 10.43 | 7.81 | 0.12 |
| 60 | 0.95 | 1.44 | 0.28 | 0.59 | 5.63 | 9.46 | 6.99 | 0.12 |
| 70 | 1.04 | 1.55 | 0.25 | 0.56 | 5.56 | 8.69 | 6.46 | 0.12 |
| 80 | 1.16 | 1.69 | 0.24 | 0.55 | 5.65 | 8.10 | 6.21 | 0.12 |
| 90 | 1.29 | 1.86 | 0.25 | 0.58 | 5.89 | 7.70 | 6.25 | 0.12 |
| 100 | 1.44 | 2.04 | 0.27 | 0.64 | 6.30 | 7.48 | 6.57 | 0.12 |
| 110 | 1.61 | 2.25 | 0.32 | 0.72 | 6.86 | 7.45 | 7.17 | 0.12 |
| 120 | 1.80 | 2.48 | 0.38 | 0.83 | 7.58 | 7.61 | 8.06 | 0.12 |

Table 3.4 Emission factors for 8 types of vehicle at various speeds in 1999 ($PM_{10}$, g $km^{-1}$)

| Speed ($km\ h^{-1}$) | Petrol cars | Petrol LGVs | Diesel cars | Diesel LGVs | Rigid HGVs | Articulated HGVs | Buses and coaches | Motorcycles |
|---|---|---|---|---|---|---|---|---|
| 10 | 0.023 | 0.037 | 0.135 | 0.326 | 0.905 | 1.077 | 0.784 | 0.087 |
| 20 | 0.023 | 0.037 | 0.108 | 0.273 | 0.641 | 0.693 | 0.695 | 0.087 |
| 30 | 0.023 | 0.037 | 0.085 | 0.231 | 0.525 | 0.535 | 0.612 | 0.087 |
| 40 | 0.023 | 0.037 | 0.068 | 0.198 | 0.455 | 0.446 | 0.535 | 0.087 |
| 50 | 0.023 | 0.037 | 0.055 | 0.175 | 0.408 | 0.387 | 0.464 | 0.087 |
| 60 | 0.023 | 0.037 | 0.047 | 0.162 | 0.373 | 0.344 | 0.400 | 0.087 |
| 70 | 0.023 | 0.037 | 0.044 | 0.159 | 0.345 | 0.312 | 0.342 | 0.087 |
| 80 | 0.023 | 0.037 | 0.046 | 0.166 | 0.323 | 0.287 | 0.290 | 0.087 |
| 90 | 0.023 | 0.037 | 0.053 | 0.183 | 0.305 | 0.266 | 0.244 | 0.087 |
| 100 | 0.023 | 0.037 | 0.064 | 0.211 | 0.290 | 0.249 | 0.205 | 0.087 |
| 110 | 0.023 | 0.037 | 0.081 | 0.248 | 0.277 | 0.234 | 0.171 | 0.087 |
| 120 | 0.023 | 0.037 | 0.102 | 0.295 | 0.265 | 0.222 | 0.144 | 0.087 |

The emission factors of $PM_{10}$ for eight types of vehicle at various speeds in 1999 are shown in Tables 3.4. The emission factors of $PM_{10}$ for petrol cars, petrol LGVs and motorcycle are low and do not vary with vehicular speed. Variations of emission factors of $PM_{10}$ for diesel cars and diesel LGVs with vehicular speed are similar to those of NOx. The emission factors of $PM_{10}$ for rigid HGVs, articulated HGVs, and buses and coaches decrease with vehicular speed

### 3.2.2 Traffic flows on major roads in Dundee

The traffic flow counts on the major roads of Dundee urban area have been undertaken by the Department of Planning and Transportation, Dundee City Council, during the past decade. The traffic flow data is available for 176 major roads or road sections. The total length of the 176 roads is 145.0 km. The name, annual average daily traffic flow (AADT), length, width and vehicle speed limit for these 176 roads or road sections are shown in Table 3.5.

The road conditions and traffic flow vary in the city's road network as would be expected. In Dundee, the annual average daily road traffic flow varies from less than 1000 vehicles to higher than 40000 vehicles. The road width varies from 10 m to 40 m. The vehicle speed limit varies from 30 mile $h^{-1}$ to 60 mile $h^{-1}$. In this thesis, the city's roads are divided into three main types. These are arterial, feeder and residential roads. The arterial roads are the city's major traffic corridors or the city bypass. The arterial road condition is good and the traffic flow and vehicle speed are generally high. The feeder roads connect the city's different districts. The traffic flow in a typical feeder road is lower than that in an arterial road and higher than that in a residential road. Residential roads connect residential area to feeder roads or arterial road. The traffic flow is low in residential roads.

If traffic flow is used as a factor to distinguish the road type in Dundee (for example: arterial road, daily traffic volume $\geq$ 20000; feeder road, daily traffic volume 10000 ~ 20000; residential road, daily traffic volume < 10000), 22 roads or road sections can be categorised as arterial roads (Table 3.5). The total length of arterial roads in Dundee is about 23.0 km. Most of these roads, such as the Kingsway, Riverside Avenue and Dock Street are the city's outer ring roads. The roads are wide (20-40 m) and the vehicle speed is high (40 – 50 mile $h^{-1}$). Some of arterial roads, such as Marketgait are the city's inner ring roads. The roads are wide (20 m) but the vehicle speed is low on these roads (30 mile $h^{-1}$).

Table 3.5 Traffic volumes and road conditions on Dundee urban road network

| Road Name | AADT (Vehicle Day$^{-1}$) | Counted Year | Road Length (m) | Road Width (m) | Speed Limit (Mile h$^{-1}$) |
|---|---|---|---|---|---|
| Kingsway | 41230 | 1999 | 792 | 40 | 50 |
| Marketagait S | 40380 | 1994 | 254 | 20 | 30 |
| Kingsway | 37682 | 1999 | 882 | 40 | 50 |
| Kingsway | 37682 | 1999 | 1546 | 40 | 50 |
| Kingsway West | 35791 | 1999 | 1157 | 40 | 50 |
| Kingsway West | 30239 | 1999 | 1307 | 40 | 50 |
| Dock St | 29741 | 1998 | 1191 | 40 | 40 |
| Kingsway West | 29122 | 1996 | 717 | 40 | 50 |
| Kingsway West | 29122 | 1999 | 777 | 40 | 50 |
| Kingsway West | 26868 | 1999 | 908 | 40 | 50 |
| Kingsway East | 25981 | 1999 | 838 | 40 | 40 |
| Marketagait N of Nethergate | 25339 | 1994 | 332 | 20 | 30 |
| Kingsway East | 25112 | 1999 | 1134 | 40 | 40 |
| Marketagait S of Nethergate | 23441 | 1994 | 375 | 20 | 30 |
| Marketagait S of S of West Part Rbt | 22974 | 1994 | 398 | 20 | 30 |
| Lochee Rd | 22548 | 1993 | 950 | 20 | 30 |
| Riverside Ave | 22272 | 1999 | 1383 | 40 | 50 |
| Riverside Ave | 22272 | 1999 | 447 | 40 | 50 |
| Arbroath Rd | 21812 | 1996 | 2393 | 20 | 40 |
| Marketgait N of West Part Rbt | 20145 | 1994 | 204 | 20 | 30 |
| Dundee Rd | 20145 | 1994 | 2235 | 40 | 40 |
| Forfar Rd | 20062 | 1993 | 2766 | 40 | 50 |
| Marketgait S of Nethergate | 19217 | 1994 | 159 | 20 | 30 |
| Marketgait N | 18546 | 1993 | 440 | 20 | 30 |
| Hawkhill | 18455 | 1994 | 394 | 20 | 30 |
| Hawkhill | 18455 | 1994 | 313 | 20 | 30 |
| Marketgait N of Ward Road | 18446 | 1994 | 311 | 20 | 30 |
| Marketgait E of Ladywell Rbt | 17909 | 1994 | 426 | 20 | 30 |
| Arbroath Rd | 17326 | 1997 | 3281 | 20 | 40 |
| Arbroath Rd | 17326 | 1997 | 822 | 20 | 40 |
| Marketgait S of King St | 17064 | 1994 | 169 | 20 | 30 |
| Macalpine Rd | 16906 | 1995 | 741 | 20 | 30 |
| Coupar Angus Rd. | 16484 | 1993 | 188 | 10 | 30 |
| Riverside Ave | 16324 | 1994 | 1144 | 50 | 40 |

Table 3.5 (continue)

| Road Name | AADT (Vehicle Day$^{-1}$) | Counted Year | Road Length (m) | Road Width (m) | Speed Limit (Mile h$^{-1}$) |
|---|---|---|---|---|---|
| Logie St | 16208 | 1993 | 754 | 20 | 30 |
| Riverside Ave | 16072 | 1998 | 1794 | 50 | 40 |
| Riverside Ave | 16072 | 1998 | 1236 | 50 | 40 |
| Riverside Ave | 16072 | 1998 | 594 | 50 | 40 |
| Riverside Ave | 16072 | 1998 | 453 | 50 | 40 |
| Coupar Angus Rd. | 15760 | 1993 | 678 | 10 | 30 |
| Arbroath Rd | 15484 | 1997 | 2425 | 20 | 50 |
| Logie St | 15479 | 1998 | 406 | 20 | 30 |
| Coupar Angus Rd. | 15425 | 1994 | 4165 | 10 | 60 |
| Dens Rd | 15247 | 1997 | 266 | 10 | 30 |
| Lochee Rd | 14714 | 1997 | 688 | 20 | 30 |
| Queen St W. of Forthill Rd | 13994 | 1993 | 466 | 10 | 30 |
| Clepington Rd | 13981 | 1993 | 826 | 10 | 30 |
| Clepington Rd | 13981 | 1993 | 884 | 10 | 30 |
| Clepington Rd | 13981 | 1993 | 2016 | 10 | 30 |
| A930 Queen St E. of Forthill Rd | 13742 | 1993 | 758 | 10 | 30 |
| Ferry Rd | 13442 | 1955 | 1618 | 40 | 40 |
| Monifieth Rd | 13352 | 1997 | 1187 | 10 | 30 |
| Dalhousie Rd | 13352 | 1997 | 1172 | 10 | 30 |
| Ferry Rd | 13352 | 1997 | 313 | 10 | 30 |
| Maule St | 13352 | 1997 | 865 | 10 | 30 |
| High St | 13352 | 1997 | 1699 | 10 | 30 |
| Arbroath Rd | 13271 | 1994 | 1627 | 10 | 30 |
| King's Cross Rd | 13021 | 1993 | 250 | 20 | 30 |
| Green Dykes Rd | 12713 | 1993 | 767 | 20 | 40 |
| Harefield Rd | 12626 | 1993 | 924 | 20 | 30 |
| Blackscroft | 11828 | 1995 | 510 | 10 | 30 |
| Dens Rd | 11439 | 1996 | 932 | 10 | 30 |
| King's Cross Rd | 11154 | 1993 | 626 | 20 | 30 |
| Albert St | 11079 | 1999 | 690 | 10 | 30 |
| Victoria Rd | 10830 | 1993 | 560 | 10 | 30 |
| Charleston Dr | 10474 | 1995 | 887 | 20 | 30 |
| Pitkerro Rd | 10090 | 1994 | 1915 | 20 | 30 |
| Happyhillock Rd | 9989 | 1995 | 278 | 20 | 40 |

Table 3.5 (continue)

| Road Name | AADT (Vehicle Day$^{-1}$) | Counted Year | Road Length (m) | Road Width (m) | Speed Limit (Mile h$^{-1}$) |
|---|---|---|---|---|---|
| Happyhillock Rd | 9989 | 1996 | 659 | 20 | 40 |
| Drumgeith Rd | 9911 | 1995 | 599 | 20 | 40 |
| Drumgeith Rd | 9911 | 1995 | 568 | 20 | 40 |
| Drumgeith Rd | 9911 | 1995 | 470 | 20 | 40 |
| Ninwells Ave | 9770 | 1994 | 398 | 20 | 40 |
| A929 Forfar Rd S. of Clepington Rd | 9737 | 1993 | 633 | 10 | 30 |
| Macalpine Rd | 9730 | 1999 | 690 | 20 | 30 |
| Craigie Dr | 9616 | 1995 | 925 | 20 | 30 |
| Claverhouse Rd | 9558 | 1995 | 601 | 20 | 40 |
| Claverhouse Rd | 9558 | 1995 | 519 | 20 | 40 |
| Claverhouse Rd | 9558 | 1995 | 514 | 20 | 40 |
| Princes St | 9186 | 1994 | 575 | 10 | 30 |
| City Rd | 9117 | 1993 | 482 | 20 | 30 |
| Pentland Ave | 9117 | 1993 | 470 | 10 | 30 |
| Balgay Rd | 9117 | 1993 | 287 | 10 | 30 |
| Forfar Rd N. of Clepington Rd | 8857 | 1993 | 288 | 20 | 30 |
| Seagate | 8849 | 1994 | 410 | 10 | 30 |
| Alexander St | 8729 | 1993 | 685 | 20 | 30 |
| Balunie Ave | 8644 | 1994 | 997 | 20 | 30 |
| Strathmore Ave | 8644 | 1994 | 1250 | 20 | 40 |
| Balunie Ave | 8644 | 1994 | 727 | 20 | 30 |
| Perth Rd | 8553 | 1998 | 853 | 10 | 30 |
| Caird Ave | 8517 | 1995 | 398 | 20 | 30 |
| Ward Rd | 8372 | 1994 | 515 | 20 | 30 |
| Dura St | 8345 | 1994 | 302 | 10 | 30 |
| Dura St | 8345 | 1994 | 288 | 10 | 30 |
| Budhope Ter | 8326 | 1993 | 895 | 10 | 30 |
| Constitution St | 8326 | 1993 | 326 | 10 | 30 |
| Drumgeith Rd | 8266 | 1995 | 742 | 20 | 40 |
| Strathearn Rd | 8249 | 1994 | 910 | 10 | 30 |
| Strathearn Rd | 8249 | 1994 | 739 | 10 | 30 |
| Charleston Dr | 8245 | 1994 | 1224 | 20 | 30 |
| Perth Rd | 8244 | 1993 | 421 | 10 | 30 |
| Blackness Rd | 8234 | 1993 | 942 | 10 | 30 |

Table 3.5 (continue)

| Road Name | AADT (Vehicle Day$^{-1}$) | Counted Year | Road Length (m) | Road Width (m) | Speed Limit (Mile h$^{-1}$) |
|---|---|---|---|---|---|
| Bellfield St | 8234 | 1993 | 269 | 10 | 30 |
| Perth Rd | 8168 | 1999 | 1938 | 20 | 30 |
| Loons Rd | 7890 | 1993 | 1132 | 10 | 30 |
| Ryron St | 7890 | 1993 | 221 | 10 | 30 |
| Ryron St | 7890 | 1993 | 406 | 10 | 30 |
| Ballindean Rd | 7861 | 1999 | 438 | 10 | 30 |
| Strathmartine Rd | 7771 | 1994 | 587 | 20 | 30 |
| Strathmartine Rd | 7771 | 1994 | 1195 | 20 | 30 |
| Strathmartine Rd | 7771 | 1994 | 1132 | 20 | 40 |
| Strathmartine Rd | 7771 | 1994 | 1504 | 20 | 40 |
| Moncur Cres | 7745 | 1995 | 319 | 10 | 30 |
| Brantwood Ave | 7487 | 1994 | 322 | 20 | 30 |
| Hawkhill | 7471 | 1993 | 578 | 20 | 30 |
| Ballindean Rd | 7193 | 1996 | 469 | 10 | 30 |
| Staffa Place | 7150 | 1996 | 277 | 10 | 30 |
| Fountainbleau Dr | 7139 | 1998 | 1112 | 20 | 40 |
| Perth Rd | 7059 | 1995 | 964 | 20 | 30 |
| Victoria St | 6873 | 1993 | 982 | 10 | 30 |
| Bell St | 6725 | 1994 | 482 | 10 | 30 |
| Blackness Rd | 6648 | 1993 | 1237 | 10 | 30 |
| Claypotts Rd | 6543 | 1994 | 1142 | 10 | 30 |
| Baldove Rd | 6517 | 1994 | 1254 | 20 | 40 |
| Old Glams Rd | 6496 | 1995 | 1131 | 10 | 30 |
| Old Glams Rd | 6496 | 1995 | 502 | 20 | 30 |
| Hilltown | 6309 | 1993 | 748 | 10 | 30 |
| South Rd | 6282 | 1993 | 1408 | 20 | 30 |
| South Rd | 6282 | 1993 | 1360 | 20 | 30 |
| Balunie Dr | 6152 | 1999 | 270 | 20 | 40 |
| Perth Rd | 6046 | 1995 | 830 | 20 | 30 |
| Ninwells Ave | 5848 | 1995 | 475 | 20 | 40 |
| Ninwells Ave | 5848 | 1995 | 349 | 20 | 40 |
| Broughty Ferry Rd | 5750 | 1997 | 1110 | 10 | 30 |
| Nethergate High St | 5634 | 1994 | 541 | 10 | 30 |
| Mallaig Ave | 5625 | 1999 | 399 | 20 | 30 |

Table 3.5 (continue)

| Road Name | AADT (Vehicle Day$^{-1}$) | Counted Year | Road Length (m) | Road Width (m) | Speed Limit (Mile h$^{-1}$) |
|---|---|---|---|---|---|
| Balgowan Ave. | 5589 | 1995 | 1572 | 20 | 40 |
| Spey Dr | 5486 | 1995 | 349 | 20 | 30 |
| Forthill Rd | 5365 | 1994 | 1094 | 10 | 30 |
| Balunie Dr | 5260 | 1999 | 407 | 20 | 40 |
| Balunie Dr | 5254 | 1999 | 454 | 20 | 40 |
| Nursery Rd | 5156 | 1998 | 1144 | 10 | 30 |
| Abertay St | 5116 | 1998 | 494 | 10 | 30 |
| Balunie Dr | 5094 | 1999 | 419 | 20 | 40 |
| Gillburn Rd | 5076 | 1993 | 1188 | 10 | 30 |
| Glamis Rd | 4934 | 1993 | 859 | 20 | 30 |
| Glamis Rd | 4934 | 1993 | 889 | 20 | 30 |
| Balunie Dr | 4813 | 1999 | 633 | 20 | 40 |
| Bagiillo Rd | 4779 | 1994 | 1118 | 20 | 40 |
| Bagiillo Rd | 4779 | 1994 | 1387 | 20 | 40 |
| Bagiillo Rd | 4779 | 1994 | 421 | 20 | 40 |
| Telford Rd | 4565 | 1996 | 252 | 10 | 30 |
| Ancrum Rd | 4540 | 1993 | 725 | 10 | 30 |
| Ballumbie Rd | 4320 | 1995 | 387 | 20 | 40 |
| Main St | 4131 | 1994 | 299 | 10 | 30 |
| Provost Rd | 4131 | 1994 | 422 | 10 | 30 |
| Harestane Rd | 4124 | 1995 | 401 | 20 | 40 |
| Camperdown Rd | 4116 | 1993 | 940 | 10 | 30 |
| West Grange Rd | 4072 | 1995 | 1209 | 10 | 30 |
| Longhaugh Rd | 3928 | 1996 | 1250 | 20 | 40 |
| Berwick Dr | 3928 | 1996 | 444 | 20 | 40 |
| Fairfield Rd | 3881 | 1994 | 688 | 10 | 30 |
| Macalpine Rd | 3772 | 1999 | 310 | 20 | 30 |
| Dickson Ave | 3620 | 1994 | 1112 | 20 | 30 |
| Blackness Ave | 3476 | 1993 | 740 | 10 | 30 |
| King's St | 3258 | 1994 | 895 | 10 | 30 |
| Dunsinane Ave | 3023 | 1993 | 1125 | 20 | 30 |
| Staffa Place | 2989 | 1996 | 1048 | 10 | 30 |
| Harestane Rd | 2704 | 1995 | 904 | 20 | 40 |
| Harestane Rd | 2704 | 1995 | 509 | 20 | 40 |

Table 3.5 (continue)

| Road Name | AADT (Vehicle Day$^{-1}$) | Counted Year | Road Length (m) | Road Width (m) | Speed Limit (Mile h$^{-1}$) |
|---|---|---|---|---|---|
| Harestane Rd | 2704 | 1995 | 368 | 20 | 40 |
| Berwick Dr | 2385 | 1996 | 645 | 20 | 40 |
| Berwick Dr | 2385 | 1996 | 843 | 20 | 40 |
| Dunholm Rd | 1331 | 1995 | 767 | 20 | 30 |
| Old Craigie Rd | 1261 | 1998 | 871 | 10 | 30 |
| Mallaig Ave | 905 | 1999 | 463 | 20 | 30 |

43 roads or road sections can be categorised as feeder roads. Total length of feeder roads in Dundee is about 40.5 km. Some of these roads, such as Lochee Road and Arbroath Road, connect residential areas with the city centre. Some of the feeder roads, such as Clepington Road and Strathmore Avenue, connect different residential areas. The road width varies from 10 m to 40 m. The vehicle speed limit varies between 30 mile h$^{-1}$ and 60 mile h$^{-1}$.

The remaining 111 roads or road sections are residential roads. Total length of residential roads in Dundee is about 81.5 km. The road width is usually less than 40 m. The vehicle speed limit is less than 40 mile h$^{-1}$ on residential roads.

### 3.3.3 Daily variation of traffic flow and composition of vehicle fleet

According to the data surveyed by the Department of Planning and Transport, Dundee City Council, the typical daily variations of traffic flow on weekdays and at weekends on arterial , feeder and residential roads are shown in Figures 3.3 – 3.5.

The daily variations of traffic flow on arterial and feeder roads are similar. There are two traffic peaks on weekdays. One appears at about 08:30 while another appears at about 17:00. The peak times are coincident with commuting times. There is only one traffic peak at weekends, with the peak value being relatively lower than on weekdays but duration of the peak value is much longer at weekends. During daytime, traffic flow on weekdays is usually higher than that at weekends. During the night, traffic flow on weekdays is usually lower than that at weekend. On arterial roads, the daily traffic flow at weekends is about 20% less than the value on weekdays. On feeder roads, the daily traffic

volume at weekends is about 35% less than the value on weekdays. The daily variations of traffic flow are consistent with people's daily work and leisure activities.

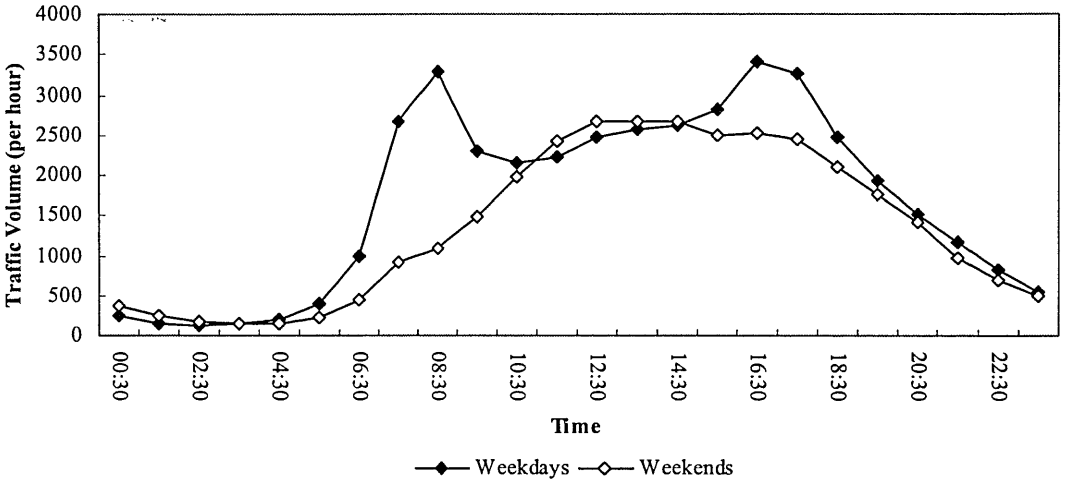


Figure 3.3 Daily variations of traffic volume on weekday and at weekend on an arterial road (Kingsway, 19/04/2000 - 26/09/2000)

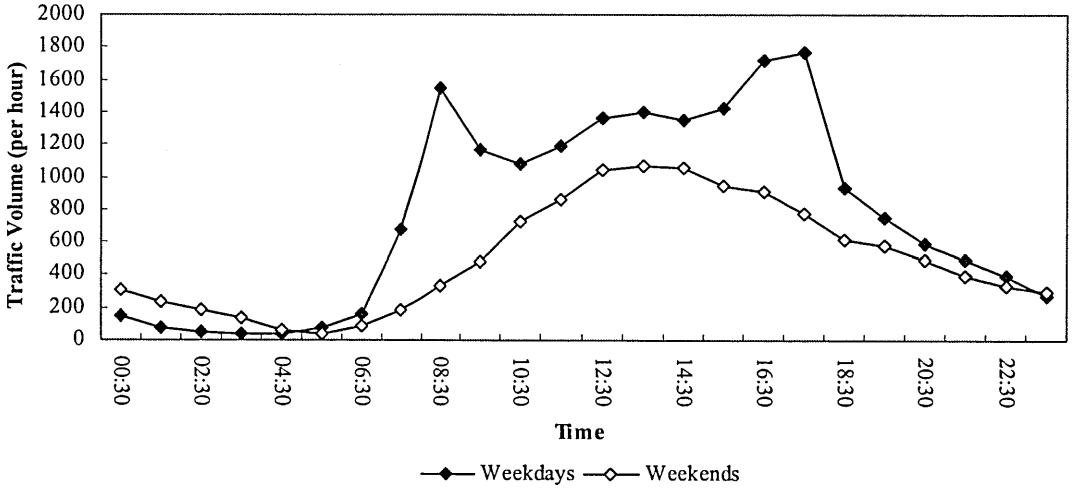


Figure 3.4 Daily variations of traffic volume on weekday and at weekend on a feeder road (Marketgait N, 28/04/1999 - 05/081999)

On residential road, the daily variations of traffic volume are generally similar to those on arterial and feeder roads. However, the variations of traffic flow on residential

roads during daytime hours are more complex. The daily traffic flow on a residential road at weekends is about 27% lower than the value on weekdays.

The vehicles on the road were divided into six types when composition of vehicle fleet was surveyed by the Department of Planning and Transportation, Dundee City Council. These six types of vehicles are cars, LGV's, rigid HGVs, articulated HGVs, Buses and Coaches, and motorcycles. The typical composition of vehicle fleet on arterial, feeder and residential roads on weekdays in Dundee are shown in Table 3.6. The compositions of vehicle fleet on the three different type roads are similar. Most of the road vehicles are cars in Dundee. They represent about 85.8% - 87.0% of the traffic flow. Of the remaining types of vehicles, buses and coaches are important in terms of composition. They form 7.8% - 9.0% of traffic flow. The composition of the other four types of vehicle in traffic flow is of less importance.

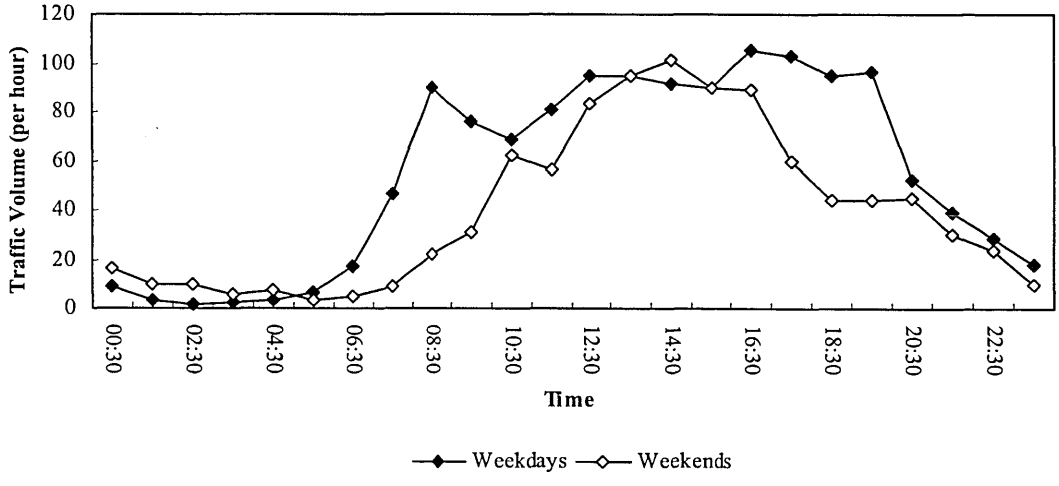


Figure 3.5 Daily variations of traffic volume on weekday and at weekend on a residential road (Old Craigie Road, 02/11/98 to 19/11/98)

Table 3.6 Compositions of vehicle fleet on different roads on weekdays

| | Cars | LGVs | Rigid HGVs | Articulated HGVs | Buses and Coaches | Motorcycles |
|---|---|---|---|---|---|---|
| Arterial road* | 87.0% | 2.8% | 1.0% | 0.8% | 8.1% | 0.2% |
| Feeder road** | 86.7% | 2.5% | 0.1% | 2.8% | 7.8% | 0.1% |
| Residential Road*** | 85.8% | 3.1% | 0.2% | 1.5% | 9.0% | 0.3% |

* Markegait S, 12/04/2000 (Wednesday)

** Perth Rd, 26/06/2000 (Monday)

*** Harefield Rd, 23/03/2000 (Thursday)

## 3.3 Atmospheric emission inventories in Dundee

The atmospheric emission inventory is a schedule of the sources of air pollutants within a particular geographical area. For satisfying the requirements of input to an atmospheric dispersion model, a good atmospheric emission inventory should include source location, pollutant's name, emission rate, emission type (point emission, line emission or area emission) and emission status (release height, smoke emission speed, smoke amount, and smoke temperature etc.). The temporal variation factors (daily, weekly or monthly) should also be included for the air pollutant emission sources that vary with time, in order to describe their temporal characteristics adequately.

A geographical coordinate system and the grids that cover the research area must be set up before creating the inventory. Selecting the University of Abertay Dundee as the origin, east and north directions were fixed as positive $x$ and $y$ axes directions, respectively. The up-direction was fixed as positive $z$ axis direction. A geographical coordinate system was set up to create the atmospheric emission inventories in Dundee. This geographical coordinate system will also be used in simulating the transport of airborne pollutants in Dundee using atmospheric dispersion model (Chapter 7). The geographical coordinate system and 1 x 1 km grids that cover the Dundee urban area are also shown in Figure 3.2.

For the atmospheric emission inventories, the datasets on air pollution sources were gathered and classified into three different types of emission sources: point, line and area emission sources.

### 3.3.1 Point emission sources

Source name, geographic coordinates, average emission rate, stack or release height, internal diameter of the chimney, smoke emission velocity, smoke temperature and temporal variation factors are the major parameters used to describe a point emission source. The data of point sources that emit NOx and particulate matter in Dundee are only available for two sources registered in Scottish Environment Protection Agency East Region, Dundee Area. The characteristics of these two point sources are:

Point emission source 1:

| | |
|---|---|
| Source name: | Michelin Tyre PLC Dundee |
| Geographic coordinates (m): | 5000 (x), 2500 (y) |
| Average emission rate (mg $s^{-1}$): | 848.8 for $NO_2$ (average emission rate in June) |

Stack or release height (m): n/a

Internal diameter of the chimney (m):n/a

Smoke emission velocity (m $s^{-1}$): n/a

Smoke temperature (°C): n/a

Temporal variation factors (monthly):

| JAN | FEB | MAR | APR | MAY | JUN |
|---|---|---|---|---|---|
| 0.89 | 1.15 | 0.97 | 2.15 | 0.97 | 1.00 |
| JUL | AUG | SET | OCT | NOV | DEC |
| 0.77 | 0.12 | 0.19 | 0 | 0 | n/a |

Point emission source 2:

Source name: Waste to Energy Plant, Dundee Energy Recycling Limited

Geographic coordinates (m): 5300 (x), 2800 (y)

Average emission rate (mg $s^{-1}$): 654.9 for PM, 7630.4 for NOx

(Guaranteed level in Table 3.2 is used)

Stack or release height (m): 70

Internal diameter of the chimney (m):n/a

Smoke emission velocity (m $s^{-1}$): 15 - 20

Smoke temperature (°C): 300 ± 5

Temporal variation factors: No

### 3.3.2 Line emission sources

In the UK Government guidance on air quality review and assessment (Department of the Environment, Transport and the Regions, 1998c), local authorities are required to study the air quality impacts of roads in their area where annual average daily traffic flow (AADT) exceeds 25,000 vehicle per day. Owen et al. (1999, 2000) used this threshold to regard the road as discrete line emission sources (AADT ≥ 25,000) or aggregated the road into area emission sources (AADT < 25,000) when they used ADMS-Urban model (McHugh et al., 1997) to simulate transport of airborne pollutants over London. In this work, this threshold was adopted as the factor for characterising roads as discrete line sources or aggregated area sources. Using this factor, 13 arterial roads or road sections in Dundee are regarded as discrete line emission sources. The remaining 163 roads or road sections will be aggregated as area emission sources.

Line source name, geographic coordinates of the line source, start point and end point of the line, average emission rate, release height, the traversed scale of the line source and temporal variation factors are the major parameters used to describe the line emission sources. The average emission rate for a road or road section regarded as line emission source ($Q_{i,j}$, mg $m^{-1}$ $s^{-1}$) is calculated using:

$$Q_{i,j} = AADT_j \times EF_{i,j} / (24 \times 3600) \quad (3.1)$$

where $i$ is the pollutant type (NOx or $PM_{10}$). $j$ is the road's name. $EF_{i,j}$ (g $km^{-1}$) is the average emission factor, which is calculated using

$$EF_{i,j} = \sum_k ef_{i,k} p_{j,k} \quad (3.2)$$

where $k$ is the type of vehicle. Vehicles are divided into 6 types (cars, LGVs, rigid HGVs, articulated HGVs, buses and coaches, motorcycle) for the composition of the road vehicle fleet in Dundee. $ef_{i,k}$ (g $km^{-1}$) is the emission factor for $k$ type vehicle at the road limit speed. Suitable value for $ef_{i,k}$ may be selected from Tables 3.3 and 3.4. $p_{j,k}$ is the percentage of $k$ type vehicle in $j$ road. The percentages of the six types of vehicle on arterial road (Table 3.6) are used.

13 line emission sources in Dundee are described in Table 3.7. All line emissions are regarded as ground surface emission sources (i.e. emission height is zero).

Daily variation factors of line emission sources on weekdays and at weekends can be calculated by the daily variations of traffic volume on arterial road (see Figure 3.2). They are shown in Table 3.8. On weekdays, the daily variation factors of line emission sources are 1.96 and 2.03 for the two traffic peaks respectively. The lowest value for the factor is 0.08, which appears during early morning. At weekends, the daily traffic flow is taken to be 20% less than the value on weekdays. The daily variation factor for the line source varies between 0.09 to 1.58.

Table 3.7 Line emission sources in Dundee

| Road name | Average emission rate (mg $m^{-1}$ $s^{-1}$) | | Start point (m) | | End point (m) | | Traversed Scale (m) |
|---|---|---|---|---|---|---|---|
| | NOx | $PM_{10}$ | X | Y | X | Y | |
| Kingsway | 0.80221 | 0.02397 | -1484 | 2219 | -719 | 2422 | 40 |
| Marketagait S | 0.73348 | 0.03084 | 594 | -641 | 781 | -469 | 20 |
| Kingsway | 0.73317 | 0.02191 | -719 | 2422 | 156 | 2313 | 40 |
| Kingsway | 0.73317 | 0.02191 | 156 | 2313 | 1656 | 1938 | 40 |

Table 3.7 (contiue)

| Road name | Average emission rate (mg $m^{-1}$ $s^{-1}$) | | Start point (m) | | End point (m) | | Traversed Scale (m) |
|---|---|---|---|---|---|---|---|
| | NOx | $PM_{10}$ | X | Y | X | Y | |
| Kingsway West | 0.69638 | 0.02081 | -2641 | 2172 | -1484 | 2219 | 40 |
| Kingsway West | 0.58836 | 0.01758 | -5172 | 1031 | -4016 | 1641 | 40 |
| Dock St | 0.54159 | 0.01975 | 953 | -109 | 2078 | 281 | 40 |
| Kingsway West | 0.56662 | 0.01693 | -4016 | 1641 | -3313 | 1781 | 40 |
| Kingsway West | 0.56662 | 0.01693 | -3313 | 1781 | -2641 | 2172 | 40 |
| Kingsway West | 0.52277 | 0.01562 | -5578 | 219 | -5172 | 1031 | 40 |
| Kingsway East | 0.47312 | 0.01725 | 2766 | 1703 | 3438 | 1203 | 40 |
| Marketagait N of Nethergate | 0.46027 | 0.01935 | -31 | -406 | 219 | -625 | 20 |
| Kingsway East | 0.45729 | 0.01668 | 1656 | 1938 | 2766 | 1703 | 40 |

Table 3.8 Daily variation factor of line emission sources on weekdays and at weekend

| Time | 0:30 | 1:30 | 2:30 | 3:30 | 4:30 | 5:30 |
|---|---|---|---|---|---|---|
| Weekdays | 0.14 | 0.09 | 0.08 | 0.08 | 0.11 | 0.24 |
| Weekends | 0.22 | 0.14 | 0.10 | 0.09 | 0.09 | 0.13 |
| Time | 6:30 | 7:30 | 8:30 | 9:30 | 10:30 | 11:30 |
| Weekdays | 0.59 | 1.58 | 1.96 | 1.36 | 1.28 | 1.32 |
| Weekends | 0.27 | 0.55 | 0.65 | 0.87 | 1.17 | 1.43 |
| Time | 12:30 | 13:30 | 14:30 | 15:30 | 16:30 | 17:30 |
| Weekdays | 1.46 | 1.53 | 1.56 | 1.67 | 2.03 | 1.94 |
| Weekends | 1.58 | 1.58 | 1.57 | 1.48 | 1.48 | 1.44 |
| Time | 18:30 | 19:30 | 20:30 | 21:30 | 22:30 | 23:30 |
| Weekdays | 1.47 | 1.14 | 0.89 | 0.69 | 0.48 | 0.32 |
| Weekends | 1.24 | 1.03 | 0.83 | 0.57 | 0.41 | 0.30 |

### 3.3.3 Area emission sources

The roads or road sections with annual average daily traffic flow less than 25,000 are aggregated as area emission sources in Dundee. Geographic coordinates for the central point of the area emission source, lateral scale of area emission source, emission rate, average release height, and temporal variation factors are the major parameters to describe the area source. The area emission is divided into 1 x 1 km grids in Dundee (Figure 3.5).

The average vehicular emission rate for a grid ($Q_i$ , mg $s^{-1}$) can be calculated by summing the emissions from all roads or road sections that are located on the grid:

$$Q_i = \sum_j Q_{i,j} L_j \tag{3.3}$$

where $i$ is the pollutant type (NOx or $PM_{10}$). $j$ is the name of the road that is located in the grid. $L_j$ (m) is the length of the road. $Q_{i,j}$ is calculated using equations (3.1) and (3.2). The coordinates of the central point of an area source, average emission rates for NOx and $PM_{10}$ for 58 area sources are shown in Table 3.9. The lateral scale of the area emission is 1,000 m. All area emissions are regarded as ground sources (i.e. average release height is zero).

Because area emission sources in Dundee are the sum of road emissions, the daily variation factors of area emission sources on weekdays and at weekends are calculated using daily variations of traffic flow on feeder road (see Figure 3.3). These factors are shown in Table 3.10. On weekdays, the daily variation factors of area emission sources are 1.99 and 2.28 for the two traffic peaks respectively. The lowest value of the factor is 0.04, which appears during early morning. At weekends, the daily traffic flow on the roads that are aggregated as area sources is taken to be 35% less than the value on weekdays. The daily variation factor of area sources varies between 0.05 to 1.38.

Table 3.9 Area emission sources in Dundee

| Coordinates of area source central point (m) | | Average Emission rate (mg $s^{-1}$) | | Coordinates of area source central point (m) | | Average Emission rate (mg $s^{-1}$) | |
|---|---|---|---|---|---|---|---|
| X | Y | NOx | $PM_{10}$ | X | Y | NOx | $PM_{10}$ |
| -6000 | 0 | 362.5 | 12.8 | 1000 | 0 | 990.2 | 41.0 |
| -5000 | 0 | 656.3 | 23.9 | 1000 | 1000 | 672.3 | 27.5 |
| -5000 | 1000 | 278.2 | 11.7 | 1000 | 3000 | 188.5 | 6.9 |
| -4000 | 0 | 223.1 | 8.9 | 2000 | 0 | 422.2 | 15.0 |
| -4000 | 1000 | 436.6 | 18.3 | 2000 | 1000 | 423.7 | 17.1 |
| -3000 | -1000 | 690.4 | 26.4 | 2000 | 2000 | 1128.8 | 34.3 |
| -3000 | 0 | 317.1 | 12.9 | 2000 | 3000 | 151.5 | 5.5 |
| -3000 | 1000 | 182.3 | 7.4 | 3000 | 1000 | 1161.0 | 42.3 |
| -3000 | 2000 | 1438.5 | 43.8 | 3000 | 2000 | 272.5 | 10.0 |
| -3000 | 3000 | 60.3 | 2.5 | 3000 | 3000 | 29.4 | 1.1 |
| -2000 | -1000 | 185.2 | 6.6 | 3000 | 4000 | 33.3 | 1.2 |
| -2000 | 0 | 249.4 | 10.5 | 4000 | 1000 | 991.3 | 37.1 |
| -2000 | 1000 | 1729.4 | 71.1 | 4000 | 2000 | 523.8 | 20.7 |

Table 3.9 (continue)

| Coordinates of area source central point (m) | | Average Emission rate (mg $s^{-1}$) | | Coordinates of area source central point (m) | | Average Emission rate (mg $s^{-1}$) | |
|---|---|---|---|---|---|---|---|
| X | Y | NOx | $PM_{10}$ | X | Y | NOx | $PM_{10}$ |
| -2000 | 2000 | 309.8 | 12.5 | 4000 | 3000 | 275.5 | 10.1 |
| -2000 | 3000 | 264.2 | 11.1 | 5000 | 1000 | 313.4 | 13.1 |
| -2000 | 4000 | 69.2 | 2.6 | 5000 | 2000 | 224.8 | 8.9 |
| -1000 | -1000 | 1174.1 | 40.9 | 5000 | 3000 | 149.0 | 5.4 |
| -1000 | 0 | 467.3 | 19.3 | 6000 | 1000 | 260.5 | 10.6 |
| -1000 | 1000 | 286.3 | 10.9 | 6000 | 2000 | 1247.1 | 45.1 |
| -1000 | 2000 | 636.9 | 25.1 | 6000 | 3000 | 155.9 | 5.7 |
| -1000 | 3000 | 506.9 | 19.1 | 7000 | 0 | 311.0 | 12.6 |
| -1000 | 4000 | 26.3 | 1.0 | 7000 | 1000 | 241.7 | 9.9 |
| 0 | -1000 | 218.6 | 9.2 | 7000 | 2000 | 239.6 | 9.4 |
| 0 | 0 | 1003.9 | 41.0 | 8000 | 1000 | 355.7 | 14.4 |
| 0 | 1000 | 823.0 | 34.2 | 8000 | 2000 | 38.4 | 1.4 |
| 0 | 2000 | 694.5 | 28.3 | 9000 | 2000 | 308.5 | 12.5 |
| 0 | 3000 | 172.5 | 6.6 | 9000 | 3000 | 276.5 | 9.8 |
| 0 | 4000 | 50.5 | 1.8 | 10000 | 2000 | 539.8 | 21.9 |
| 1000 | -1000 | 193.9 | 5.8 | 10000 | 3000 | 767.0 | 22.6 |

Table 3.10 Daily variation factors for area emission sources

| Time | 0:30 | 1:30 | 2:30 | 3:30 | 4:30 | 5:30 |
|---|---|---|---|---|---|---|
| Weekdays | 0.19 | 0.09 | 0.06 | 0.04 | 0.04 | 0.09 |
| Weekends | 0.39 | 0.30 | 0.24 | 0.18 | 0.08 | 0.05 |
| Time | 6:30 | 7:30 | 8:30 | 9:30 | 10:30 | 11:30 |
| Weekdays | 0.20 | 0.87 | 1.99 | 1.50 | 1.40 | 1.54 |
| Weekends | 0.11 | 0.24 | 0.43 | 0.62 | 0.94 | 1.11 |
| Time | 12:30 | 13:30 | 14:30 | 15:30 | 16:30 | 17:30 |
| Weekdays | 1.75 | 1.80 | 1.74 | 1.83 | 2.22 | 2.28 |
| Weekends | 1.34 | 1.38 | 1.36 | 1.21 | 1.17 | 0.98 |
| Time | 18:30 | 19:30 | 20:30 | 21:30 | 22:30 | 23:30 |
| Weekdays | 1.19 | 0.96 | 0.76 | 0.63 | 0.51 | 0.34 |
| Weekends | 0.79 | 0.74 | 0.64 | 0.51 | 0.43 | 0.37 |

### 3.3.4 Discussion on atmospheric emission inventories in Dundee

Based on available and investigated data, atmospheric emission inventories in Dundee have been compiled according to point, line and area emissions. The source characteristics have been described in detail, to satisfy the requirements of input to the atmospheric dispersion model. There are two major point emission sources for NOx covered by the inventories. The total annual emission of NOx from these two point sources is 258.77 tonnes. Most of it come from Baldovie Waste to Energy Plant (240.63 tonnes). There is only one major point emission source for particulate matter. The total annual emission of particulate matter is 20.62 tonnes. The total annual emissions for Baldovie Waste to Energy Plant may have been overestimated because they have been calculated on the assumption that the plant operates 365 days per annum. There are 13 line emission sources covered by the inventories. The total annual emissions from line emission sources are 227.41 tonnes for NOx and 7.25 tonnes for $PM_{10}$ respectively. There are 58 area emission sources covered by the inventories. The total annual emissions from area emission sources are 850.83 tonnes for NOx and 32.17 tonnes for $PM_{10}$, respectively.

The total annual emissions covered by the atmospheric emission inventories compiled in this research project are 1337.01 tonnes for NOx and 60.04 tonnes for airborne particulate matter. They, in general, underestimate both NOx and $PM_{10}$ emissions in Dundee for the reasons discussed below. Most of the NOx emissions come from anthropogenic sources, being produced from various combustion processes. There are many small industrial and commercial combustion processes for which emission data are unavailable in Dundee. These processes are not covered in the inventories. Another important NOx emission source is the domestic gas consumed for cooking and heating. The NOx emission from domestic gas should be large, particularly in winter. This has not been compiled in the inventories, because the data for domestic gas consumption is unavailable. The NOx emissions from traffic on many minor roads have not been compiled in the inventories as well, because the traffic flow data are unavailable.

The sources of $PM_{10}$ are very complex. They come from various anthropogenic activities as well as natural and fugitive emissions. With the exception of combustion processes, road dust and construction dust are the two important $PM_{10}$ emission sources in an urban area. Crustal dust and biological emission are two important natural emission sources. Some important components such as sulphate and nitrate are secondary pollutants. They come mainly from transboundary transportation. Dundee is a city located on the

coastline. The marine source aerosol is another important $PM_{10}$ source. The $PM_{10}$ emissions from these sources are not compiled in the inventories, because the data is unavailable. The annual average concentrations of NOx and $PM_{10}$ measured in Dundee are in the same order. However, the total annual emission of $PM_{10}$ compiled in the inventories is about 4.5% of the value for NOx. It implies that most of $PM_{10}$ emission sources are not compiled in the atmospheric emission inventories.

# Chapter 4 Field monitoring and laboratory work

Air quality monitoring data provides the basic data for air quality management. Combined with an atmospheric emission inventory and meteorological conditions, a systematic set of air quality data provides a comprehensive database for model development and testing. The available air quality data, especially the data that can show urban background air quality, is not very comprehensive in Dundee. In order to gather a systematic air quality dataset, an automatic air pollution monitoring station was set up on the roof of the University of Abertay Dundee library to monitor urban background air quality and atmospheric dispersion conditions.

$PM_{10}$ and TSP were sampled, on weekdays and at weekends, at the automatic air pollution monitoring station. The concentrations of NO, $NO_2$ and NOx as well as wind speed, wind direction, ambient temperature and the amount of rainfall were measured continuously. The station was operated from December 1999 to December 2000. One year of systematic data for air quality and meteorological conditions were gathered at the monitoring station. $PM_{10}$ was sampled using a Partisol Model 2000 Air Sampler (Rupprecht & Patashnich Co., Inc., 1996). TSP was sampled using a High Volume Air Sampler (Bird & Tole Ltd.). The concentrations of NO, $NO_2$ and NOx were analysed using APNA-360Ambient NOx Monitor (HORIBA, Ltd., 1996). Wind speed, wind direction, ambient temperature and amount of rainfall were measured using ELE MM900 environmental monitoring station (ELE International, 1993).

Small airborne particulate pollution is causing concern in the UK (AEA Technology, 1995). It is believed that these particulates can adversely affect health. Some important information about the sources of airborne pollutants could be derived from the chemical composition of the airborne particulates. $PM_{10}$ and TSP samples were analysed in the laboratory after they were sampled. BDH AA-200DS balance (BDH Balance Service Unit) was used to weigh the masses of $PM_{10}$ and TSP. Wet chemical analyses were used to determine the chemical components of $PM_{10}$ and TSP. The metal elements ($Ca^{2+}$, $Mg^{2+}$, Zn, Cu, Ni and Pb) were analysed using an Atomic Absorption Spectrophotometer (AAS). The ions ($SO_4^{2-}$, $NO_3^-$, $Cl^-$, $NH_4^+$, $Na^+$ and $K^+$) were analysed using High Performance Liquid Chromatography (HPLC).

## 4.1 Site of the automatic monitoring station

The automatic air pollution monitoring station was set up on the roof of the University of Abertay Dundee library. The library is a four-floor building located on the north side of Bell Street, in the city centre of Dundee, UK (Figure 4.1). There are no high buildings around the library to cause air current interference from any direction. In the immediate vicinity of the library, there are no important air pollution sources except traffic emissions. The daily traffic flow on Bell street is small with a value of 6751. North Marketgait and West Marketgait, two links of Dundee's ring road, are about 100 m north and 180 m west of the library respectively. The daily traffic flows are relatively large on these two roads with the values of 25339 and 18546 respectively. The automatic air pollution monitoring station is about 18 m above the ground. Because the study station is located in the city centre and not affected by any specific source emissions or air flow that is blocked from some directions, the data measured at the station can reasonably represent the ambient air quality in the city centre of Dundee.

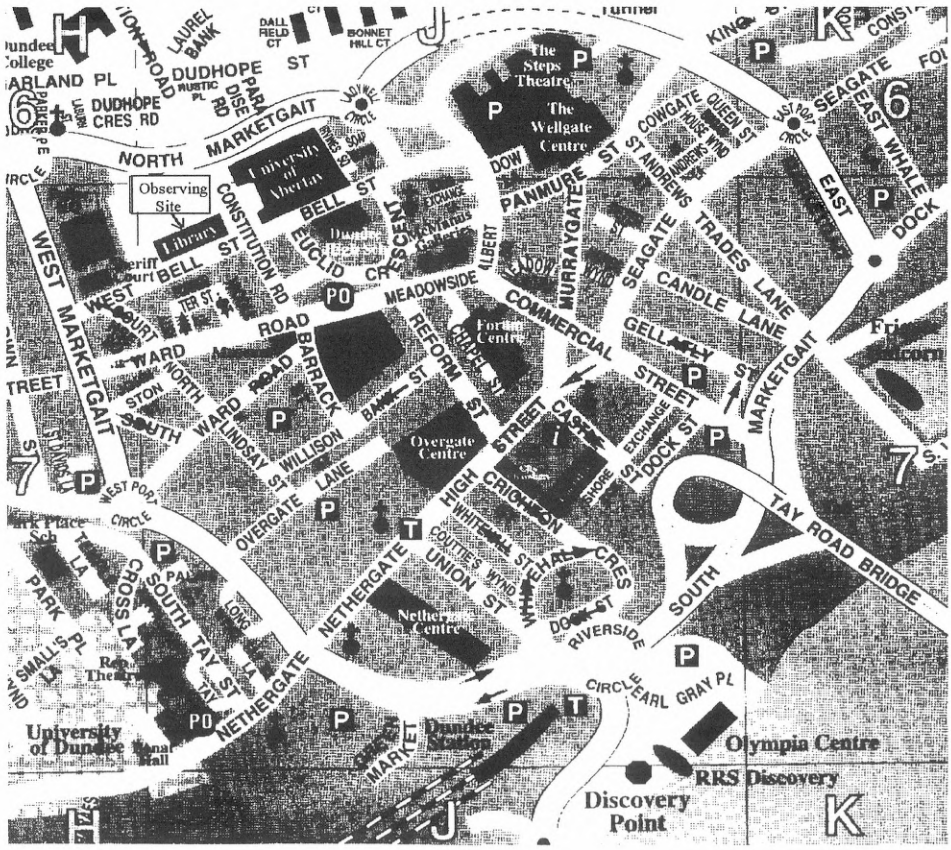


Figure 4.1 Location of automatic air quality monitoring station

## 4.2 Monitoring instrumentation and operation

### 4.2.1 Partisol Model 2000 Air Sampler

The Partisol Model 2000 Air Sampler (Rupprecht & Patashnich Co., Inc., 1996) is a microprocessor-controlled manual airborne particulate sampler. It may be used to sample different sizes of particulates by selecting a different inlet. The $PM_{10}$ inlet was used to sample $PM_{10}$ at the monitoring station (Figure 4.2). The instrumentation has an internal diagnostic program to determine whether other status conditions are present. It can store operating data half hourly for each filter exposed to a sample flow, including the average pressure and temperature during the filter exposure, the mass volume through the filter, the presence of any error conditions and the total exposure time.

The $PM_{10}$ inlet operates at a flow rate of 16.7 l $min^{-1}$ (1 $m^3$ $h^{-1}$). The Partisol Model 2000 Air Sampler maintains a constant volumetric flow rate during the sampling period. The flow volume reported by the instrumentation is in accordance with the US EPA standard, with a standard temperature of 25 °C and a standard pressure of 1 atmosphere. The ambient temperature and pressure are measured by two sensors fixed to the sampler. The ambient temperature sensor has an accuracy of ±1% over a range of –25 to 60°C. The ambient pressure sensor is rated from 0.68 to 1.09 atmospheres and is specified to have a maximum error of 1.5% in a temperature range of 0 to 85°C .

Whatman 2 μm PTFE 46.2 mm filters (Whatman Inc.) and Gelman Laboratory 2 μm Teflo 47 mm filters (PALL Gelman Sciences) were used to collect $PM_{10}$ samples. Two $PM_{10}$ samples a week, one for weekdays (Monday to Friday) and another one for weekends (Saturday and Sunday), were sampled for one year. The flow rate of the instrumentation was calibrated, using an external flow meter every four weeks. The $PM_{10}$ inlet was cleaned every two weeks. The temperature and pressure sensors were calibrated every three months.

### 4.2.2 High Volume Air Sampler

The High Volume Air Sampler (Bird & Tole Ltd.) was a simple air pump equipped with a flow meter (Figure 4.3). The ambient air is drawn through the paticulates collector by the air pump. The times and flow rates at the sample start and end were recorded manually. The volume of ambient air through the filter was calculated using average flow rate and sample time. A Cole-Parmer 1.0 μm PTFE 47 mm (Cole-Parmer Instrument

Company) filter was used to collect the TSP. In a similar manner to the method used for $PM_{10}$, two samples were collected each week. The flow rate of the High Volume Air Sampler was calibrated every 4 weeks.

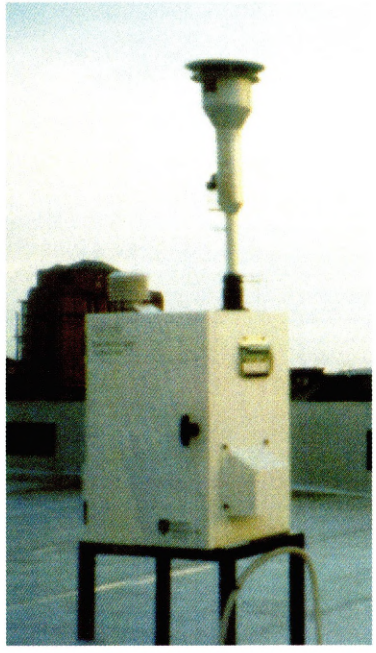

Figure 4.2 Partisol Model 2000 Air Sampler

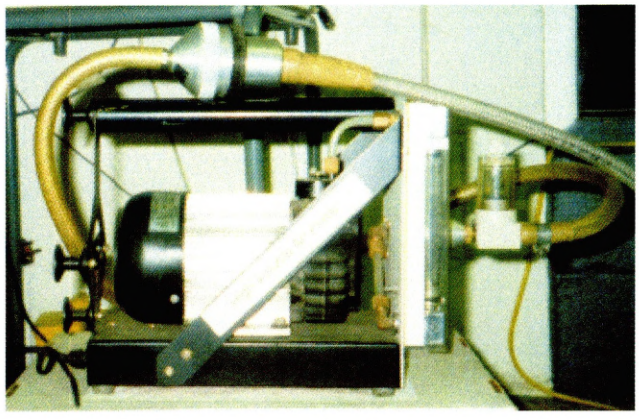

Figure 4.3 High Volume Air Sampler

### 4.2.3 APNA-360 Ambient NOx Monitor

The APNA-360 Ambient NOx Monitor (HORIBA, Ltd., 1996) shown in Figure 4.4 can measure ambient concentrations of NO, $NO_2$ and NOx continuously. It is based on the chemiluminescence method (CLD). Part of the NO is oxidised to $NO_2$ when NO and $NO_2$ in the sample gas reacts with ozone. The newly generated $NO_2$ is in the excited state

($NO_2$') and radiates light when it returns to the ground state. This phenomenon is called chemiluminescence and can be described as:

$$NO + O_3 = NO_2^* + O_2 \quad (4.1)$$

$$NO_2^* \rightarrow NO_2 + h\nu \quad (4.2)$$


Figure 4.4 APNA-360 Ambient NOx Monitor

This reaction is extremely fast and only NO is involved, with almost no effect on the other coexistent gases. If the NO is at a low concentration, the quantity of luminescence is in proportion to that concentration. The APNA-360 separates the sampled gas into two portions. In one portion, $NO_2$ is reduced to NO by the NOx converter and then used as the sample gas for measuring NOx. In the other, the NO sample gas is used directly. These sample gases are switched to NOx, NO and reference gas lines by the solenoid valves every 0.5 seconds and are in turn introduced to the reaction chamber.

In the reaction chamber, the sample gas reacts with ozone that comes from the ozone generator. The light emission involved in the reaction is detected by a photodiode. The output obtained by the photodiode is in proportion to the concentration of NOx and NO. The results are calculated to output the concentrations of NO, $NO_2$ and NOx as continuous signals. The important parameters for APNA-360 are shown in Table 4.1.

1 hour mean concentrations of NO, $NO_2$ and NOx were recorded by the instrument. 15 min mean concentrations were also recorded as a reference. The recorded data were downloaded every week. The APNA-360 Ambient NOx Monitor was calibrated using

standard gases every week. Pure $N_2$ gas was used to calibrate the zero points. NOx standard gas (BOC GASES, NO: 454.00 ppb; NOx: 461.00 ppb) was used to calibrate the measurement span.

Table 4.1 The important parameters for APNA-360

| | |
|---|---|
| Standard measurement range | 0 - 0.1, 0.2, 0.5, 1.0 ppm auto-switching |
| Lower detection limit | 0.5 ppb |
| Repeatability | ±1.0% full scale |
| Accuracy of graduation | ±1.0% full scale |
| Zero drift and Span drift | ±1.0% of full-scale value per day<br>±2.0% of full-scale value per week |
| Response time $T_{90}$ | Within 120 seconds |
| Interference effect | ±2.0% ppb for 2% $H_2O$ and 0.2 ppm $NH_3$ |
| Sample flow rate | Approx. 0.8 l $min^{-1}$ |
| Working temperature range | 0 – 40°C |
| Working humidity range | 85% maximum |

### 4.2.4 ELE MM900 environmental monitoring station

The ELE MM900 environmental monitoring station shown in Figure 4.6 (ELE International, 1993) is a station combining environmental monitoring and data logging. ELE MM900 environmental monitoring system supports up to a maximum of ten sensors, both meteorological factors and gaseous pollutants. ELE International provides a series of meteorological sensors and gaseous pollutant sensors optional to the user. Seven gaseous pollutant sensors for monitoring concentrations of hydrogen sulphide, hydrogen cyanide, hydrogen, chlorine, sulphur dioxide, nitrogen dioxide and carbon monoxide are available. The important parameters for these gaseous pollutant sensors are shown in Table 4.2.

As shown in Table 4.2, the accuracy of the seven gaseous pollutant sensors is too low to be used to measure ambient concentrations for these gases. Except carbon monoxide, the concentrations of these gases in ambient air are significantly lower than the accuracy of these sensors. Although the ambient concentration of carbon monoxide approaches the sensor's accuracy, carbon monoxide sensor can not measure temporal variation of carbon monoxide concentration reliably for the aims of this project to be met.

Therefore gaseous pollutant sensors were not installed on ELE MM900 environmental monitoring station.

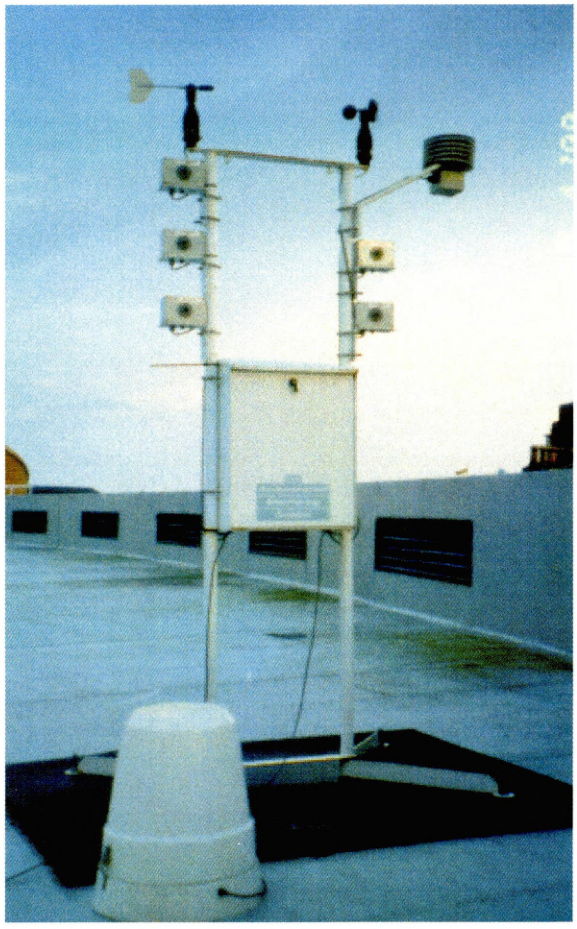

Figure 4.5 ELE MM900 environmental monitoring station

Table 4.2 The important parameters for the gaseous pollutant sensors

| Sensor's name | Measuring rang (ppm) | Accuracy (ppm) | Response time (s) | Drift (% of full signal month$^{-1}$) |
|---|---|---|---|---|
| Hydrogen sulphide | 0 – 200 | ± 1 | 60 | <2 |
| Hydrogen cyanide | 0 – 200 | ± 1 | 60 | <2 |
| Hydrogen | 0 – 2000 | ± 1 | 70 | <2 |
| Chlorine | 0 – 100 | ± 1 | 40 | <2 |
| Sulphur dioxide | 0 – 100 | ± 1 | 20 | <2 |
| Nitrogen dioxide | 0 – 100 | ± 1 | 30 | <2 |
| Carbon monoxide | 0 – 2000 | ± 1 | 30 | <2 |

A number of sensors for measuring various kinds of meteorological factors such as wind, temperature, humidity, radiation, rainfall etc are available. An anemometer, wind direction sensor, ambient temperature sensor and rain gauge were installed on ELE MM900 environmental monitoring station to measure meteorological conditions. The important parameters for these meteorological sensors are shown in Table 4.3.

Table 4.3 The important parameters for the meteorological sensors

| Sensor Type | Measuring range | Accuracy | Other parameters |
|---|---|---|---|
| Anemometer | 0.25 – 75 m $s^{-1}$ | 1% ± 0.1 m $s^{-1}$ | 1 rotation = 4 pluses |
| Wind direction | 0 - 360 | ± 2 degree | Max wind speed: 75 m $s^{-1}$ |
| Temperature | -20 – 70 °C | 0.2°C at 20°C | |
| Rain gauge | n/a | n/a | Capacity: 0.2 mm per tip<br>Respond: <100 ms for 0.2 mm rain |

The MM900 logging systems consist of two elements, an MM900/950 series data logger and Dialog 900 management software. They provide a convenient tool for the operation of ELE MM900 environmental monitoring station. The MM900/950 data logger is designed to accommodate the various meteorological and gaseous pollutant sensors. The logger has a built in measuring system that can accept various kinds of digital or analogue inputs such as voltages, resistances, pulses and frequencies coming from various sensors. Each input channel of the data logger is separately configured to match the characteristics of the connected sensor, and to convert the reading from the measured units (volts, ohms, counts, etc.) to engineering units. Reading from the input channels can be logged at regular time intervals, where the interval can be different for each channel, and intermittently in response to alarms or events. Another important feature of the data logger is its ability to apply data compression functions to information from an input channel.

A dialog 900 management software provides the means to set up and operate the MM900/950 data logger and download data to a computer. Once the experiment has been defined, and the relevant sensors connected, the logger can be quickly and easily configured. Once the logger has been configured, it will run independently from the computer until data has to be collected. Dialog 900 is supplied with a database containing the configuration data for sensors supplied by ELE International. This database can be

edited and updated so that new sensors can be incorporated. The data held for a sensor contains all information required by the MM900/950 data logger to measure the sensor's signal, and to convert it to engineering units.

The readings of average wind speed, basic wind direction, average ambient temperature and total rainfall from four installed meteorological sensors were recorded and stored every 10 min by the data logger. The data were downloaded to a computer once a week during the period of investigation.

## 4.3 Laboratory analysis instrumentation and methods

### 4.3.1 Instruments and methods used for determining masses of $PM_{10}$ and TSP measurement

The gravimetric method was used for mass measurements of $PM_{10}$ and TSP. The net masses of $PM_{10}$ and TSP collected on filter papers were measured by weighing the filter papers before and after sampling. A semi-micro balance, BDH AA-200DS balance (BDH Balance Service Unit), with a minimum resolution of 0.01 mg was used to weigh the filter papers. According to standard procedure, the 'blank' filter papers and the sampled filter papers should be equilibrated for 24 hours at a constant relative humidity between 20 and 40% (within ±5%) and at a constant temperature of between 15 and 30°C (within ±3°C) before they are weighed. A cabinet that could maintain a constant relative humidity and a constant temperature was unavailable in the laboratory. Instead, the filter papers were placed in a dessicator to equilibrate for at least 24 hours before they were weighed.

BDH AA-200DS balance was turned on for at least 1 hour to warm up before performing any weighing. Each blank or sampled filter paper was weighed twice. Auto calibration is conducted before each weighing section. Average mass reading is used to calculate the net masses of $PM_{10}$ and TSP. One of ten filter papers taken randomly was weighed again at the next weighing session. These re-weights were used to estimate the precision of the measurement.

The minimum resolution of BDH AA-200DS balance is 0.01 mg. It is reasonable to suppose its detection limit is 0.005 mg. The detection limit for net weight of particulates is also 0.005 mg. The ambient air volume drawn through the $PM_{10}$ filter paper is about 100$m^3$ for weekday samples and 68 $m^3$ for weekend samples. Thus, the detection limit for

concentration of $PM_{10}$ is 0.050 μg $m^{-3}$ (0.005*1000/100) for weekday samples and 0.074 μg $m^{-3}$ (0.005*1000/68) for weekend samples.

After mass analysis, the sampled filter papers were stored in a refrigerator before their chemical compositions were analysed using wet chemical analysis method. For the chemical composition analysis, the sampled filter paper was divided into two parts. The weights of two parts were measured using the BDH AA-200DS balance. A half of the sampled filter was used to analyse for metal elements ($Ca^{2+}$, $Mg^{2+}$, Zn, Cu, Ni and Pb) using Atomic Absorption Spectrophotometer (AAS). Another half of the sampled filter was used to analyse for water soluble ions ($SO_4^{2-}$, $NO_3^-$, $Cl^-$, $NH_4^+$, $Na^+$ and $K^+$) using High Performance of Liquid Chromatography (HPLC).

### 4.3.2 Atomic Absorption Spectrophotometer (AAS) and metal elements analysis methods

A Perkin Elmer 1100 B AAS, supported by an acetylene flame, shown in Figure 4.6 was used to analyse metal elements (Perkin Elmer, 1989). It is a microcomputer-controlled atomic absorption spectrophotometer with an integrated CRT screen. All operating parameters and functions for the spectrophotometer are entered via an incorporated keyboard. The spectrometer features a single-beam, all-reflecting optical system. The optics are coated with silica for durability. The photomultiplier gain, hollow cathode lamp current, optional background corrector brightness, signal processing and data processing are automatically controlled.

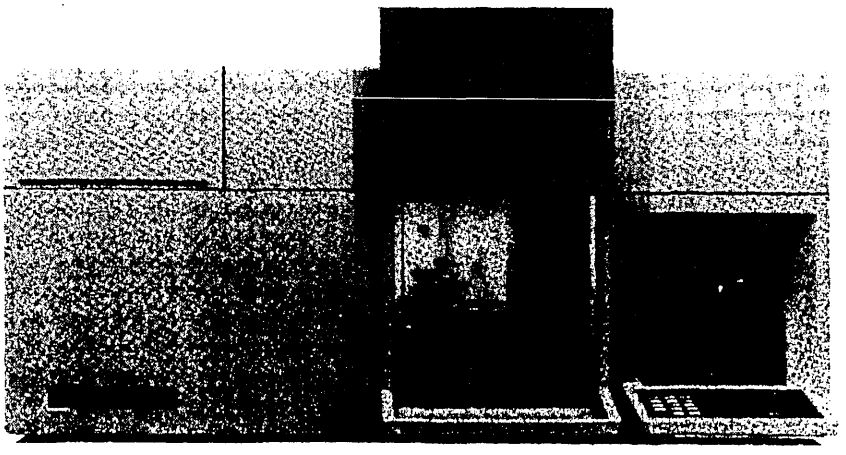

Figure 4.6 PERKIN ELMER 1100 B atomic absorption spectrophotometer

The fundamental principles of flame atomic absorption spectrophotometer were described by Welz (1986). The flame atomic absorption spectrophotometer consists of a resonance line source, a prism system, a flame atomiser, a monochromator, a detector and amplifier, and a computer. The light from the source lamp (a hollow cathode lamp or electrodeless discharge lamp) generates a sharp line spectrum characteristic of the desired element, passes through the flame into which the sample solution is sprayed as fine mist. The region of the spectrum in the immediate neighbourhood of the resonance line to be measured is selected by the monochromator. The isolated resonance line falls on to the detector, a photomultiplier, the output is amplified and connected to the computer. The intensity of the resonance line is measured with and without the sample passing into the flame. The ratio of these readings is a measure of the absorption and therefore of the amount of the element being determined. The important parameters for a Perkin Elmer 1100 B atomic absorption spectrophotometer are shown in Table 4.4.

Table 4.4 The important parameters for a Perkin Elmer 1100 B atomic absorption spectrophotometer

| | | |
|---|---|---|
| Radiation sources | Hollow cathode lamps (HCLs) and electrodeless discharge lamps (EDLs) | |
| Burner | Single slot, 10 cm, all-titanium, removable burner head for air/acetylene operation | |
| Monochromator | Grating monochromator in Littrow configuration | |
| | Ruled area: | 64 mm x 71 mm, 1800 lines/mm |
| | Reciprocal linear dispersion (nominal): | 1.6 nm/mm |
| | Blaze wavelengths: | 236 nm and 598 nm |
| | Focal length: | 267 mm |
| | Wavelength range: | 190 nm to 870 nm |
| | Resolution: | 0.2, 0.7, 2.0 nm |
| Detector | Wide-range photomultiplier with UV transmitting window | |

#### 4.3.2.1 Sample preparation

One half of the sampled filter for metal element analysis was cut into small pieces. These small pieces were digested for 30 min in 10 ml of concentrated $HNO_3$ over a low heat. The solution was removed and the remaining solid was extracted three times, for 15 min each time, with deionized water (50 ml for each time). The extracts were combined with the acid solution and were then evaporated nearly to dryness. Then, the sample was redissolved using 5 ml $HNO_3$. The solutions were transferred to a 50 ml volumetric flask

and made to the prescribed volume with deionized water. Finally, the sample solution was filtered through a filter paper and was then ready for AAS analysis.

Two half blank filter papers for $PM_{10}$ as well as two half blank filter papers for TSP were treated in the same manner as described above in order to prepare the blank samples. Results of the analysis of blank samples were used to estimate the element concentration produced by the filter and sample preparation.

After the sample solution concentration was analysed by AAS, the concentration of element in ambient aerosol ($C$, ng $m^{-3}$) can be calculated using:

$$C = 50( C_l - C_b) M_f/(V_a M_h) \quad (4.3)$$

where $C_l$ (ng $ml^{-1}$) is the concentration of sample solution measured by AAS, $C_b$ (ng $ml^{-1}$) is the average concentration of blank sample solutions, $M_f$ (mg) is the weight of the sampled filter, $M_h$ (mg) is the weight of a half of the sampled filter used for AAS analysis. $V_a$($m^3$) is the ambient air volume pumped through the filter paper.

#### 4.3.2.2 Instrumentation calibration

Quantitative measurements in atomic absorption are based on Beer's law, which states that absorbance is proportional to concentration. However, for most elements, particularly at high concentrations, the relationship between concentration and absorbance is not linear. The readout of the Perkin Elmer 1100 B AAS may be calibrated directly in units of concentration. The concentrations of the reference solutions are input in the program element mode. In the run mode, the reference solutions are measured in turn and the absorbance reading are equated with the respective concentration values. The AAS then constructs an appropriate analytical curve, using the technique of calibration provided by the manufacturer. There are six available calibration techniques which may be selected when using the AAS. These techniques are linear, 2-coefficient equation, 3-coefficient equation, auto select, technique of standard addition, technique of standard addition calibration, and reslope.

The selection of the calibration technique, the number of standard solution and their concentration is very important in AAS analysis.

The concentration in the sample solution is very low for most metal elements and therefore linear calibration technique was selected in AAS analysis. Five standard solutions were used to calibrate the instrument for each metal element. The concentrations of the five standard solutions were selected at equal intervals from zero to the maximum

concentration that may be measured in all samples. Ten random samples (5 for $PM_{10}$ and 5 for TSP) were analysed prior to analysing all samples formally for a metal element. Then, the maximum possible concentration of the metal was estimated and used to prepare standard solution. The concentrations and absorbances of five standard solutions for six metals are shown in Table 4.5.

The minimum resolution of absorbance of the Perkin Elmer 1100B AAS is 0.001. It is reasonable to suppose that its detection limits for absorbance is 0.0005. The concentration of standard solution for the metal element that can produce 0.0005 absorbance may be regarded as detection limit for the metal. The detection limit of the Perkin Elmer 1100B AAS for metal element standard solutions can be estimated from Table 4.5. It is about 11.8 ng $ml^{-1}$ for $Ca^{2+}$, 0.9 ng $ml^{-1}$ for $Mg^{2+}$, 4.8 ng $ml^{-1}$ for Cu, 41.7 ng $ml^{-1}$ for Pb, 8.9 ng $ml^{-1}$ for Ni, and 2.1 ng $ml^{-1}$ for Zn (calculated using concentration and absorbance of standard 5 in Table 4.5). The detectiion limit of Perkin Elmer 1100B AAS for the concentration of metal element in the airborne particulates can be estimated by substituting above values into equation 4.3. The detection limit for concentration of metal element in $PM_{10}$ weekdays sample is 11.8 ng $m^{-3}$ for $Ca^{2+}$, 0.9 ng $m^{-3}$ for $Mg^{2+}$, 4.8 ng $m^{-3}$ for Cu, 41.7 ng $m^{-3}$ for Pb, 8.9 ng $m^{-3}$ for Ni, and 2.1 ng $m^{-3}$ for Zn respectively.

Table 4.5 Concentrations and absorbances of standard solutions

| | Standard | 1 | 2 | 3 | 4 | 5 |
|---|---|---|---|---|---|---|
| $Ca^{2+}$ | Concentration (ng $ml^{-1}$) | 500 | 1000 | 1500 | 2000 | 2500 |
| | Absorbance | 0.028 | 0.050 | 0.072 | 0.088 | 0.106 |
| $Mg^{2+}$ | Concentration (ng $ml^{-1}$) | 80 | 160 | 240 | 320 | 400 |
| | Absorbance | 0.065 | 0.102 | 0.147 | 0.186 | 0.225 |
| Cu | Concentration (ng $ml^{-1}$) | 40 | 80 | 120 | 160 | 200 |
| | Absorbance | 0.004 | 0.010 | 0.015 | 0.017 | 0.021 |
| Pb | Concentration (ng $ml^{-1}$) | 100 | 200 | 300 | 400 | 500 |
| | Absorbance | 0.001 | 0.002 | 0.004 | 0.005 | 0.006 |
| Ni | Concentration (ng $ml^{-1}$) | 50 | 100 | 150 | 200 | 250 |
| | Absorbance | 0.003 | 0.006 | 0.009 | 0.012 | 0.014 |
| Zn | Concentration (ng $ml^{-1}$) | 30 | 60 | 90 | 120 | 150 |
| | Absorbance | 0.006 | 0.014 | 0.021 | 0.028 | 0.035 |

#### 4.3.2.3 Interference

Six categories of interferences exist in AAS analysis (Perkin Elmer, 1989). They are chemical interferences, ionisation interferences, matrix interferences, emission interferences, spectral interferences and background absorption. The interferences in AAS analysis are easy to eliminate, because they are well defined.

Matrix interferences can cause a suppression or enhancement of the analysis signal. Matrix interferences occur when the physical characteristics (viscosity, burning characteristics, surface tension) of the sample solution and standard solution differ considerably. This can happen when the sample solution contains a high concentration of dissolved salts or acid, when different solvents are used for sample and standard solutions, or when the sample and standard solutions are at radically different temperatures.

The proportion of acid to deionized water in the sample solutions is 1:9. The viscosity of the sample solutions increases, because acid is added to the solutions. Acid in the solutions will decrease the absorbance. To eliminate the matrix interferences, all standard solutions were prepared using solution with the proportion of 1:9 for acid and deionized water.

There are two causes of background absorption in AAS: light scattering by particles in the flame and molecular absorption of light from the lamp by molecules in the flame. The most common way to compensate for background absorption is to use a background corrector, which utilises a continuum source (a deuterium arc lamp in the ultraviolet or a tungsten-iodide lamp for visible wavelengths). A continuum source emits light over a broad spectrum of wavelengths instead of at specific lines. With background correction, simultaneous compensation is obtained at the same wavelength used to measure atomic absorption. With this system, light from the primary source and the continuum source are passed alternately through the flame. The element being determined effectively absorbs light only from the primary source, while background absorption affects both beams equally. Therefore, when the ratio of the two beams is measured electronically, the effect of the background absorption is eliminated.

The background corrector was used in the analysis of $Mg^{2+}$, Pb, Ni, and Zn.

#### 4.3.2.4 Analysis of Sample

The standard atomic absorption conditions for $Ca^{2+}$, $Mg^{2+}$, Cu, Pb, Ni and Zn are described in the users manual of the Perkin Elmer 1100B AAS. They are shown in Table 4.6. Air-acetylene flame was used in the analysis.

The sample solution was aspirated into the flame of AAS and the concentration was read five times. Average concentration and standard deviation were recorded. Auto zero using deionized water and checking analysis span using standard solutions were conducted every ten times when analysing a sample solution. It was regarded as zero if average concentration was less than the detection limits. The average standard deviations are used to estimate the analysis precision. They are shown in Table 4.7.

Table 4.6 Standard atomic absorption conditions for various metal elements

| Element | Wavelength (nm) | Slit (nm) | Relative Noise | Sensitivity (mg $L^{-1}$) | Sensitivity Check (mg $L^{-1}$) | Linear Range (mg $L^{-1}$) |
|---|---|---|---|---|---|---|
| $Ca^{2+}$ | 422.7 | 0.7 | 1.0 | 0.077 | 4.0 | 5.0 |
| $Mg^{2+}$ | 285.2 | 0.7 | 1.0 | 0.0078 | 0.30 | 0.50 |
| Cu | 324.7 | 0.7 | 1.0 | 0.077 | 4.0 | 5.0 |
| Pb | 283.3 | 0.7 | 0.43 | 0.45 | 20.0 | 20.0 |
| Ni | 232.0 | 0.2 | 1.0 | 0.14 | 7.0 | 2.0 |
| Zn | 213.9 | 0.7 | 1.0 | 0.018 | 1.0 | 1.0 |

Table 4.7 Analysis precision for metal elements (%)

| Element | $Ca^{2+}$ | $Mg^{2+}$ | Cu | Pb | Ni | Zn |
|---|---|---|---|---|---|---|
| Precision | 0.9 | 0.5 | 19.1 | 7.8 | 14.3 | 2.4 |

### 4.3.3 High Performance Liquid Chromatography (HPLC) and ions analysis methods

High Performance Liquid Chromatography (HPLC) is a technique that has arisen from the application to liquid chromatography (LC) of theories and instrumentation that were originally developed for gas chromatography (GC) (Lindsay, 1992). A typical HPLC consists of a high pressure pump, a supply of mobile phase, a column containing a high

efficiency stationary phase, an injection unit for introducing samples on to the column, an in-line detector and some instruments to record, treat and display the detector signal.

In an analytical HPLC the mobile phase is normally pumped through the column with a stable flow rate. If the composition of the mobile phase is constant, the method is called 'isocratic' elution. If the composition of the mobile phase can be made to change in a predetermined way during the separation, the method is called 'gradient' elution. After passing through the column, the separated solutes are sensed by an inline detector. The output of the detector is an electrical signal, the variation of which is treated and displayed by a computing integrator.

The height of the chromatographic peak can be used to estimate the concentration of the solute represented by the peak. This is easy to measure. However, the area of the chromatographic peak is a more satisfactory analytical parameter than peak height because peak area is independent of broadening effects.

The HPLC system shown in Figure 4.7, was used to analyse the ions. The system consists of an isocratic pump (IsoChrom, Spectra-Physics, 1988a), an injection unit, a HPLC column (PRP-X100 for anions and PRP-X200 for cations, Hamilton Company), a conductivity detector (Conductor Monitor III, Milton Roy) and an integrator (SP4400, Spectra-Physics, 1988b).

The IsoChrom isocratic pump provides a constant flow through the HPLC system. The important parameters for the IsoChrom isocratic pump are shown in Table 4.8.

The injection unit allows 20 μL sample solution to be injected in the column.

A PRP-X100 anion exchange HPLC column was used to analyse the concentrations of $SO_4^{2-}$, $NO_3^-$ and $Cl^-$. PRP-X200 cation exchange HPLC column was used to analyse the concentrations of $NH_4^+$, $Na^+$ and $K^+$. The column descriptions, operating limits, chromatographic test conditions and efficiencies for the two columns are shown in Table 4.9.

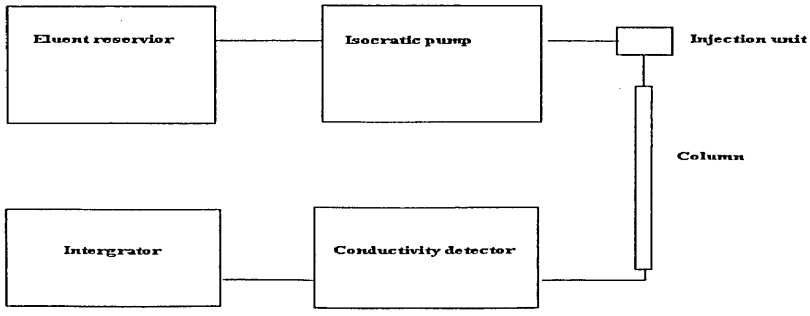


Figure 4.7 The HPLC system for ions analysis

Table 4.8 The important parameters for IsoChrom isocratic pump (Spectra-Physics)

| | |
|---|---|
| Flow range | 0.01 to 10 ml/min standard; |
| | Up to 30 ml/min using prep option. |
| Flow precision | 0.2% RSD* |
| Maximum pressure | 5000 psi for standard head; |
| | 2500 psi for prep option. |
| Compressibility compensation | Automatic |
| Flow stability test | Pump flow diagnostic to verify proper pump performance. |

*: Typical RSD obtained on chromatographic retention times.

Table 4.9 The descriptions, operating limits, chromatographic test conditions and efficiencies for PRP-X100 and PRP-X200 HPLC columns (Hamilton company)

| | PRP-X100 | PRP-X200 |
|---|---|---|
| Description | | |
| Dimensions | 100 x 4.1 mm | 150 x 4.1 mm |
| Particle size | 10 μm | 10 μm |
| Operating limits | | |
| Mobile phase | pH 1-13, 0-100% aqueous | PH 1-9, 0-100% aqueous |
| Temperature | 5-30 °C pH 1-13, 30-60 °C PH 1-7.9 | 5-60 °C |
| Chromatographic test conditions | | |
| Eluent | 4mM p-Hydroxybenzoic acid 2.5% MeOH pH=8.5 | 4mM $HNO_3$ in 7:3 water:MeOH |
| Flow rate | 2.0 ml $min^{-1}$ | 2.0 ml $min^{-1}$ |
| Test pressure | <700 psi | <1600 psi |
| Temperature | Ambient | Ambient |
| Detection | Conductivity | Conductivity |
| Efficiency | | |
| Guarantee efficiency | 750 plates | 1000 plates |
| Actual efficiency | 972 plates | 1665 plates |

Conductor Monitor III (Milton Roy) detects the conductivity of separated solutes and transfers the signal to a SP400 integrator (Spectra-Physics). SP400 integrator is a microcomputer with powerful functions for HPLC analysis. It provides methods for peak identification and its area calculation, data processing and storing and output of results of analysis.

#### 4.3.3.1 Sample preparation

Preparation of sample for HPLC analysis is relatively simple. A half of sampled filter for ion analysis was cut into small pieces. The pieces were extracted for 30 min in 25 ml of deionized water on an ultrasonic bath. The solid was removed and the resulting sample was ready for the HPLC analysis.

Two half blank filters for $PM_{10}$ as well as two half blank filters for TSP were extracted for 30 min in 25 ml of deionized water to prepare blank sample. Analysis results of blank samples were used to estimate the ion concentration produced by the filter.

After the sample extract concentration was analysed by HPLC, the concentration of ion in ambient aerosol ($C$, ng $m^{-3}$) can be calculated using

$$C = 25( C_l - C_b) M_f/(V_a M_h) \quad (4.4)$$

where $C_l$ (ng $ml^{-1}$) is the concentration of sample extract measured by HPLC, $C_b$ (ng $ml^{-1}$) is the average concentration of blank sample extracts, $M_f$ (mg) is the weight of the sampled filter, $M_h$ (mg) is the weight of a half of sampled filter used for HPLC analysis. $V_a$($m^3$) is the ambient air volume through the filter.

#### 4.3.3.2 Instrumentation calibration

The most straightforward method for quantitative chromatographic analysis involves the preparation of a series of standard solutions that approximate the composition of the unknown. Chromatograms for the standard solutions are then obtained. The peak areas are plotted as a function of concentration. The plot of the data should yield a straight line passing through the origin. The quantitative chromatographic analysis is based on this line. Thus, selection of the number and concentration for standard solution is important in HPLC analysis.

Five standard solutions for cations as well as five standard solutions for anions were used to calibrate the instrument. The concentration of each ion in the five standard solutions was increased at equal intervals from zero to the maximum concentration that may be measured in all samples. Like AAS analysis, 10 random samples (5 for $PM_{10}$ and 5 for TSP) were analysed prior to analysing cation and anion real samples. The maximum concentration for each cation and anion were estimated to prepare the standard solutions. The concentrations of $SO_4^{2-}$, $NO_3^-$ and $Cl^-$ in the five standard solutions for anion analysis and the concentration of $NH_4^+$, $Na^+$ and $K^+$ in the five standard solutions for cation analysis are shown in Table 4.10.

The standard solutions were analysed before sample analysis. They were analysed again when ten samples were analysed. Five chromatograms for each standard solution were obtained. The average peak areas were used to plot the calibration lines. The standard deviations of the peak areas were used to estimate the precisions of the analysis.

Table 4.10 Ion concentrations of standard solutions (μg $ml^{-1}$)

| Standard | 1 | 2 | 3 | 4 | 5 |
|---|---|---|---|---|---|
| $SO_4^{2-}$ | 2.0 | 4.0 | 6.0 | 8.0 | 10.0 |
| $NO_3^-$ | 2.0 | 4.0 | 6.0 | 8.0 | 10.0 |
| $Cl^-$ | 2.0 | 4.0 | 6.0 | 8.0 | 10.0 |
| $NH_4^+$ | 0.6 | 1.2 | 1.8 | 2.4 | 3.0 |
| $Na^+$ | 0.6 | 1.2 | 1.8 | 2.4 | 3.0 |
| $K^+$ | 0.2 | 0.4 | 0.6 | 0.8 | 1.0 |

### 4.3.3.3 Analysis of sample

The sample solution was injected into the column of the HPLC using 4 mm syringe filters (0.2 μm NYL w/tube tip, Whatman). The blank samples were analysed along with the samples to correct for the ions extracted from Teflon-membrane filters. The concentration of $SO_4^{2-}$, $NO_3^-$ and $Cl^-$ were analysed using PRP-X100 HPLC column. 4mM p-Hydroxybenzoic acid, 2.5% MeOH (PH=8.5) solution was used as eluant. The eluant was degassed using supersonic bath before serving as mobile phase. The flow rate was set at 1.5 ml $min^{-1}$. A typical chromatogram for cation analysis is shown in Figure 4.8. The concentrations of $NH_4^+$, $Na^+$ and $K^+$ were determined with a PRP-X200 HPLC column. 4mM $HNO_3$ in 7:3 Water:MeOH solution was used as eluant. It was also degassed using a supersonic bath before serving as mobile phase. The flow rate was set up as 2.0 mL $min^{-1}$. A typical chromatogram for ion analysis is shown in Figure 4.9.

The peak area was used to determine analysis concentration based on the plotted lines from standard solution analysis. The precision of the analysis was estimated using the standard deviation of the results of the analysis for the standard solutions. They are shown in Table 4.11.

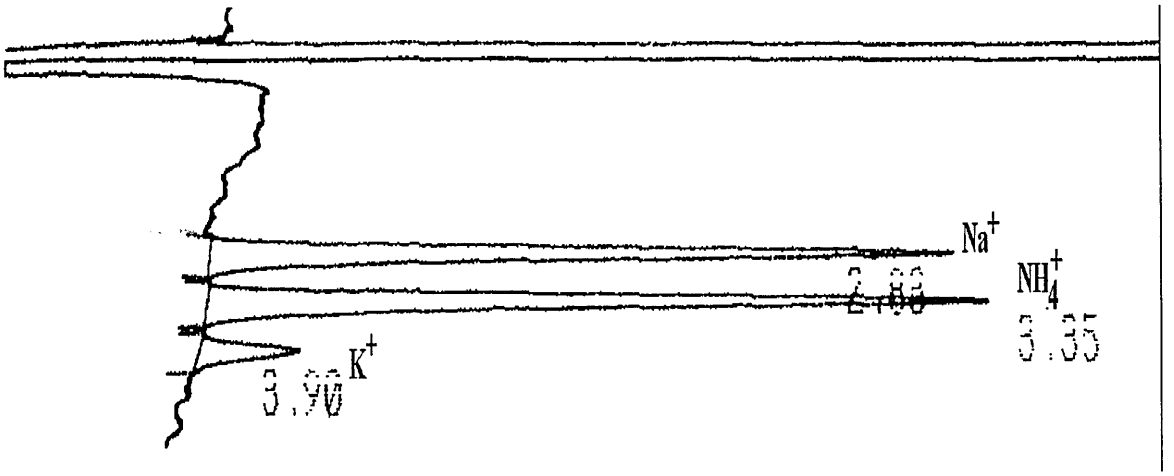


Figure 4.8 Typical chromatogram for cation analysis

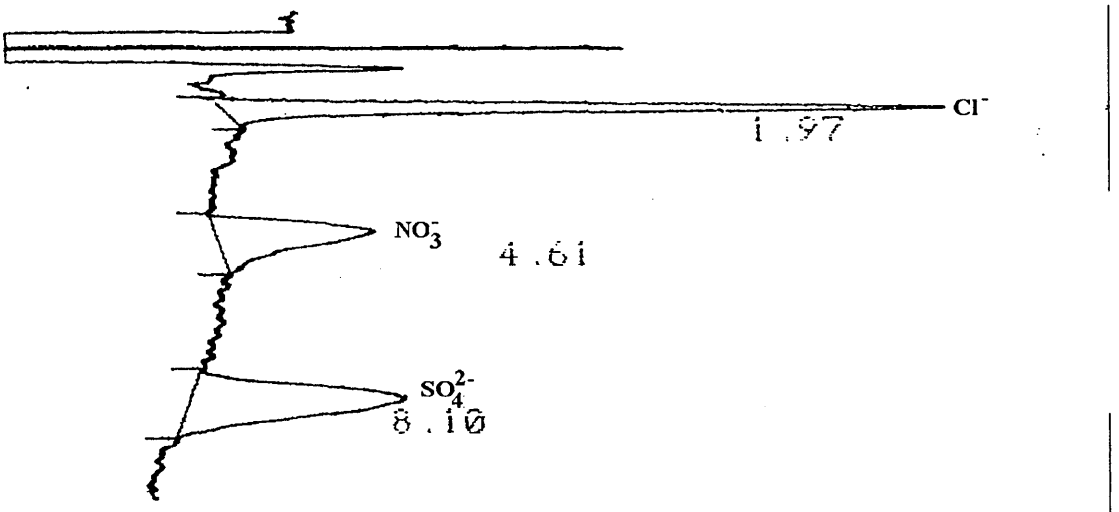


Figure 4.9 Typical chromatogram for anion analysis

Table 4.11 Analysis precision for ions (%)

| Iron | $SO_4^{2-}$ | $NO_3^-$ | $Cl^-$ | $NH_4^+$ | $Na^+$ | $K^+$ |
|---|---|---|---|---|---|---|
| Precision | 23.5 | 13.5 | 11.3 | 5.2 | 4.2 | 9.0 |

## 4.4 Discussion on field monitoring and laboratory analysis

94 $PM_{10}$ samples and 95 TSP samples were sampled at the monitoring station used for this study. Analysing chemical compositions for such a large number of samples using both AAS and HPLC was a difficult and time consuming job. The chemical compositions for 59 $PM_{10}$ samples and 60 TSP samples were analysed in laboratory.

In planning the field monitoring, the author tried to use all available equipment to measure as many as possible airborne pollutants and get a comprehensive database for urban background air quality and atmospheric dispersion conditions in Dundee. However, the field monitoring was limited by the available equipment. $O_3$, CO, $SO_2$, Benzene and 1,3 butadiene are other five criteria pollutants apart from $NO_2$ and NOx pollution gases, that are usually measured at the UK's air quality automatic monitoring stations. These pollution gases could not be measured at the monitoring station used for this study because the requisite automatic analysers were unavailable.

Solar radiation and cloud cover are two important parameters used for determining atmospheric stability. They could not be measured at the station because the requisite instrument and technician were unavailable.

The laboratory analysis was also limited by analysis instruments and time. Carbon, the most important component of an aerosol, was not analysed. The range of metal elements analysed was limited by available light sources and the detection limits of AAS. Aluminium (Al) and Silicone (Si) are two important elements in ambient $PM_{10}$ and TSP. They come from crustal dust. These two metals could not be analysed because the light sources (bulbs) and the flame of nitrous oxide-acetylene were unavailable. Arsenic (As) and Vanadium (V) are another two important trace elements of $PM_{10}$ and TSP because they can serve as the source markers of coal combustion emission and oil combustion emission respectively. These two trace metals could not be analysed, again because equipment was unavailable. Compared with concentrations in ambient of $PM_{10}$ and TSP, the AAS detection limits for Pb and Ni may have been too high.

# Chapter 5 Results and analysis of field monitoring and laboratory analysis

## 5.1 Meteorological conditions

### 5.1.1 Summary of meteorological data

Meteorological conditions are the most important factors that can affect the transport, transformation and deposition of airborne pollutants after they are emitted into ambient atmosphere, from emission sources. In 2000, wind speed, wind direction, ambient temperature and total rainfall were measured continually at the automatic monitoring station. A statistical summary of a year's data for wind speed, temperature and total rainfall is shown in Table 5.1.

Table 5.1 Wind speed, temperature and total rainfall

| Month | JAN | FEB | MAR | APR | MAY | JUN | JUL | AUG | SEP | OCT | NOV | DEC |
|---|---|---|---|---|---|---|---|---|---|---|---|---|
| Wind speed (m $s^{-1}$) | | | | | | | | | | | | |
| Max | 7.7 | 7.6 | 7.5 | 6.4 | 5.7 | 6.9 | 4.3 | 4.9 | 7.3 | 8.0 | 7.2 | 7.0 |
| Average | 2.0 | 2.6 | 2.2 | 1.9 | 1.8 | 2.1 | 1.5 | 1.6 | 1.8 | 1.7 | 1.6 | 1.9 |
| Temperature (°C) | | | | | | | | | | | | |
| Max | 12.1 | 13.6 | 16.4 | 15.8 | 20.7 | 20.9 | 23.1 | 24.5 | 21.5 | 19.5 | 12.8 | 12.9 |
| Min | 0.2 | -0.1 | -0.6 | 0.7 | 6.2 | 6.6 | 8.3 | 10.4 | 7.2 | 4.7 | 2.6 | -1.0 |
| Average | 5.8 | 5.9 | 8.0 | 8.0 | 10.9 | 12.9 | 14.5 | 16.0 | 13.9 | 10.4 | 7.0 | 5.2 |
| total rainfall (mm) | 16.2 | 24.2 | 39.2 | 56.2 | 46.4 | 44.0 | 8.4 | 45.8 | 127.8 | 88.8 | 88.8 | 88.2 |

The wind is not too strong in Dundee. In 2000, the average wind speed measured at the station is 1.9 m $s^{-1}$. The max. wind speed is 8.0 m $s^{-1}$. It occurred at 03:00 on 29 October 2000. Wind speed varies with season, as one would expect. It is relatively higher in the winter (December, January and February) and lower in the summer (June, July and August). The strongest monthly-averaged wind speed in Dundee is in February with an average speed for the month as 2.6 m $s^{-1}$. The weakest wind is in July, with an average speed of 1.5 m $s^{-1}$.

The variation of ambient temperature is moderate in Dundee. In 2000, the average temperature measured at the station is 10.1 °C. The highest temperature is 24.5 °C. It occurred at 13:00 on 6 August 2000. The lowest temperature is –1.0 °C and it occurred at 09:00 on 17 December 2000. The hottest month is August with an average temperature of 16.0 °C. The coldest month is December with an average temperature of 5.2 °C.

In 2000, the total rainfall measured at the station is 674 mm. Rainfall also varies with season as one would expect. Autumn (September, October and November) is the wettest season. The total rainfall in the autumn is 305 mm, accounting for about 45.3% of the annual total rainfall. Summer is the driest season. The total rainfall in the summer is 98 mm, which accounts for about 14.6% of the annual total rainfall. The highest rainfall is in September (127.8 mm) while lowest rainfall is in July (8.4 mm).

For the region of Tayside, especially Dundee and its surrounding areas, the meteorological data are usually obtained from the weather station at the air base of the Royal Air Force, Leuchars. It is located 12 km south of Dundee. For comparison with the measured data, the summary of multi-year data for temperature and total rainfall gathered at this weather station from 1959 to 1992 are shown in Table 5.2 (Dundee Energy Resources Ltd., 1994).

Table 5.2 Temperature and total rainfall at Leuchars (1959 – 1992)

| Month | JAN | FEB | MAR | APR | MAY | JUN | JUL | AUG | SEP | OCT | NOV | DEC |
|---|---|---|---|---|---|---|---|---|---|---|---|---|
| Temperature (°C) | | | | | | | | | | | | |
| Max | 10.5 | 11.0 | 13.3 | 17.3 | 20.2 | 24.3 | 23.9 | 23.7 | 21.2 | 17.2 | 13.6 | 11.4 |
| Min | -4.8 | -4.0 | -2.3 | -0.7 | 2.2 | 5.1 | 6.7 | 6.2 | 3.8 | 1.0 | -2.8 | -4.0 |
| Total rainfall (mm) | 69 | 46 | 52 | 45 | 52 | 57 | 59 | 66 | 67 | 67 | 62 | 63 |

The highest temperature measured at Leuchars is 24.3 °C, representing the June data. The lowest temperature is –4.8 °C, which occurred in January. In comparison with the multi-year data collected at Leuchars, the ambient temperature measured at the 'study' station in 2000 is relatively high especially in winter. Leuchars station is located in a rural area. The station used for this study is located in an urban area. Higher ambient temperature measured at the study station may show the urban effect on climate. Heat island effects in an urban area can increase the ambient temperature especially at night (Pasquill and Smith, 1983). The multi-year average total rainfall measured at Leuchars is

705 mm, with a uniform annual distribution. The total rainfall measured at the study station is somewhat less and it shows a seasonal variation.

### 5.1.2 Distributions of wind speed and direction

Wind is the most important factor in atmospheric dispersion. In analysing distributions of wind speed and direction, the wind direction was divided into 16 sectors (N, NNE, NE, ENE, E, ESE, SE, SSE, S, SSW, SW, WSW, W, WNW, NW and NNW). Condition is regarded as calm (C) or stagnation if the wind speed is less than 1.0 m $s^{-1}$. Wind speeds greater than or equal to 1 m $s^{-1}$ are divided into four categories (1~3, 3~5, 5~7 and >7). The yearly distributions of wind direction and speed, measured at the study station are shown in Table 5.3. The yearly wind rose and the wind roses for typical months (February, May, August and November) are shown in Figure 5.1.

The prevailing wind measured at the monitoring station is westerly. The yearly average frequency for westerly wind (WSW, W and WNW) is 33.61%. The yearly average frequency for easterly wind (ENE, E and ESE) is 20.66%. The frequency for calm conditions is high in Dundee, with a yearly average value of 26.85%.

There is a seasonal variation in wind direction measured at the station. In February, the dominating wind is westerly. The frequency for westerly wind during the month is 57.70%, with the frequency for calm condition being 18.49%. As mentioned above, average wind speed is highest in February. In May, the easterly wind is more prevalent than westerly wind. During this month, the frequency for easterly wind is 32.54% while the frequency for westerly wind is 22.63%. The frequency for calm condition is 28.32%, which is similar to yearly average value. In August, the westerly wind becomes stronger again, with the frequency for westerly wind being 27.58%. The frequency for the easterly wind is 22.63%. The frequency for calm condition is 31.38%. In November, the westerly wind was more prevalent than easterly wind. The frequency for westerly wind is 32.95% while the frequency for easterly wind is 15.28%. The frequency for calm condition is 32.32%, which is higher than the yearly average value.

Table 5.3 Distributions (%) of wind direction and speed in 2000

| Month | Speed ($m\ s^{-1}$) | N | NNE | NE | ENE | E | ESE | SE | SSE | S | SSW | SW | WSW | W | WNW | NW | NNW | C | Summary |
|---|---|---|---|---|---|---|---|---|---|---|---|---|---|---|---|---|---|---|---|
| JAN | 1.0~3.0 | 0.76 | 0.45 | 0.57 | 0.79 | 0.93 | 0.57 | 0.34 | 0.23 | 0.11 | 1.13 | 2.72 | 7.85 | 15.01 | 13.63 | 6.20 | 1.50 | | 52.80 |
| | 3.0~5.0 | 0.08 | 0.06 | 0.00 | 0.00 | 0.00 | 0.00 | 0.00 | 0.06 | 0.11 | 0.28 | 0.37 | 2.32 | 4.62 | 4.90 | 2.07 | 0.40 | | 15.27 |
| | 5.0~7.0 | 0.03 | 0.00 | 0.00 | 0.00 | 0.00 | 0.00 | 0.00 | 0.00 | 0.06 | 0.17 | 0.31 | 1.42 | 1.33 | 1.22 | 0.65 | 0.08 | | 5.27 |
| | >7.0 | 0.00 | 0.00 | 0.00 | 0.00 | 0.00 | 0.00 | 0.00 | 0.00 | 0.00 | 0.00 | 0.03 | 0.06 | 0.25 | 0.20 | 0.06 | 0.00 | | 0.59 |
| | Total | 0.88 | 0.51 | 0.57 | 0.79 | 0.93 | 0.57 | 0.34 | 0.28 | 0.28 | 1.59 | 3.43 | 11.64 | 21.22 | 19.94 | 8.98 | 1.98 | 26.06 | 100.00 |
| FEB | 1.0~3.0 | 0.72 | 0.48 | 0.48 | 0.82 | 0.00 | 0.96 | 0.48 | 0.17 | 0.34 | 0.96 | 2.23 | 6.83 | 10.89 | 10.48 | 3.88 | 1.39 | | 41.10 |
| | 3.0~5.0 | 0.26 | 0.12 | 0.10 | 0.02 | 0.00 | 0.05 | 0.00 | 0.12 | 0.19 | 0.89 | 2.71 | 7.00 | 9.26 | 7.46 | 3.02 | 0.79 | | 31.99 |
| | 5.0~7.0 | 0.00 | 0.00 | 0.00 | 0.00 | 0.00 | 0.00 | 0.05 | 0.00 | 0.05 | 0.14 | 0.38 | 1.82 | 2.21 | 1.32 | 0.43 | 0.14 | | 6.55 |
| | >7.0 | 0.00 | 0.00 | 0.00 | 0.00 | 0.00 | 0.00 | 0.00 | 0.00 | 0.00 | 0.00 | 0.12 | 0.22 | 0.12 | 0.10 | 0.00 | 0.00 | | 0.55 |
| | Total | 0.98 | 0.60 | 0.58 | 0.84 | 1.32 | 1.01 | 0.53 | 0.29 | 0.58 | 1.99 | 5.44 | 15.88 | 22.47 | 19.35 | 7.34 | 2.33 | 18.49 | 100.00 |
| MAR | 1.0~3.0 | 0.68 | 0.68 | 1.12 | 3.19 | 4.11 | 2.99 | 0.92 | 0.51 | 0.66 | 0.75 | 2.55 | 6.01 | 8.51 | 9.27 | 3.65 | 0.92 | | 46.52 |
| | 3.0~5.0 | 0.19 | 0.19 | 0.29 | 0.63 | 0.63 | 0.85 | 0.41 | 0.15 | 0.32 | 0.34 | 1.43 | 4.23 | 6.37 | 6.30 | 2.70 | 0.78 | | 25.83 |
| | 5.0~7.0 | 0.00 | 0.00 | 0.07 | 0.15 | 0.22 | 0.34 | 0.17 | 0.12 | 0.02 | 0.07 | 0.07 | 0.61 | 0.49 | 0.78 | 0.34 | 0.07 | | 3.53 |
| | >7.0 | 0.00 | 0.00 | 0.00 | 0.00 | 0.00 | 0.00 | 0.00 | 0.00 | 0.00 | 0.00 | 0.00 | 0.00 | 0.05 | 0.07 | 0.00 | 0.00 | | 0.12 |
| | Total | 0.88 | 0.88 | 1.48 | 3.96 | 4.96 | 4.18 | 1.51 | 0.78 | 1.00 | 1.17 | 4.06 | 10.85 | 15.42 | 16.42 | 6.69 | 1.78 | 24.00 | 100.00 |
| APR | 1.0~3.0 | 0.88 | 1.40 | 3.79 | 7.38 | 8.03 | 4.87 | 1.47 | 0.78 | 0.82 | 1.01 | 2.25 | 1.73 | 7.38 | 5.78 | 2.48 | 1.14 | | 51.21 |
| | 3.0~5.0 | 0.16 | 0.33 | 1.24 | 3.85 | 4.57 | 1.47 | 0.36 | 0.03 | 0.10 | 0.07 | 0.52 | 0.62 | 0.75 | 3.46 | 0.16 | 0.10 | | 17.80 |
| | 5.0~7.0 | 0.10 | 0.36 | 0.65 | 1.86 | 1.44 | 0.29 | 0.03 | 0.00 | 0.00 | 0.00 | 0.03 | 0.00 | 0.03 | 0.03 | 0.00 | 0.00 | | 4.83 |
| | >7.0 | 0.00 | 0.00 | 0.00 | 0.00 | 0.03 | 0.00 | 0.00 | 0.00 | 0.00 | 0.00 | 0.00 | 0.00 | 0.00 | 0.00 | 0.00 | 0.00 | | 0.03 |
| | Total | 1.14 | 2.09 | 5.68 | 13.10 | 14.08 | 6.63 | 1.86 | 0.82 | 0.95 | 1.08 | 2.81 | 2.35 | 8.16 | 9.27 | 2.65 | 1.24 | 26.09 | 100.00 |

Table 5.3 (Continue)

| Month | Speed ($m\ s^{-1}$) | N | NNE | NE | ENE | E | ESE | SE | SSE | S | SSW | SW | WSW | W | WNW | NW | NNW | C | Summary |
|---|---|---|---|---|---|---|---|---|---|---|---|---|---|---|---|---|---|---|---|
| MAY | 1.0~3.0 | 0.39 | 0.73 | 2.90 | 6.84 | 7.94 | 6.38 | 1.78 | 0.51 | 0.51 | 0.68 | 1.39 | 7.57 | 6.82 | 3.92 | 2.90 | 0.93 | | 52.19 |
| | 3.0~5.0 | 0.07 | 0.12 | 0.85 | 2.44 | 4.19 | 3.87 | 1.00 | 0.29 | 0.12 | 0.19 | 0.44 | 1.44 | 1.61 | 1.27 | 0.34 | 0.17 | | 18.41 |
| | 5.0~7.0 | 0.00 | 0.00 | 0.00 | 0.15 | 0.22 | 0.51 | 0.12 | 0.02 | 0.00 | 0.00 | 0.05 | 0.00 | 0.00 | 0.00 | 0.00 | 0.00 | | 1.07 |
| | >7.0 | 0.00 | 0.00 | 0.00 | 0.00 | 0.00 | 0.00 | 0.00 | 0.00 | 0.00 | 0.00 | 0.00 | 0.00 | 0.00 | 0.00 | 0.00 | 0.00 | | 0.00 |
| | Total | 0.46 | 0.85 | 3.75 | 9.43 | 12.35 | 10.76 | 2.90 | 0.83 | 0.63 | 0.88 | 1.88 | 9.01 | 8.43 | 5.19 | 3.24 | 1.10 | 28.32 | 100.00 |
| JUN | 1.0~3.0 | 0.52 | 1.47 | 4.01 | 8.61 | 8.54 | 5.05 | 1.97 | 0.85 | 0.62 | 1.04 | 2.32 | 5.05 | 8.02 | 6.88 | 2.73 | 0.93 | | 58.61 |
| | 3.0~5.0 | 0.14 | 0.05 | 0.55 | 1.85 | 2.75 | 2.99 | 0.66 | 0.12 | 0.17 | 0.45 | 0.71 | 3.08 | 2.99 | 2.23 | 0.76 | 0.12 | | 19.62 |
| | 5.0~7.0 | 0.00 | 0.00 | 0.00 | 0.00 | 0.07 | 0.19 | 0.00 | 0.02 | 0.02 | 0.05 | 0.28 | 0.45 | 0.88 | 0.55 | 0.14 | 0.07 | | 2.73 |
| | >7.0 | 0.00 | 0.00 | 0.00 | 0.00 | 0.00 | 0.00 | 0.00 | 0.00 | 0.00 | 0.00 | 0.00 | 0.00 | 0.00 | 0.00 | 0.00 | 0.00 | | 0.00 |
| | Total | 0.66 | 1.52 | 4.55 | 10.46 | 11.36 | 8.23 | 2.63 | 1.00 | 0.81 | 1.54 | 3.32 | 8.59 | 11.88 | 9.65 | 3.63 | 1.11 | 19.05 | 100.00 |
| JUL | 1.0~3.0 | 0.61 | 1.04 | 3.73 | 7.86 | 15.90 | 7.45 | 2.06 | 0.79 | 0.50 | 0.68 | 1.36 | 3.79 | 7.68 | 6.42 | 2.28 | 1.04 | | 63.18 |
| | 3.0~5.0 | 0.02 | 0.11 | 0.50 | 1.33 | 2.53 | 2.53 | 0.66 | 0.14 | 0.09 | 0.05 | 0.18 | 0.45 | 0.90 | 1.13 | 0.32 | 0.05 | | 10.98 |
| | 5.0~7.0 | 0.00 | 0.00 | 0.00 | 0.00 | 0.00 | 0.00 | 0.00 | 0.00 | 0.00 | 0.00 | 0.00 | 0.00 | 0.00 | 0.00 | 0.00 | 0.00 | | 0.00 |
| | >7.0 | 0.00 | 0.00 | 0.00 | 0.00 | 0.00 | 0.00 | 0.00 | 0.00 | 0.00 | 0.00 | 0.00 | 0.00 | 0.00 | 0.00 | 0.00 | 0.00 | | 0.00 |
| | Total | 0.63 | 1.15 | 4.22 | 9.10 | 18.43 | 9.98 | 2.71 | 0.93 | 0.59 | 0.72 | 1.54 | 4.25 | 8.58 | 7.54 | 2.60 | 1.08 | 25.93 | 100.00 |
| AUG | 1.0~3.0 | 0.48 | 1.35 | 3.41 | 6.50 | 6.92 | 5.02 | 1.69 | 0.80 | 0.48 | 0.89 | 2.13 | 6.05 | 8.80 | 8.04 | 3.25 | 1.51 | | 57.33 |
| | 3.0~5.0 | 0.05 | 0.09 | 0.32 | 0.87 | 1.63 | 1.69 | 0.53 | 0.11 | 0.02 | 0.07 | 0.62 | 1.28 | 1.74 | 1.67 | 0.44 | 0.16 | | 11.29 |
| | 5.0~7.0 | 0.00 | 0.00 | 0.00 | 0.00 | 0.00 | 0.00 | 0.00 | 0.00 | 0.00 | 0.00 | 0.00 | 0.00 | 0.00 | 0.00 | 0.00 | 0.00 | | 0.00 |
| | >7.0 | 0.00 | 0.00 | 0.00 | 0.00 | 0.00 | 0.00 | 0.00 | 0.00 | 0.00 | 0.00 | 0.00 | 0.00 | 0.00 | 0.00 | 0.00 | 0.00 | | 0.00 |
| | Total | 0.53 | 1.44 | 3.73 | 7.38 | 8.54 | 6.71 | 2.22 | 0.92 | 0.50 | 0.96 | 2.75 | 7.33 | 10.54 | 9.71 | 3.69 | 1.67 | 31.38 | 100.00 |

Table 5.3 (Continue)

| Month | Speed ($m\ s^{-1}$) | N | NNE | NE | ENE | E | ESE | SE | SSE | S | SSW | SW | WSW | W | WNW | NW | NNW | C | Summary |
|---|---|---|---|---|---|---|---|---|---|---|---|---|---|---|---|---|---|---|---|
| SEP | 1.0~3.0 | 0.62 | 1.43 | 3.01 | 6.98 | 6.58 | 3.94 | 1.36 | 0.59 | 0.64 | 0.89 | 2.27 | 5.47 | 7.82 | 5.05 | 3.11 | 1.08 | | 50.84 |
| | 3.0~5.0 | 0.10 | 0.42 | 1.63 | 3.62 | 3.60 | 2.86 | 0.81 | 0.25 | 0.12 | 0.15 | 0.44 | 1.16 | 1.04 | 0.99 | 0.47 | 0.10 | | 17.75 |
| | 5.0~7.0 | 0.00 | 0.00 | 0.10 | 0.10 | 0.35 | 0.47 | 0.27 | 0.00 | 0.00 | 0.00 | 0.07 | 0.10 | 0.12 | 0.12 | 0.07 | 0.00 | | 1.78 |
| | >7.0 | 0.00 | 0.00 | 0.00 | 0.10 | 0.12 | 0.22 | 0.07 | 0.00 | 0.00 | 0.00 | 0.00 | 0.00 | 0.00 | 0.00 | 0.00 | 0.00 | | 0.52 |
| | Total | 0.71 | 1.85 | 4.73 | 10.80 | 10.65 | 7.50 | 2.51 | 0.84 | 0.76 | 1.04 | 2.79 | 6.73 | 8.97 | 6.16 | 3.65 | 1.18 | 29.12 | 100.00 |
| OCT | 1.0~3.0 | 0.28 | 0.50 | 0.99 | 2.15 | 3.66 | 2.87 | 1.38 | 0.72 | 0.77 | 1.67 | 3.40 | 8.11 | 11.46 | 8.76 | 2.89 | 0.92 | | 50.53 |
| | 3.0~5.0 | 0.04 | 0.09 | 0.11 | 0.35 | 0.53 | 0.50 | 0.46 | 0.09 | 0.07 | 0.20 | 1.07 | 1.86 | 2.94 | 2.39 | 0.72 | 0.15 | | 11.57 |
| | 5.0~7.0 | 0.02 | 0.00 | 0.04 | 0.09 | 0.20 | 0.35 | 0.11 | 0.00 | 0.02 | 0.04 | 0.26 | 0.39 | 0.57 | 0.22 | 0.04 | 0.00 | | 2.37 |
| | >7.0 | 0.00 | 0.00 | 0.02 | 0.00 | 0.00 | 0.04 | 0.00 | 0.00 | 0.00 | 0.04 | 0.15 | 0.20 | 0.20 | 0.26 | 0.00 | 0.00 | | 0.92 |
| | Total | 0.35 | 0.59 | 1.16 | 2.59 | 4.38 | 3.77 | 1.95 | 0.83 | 0.85 | 1.95 | 4.89 | 10.60 | 15.16 | 13.83 | 3.66 | 1.07 | 32.36 | 100.00 |
| NOV | 1.0~3.0 | 0.46 | 1.09 | 2.01 | 4.07 | 4.51 | 2.80 | 1.20 | 0.44 | 0.42 | 0.93 | 2.75 | 6.76 | 12.80 | 9.70 | 3.66 | 1.06 | | 54.68 |
| | 3.0~5.0 | 0.09 | 0.23 | 0.81 | 1.53 | 1.53 | 0.53 | 0.32 | 0.14 | 0.12 | 0.09 | 0.39 | 1.00 | 1.74 | 1.48 | 0.35 | 0.19 | | 10.53 |
| | 5.0~7.0 | 0.02 | 0.02 | 0.39 | 0.72 | 0.42 | 0.16 | 0.09 | 0.00 | 0.00 | 0.00 | 0.09 | 0.14 | 0.16 | 0.05 | 0.00 | 0.07 | | 2.34 |
| | >7.0 | 0.00 | 0.00 | 0.00 | 0.00 | 0.00 | 0.00 | 0.00 | 0.00 | 0.00 | 0.00 | 0.02 | 0.07 | 0.00 | 0.00 | 0.00 | 0.05 | | 0.14 |
| | Total | 0.58 | 1.34 | 3.22 | 6.32 | 6.46 | 3.50 | 1.62 | 0.58 | 0.53 | 1.02 | 3.26 | 7.96 | 14.70 | 11.23 | 4.00 | 1.37 | 32.31 | 100.00 |
| DEC | 1.0~3.0 | 0.54 | 0.65 | 2.12 | 4.21 | 5.68 | 4.42 | 2.12 | 1.01 | 0.72 | 1.19 | 2.25 | 5.04 | 6.12 | 8.08 | 2.27 | 2.45 | | 48.86 |
| | 3.0~5.0 | 0.13 | 0.05 | 0.46 | 0.49 | 1.08 | 1.03 | 0.46 | 0.18 | 0.23 | 0.46 | 1.34 | 4.75 | 4.80 | 2.76 | 0.39 | 0.75 | | 19.40 |
| | 5.0~7.0 | 0.00 | 0.05 | 0.10 | 0.36 | 0.18 | 0.05 | 0.03 | 0.03 | 0.05 | 0.15 | 0.23 | 0.93 | 0.77 | 0.44 | 0.10 | 0.05 | | 3.54 |
| | >7.0 | 0.00 | 0.00 | 0.00 | 0.00 | 0.00 | 0.00 | 0.00 | 0.00 | 0.00 | 0.00 | 0.03 | 0.03 | 0.08 | 0.00 | 0.00 | 0.00 | | 0.13 |
| | Total | 0.67 | 0.75 | 2.69 | 5.06 | 6.95 | 5.50 | 2.61 | 1.21 | 1.01 | 1.81 | 3.85 | 10.74 | 11.78 | 11.29 | 2.76 | 3.25 | 28.07 | 100.00 |

Table 5.3 (Continue)

| Annual | Speed ($m\ s^{-1}$) | N | NNE | NE | ENE | E | ESE | SE | SSE | S | SSW | SW | WSW | W | WNW | NW | NNW | C | Summary |
|---|---|---|---|---|---|---|---|---|---|---|---|---|---|---|---|---|---|---|---|
| | 1.0~3.0 | 0.57 | 0.94 | 2.34 | 4.95 | 6.12 | 3.97 | 1.41 | 0.62 | 0.55 | 0.99 | 2.30 | 5.94 | 9.29 | 7.99 | 3.25 | 1.23 | | 52.45 |
| | 3.0~5.0 | 0.11 | 0.15 | 0.56 | 1.37 | 1.87 | 1.55 | 0.48 | 0.14 | 0.14 | 0.27 | 0.86 | 2.44 | 3.24 | 2.95 | 0.98 | 0.31 | | 17.41 |
| | 5.0~7.0 | 0.01 | 0.03 | 0.10 | 0.25 | 0.23 | 0.20 | 0.07 | 0.02 | 0.02 | 0.05 | 0.15 | 0.48 | 0.54 | 0.39 | 0.14 | 0.04 | | 2.72 |
| | >7.0 | 0.00 | 0.00 | 0.00 | 0.01 | 0.01 | 0.02 | 0.01 | 0.00 | 0.00 | 0.00 | 0.03 | 0.05 | 0.06 | 0.05 | 0.00 | 0.00 | | 0.25 |
| | Total | 0.69 | 1.12 | 3.00 | 6.57 | 8.36 | 5.74 | 1.97 | 0.78 | 0.70 | 1.31 | 3.34 | 8.91 | 13.12 | 11.58 | 4.38 | 1.58 | 26.85 | 100.00 |
| Leuchars | | 2.85 | | 3.57 | 6.16 | 7.94 | | 5.76 | 2.82 | 2.57 | | 9.08 | 29.30 | 9.20 | | 4.07 | 2.42 | | 100.00 |

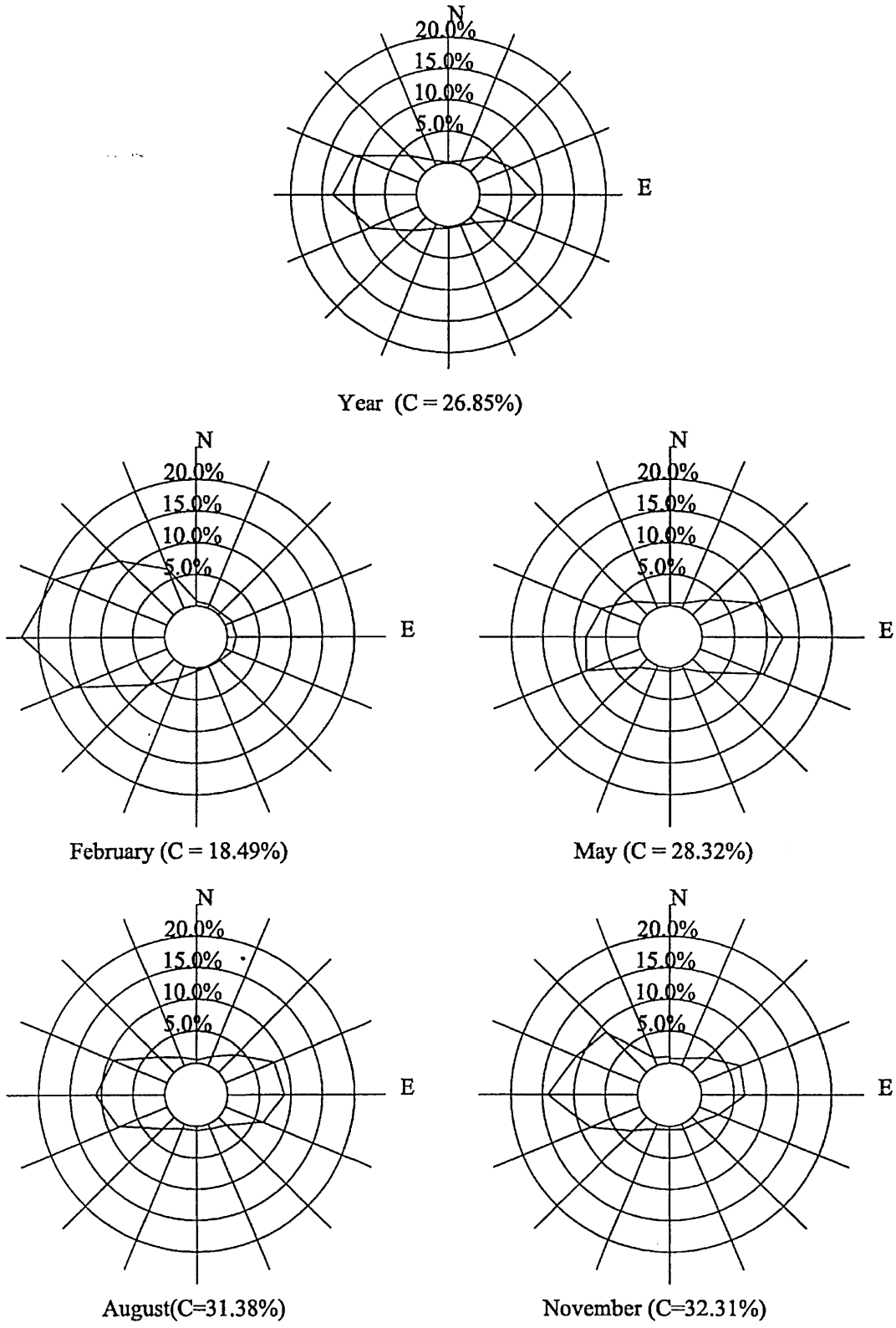


Figure 5.1 Yearly wind rose and typical monthly wind rose measured at the station in 2000

For comparison purposes, the multi-year monitoring results (1959 ~ 1992) for wind direction at Leuchars are also shown in Table 5.3. The method used to divide the wind direction is different in the data obtained from the weather station at Leuchars. The wind direction is divided into 12 categories (i.e. with 30° sector width) and no calm condition has been defined. The south westerly wind (240°) is the prevailing wind in the Leuchars data. Its frequency is 29.30%. The frequency for westerly wind (240°, 270° and 300°) is 42.57% while the frequency for easterly wind (60°, 90° and 120°) is 18.86%.

There are some differences in the distribution of wind direction between the data measured at the study station and Leuchars. The prevailing wind measured at the study station is westerly while the prevailing wind measured at Leuchars is south westerly. The ratio of westerly wind frequency to easterly wind frequency is 1.63 at the study station. It is 2.26 at Leuchars. The frequency for easterly wind at the study station is higher than that at Leuchars. The wind direction data measured at the study station shows the effect of local landscape on the monitoring result. There is an east-west oriented hill located at about 150m north of the study monitoring station. The wind direction may have been modified by this hill. Thus, the wind direction measured at the station is mainly westerly and easterly.

The wind speed measured at the study monitoring station is relatively low. The yearly average wind speed is 1.9 m $s^{-1}$. 52% of wind speed varies between 1.0 ~ 3.0 m $s^{-1}$. Including calm condition, 79.30% of wind speed is less than 3.0 m $s^{-1}$. Another 17.41% of wind speed varies between 3.0 ~ 5.0 m $s^{-1}$. Only about 2.97% of wind speed is higher than 5.0 m $s^{-1}$.

### 5.1.3 Daily variations of wind speed and direction

The daily variations of wind speed and wind direction distributions measured at the study station are shown in Figures 5.2 and 5.3.

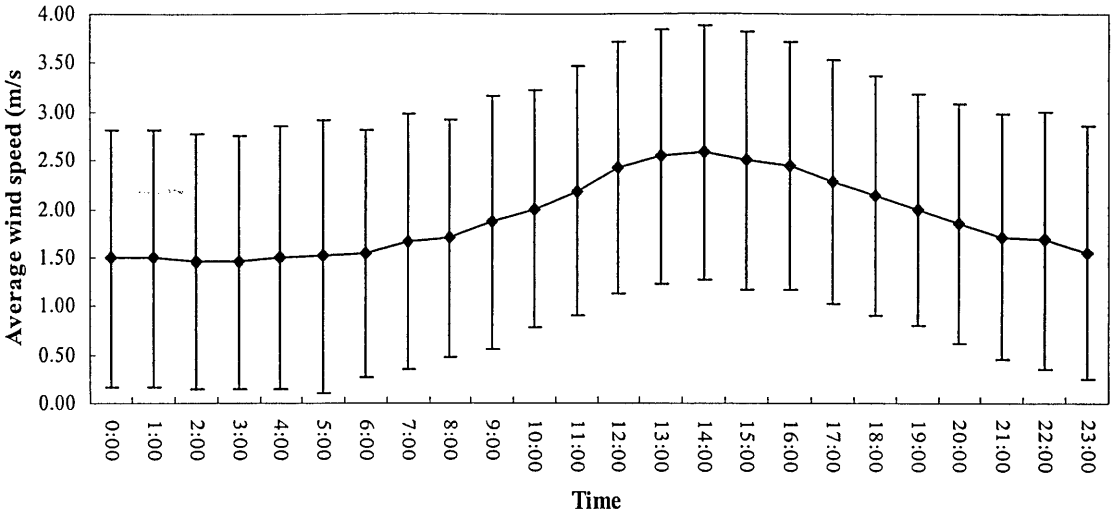


Figure 5.2 Daily variation of wind speed at the study station

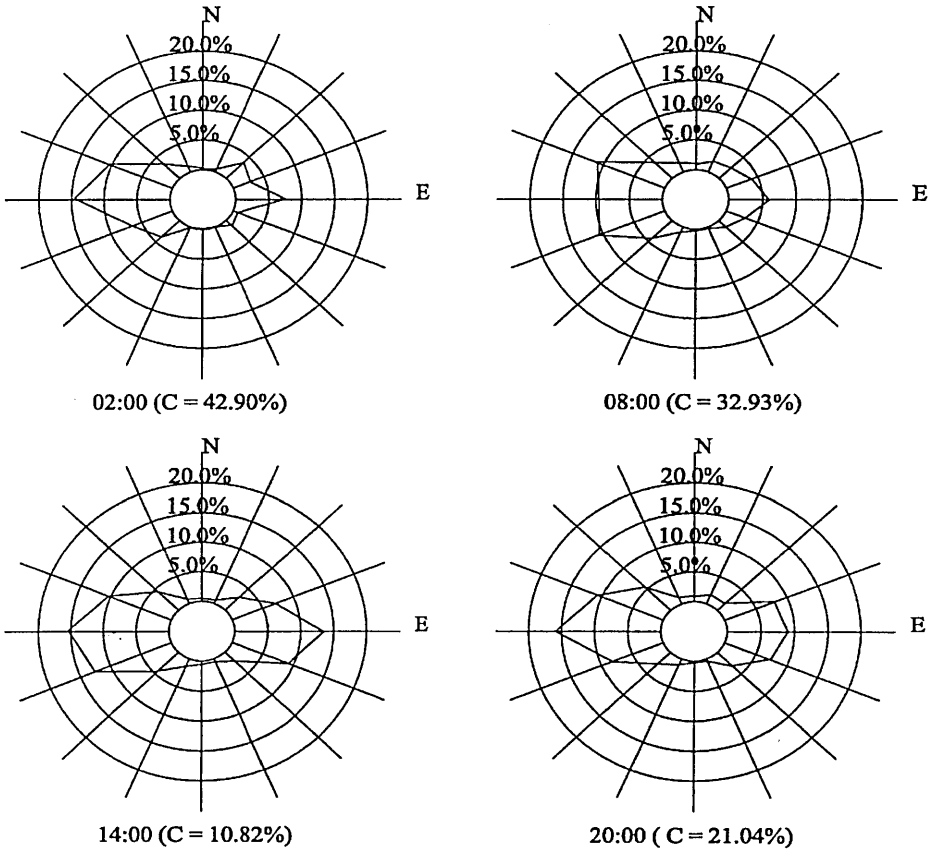


Figure 5.3 Daily variation of wind direction at the study station

This information (Figure 5.2) suggests a definite daily variation for wind speed in Dundee. Wind speed measured at the study station is high during daytime and low at night (Figure 5.2). Highest average wind speed is 2.5 m $s^{-1}$. It occurred at 14:00. The frequency for calm condition is only 10.82% at this time. The lowest average wind speed is 1.5 m $s^{-1}$, which occurred at 03:00. The frequency for calm condition is 42.90% at 02:00. Although it is not as obvious as the wind speed, the distributions of wind direction measured at the study station also show regular daily variation. The frequency of easterly wind increases in the afternoon (14:00) and at early night time (20:00). This frequency decreases at late night and in the morning.

Dundee is a coastal city. On the eastern side of the city is the North Sea. The daily variations of wind speed and wind direction show the effect of sea-land boundary layer on the local wind field. Although the wind measured at the study station is mainly dominated by large weather systems, local sea-land boundary can affect daily variation of wind speed and direction. During the period that sea breeze occurs (afternoon and early night), the frequency of easterly wind increases and the frequency of calm condition decreases.

## 5.2 NO, $NO_2$ and NOx data

### 5.2.1 Summary of NO, $NO_2$ and NOx data

NOx is one of the major gaseous pollutants that can cause concerns in the UK. The concentrations of NO, $NO_2$ and NOx were measured continually at the study station for one year. A summary of the data for one hour mean concentrations of NO, $NO_2$ and NOx in 2000 is shown in Table 5.4.

In year 2000, variation range of one hour mean concentration measured at the station is 0.000 to 0.323 ppm for NO, 0.000 to 0.049 ppm for $NO_2$ and 0.000 to 0.372 ppm for NOx. The highest concentrations of NO, $NO_2$ and NOx occurred at the same time, at 16:30 on 18 December 2000. These peak concentrations coincide with a traffic rush time on a Monday afternoon. On 18 December 2000, the weather was calm, dry and cold. The calm condition continued for more than 20 hours. During the daytime on 18 December 2000, the highest wind speed measured at the station was only 1.3 m $s^{-1}$. The daily average wind speed was just 0.4 m $s^{-1}$. There was no rainfall in the 5 days period to 18 December 2000. The ambient temperature was low and stable. The daily averaged ambient temperature measured at the station was 4.4 °C. The highest temperature was only 5.5 °C.

At 16:30 on the day, the wind speed measured at the station was 0.0 m $s^{-1}$ and the ambient temperature was 3.8 °C, the lowest temperature for the whole day.

Table 5.4 Summary of one hour average concentrations of NO, $NO_2$ and NOx (ppm)

| | NO | | | | $NO_2$ | | | | NOx | | | |
|---|---|---|---|---|---|---|---|---|---|---|---|---|
| | Max | Min | Average | SD* | Max | Min | Average | SD | Max | Min | Average | SD |
| JAN | 0.152 | 0.000 | 0.010 | 0.020 | 0.041 | 0.001 | 0.015 | 0.010 | 0.188 | 0.001 | 0.025 | 0.028 |
| FEB | 0.130 | 0.000 | 0.006 | 0.013 | 0.041 | 0.001 | 0.013 | 0.009 | 0.171 | 0.001 | 0.019 | 0.020 |
| MAR | 0.053 | 0.000 | 0.003 | 0.005 | 0.035 | 0.001 | 0.011 | 0.007 | 0.073 | 0.001 | 0.014 | 0.010 |
| APR | 0.055 | 0.000 | 0.003 | 0.005 | 0.039 | 0.002 | 0.012 | 0.007 | 0.074 | 0.002 | 0.015 | 0.010 |
| MAY | 0.054 | 0.000 | 0.003 | 0.005 | 0.044 | 0.002 | 0.011 | 0.006 | 0.087 | 0.002 | 0.014 | 0.010 |
| JUN | 0.037 | 0.000 | 0.003 | 0.004 | 0.043 | 0.000 | 0.009 | 0.006 | 0.067 | 0.000 | 0.012 | 0.009 |
| JUL | 0.036 | 0.000 | 0.002 | 0.004 | 0.022 | 0.000 | 0.007 | 0.004 | 0.051 | 0.000 | 0.009 | 0.007 |
| AUG | 0.053 | 0.000 | 0.004 | 0.005 | 0.029 | 0.000 | 0.009 | 0.005 | 0.061 | 0.000 | 0.012 | 0.009 |
| SEP | 0.074 | 0.000 | 0.005 | 0.007 | 0.032 | 0.001 | 0.012 | 0.006 | 0.099 | 0.001 | 0.016 | 0.012 |
| OCT | 0.070 | 0.000 | 0.005 | 0.008 | 0.037 | 0.000 | 0.013 | 0.007 | 0.103 | 0.000 | 0.019 | 0.014 |
| NOV | 0.277 | 0.000 | 0.010 | 0.023 | 0.045 | 0.001 | 0.016 | 0.009 | 0.322 | 0.001 | 0.027 | 0.029 |
| DEC | 0.323 | 0.000 | 0.016 | 0.036 | 0.049 | 0.000 | 0.018 | 0.010 | 0.372 | 0.001 | 0.034 | 0.043 |
| Year | 0.323 | 0.000 | 0.006 | 0.014 | 0.049 | 0.000 | 0.012 | 0.008 | 0.372 | 0.000 | 0.017 | 0.020 |

* SD Standard Deviation

The variations of concentrations of NO, $NO_2$ and NOx measured at the station are inversely proportional to the ambient temperature. The higher concentrations appear in November, December and January with lower ambient temperature. The highest monthly mean concentrations of NO, $NO_2$ and NOx are in December. The lower concentrations appear in June, July and August with higher ambient temperature. The lowest monthly mean concentrations of NO, $NO_2$ and NOx are in July. The annual variations of NO, $NO_2$ and NOx concentrations with ambient temperature measured at the station show similar characteristics to the variation of vehicular NOx emission with ambient temperature. The lower the ambient temperature is, the higher the NOx emitted by vehicle. It implies that traffic emission is the major source that affects the NOx concentration at the station.

The annual mean concentrations of NO, $NO_2$ and NOx measured at the station in 2000 are 0.006 ppm, 0.012 ppm and 0.017 ppm, respectively.

The air quality standards for $NO_2$ have been recommended in the UK National Air Quality Strategy (Department of the Environment, Transport and the Regions, 1999). They are 0.150 ppm for one hour mean concentration (maximum of 18 exceedances per year)

and 0.021 ppm for annual mean concentration. The maximum one hour mean concentration of $NO_2$ measured at the station in 2000 is 0.049 ppm. This is much less than the concentration objective value in the air quality strategy. The annual mean concentration of $NO_2$ measured at the station in 2000 is 0.012 ppm. It is also less than the concentration value in the air quality strategy.

### 5.2.2 Daily variations of NO, $NO_2$ and NOx

According to the source emission survey discussed in Chapter 3, traffic emission is the major air pollution source in Dundee. The annual variations of concentrations of NO, $NO_2$ and NOx imply that vehicle emission is the major source that affects NOx data at the station. The daily variation of road traffic flow is different on weekdays and at weekends (see section 3.3.3). For analysing the daily variations of concentrations, the NO, $NO_2$ and NOx data have been divided into two parts, weekdays and weekends. The average daily variations of concentrations of NO, $NO_2$ and NOx on weekdays are shown in Figures 5.4.

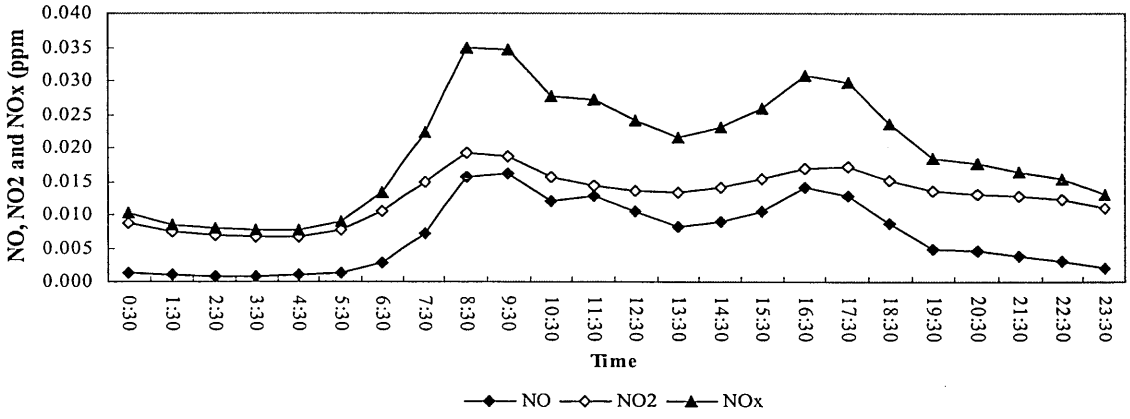


Figure 5.4 Average daily variations of concentrations of NO, $NO_2$ and NOx on weekdays

The average daily variations of hourly mean concentrations of NO, $NO_2$ and NOx on weekdays correlate well with the daily variation of traffic flow on arterial and feeder roads in Dundee (Figures 3.2 and 3.3). There are two peaks and two troughs in the curves describing the daily variations of concentrations. 08:30, the time of the first peak concentrations, coincides with the time of the first of the traffic flow peaks. However, the duration of the first peak concentrations is about one hour longer than the traffic flow peak. The time that second peak concentrations occurred and the duration of the second peak concentrations coincide well with the characteristics of the second traffic peak. The values of the second peaks for concentrations of NO, $NO_2$ and NOx are generally lower than the

values of the first peaks. However, the values of the second peaks for traffic flow are generally higher than the values of the first peaks. Like traffic flow, the average daily variation of NO is sharper than the average daily variation of $NO_2$. Most of the NOx emitted freshly by vehicle is NO. Most of $NO_2$ is formed by oxidation of NO in atmospheric environment. Thus, daily variation of concentration of NO shows the effect of traffic flow variation directly.

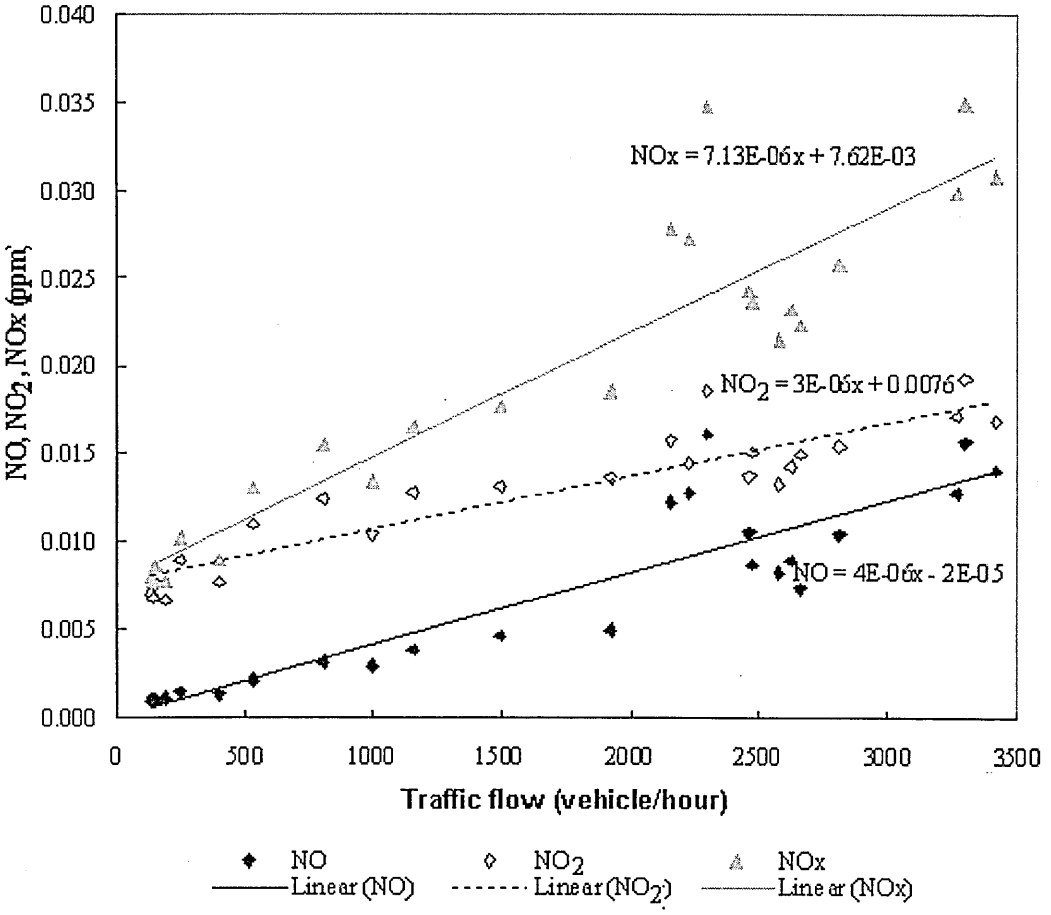


Figure 5.5 Linear relationships of NO, $NO_2$, NOx and Traffic flow on weekdays

The linear relationships between hourly average concentrations of NO, $NO_2$, NOx and hourly traffic flows on arterial road on weekdays are shown in Figure 5.5. The linear correlations between hourly average concentrations of NO, $NO_2$, NOx and traffic flows are good on weekdays with the values of correlation coefficients ($r$) of 0.90 for NO, 0.92 for $NO_2$ and 0.93 for NOx. The small scatter evident in Figure 5.5 probably represents the effect of meteorological parameters, which have not been plotted in the figure.

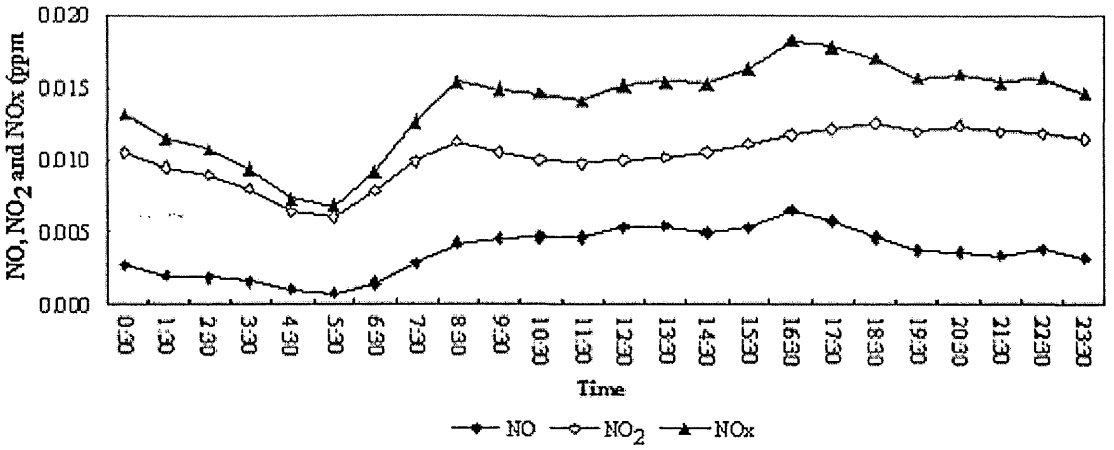


Figure 5.6 Average daily variations of concentrations of NO, $NO_2$ and NOx at weekends

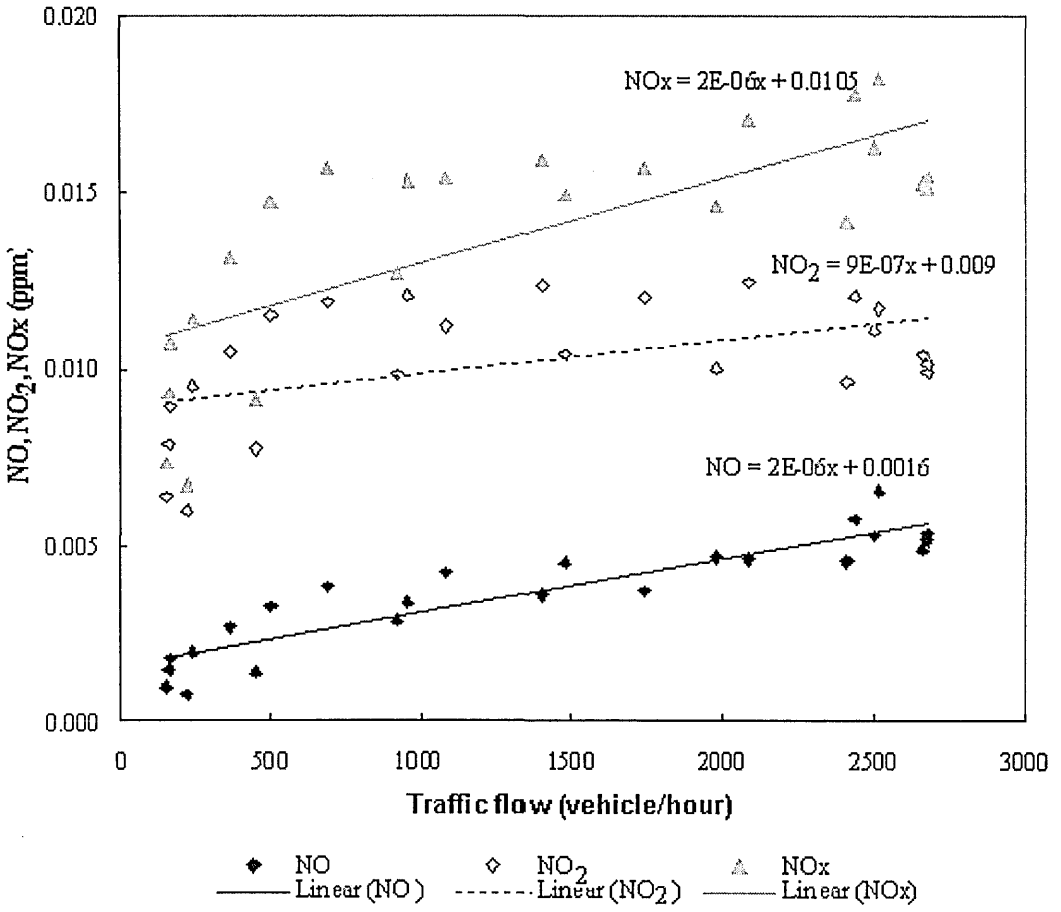


Figure 5.7 Linear relationships of NO, $NO_2$, NOx and Traffic flow at weekends

The average daily variations of concentrations of NO, $NO_2$ and NOx at weekends are shown in Figure 5.6. They are also similar to the daily variation of traffic flow on

arterial and feeder roads at weekends. There is only one clear peak, with relatively lower value than on weekdays but the duration of the peak is much longer. The time of the peak concentration and the duration of peak concentration for NO are identical to those for the traffic flow. However, the duration of the peak concentration for $NO_2$ and NOx is much longer than for the traffic flow.

The linear relationships between hourly average concentrations of NO, $NO_2$, NOx and hourly traffic flows on arterial road at weekends are shown in Figure 5.7. The linear correlation between hourly average concentrations of NO and traffic flows at weekends is as good as that on weekdays. The correlation coefficient (r) is 0.91. However, the linear correlation between hourly average concentrations of $NO_2$ and traffic flows at weekends is not as good as that for the weekdays, with a value of 0.49 for the correlation coefficient (r), probably because traffic emission source reduces at weekends. The correlation coefficient (r) for NOx vs traffic flow is 0.75 at weekends.

### 5.2.3 Variations of NO, $NO_2$ and NOx with wind speed, wind direction and temperature

The concentrations of NO, $NO_2$ and NOx measured at the study station depend on emission sources and various weather factors such as wind speed, wind direction and ambient temperature. The average daily variations of concentrations of NO, $NO_2$ and NOx have proved further that road traffic emission is the major NOx emission source that affects the data measured at the station. The road traffic emission source has a daily variation. This daily variation is different on a weekday and at weekends. For the analysis of the variations of NO, $NO_2$ and NOx with wind speed, wind direction and ambient temperature separately, the hourly average concentrations of NO, $NO_2$ and NOx collected at the station in 2000 were divided by the hourly traffic flows (TF) on arterial road (Kingsway). The variations of the ratio of concentrations of NO, $NO_2$, NOx and traffic flows with wind speed, wind direction and ambient temperature are shown in Figures 5.8, 5.9 and 6.0.

Although the plots of the ratios of concentrations of nitrogen oxides to traffic flows vs. wind speed contain scattered point, the plots show weak trends. These trends are possible marked by the influence of some other relevant factors, but they generally show that the ratio of the concentrations of nitrogen oxides to traffic flows are generally inversely proportional to wind speed. (Figures 5.8). The regression analysis indicates that

the exponential regressions can approximately describe the variations of the ratios of the concentrations of nitrogen oxides and traffic flows with wind speed. The correlation coefficients ($r$) are 0.41, 0.51 and 0.56 for NO, $NO_2$ and $NO_x$, respectively.

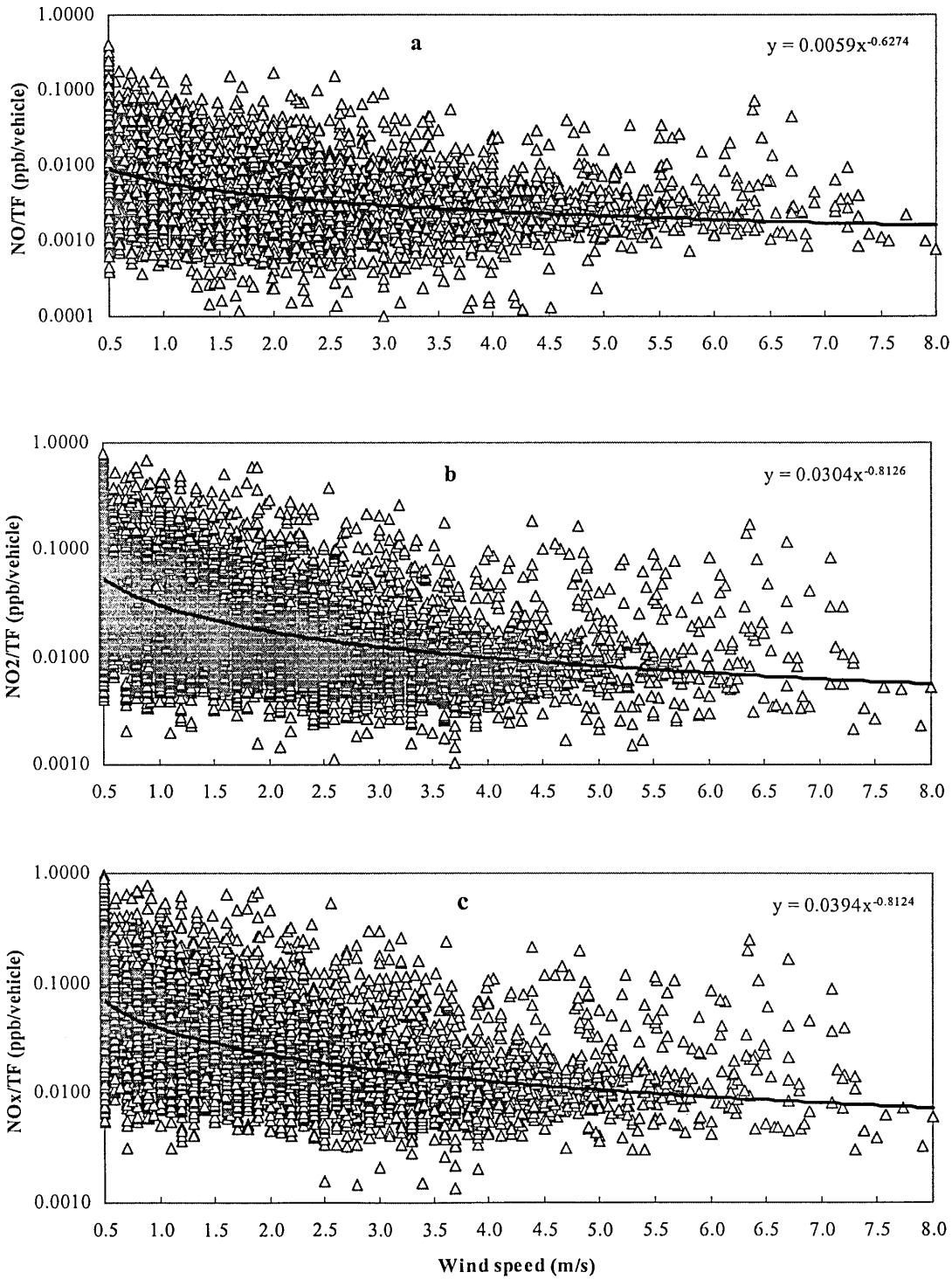


Figure 5.8 Variations of NO, $NO_2$ and NOx with wind speed

The variation of airborne pollutant with wind direction can show the direction of major air pollution sources that affect the receptor. Figure 5.9 indicates that the effect of wind direction on the ratios of concentrations of NO, $NO_2$ and NOx and traffic flows is less. It is simply that there is no special NOx emission source in an aspect that may significantly affect the monitoring results at the study station.

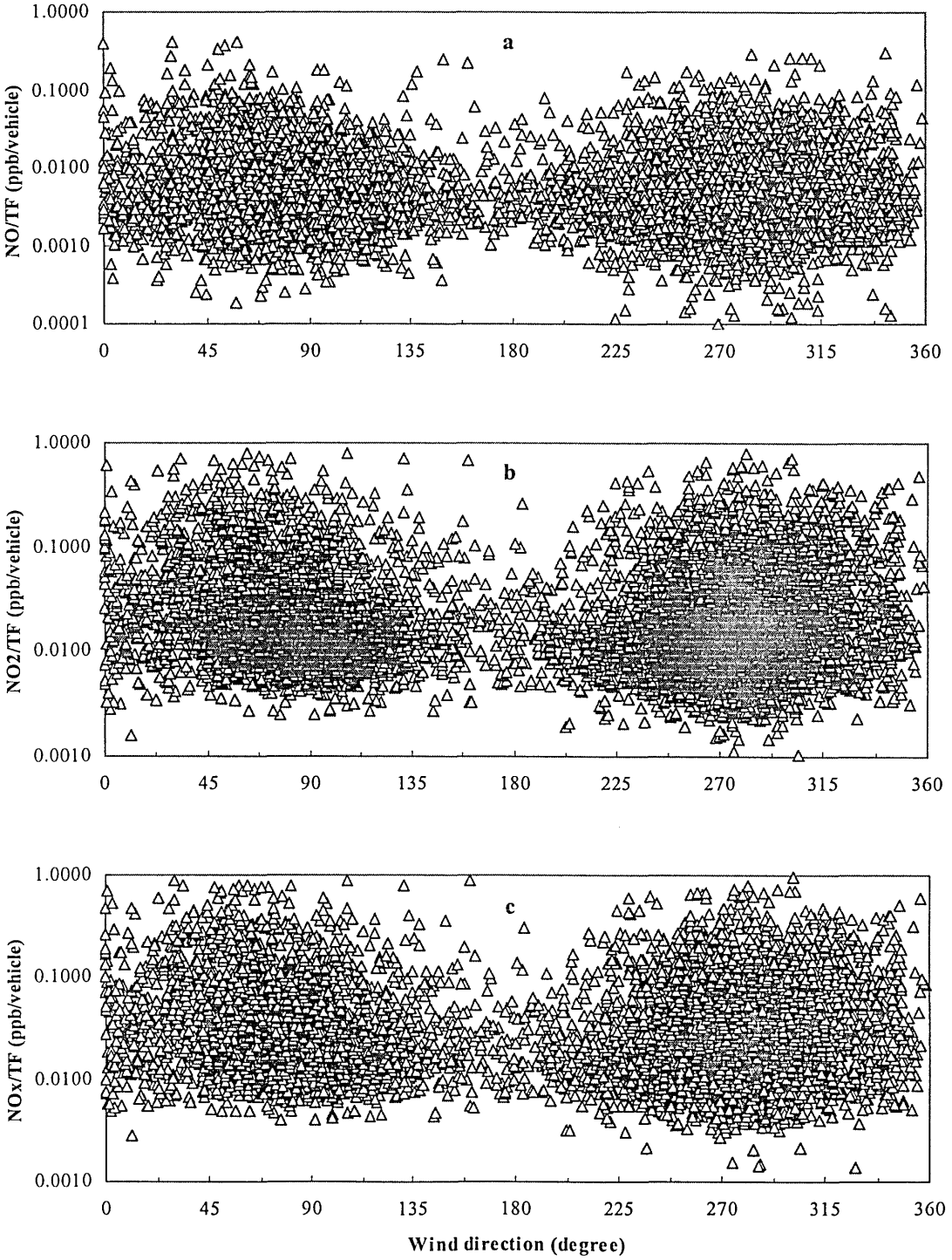


Figure 5.9 Variations of NO, $NO_2$ and NOx with wind direction

The relationship of the ratios of concentrations of nitrogen oxides and traffic flows with ambient temperature is scattered. Exponential regression can approximately describe the decreases of the ratios of nitrogen oxides and traffic flows with ambient temperature (Figure 5.10). The correlation coefficients ($r$) are 0.27, 0.40 and 0.39 for NO, $NO_2$ and $NO_x$, respectively.

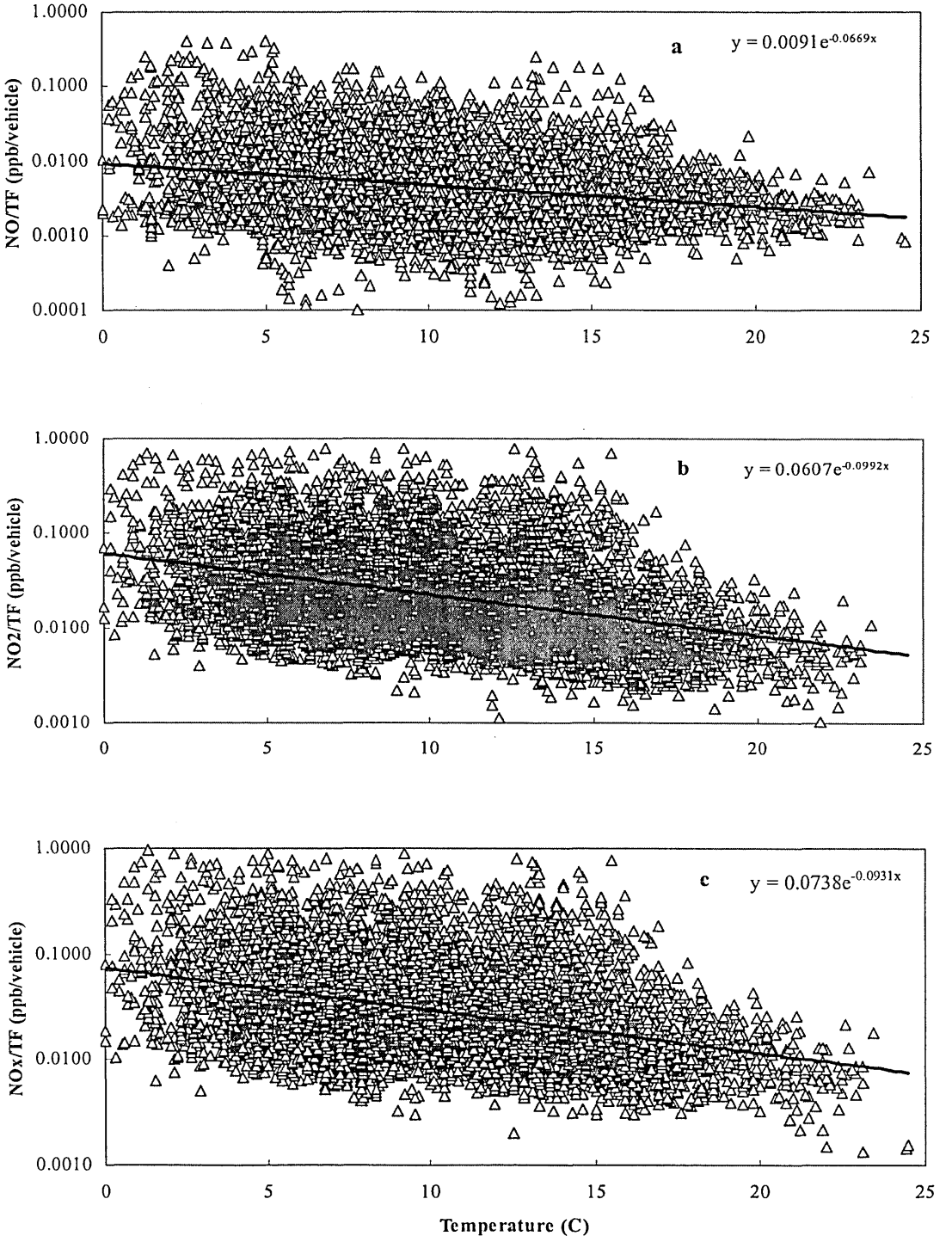


Figure 5.10 Variations of NO, $NO_2$ and NOx with ambient temperature

### 5.2.4 Multi variations of NO, $NO_2$ and NOx with traffic flow, wind speed and ambient temperature

As analysed in sections 5.2.2 and 5.2.3, NO, $NO_2$ and NOx measured at the station are the complex functions of source emission (coming from road traffic mainly), wind speed and ambient temperature. The impact of wind direction on concentrations of NO, $NO_2$ and NOx is not obvious. The correlations among average concentrations of NO, $NO_2$ and NOx and traffic flow on arterial road, as demonstrated in Figures 5.5 and 5.7, are good. However, the relationships among concentrations of NO, $NO_2$ and NOx and single weather factors such as wind speed and ambient temperature (figure 5.8-5.10) are scattered. Multi regressions have been done to derive the relationships among 7800 sets of NO, $NO_2$, NOx hourly concentrations measured at the station and traffic flow on arterial road, wind speed and ambient temperature. The multi regression equations at 95% confidence level that describe relationships among NO, $NO_2$, NOx (ppm) and traffic flow (*TF*, vehicles $h^{-1}$), wind speed (*WS*, m $s^{-1}$) and ambient temperature (*T*, °C) are shown in equations 5.1-5.3.

$$NO=(4.743\pm0.15)*10^{-6}*TF-(2.74\pm0.12)*10^{-3}*WS-(7.00\pm0.36)*10^{-4}*T+(1.05\pm0.04)*10^{-2} \quad (5.1)$$

$$NO_2=(4.06\pm0.07)*10^{-6}*TF-(2.67\pm0.05)*10^{-3}*WS-(6.40\pm0.16)*10^{-4}*T+(1.84\pm0.03)*10^{-2} \quad (5.2)$$

$$NOx=(8.80\pm0.19)*10^{-6}*TF-(5.41\pm0.16)*10^{-3}*WS-(13.40\pm0.48)*10^{-4}*T+(2.77\pm0.06)*10^{-2} \quad (5.3)$$

The relationships among NO, $NO_2$, NOx and traffic flow, wind speed, wind direction and temperature are similar. As expected, the concentrations of NO, $NO_2$ and NOx increase with traffic flow and decrease with wind speed and ambient temperature. These variation trends have been identified in separate analyses of relationship among NO, $NO_2$ and NOx, traffic flow and single weather factors (sections 5.2.2 and 5.2.3). The multi correlation coefficients (*r*) for the 7800 sets of samples are 0.40, 0.43 and 0.55 for NO, $NO_2$ and NOx, respectively.

## 5.3 Mass and chemical species of $PM_{10}$ and TSP

Two $PM_{10}$ and TSP samples a week, one for weekdays and another one for weekends, were sampled at the study station for one year. A total of 94 $PM_{10}$ samples and

95 TSP samples have been collected. The masses of $PM_{10}$ and TSP were measured using the gravimetric method (section 4.3.1). Metal elements of the particulates ($Ca^{2+}$, $Mg^{2+}$, Pb, Ni, Zn and Cu) were analysed using an atomic absorption spectrophotometer (AAS, section 4.3.2). Ions of the particulates ($SO_4^{2-}$, $NO_3^-$, $NH_4^+$, $Cl^-$, $Na^+$ and $K^+$) were analysed using high performance liquid chromatography (HPLC, section 4.3.3). Gravimetric analysis was conducted for all $PM_{10}$ and TSP samples. Wet chemical analysis was conducted for 59 $PM_{10}$ samples and 60 TSP samples. These 59 $PM_{10}$ samples and 60 TSP samples were collected from 9 December 1999 to 31 July 2000.

### 5.3.1 Summary of results for mass and chemical species of $PM_{10}$ and TSP

A summary of mass and chemical species data results for 59 RSP samples are shown in Table 5.5. The mass concentration of $PM_{10}$ measured at the station ranges from 5000 ng $m^{-3}$ to 36500 ng $m^{-3}$. The average concentration is 12200 ng $m^{-3}$. In comparison to the $PM_{10}$ database gathered in this work (Table 2.3), the mass concentration of $PM_{10}$ measured at the station is low. The average mass concentration of $PM_{10}$ equates to the lowest value in the gathered $PM_{10}$ database, which was measured at a remote site located in Oki Island, Japan.

The air quality standards for $PM_{10}$ and Pb have been recommended in the UK National Air Quality Strategy (Department of the Environment, Transport and the Regions, 1999). They are 50000 ng $m^{-3}$ for 24 hours mean concentration of $PM_{10}$ (maximum of 4 exceedances per year) and 500 ng $m^{-3}$ for annual mean concentration of Pb. The maximum concentration of $PM_{10}$ (36500 ng $m^{-3}$) measured at the study station is less than the limit in the air quality strategy. However, the concentration measured at the station are averaged over 3 or 4 days. The maximum 24 hours mean concentration at the station may be much larger than the maximum of the 3 or 4 days average. The average concentration of Pb measured at the station (38 ng $m^{-3}$) is much less than the limit in the air quality strategy (Department of the Environment, Transport and the Regions, 1999).

Table 5.5 Summary of mass and chemical species analysis results for $PM_{10}$ (ng $m^{-3}$)

| | Mass | $SO_4^{2-}$ | $NO_3^-$ | $NH_4^+$ | $Ca^{2+}$ | $K^+$ | $Cl^-$ | $Na^+$ | $Mg^{2+}$ | Pb | Ni | Zn | Cu |
|---|---|---|---|---|---|---|---|---|---|---|---|---|---|
| Min | 5000 | 422 | 0 | 80 | 0 | 0 | 79 | 70 | 0 | 0 | 0 | 0 | 0 |
| Max | 36500 | 7455 | 7692 | 3121 | 2310 | 1432 | 2888 | 3915 | 560 | 133 | 93 | 168 | 62 |
| Average | 12200 | 2154 | 1107 | 670 | 779 | 110 | 980 | 1164 | 127 | 21 | 25 | 28 | 24 |
| SD* | 6000 | 1543 | 1261 | 602 | 526 | 185 | 672 | 656 | 132 | 38 | 25 | 30 | 14 |

*SD Standard Deviation

On average, the 12 chemical species analysed using AAS and HPLC hold about 60.7% of the $PM_{10}$ mass. C, the most important component of the aerosol, and Si and Al, two other important components of the aerosol, have not been analysed in this study because analysis equipment was unavailable.

Most of $SO_4^{2-}$, $NO_3^-$ and $NH_4^+$ come from secondary origin. They are formed from precursors of gaseous $SO_2$, NOx and $NH_3$. $SO_4^{2-}$, $NO_3^-$ and $NH_4^+$ are three major components for $PM_{10}$ measured at the study station. They hold about 31.4% of $PM_{10}$ mass (range from 7.2% to 73.6%). In comparison with the $PM_{10}$ database (Table 2.3), the concentrations of $SO_4^{2-}$, $NO_3^-$ and $NH_4^+$ measured at the station are similarly low. The average concentration of $SO_4^{2-}$ is 2154 ng $m^{-3}$. It is lower than each of the remaining values in the $PM_{10}$ database, except for the value at Alert, an arctic site in Canada. The average concentrations of $NO_3^-$ and $NH_4^+$ are 1107 ng $m^{-3}$ and 670 ng $m^{-3}$ respectively. They are lower than most of the values in the $PM_{10}$ database.

$Ca^{2+}$ and $K^+$ are regarded as crustal elements. They are important components for $PM_{10}$ measured at the station. Two elements hold about 8.5% of $PM_{10}$ mass. (range from 0.0% to 23.3%). The average concentration of $Ca^{2+}$, measured at the station, is 779 ng $m^{-3}$. This value is similar to the value measured in Brisbane, Australia. It is lower than most values measured in America and Asia, but higher than the values measured in the Czech Republic and South Africa. The concentration of $K^+$ measured at the station is low. Its average value is 110 ng $m^{-3}$. This value is lower than all the values in the $PM_{10}$ database, except for the value at the arctic site.

$Cl^-$, $Na^+$ and $Mg^{2+}$ are major components of marine aerosols. The concentrations of $Cl^-$, $Na^+$ and $Mg^{2+}$ measured at the station are high. They show the impact of marine aerosols on airborne particulates in Dundee. Three species hold about 19.8% of $PM_{10}$ mass (range from 1.52% to 42.3%). The average concentration of $Cl^-$ is 980 ng $m^{-3}$. Although it is lower than the values measured at most sites in the UK, this value is similar to the values measured at Haverah Park, the UK and other coastal sites such as Sapporo, Japan, Hong Kong and Singapore. The average concentration of $Na^+$ is 1164 ng $m^{-3}$. It is similar to the values measured at seven sites in the UK (Altrincham, Manchester, Brent, Chilton, Flixtton, Walsall, Windermere).

Pb, Ni, Zn and Cu are usually considered as trace elements that come from anthropogenic sources (Qin et al., 1997). These four elements measured at the station hold

about 0.9% of the $PM_{10}$ mass (ranging from 0.1% to 5.6%). Average concentration of Pb measured at the station is 21 ng $m^{-3}$. The value is lower than most values in the $PM_{10}$ database. Ni may be regarded as a tracer of fuel oil burning emission. Average concentration of Ni measured at the station is 25 ng $m^{-3}$. It is higher than most of the values in the $PM_{10}$ database. Zn and Cu may come from various sources. Average concentrations measured at the station are 28 ng $m^{-3}$ for Zn and 24 ng $m^{-3}$ for Cu. These values are relatively low in comparison to the other values in the $PM_{10}$ database.

The anions and cations in the $PM_{10}$ data measured at the station are well balanced. The average equivalent anion to cation ratio is 1.00. The average equivalent concentration ratio of $Cl^-$ to $Na^+$ is 0.55. It is much lower than the value of 1.16 in seawater (Wilson, 1975), indicating the existence of the $Cl^-$ loss reaction. $SO_4^{2-}$ is a major ion for $PM_{10}$. Its average equivalent concentration is 44.8 neq $m^{-3}$. The equivalent concentration of sea salt $SO_4^{2-}$ can be estimated using 0.12 (typical ratio of $SO_4^{2-}$ to $Na^+$ in seawater) times equivalent concentration of $Na^+$. The estimated concentration of sea salt $SO_4^{2-}$ is about 6.1 neq $m^{-3}$, which is only 13.5% of total sulphate in Dundee. Most of the sulphate is therefore non-sea salt sulphate (NSS) in Dundee. The fraction of the NSS that is not associated with ammonium can be defined as excess sulphate, which can be estimated by using the expression: NSS (neq $m^{-3}$) – [total ammonium (neq $m^{-3}$) – total nitrate (neq $m^{-3}$)]. The average equivalent concentration of excess sulphate is estimated to be 19.4 neq $m^{-3}$. It is about 43.3% of total sulphate.

A summary of mass and chemical species data for 60 TSP samples is shown in Table 5.6. In comparison with data from other sites (Table 2.4), the mass concentration of TSP measured at the station is low. It ranges from 6400 ng $m^{-3}$ to 66600 ng $m^{-3}$. The average concentration is 17600 ng $m^{-3}$. It is much lower than the values measured at Agra , India (368520 ng $m^{-3}$) and Hong Kong (88347 ng $m^{-3}$).

On average, the 12 analysed chemical species hold about 65.3% of TSP mass. This percentage is only marginally higher than the corresponding $PM_{10}$ value.

Table 5.6 Summary of mass and chemical species analysis results for TSP (ng $m^{-3}$)

| | Mass | $SO_4^{2-}$ | $NO_3^-$ | $NH_4^+$ | $Ca^{2+}$ | $K^+$ | $Cl^-$ | $Na^+$ | $Mg^{2+}$ | Pb | Ni | Zn | Cu |
|---|---|---|---|---|---|---|---|---|---|---|---|---|---|
| Min | 6400 | 640 | 0 | 0 | 115 | 0 | 34 | 51 | 10 | 0 | 0 | 0 | 0 |
| Max | 66600 | 20769 | 4179 | 5292 | 6038 | 6047 | 7354 | 5301 | 739 | 219 | 442 | 549 | 282 |
| Average | 17600 | 4341 | 398 | 1246 | 998 | 489 | 1428 | 1520 | 132 | 47 | 77 | 87 | 29 |
| SD* | 10700 | 3709 | 690 | 1208 | 757 | 879 | 1537 | 1359 | 107 | 60 | 91 | 91 | 39 |

$SO_4^{2-}$, $NO_3^-$ and $NH_4^+$ are also three major components for TSP measured at the study station. They hold about 32.5% of TSP mass (range from 8.6% to 90.3%). This percentage is similar to the value in $PM_{10}$ (31.4%). The average concentration of $SO_4^{2-}$ is 4341 ng $m^{-3}$. This value is lower than the values measured in Asia. The average concentration of $NO_3^-$ is 398 ng $m^{-3}$. It is much lower than the values measured in Asia. The author has observed that the average concentration of $NO_3^-$ measured in TSP is much lower than the value measured in $PM_{10}$. A possible explanation for this is that a system error may have occurred in the TSP sampling and analysis for nitrate, because of its semi-volatile property. The average concentration of $NH_4^+$ is 670 ng $m^{-3}$. It is lower than the values measured in Korea and Hong Kong.

$Ca^{2+}$ and $K^+$ hold about 14.9% of TSP mass measured at the station. (ranging from 1.2% to 69.0%). This percentage is significantly higher than the value in the $PM_{10}$ sample (8.9%), because crustal elements favour coarse particulate. The average concentration of $Ca^{2+}$ is 998 ng $m^{-3}$. It is lower than the values measured in Turkey, Hong Kong and India but higher than the values measured in Korea and Venezuela. The average concentration of $K^+$ is 489 ng $m^{-3}$. It is lower than the values measured in Hong Kong and India but higher than the values measured in Korea and Venezuela.

$Cl^-$, $Na^+$ and $Mg^{2+}$ hold about 21.0% of TSP mass measured at the station (ranging from 1.6% to 98.7%). This percentage is similar to the value in $PM_{10}$ (19.8%), The average concentration of $Cl^-$ is 1428 ng $m^{-3}$. It is lower than the values measured at other sites. The average concentration of $Na^+$ is 1520 ng $m^{-3}$ which is lower than the values measured in Turkey and Asia but higher than the values measured in Venezuela.

Pb, Ni, Zn and Cu hold about 1.6% of TSP mass measured at the station (range from 0.3% to 10.2%). This percentage is higher than the value in $PM_{10}$ (0.9%). Average concentration of Pb is 47 ng $m^{-3}$. It is lower than the values measured in India and Hong Kong but higher than the value measured in Turkey. Average concentration of Ni is 77 ng $m^{-3}$. It is lower than the value measured at Agra, India, but much higher than the values measured at other sites. Average concentration of Zn is 87 ng $m^{-3}$. It is much lower than the values measured in Asia but higher than the values measured in Turkey and Venezuela. Average concentration of Cu is 29 ng $m^{-3}$. It is much lower than the values measured at other sites.

The anions and cations in the TSP measured at the station are also well balanced. The average equivalent anion to cation ratio is 1.08. The average equivalent concentration ratio of $Cl^-$ to $Na^+$ is 0.61. It is also lower than the value in seawater. Average equivalent concentration of $SO_4^{2-}$ is 90.4 neq $m^{-3}$. The equivalent concentration of sea salt $SO_4^{2-}$ is about 7.9 neq $m^{-3}$, which is only 8.8% of total sulphate. 91.8% of sulphate are NSS in TSP. The average equivalent concentration of excess sulphate is estimated to be 19.8 neq $m^{-3}$. It is about 21.9% of total sulphate.

Summarising the above discussion, the mass concentrations of $PM_{10}$ and TSP measured at the study station are very low. The concentration for most of the chemical species of $PM_{10}$ and TSP, except $Cl^-$ and $Na^+$, are lower or much lower than the values measured at other sites around the world. Like other sites in the UK, the concentrations for $Cl^-$ and $Na^+$ are relatively high and they show characteristics of marine aerosol.

### 5.3.2 Temporal variations of masses and chemical species of $PM_{10}$ and TSP

Temporal variations of mass concentrations of $PM_{10}$ and TSP are shown in Figure 5.11. They fluctuate with time. Relatively high concentrations of $PM_{10}$ and TSP appear in spring (March, April and May). Temporal variations of mass concentration of $PM_{10}$ and TSP show good comparison except for the samples collected on 6 April 2000. The linear correlation coefficient (r) between mass concentrations of $PM_{10}$ and TSP is 0.89. It implies that $PM_{10}$ and TSP measured at the station come from similar sources.

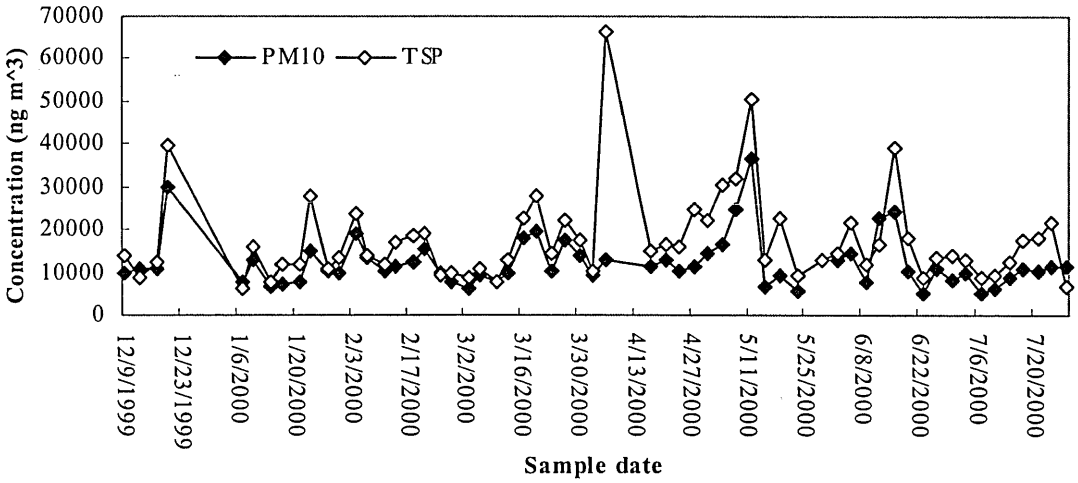


Figure 5.11 Temporal variations of mass concentrations of $PM_{10}$ and TSP

The highest mass concentration of $PM_{10}$ occurred on 12 May 2000. It is a weekend sample. In the past half month before the sample was collected, the total rainfall record was only 0.2 mm. The dominant wind was easterly. The mass concentration of $PM_{10}$ measured at the station increased continually. During the sample period, there was no rainfall. Average ambient temperature was 12.1 °C. Average wind speed was 1.9 m $s^{-1}$. The dominant wind was also easterly. The frequency of easterly wind (ENE, E and ESE) was 52.1% while the frequency of calm conditions (C) was 31.4%. The 12 analysed chemical species hold about 58.7% of the sample mass, approaching the average value of 60.7%. Among the chemical species, secondary aerosol ($SO_4^{2-}$, $NO_3^-$ and $NH_4^+$) hold about 50.1%. This percentage is much larger than the average value for all the samples (31.4%). Crustal elements ($Ca^{2+}$ and $K^+$), marine aerosol ($Cl^-$, $Na^+$ and $Mg^{2+}$) and trace elements (Pb, Ni, Zn and Cu) hold about 0.9%, 7.4% and 0.3% of the $PM_{10}$ mass, respectively. These percentages are much less than average values (8.5%, 19.8% and 0.9% respectively). The results indicate that high concentration of $PM_{10}$ is accompanied by high concentrations of secondary pollution species.

The highest mass concentration of TSP occurred on 6 April 2000. This high value may have been caused by fugitive emission sources because the temporal variation was sharply fluctuating and the mass concentration of $PM_{10}$ measured at the same time was at a normal level. It may be more significant to analyse the sample with the second highest mass concentration that occurred at the same time as the highest concentration of $PM_{10}$. For the TSP sample with the second highest mass concentration, 12 analysed chemical species hold about 31.1% of the sample mass. It is much less than the average value (65.3%). Among the chemical species, secondary aerosol, crustal elements, marine aerosol, trace elements hold about 22.6%, 2.9%, 4.2% and 1.4% of the sample mass respectively. These percentages are less than the average values (32.5%, 14.9%, 21.0% and 1.6% respectively). These results indicate that high concentration of TSP is not caused by the analysed chemical species. C may be the major species causing high concentration of TSP.

Temporal variations of chemical species concentrations of $PM_{10}$ are shown in Figure 5.12. In general, temporal variations of $SO_4^{2-}$, $NO_3^-$ and $NH_4^+$ in $PM_{10}$ are similar (Figure 5.12a). The linear correlation coefficients (r) between $SO_4^{2-}$ and $NO_3^-$, $SO_4^{2-}$ and $NH_4^+$ and $NO_3^-$ and $NH_4^+$ are 0.80, 0.87 and 0.92, respectively. This shows that the species come from similar sources. The concentration $SO_4^{2-}$, $NO_3^-$ and $NH_4^+$ are high in the spring, when easterly wind is more prevalent than westerly. $SO_4^{2-}$ concentrations are still high in

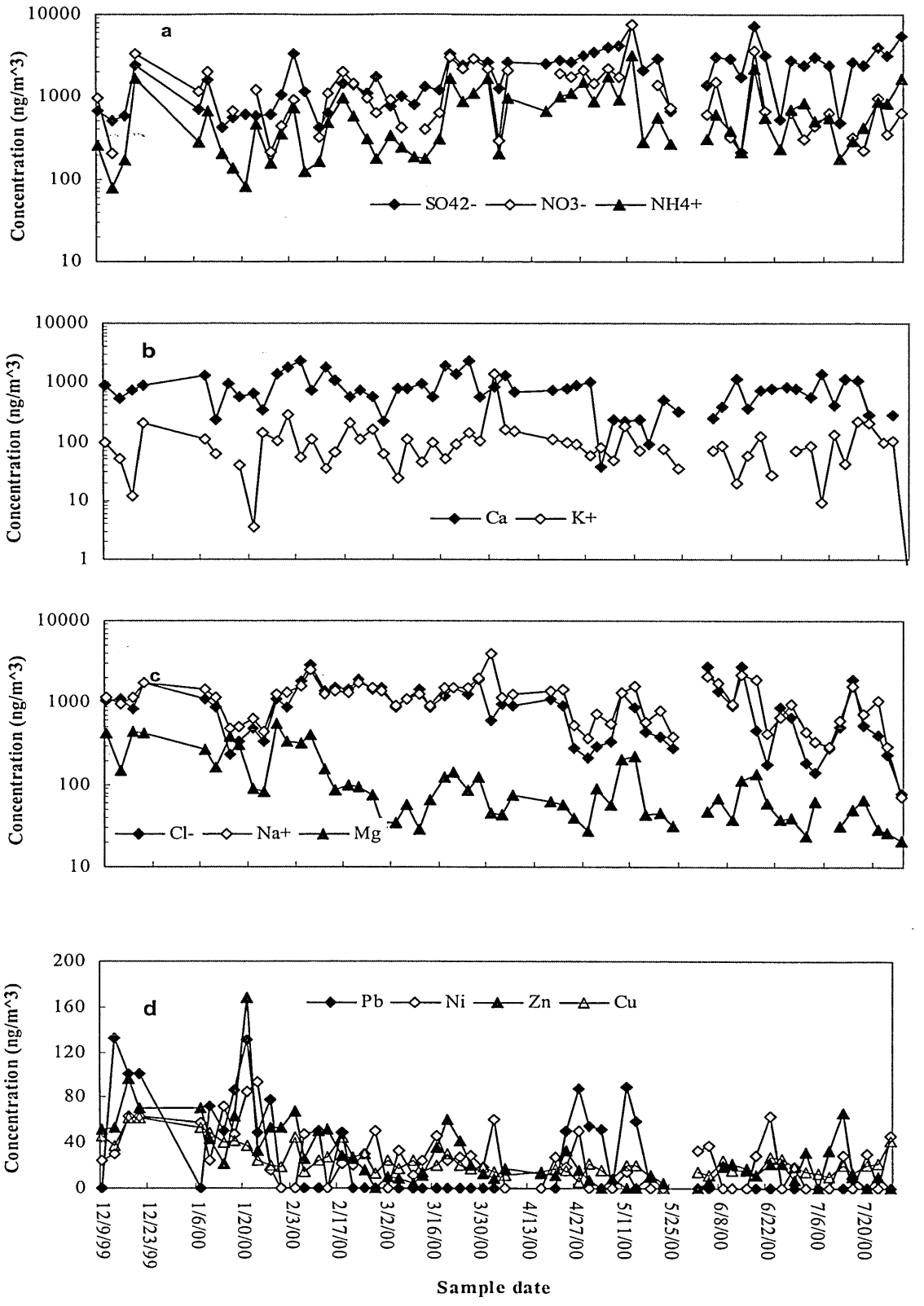


Figure 5.12 Temporal variations of chemical species concentrations of $PM_{10}$

the summer while $NO_3^-$ and $NH_4^+$ fall to average levels. This may be caused by the impact of ambient temperature on the particulate sample. High ambient temperature may evaporate the nitrate and ammonium from the particulate sample. Although both of them are regarded as crustal elements, the temporal variation of $Ca^{2+}$ and $K^+$ in $PM_{10}$ are not similar (Figure 5.12b). This indicates that the species come from different sources. The temporal variation of $Ca^{2+}$ is gentler than that of $K^+$. It means that $Ca^{2+}$ sources are relatively stable.

The temporal variations of $Cl^-$ and $Na^+$ in $PM_{10}$ are very similar except the samples collected on 27 March 2000. The linear correlation coefficient (r) between $Cl^-$ and $Na^+$ is 0.93. This shows that they come from the same source, possibly marine aerosol (Figure 5.12c). Concentrations of $Cl^-$ and $Na^+$ were high and stable during the period 7 February 2000 to 27 Mach 2000. Their concentrations were relatively low and fluctuate during summer. The temporal variation of $Mg^{2+}$ is not coincident with those for $Cl^-$ and $Na^+$. It is the higher in the winter and lower in the spring and summer. There are possibly some $Mg^{2+}$sources other than marine aerosol that affected the data at the station.

The concentrations of trace elements (Pb, Ni, Zn and Cu) in $PM_{10}$ are relatively higher in the winter and lower in the spring and summer (Figure 5.12d). This may show the impact of seasonal variation of anthropogenic emission source (for example, house heating emission) in the measured data. The temporal variations of the trace elements fluctuated a lot and are not coincident, because their sources are very complex.

Temporal variations of chemical species concentration of TSP are shown in Figure 5.13.

Similar to those of $PM_{10}$, temporal variations of $SO_4^{2-}$, $NO_3^-$ and $NH_4^+$ in TSP are generally coincident (Figure 5.13a). The concentration of $SO_4^{2-}$, $NO_3^-$ and $NH_4^+$ are high in the spring. However, concentration of $SO_4^{2-}$ in TSP, like $NO_3^-$ and $NH_4^+$ concentrations, falls to average levels in summer.

The temporal variation of $Ca^{2+}$ and $K^+$ in TSP are also not coincident (Figure 5.13b). The concentration of $Ca^{2+}$ in TSP keeps a relatively stable level. This indicates that $Ca^{2+}$ sources for TSP are stable.

The temporal variations of $Cl^-$ and $Na^+$ in TSP are very coincident (Figure 5.13c). Concentrations of $Cl^-$ and $Na^+$ in TSP were high and stable during the period 28 January 2000 to 14 February 2000. This period is a little early and much shorter than the period for

the $PM_{10}$. In contrast to that of $PM_{10}$, there is no obvious seasonal variation for concentration of $Mg^{2+}$ in TSP.

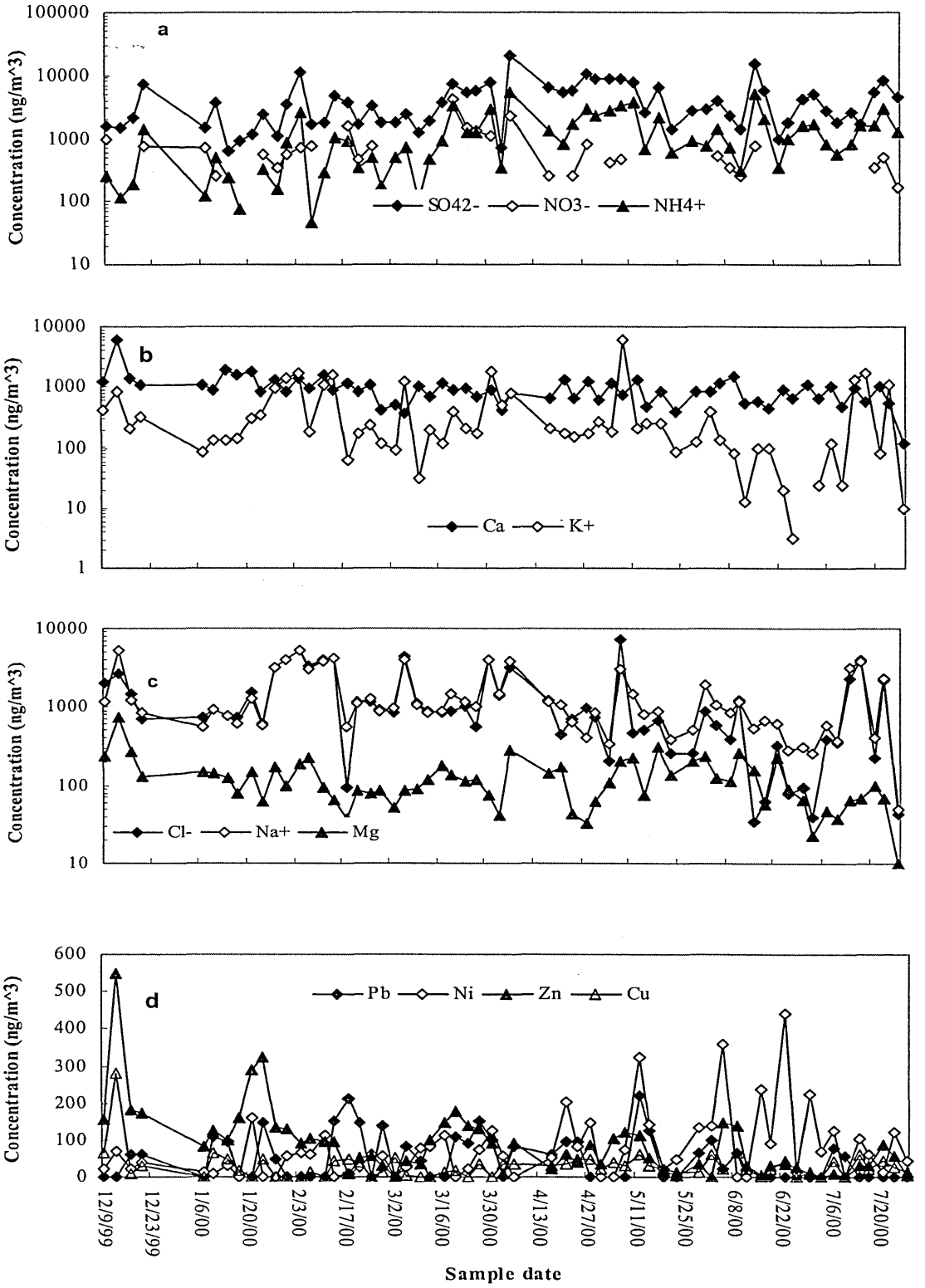


Figure 5.13 Temporal variations of chemical species concentrations of TSP

The concentrations of trace elements in TSP are much higher than those in $PM_{10}$ (Figure 5.13d). There are no significant seasonal variations for the concentrations of trace elements in TSP.

### 5.3.3 Variations of masses and chemical species of $PM_{10}$ and TSP with rainfall

Precipitation is a major 'cleaning' process for atmospheric aerosol. The rainfall increases ground soil moisture and reduces fugitive dust source emissions. Variations of mass concentration of $PM_{10}$ and TSP with the total rainfall during the sample period are shown in Figure 5.14.

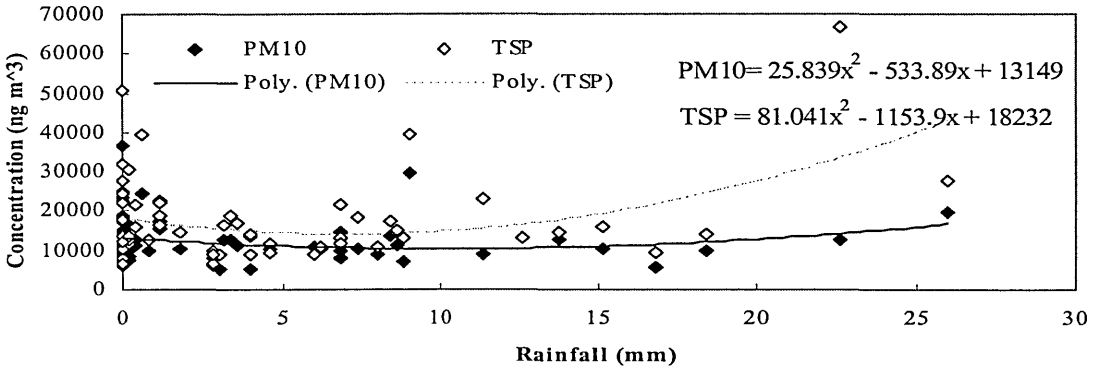


Figure 5.14 Variations of mass concentrations of $PM_{10}$ and TSP with rainfall

The effect of rainfall on mass concentrations of $PM_{10}$ and TSP is not so obvious, as expected. Second order polynomial regressions can approximately describe the variations of mass concentration with rainfall for both $PM_{10}$ and TSP. The correlation coefficients ($r$) are 0.20 for $PM_{10}$ (59 samples) and 0.42 for TSP (60 samples). These suggest that relationship between mass concentration and the total rainfall is better for TSP than for $PM_{10}$. When the total rainfall is low, the mass concentrations of $PM_{10}$ and TSP decrease slowly with the rainfall. When total rainfall is high, the mass concentrations keep at a soundly low level except for a few special cases. It seems that mass concentrations of $PM_{10}$ and TSP are affected by rainfall record during the sampling time as well as the continued rainfall record. The rainfall record was zero during the sample time of the highest $PM_{10}$ concentration and second highest TSP concentration. As mentioned above, the total rainfall was just 0.2 mm in the half a month before the samples were collected.

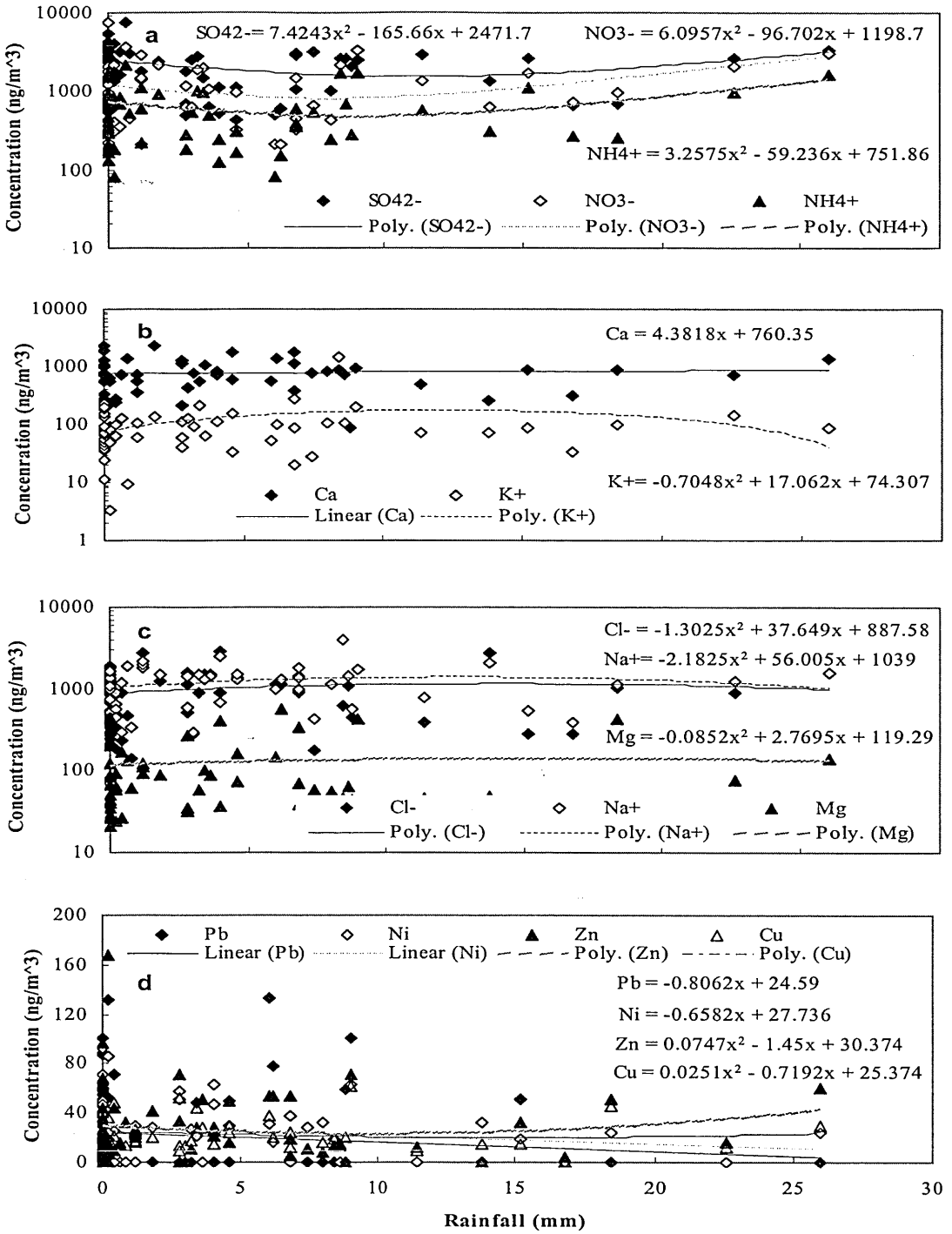


Figure 5.15 Variations of chemical species concentrations of $PM_{10}$ wi th rainfall

Variations of chemical species concentrations of $PM_{10}$ with total rainfall during the sample time are shown in Figure 5.15. Variation trends of secondary species in $PM_{10}$ with the total rainfall are similar (Figure 5.15a). The second order polynomial regressions can

approximately describe these trends. The correlation coefficients of concentration and rainfall ($r$) are also similar with the values of 0.24, 0.25 and 0.25 for $SO_4^{2-}$, $NO_3^-$ and $NH_4^+$, respectively. When the rainfall is low, the secondary species decrease with the rainfall slowly. When the rainfall is high, the secondary species increase with the rainfall.

Although they are crustal elements believed to be related to soil dust, the variation trends with the rainfall are different for $Ca^{2+}$ and $K^+$ in $PM_{10}$ (Figure 5.15b). There is no noticeable variation with the rainfall for $Ca^{2+}$ although a linear regression can be fitted to the data. The linear regression coefficient ($r$) is 0.05. A second order polynomial regression can approximately describe the variation with the rainfall for $K^+$. The correlation coefficient ($r$) is 0.21. These may indicate that local fugitive dust emissions are not the major sources that affect the $PM_{10}$ datasets at the station.

Variations of $Cl^-$ and $Na^+$ in $PM_{10}$ with the rainfall are similar (Figure 5.15c). The second order polynomial regressions can approximately describe these variations. The correlation coefficients ($r$) are 0.14 and 0.20 for $Cl^-$ and $Na^+$, respectively. Variation of $Mg^{2+}$ in $PM_{10}$ with the rainfall may be described using a second order polynomial regression. However, the correlation is very poor with a value of 0.06 for the correlation coefficient ($r$).

No significant relationships between trace elements in $PM_{10}$ and the rainfall can be derived (Figure 5.15d). The linear regressions may be fitted to the variations of Pb and Ni with the rainfall. The correlation coefficients ($r$) are 0.13 for Pb and 0.16 for Ni. The second order polynomial regressions may be fitted for Zn and Cu. The correlation coefficients ($r$) are 0.12 and 0.13, respectively.

Variations of chemical species concentrations of TSP with the total rainfall during the sample time are shown in Figure 5.16. The relationships between secondary species and the total rainfall are better for TSP than for $PM_{10}$ (Figure 5.16a). The second order polynomial regressions can approximately describe variations of secondary species in TSP with the total rainfall. The correlation coefficients ($r$) are 0.38, 0.42 and 0.72 for $SO_4^{2-}$, $NO_3^-$ and $NH_4^+$, respectively. When the rainfall is low, the concentrations of secondary species decrease with the rainfall. When the rainfall is high, the concentrations of secondary species increase with the rainfall.

No noticeable variations of the $Ca^{2+}$ and $K^+$ in TSP with the rainfall may be derived (Figure 5.16b). The second order polynomial regression can be fitted for $Ca^{2+}$ and $K^+$.

However, the correlation coefficients of concentration vs the rainfall ($r$) are very small, with values of 0.11 for $Ca^{2+}$ and 0.04 for $K^+$.

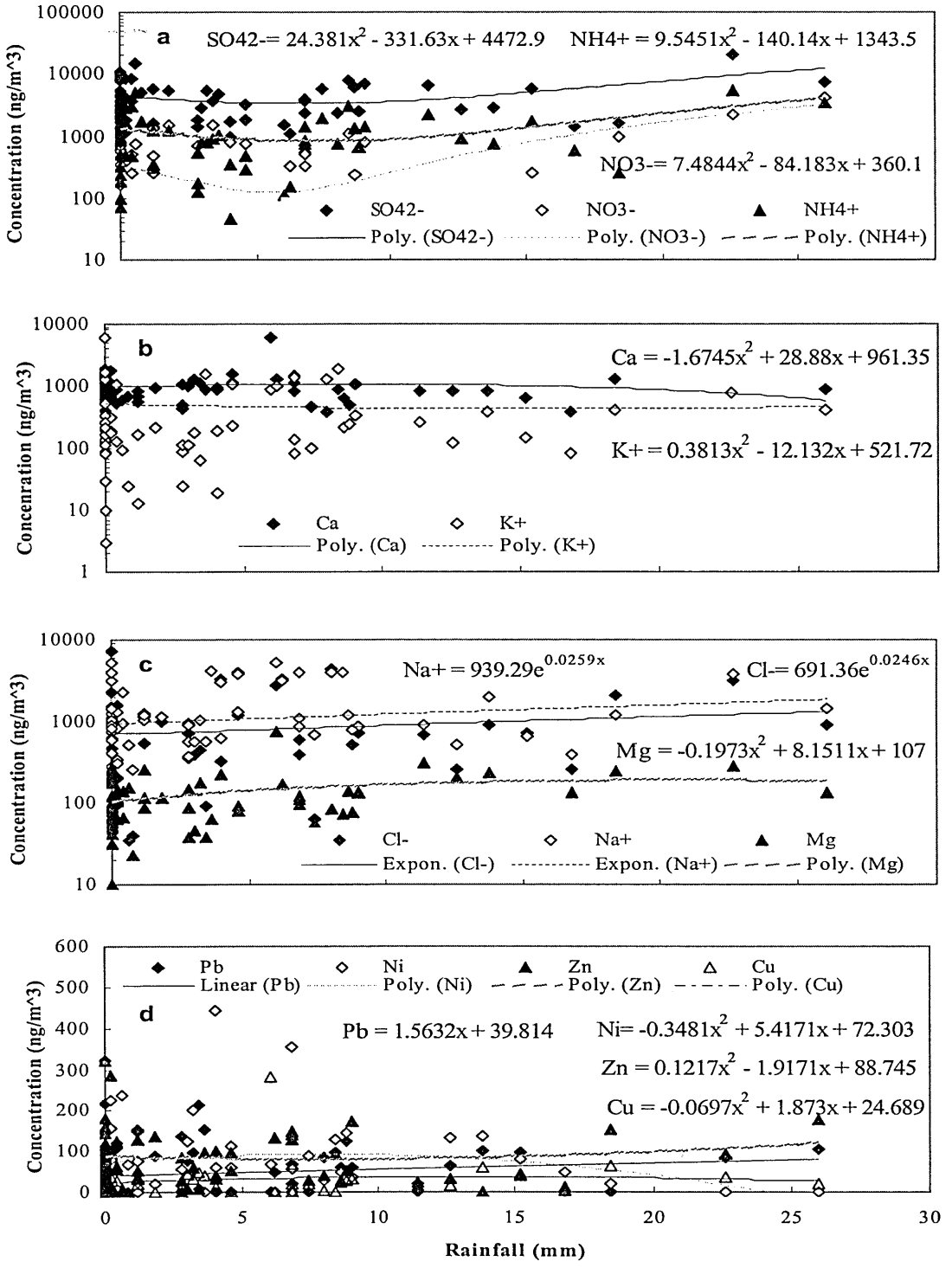


Figure 5.16 Variations of chemical species concentrations of TSP with rainfall

Variations of $Cl^-$ and $Na^+$ in TSP with the rainfall are similar (Figure 5.16c). The exponential regressions may approximately describe these variations. The correlation coefficients (r) are 0.12 for $Cl^-$ and 0.17 for $Na^+$. Variation of $Mg^{2+}$ in TSP with the rainfall may be represented using a second order polynomial regression. The correlation is better than for $Mg^{2+}$ in $PM_{10}$ with a value of 0.26 for the correlation coefficient ($r$).

No significant relationships between trace elements in TSP and the rainfall can be derived (Figure 5.16d). The linear regression may be fitted for the variation of Pb with rainfall. The correlation coefficient ($r$) is 0.16. The second order polynomial regressions may be fitted for Ni, Zn and Cu. The correlation coefficients ($r$) are 0.20, 0.07 and 0.12, respectively.

Except in a few number of cases, effect of rainfall on chemical species of aerosol is not as obvious as expected. Low correlation coefficients suggest that some other factors except rainfall could affect concentration of chemical species in aerosol.

### 5.3.4 Variations of masses and chemical species of $PM_{10}$ and TSP with temperature

Ambient temperature may affect some anthropogenic source emissions (for example, house heating emission). Temperature can interfere with the sampling process for some volatile species such as $NO_3^-$ and $NH_4^+$. High ambient temperature will evaporate volatile species from the filer paper.

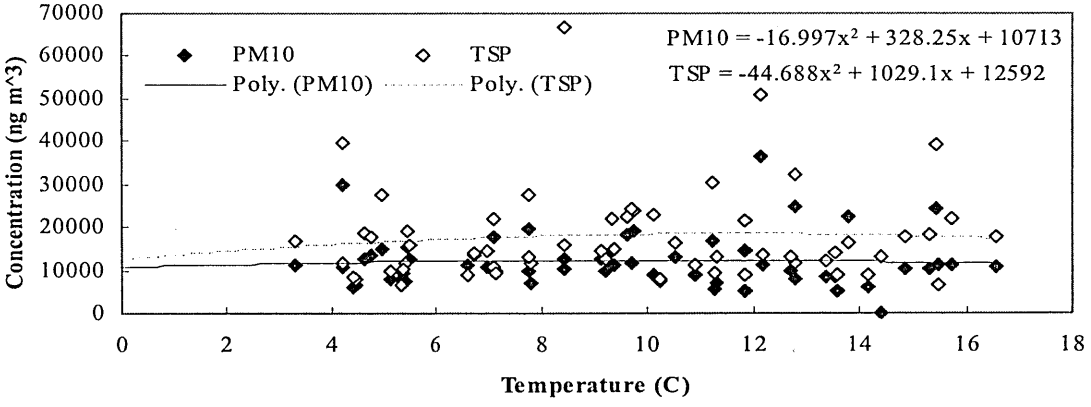


Figure 5.17 Variations of mass concentration of $PM_{10}$ and TSP with temperature

Variations of mass concentration of $PM_{10}$ and TSP with the average ambient temperature during the sampling period are shown in Figure 5.17. No noticeable variations

of mass concentrations with ambient temperature for $PM_{10}$ and TSP can be derived. The second order polynomial regressions may be fitted for both $PM_{10}$ and TSP. However, the correlation coefficients ($r$) are small with the values of 0.07 for $PM_{10}$ and 0.12 for TSP.

Variations of chemical species concentrations of $PM_{10}$ with the average ambient temperature during the sampling period are shown in Figure 5.18. Concentration of $SO_4^{2-}$ in $PM_{10}$ linearly increases with ambient temperature (Figure 5.18a). The linear correlation coefficient ($r$) is 0.55. The second order polynomial regressions can be fitted to the $NO_3^-$ and $NH_4^+$ in $PM_{10}$ vs ambient temperature. The correlation coefficients ($r$) are 0.12 for $NO_3^-$ and 0.22 for $NH_4^+$, respectively.

A linear regression can be fitted for $K^+$ in $PM_{10}$ vs ambient temperature while a second order polynomial regression had to be fitted for $Ca^{2+}$ (Figure 5.18b). The correlation coefficients ($r$) are 0.17 for $K^+$ and 0.31 for $Ca^{2+}$, respectively.

Concentrations of marine aerosol in $PM_{10}$ generally decrease with ambient temperature (Figure 5.18c). Variations of $Cl^-$ and $Na^+$ with ambient temperature are similar The exponential regressions can be used to describe these relationships. The correlation coefficients (r) are 0.39 for $Cl^-$ and 0.37 for $Na^+$, respectively. A second order polynomial regression may adequately represent the variation of $Mg^{2+}$ with ambient temperature. The correlation coefficient ($r$) is 0.53.

Concentrations of trace elements in $PM_{10}$ linearly decrease with ambient temperature (Figure 5.18d). The linear correlation coefficients ($r$) are 0.38 for Pb, 0.48 for Ni, 0.47 for Zn, and 0.51 for Cu, respectively. These can be attributed to impact of seasonal variation sources on trace elements in $PM_{10}$.

Variations of chemical species concentrations of TSP with the average ambient temperature during the sampling period are shown in Figure 5.19. An exponential regression can be fitted for $SO_4^{2-}$ in TSP vs ambient temperature (Figure 5.19a). The correlation coefficient ($r$) is 0.23. The linear regressions may be fitted for $NO_3^-$ and $NH_4^+$ in TSP vs ambient temperature. The linear correlation coefficients ($r$) are 0.18 for $NO_3^-$ and 0.35 for $NH_4^+$, respectively. Concentration of $NO_3^-$ decreases with ambient temperature while $NH_4^+$ increases with ambient temperature.

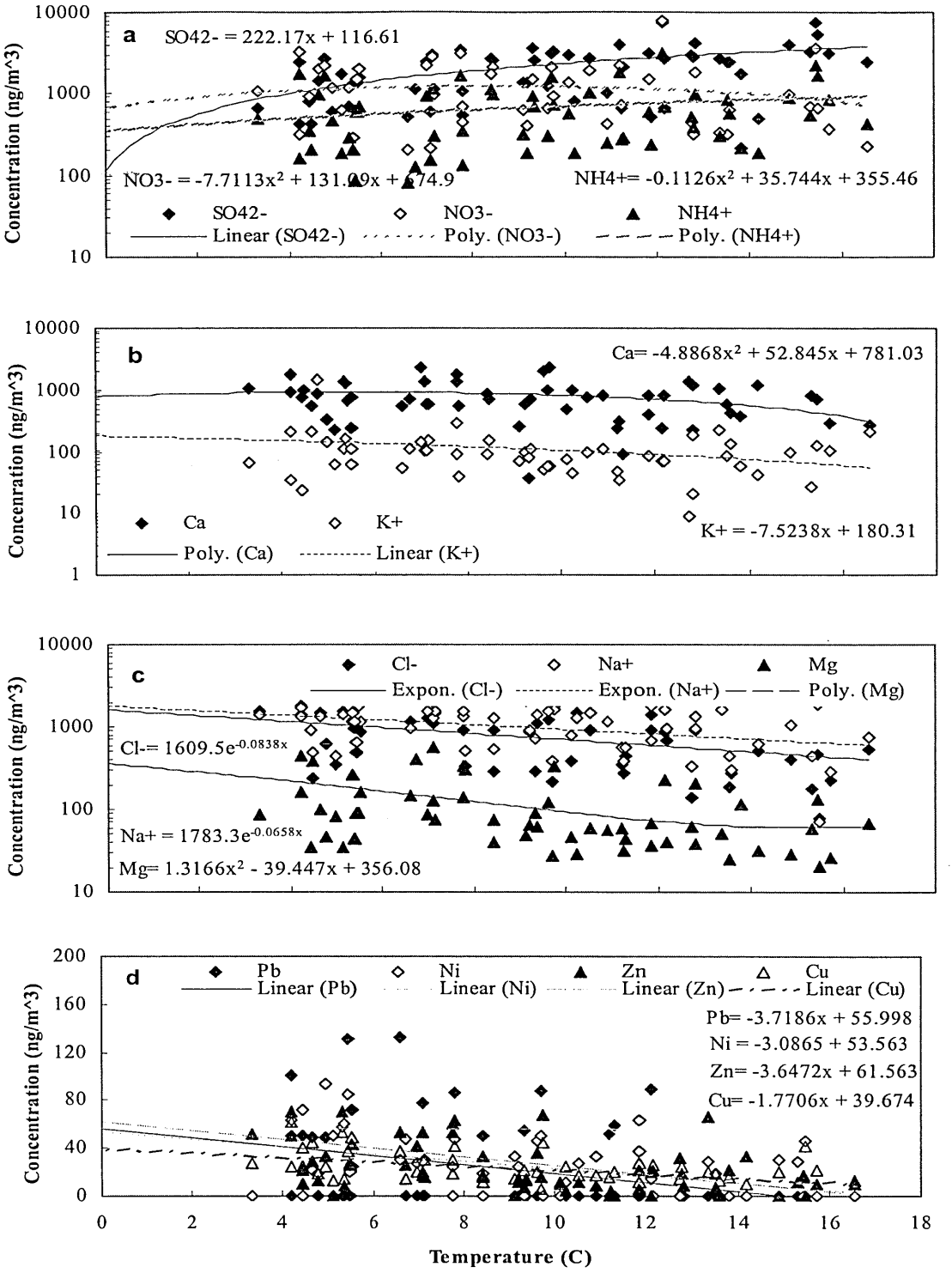


Figure 5.18 Variations of chemical species concentrations of $PM_{10}$ with ambient temperature

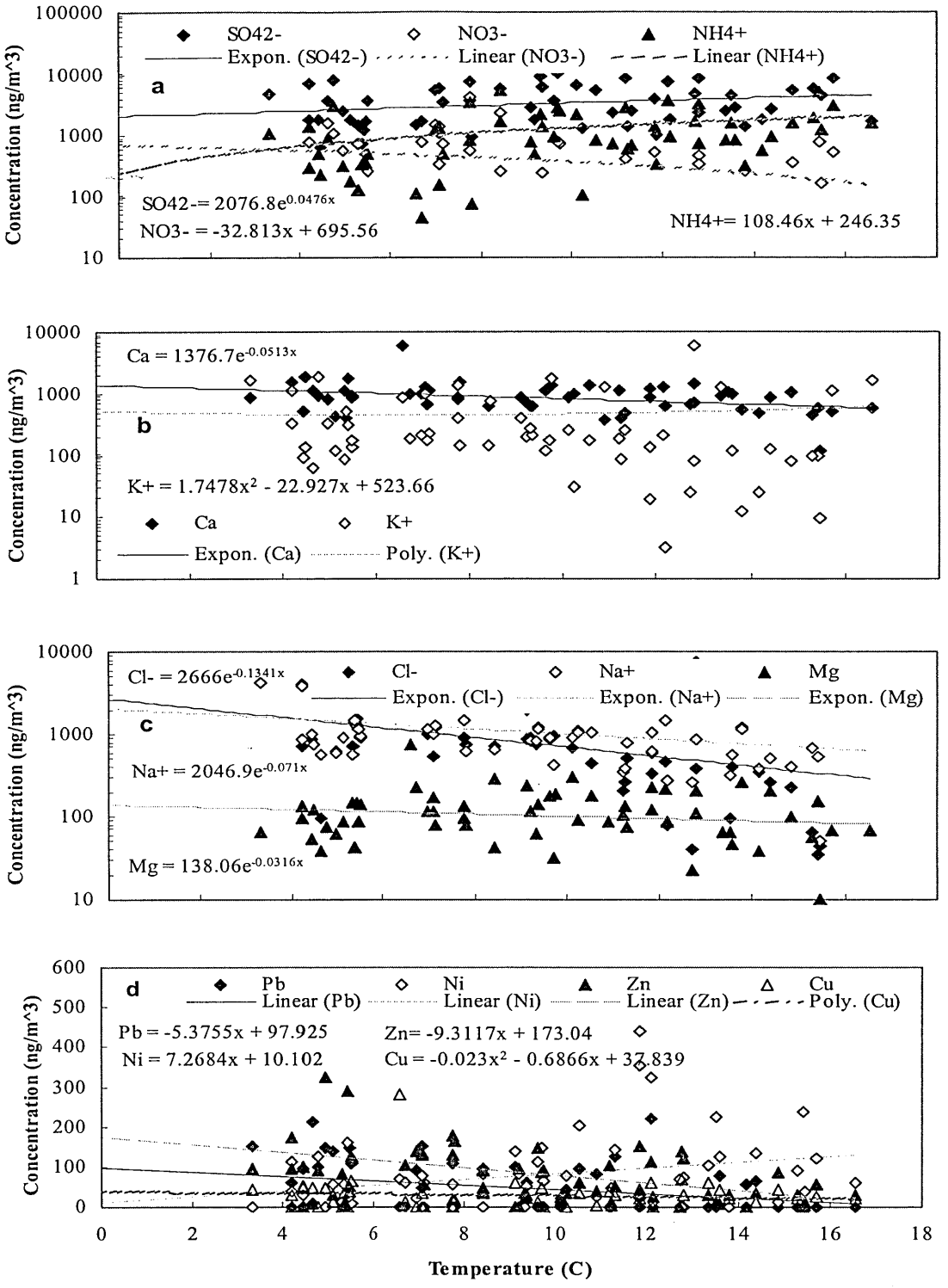


Figure 5.19 Variations of chemical species concentrations of TSP with ambient temperature

An exponential regression may be fitted for $Ca^{2+}$ in TSP vs ambient temperature while a second order polynomial regression had to be fitted for $K^+$ (Figure 5.19b). The correlation coefficients ($r$) are 0.37 for $Ca^{2+}$ and 0.05 for $K^+$, respectively.

Like those in $PM_{10}$, concentrations of marine aerosol in TSP generally decrease with ambient temperature (Figure 5.19c). The exponential regressions can be used to describe these relationships. The correlation coefficients ($r$) are 0.41 for $Cl^-$, 0.30 for $Na^+$ and 0.17 for $Mg^{2+}$, respectively.

The relationships between trace elements in TSP with ambient temperature are more complex than those in $PM_{10}$ (Figure 5.19d). Concentrations of Pb and Zn also linearly decrease with ambient temperature. The linear correlation coefficients ($r$) are 0.35 for Pb and 0.47 for Zn. However, concentration of Ni linearly increases with ambient temperature. The correlation coefficient ($r$) is 0.31. A second order polynomial regression had to be fitted for Cu. The correlation coefficient ($r$) is 0.11. These suggest there are some trace element sources for TSP other than for $PM_{10}$.

### 5.3.5 Variations of masses and chemical species of $PM_{10}$ and TSP with wind speed

High wind speed means a high degree of atmospheric transport and dilution. High wind speed is known to reduce the concentration of particulates coming from local emission sources. However, it can not significantly affect the concentration of particulates coming from a long distance. For crustal elements coming from fugitive dust, high wind speed will increase their emission sources because strong wind blows the dust from the ground into air.

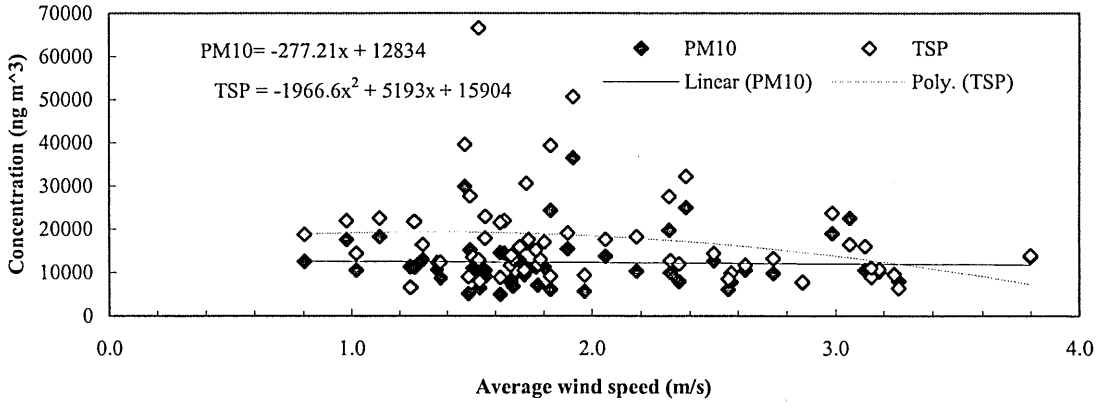


Figure 5.20 Variations of mass concentration of $PM_{10}$ and TSP with wind speed

Variations of mass concentrations of $PM_{10}$ and TSP with the average wind speed during the sampling period are shown in Figure 5.20. As with the sutuation for

temperature, no noticeable relationship between $PM_{10}$ mass concentrations and the average wind speeds may be derived. Linear regression can be fitted for $PM_{10}$ mass concentrations and average wind speed. However, the correlation coefficient is only 0.03. The scattered relationship between $PM_{10}$ mass and wind speed is caused by other factors such as rainfall and ambient temperature. A second order polynomial regression can describe the variation of TSP mass concentrations vs. average wind speed. The correlation coefficient is 0.24. The mass concentration of TSP increases first with wind speed. Then, it decreases with wind speed.

Variations of chemical species concentrations of $PM_{10}$ with the average wind speed during the sample period are shown in Figure 5.21. Variation trends of secondary species in $PM_{10}$ with average wind speed are different (Figure 5.21a). Linear regressions can be fitted for $SO_4^{2-}$ and $NO_3^-$. The linear correlation coefficients are 0.27 and 0.19 for $SO_4^{2-}$ and $NO_3^-$, respectively. Concentration of $SO_4^{2-}$ increases with wind speed while concentration of $NO_3^-$ decreases with wind speed. A second order polynomial regression can represent variation of $NH_4^+$ in $PM_{10}$ with average wind speed. The correlation coefficient is 0.68.

Concentration of $Ca^{2+}$ in $PM_{10}$ decreases with wind first (Figure 5.21b). Then, it increases with wind. A second order polynomial regression can be fitted. The correlation coefficient is 0.22. Variation of $K^+$ concentration in $PM_{10}$ with wind speed is very complex. A second order polynomial regression had to be fitted to describe this variation. The correlation coefficient is only 0.06.

The second order polynomial regressions can represent variations of marine aerosol in $PM_{10}$ with average wind speed (Figure 5.21c). The correlation coefficients are 0.49, 0.32 and 0.37 for $Cl^-$, $Na^+$ and $Mg^{2+}$, respectively. Concentrations of Na+ and $Mg^{2+}$ generally increase with wind speed. However, $Cl^-$ concentration decreases with wind speed first. Then, it increases with wind speed.

Concentrations of trace elements in $PM_{10}$ decrease with average wind speed first (Figure 5.21d). Then, they increase with wind. The second order polynomial regressions can describe these variations. The correlation coefficients are 0.11, 0.25, 0.13 and 0.20 for Pb, Ni, Zn and Cu, respectively.

Variations of concentrations of chemical species in TSP with the average wind speed during the sampling period are shown in Figure 5.22. No significant trends can be found for variations of secondary species in TSP with average wind speed (Figure 5.22a).

Second order polynomial regressions had to be fitted variations of $SO_4^{2-}$, $NO_3^-$ vs. average wind speed while liner regressions was fitted variations of $NH_4^+$ and wind speed. The correlation coefficients are 0.01, 0.24 and 0.20 for $SO_4^{2-}$, $NO_3^-$ and $NH_4^+$, respectively.

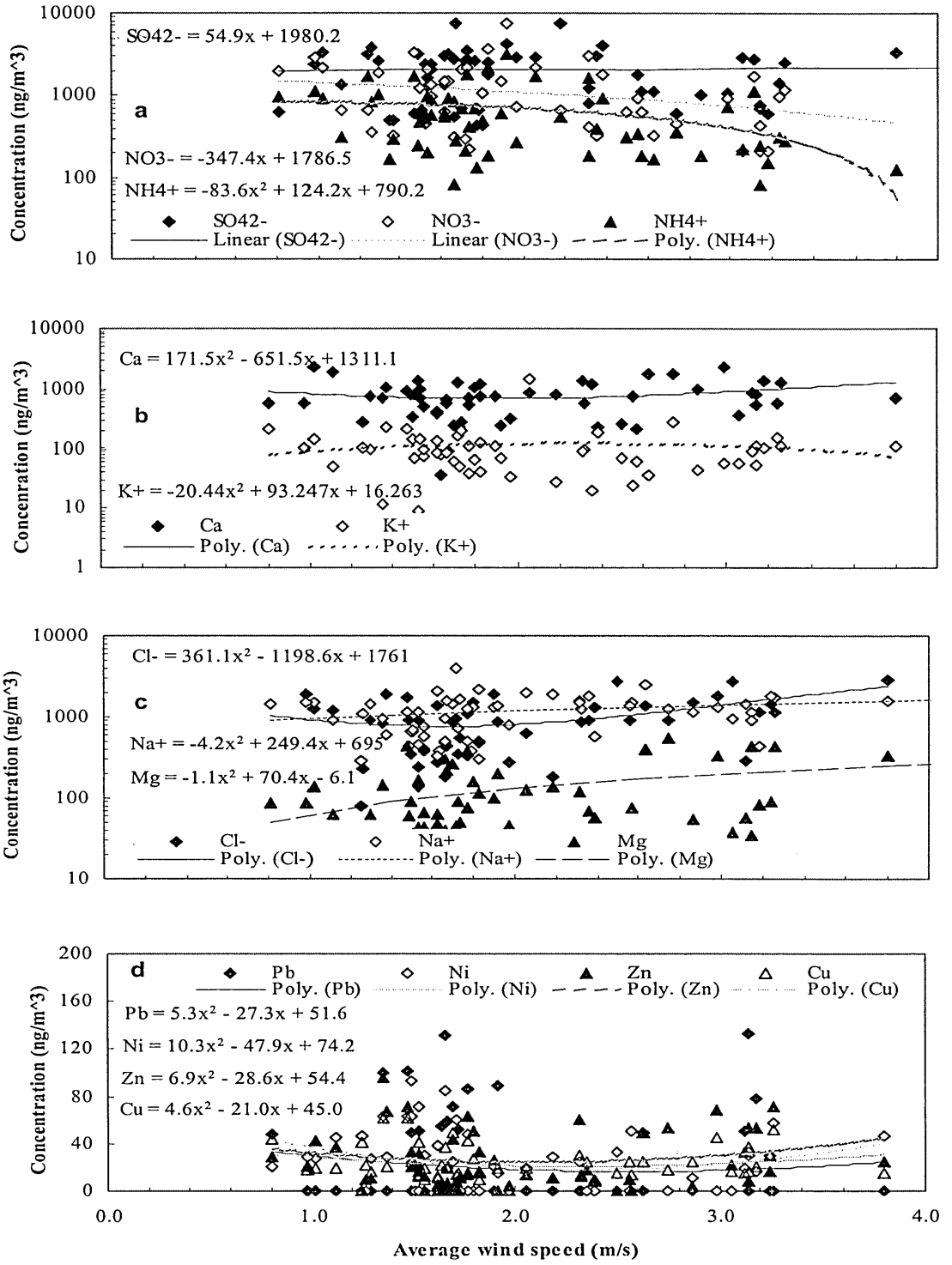


Figure 5.21 Variations of chemical species concentrations of $PM_{10}$ with wind speed

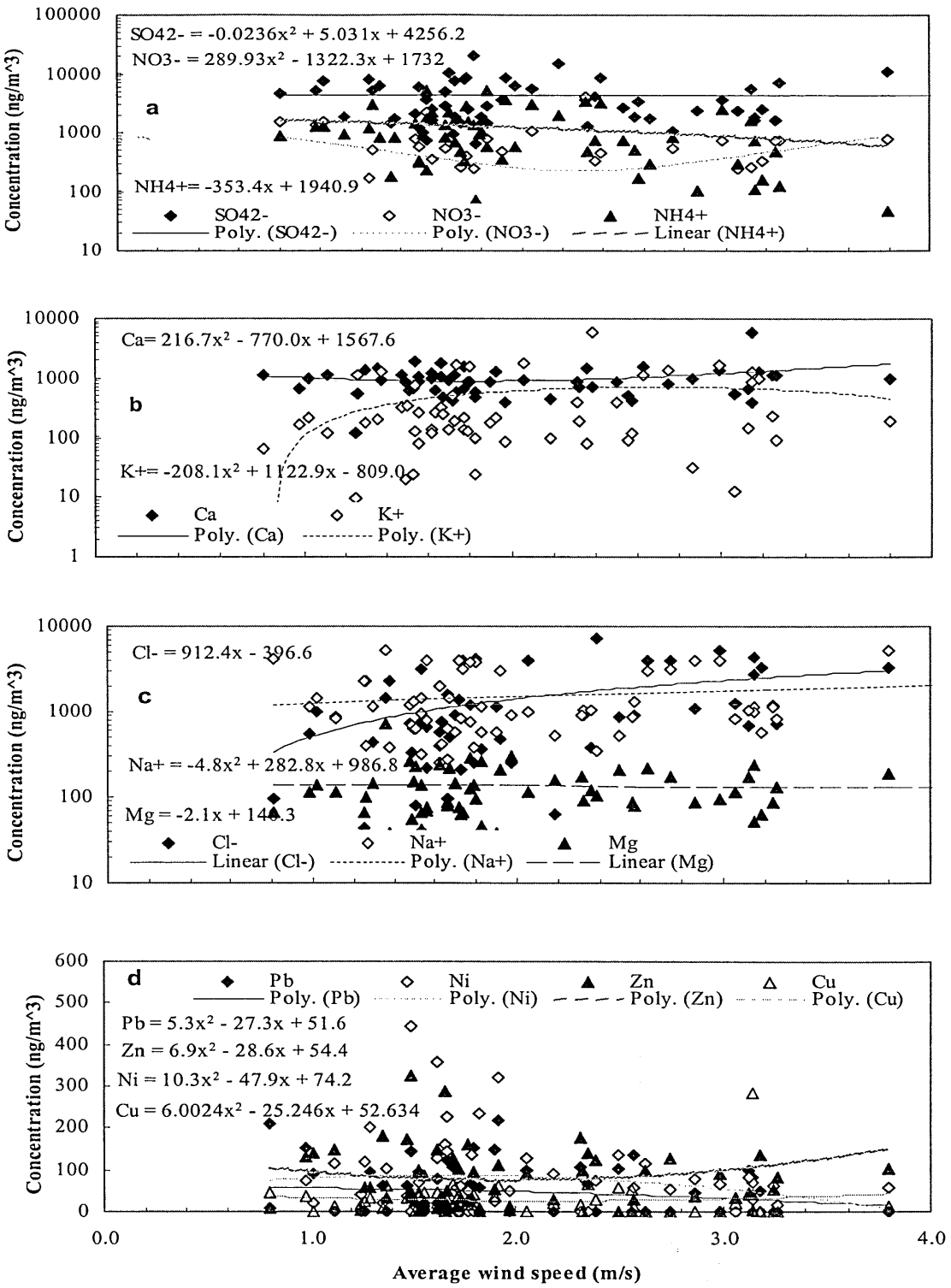


Figure 5.22 Variations of chemical species concentrations of TSP with wind speed

Variation trends of $Ca^{2+}$ and $K^+$ in TSP with wind speed are different (Figure 5.22b). The second order polynomial regressions can represent the variation of $Ca^{2+}$ and $K^+$ with wind speed. The correlation coefficients are 0.23 for $Ca^{2+}$ and 0.22 for $K^+$.

Variations of marine aerosol in TSP with average wind speed are different (Figure 5.22c). Linear relationships can describe the variations of $Cl^-$ and $Mg^{2+}$ with wind speed. The correlation coefficients are 0.40 for $Cl^-$ and 0.15 for $Mg^{2+}$. Concentration of $Cl^-$ increases with wind speed while concentration of $Mg^{2+}$ decreases with wind speed. A second order polynomial regression had to be fitted for $Na^+$ in TSP vs average wind speed The correlation coefficient is 0.19.

Variations of trace elements in TSP with average wind speed are more complex than those in $PM_{10}$ (Figure 5.22d). Concentration of Pb generally decreases with wind speed. The linear correlation coefficient is 0.21. The second order polynomial regressions can represent variations of Ni, Zn and Cu with wind speed. The correlation coefficients are 0.18, 0.16 and 0.09 for Ni, Zn and Cu, respectively.

### 5.3.6 Contributions of wind aspects to concentrations of masses and chemical species of $PM_{10}$ and TSP

An investigation into the effect of wind aspects on airborne particulates may show the direction of the source. The source direction that affects the monitoring and analysis results of $PM_{10}$ and TSP at the study station can be identified roughly by comparing average contribution of wind aspect with the average frequency of wind direction. If the average contribution of the wind aspect to a chemical species is higher than the wind direction frequency, it means the contribution of source from this aspect to this specie is higher than the average level and the sources related to the species are strong in this direction. On the other hand, if the average contribution of the wind aspect to a chemical species is lower than the wind direction frequency, it means the contribution of source from this aspect to this species is lower than the average level and the sources related to the species are weak in this direction.

Average contributions of wind aspects to concentrations of masses and chemical species of $PM_{10}$ and TSP can be calculated using

$$E_{jk} = \sum_{i=1}^{N} C_{ik} P_{ij} / \sum_{i=1}^{N} C_{ik} \qquad (5.7)$$

Where $E_{jk}$ (%) is average contribution of $j$ wind aspect to $k$ chemical species, $C_{ik}$ is the concentration of $k$ chemical species in $i$ sample, $P_{ij}$ (%) is the frequency of $j$ wind aspect

during sampling period for $i$ sample. $N$ is the sample number. Average contributions of wind aspects on mass and chemical species of $PM_{10}$ and TSP calculated using the above formula are shown in Tables 5.7 and 5.8. For comparison, annual average frequency distribution of wind direction is listed in the tables as well.

The two prevailing winds measured at the station are westerly (WSW, W and WNW) and easterly (ENE, E and ESE) with annual average frequency of 33.61% and 20.66% respectively. The average contribution of westerly wind to $PM_{10}$ mass is 30.63% (Table 5.7). It is lower than the value of wind frequency. The average contribution of easterly wind to $PM_{10}$ mass is 24.15%. On the other hand, this is higher than the value of wind frequency. A comparison of the wind aspect contribution and wind frequency indicates that $PM_{10}$ sources located in the easterly direction is stronger than those in westerly direction.

Table 5.7 Average contributions of wind aspects on mass and chemical species of $PM_{10}$ (%)

| | AWF* | Mass | $SO_4^{2-}$ | $NO_3^-$ | $NH_4^+$ | $Ca^{2+}$ | $K^+$ | $Cl^-$ | $Na^+$ | $Mg^{2+}$ | Pb | Ni | Zn | Cu |
|---|---|---|---|---|---|---|---|---|---|---|---|---|---|---|
| C | 26.85 | 26.49 | 28.04 | 30.21 | 30.04 | 24.48 | 27.18 | 23.45 | 24.83 | 23.82 | 27.38 | 27.50 | 25.49 | 26.40 |
| N | 0.69 | 0.84 | 0.76 | 0.82 | 0.81 | 0.96 | 1.11 | 0.88 | 0.91 | 0.92 | 0.96 | 0.96 | 0.99 | 0.94 |
| NNE | 1.12 | 1.15 | 1.25 | 1.18 | 1.26 | 1.20 | 1.29 | 1.11 | 1.16 | 0.85 | 0.79 | 1.12 | 0.91 | 0.96 |
| NE | 3.00 | 3.28 | 4.01 | 4.01 | 4.26 | 2.39 | 3.96 | 2.58 | 2.99 | 1.97 | 2.14 | 2.12 | 1.79 | 2.35 |
| ENE | 6.57 | 7.74 | 9.38 | 9.51 | 10.02 | 5.60 | 9.36 | 6.13 | 7.04 | 4.49 | 5.07 | 4.88 | 4.29 | 5.33 |
| E | 8.36 | 9.45 | 11.72 | 11.81 | 12.49 | 6.65 | 11.26 | 6.83 | 8.30 | 5.65 | 6.18 | 5.69 | 5.05 | 6.61 |
| ESE | 5.74 | 6.96 | 9.02 | 8.70 | 9.26 | 4.27 | 6.89 | 4.94 | 5.77 | 4.05 | 4.02 | 3.94 | 3.33 | 4.76 |
| SE | 1.97 | 2.17 | 2.69 | 2.64 | 2.80 | 1.46 | 2.04 | 1.60 | 1.84 | 1.40 | 1.38 | 1.54 | 1.21 | 1.59 |
| SSE | 0.78 | 0.71 | 0.84 | 0.77 | 0.83 | 0.71 | 0.73 | 0.64 | 0.68 | 0.58 | 0.53 | 0.66 | 0.69 | 0.67 |
| S | 0.70 | 0.67 | 0.65 | 0.67 | 0.65 | 0.77 | 0.77 | 0.78 | 0.76 | 0.65 | 0.71 | 0.66 | 0.70 | 0.67 |
| SSW | 1.31 | 1.27 | 1.03 | 0.96 | 0.95 | 1.63 | 1.36 | 1.52 | 1.42 | 1.56 | 1.55 | 1.57 | 1.69 | 1.50 |
| SW | 3.34 | 2.87 | 2.35 | 2.15 | 2.03 | 3.59 | 2.51 | 3.70 | 3.29 | 3.61 | 2.78 | 3.36 | 3.53 | 3.28 |
| WSW | 8.91 | 7.80 | 6.23 | 5.83 | 5.41 | 9.98 | 6.83 | 10.11 | 8.92 | 10.47 | 8.14 | 9.20 | 9.96 | 9.36 |
| W | 13.12 | 11.87 | 9.38 | 8.79 | 8.13 | 15.04 | 10.43 | 15.02 | 13.45 | 16.48 | 14.59 | 15.00 | 16.49 | 14.65 |
| WNW | 11.58 | 10.96 | 8.27 | 7.75 | 7.23 | 13.77 | 9.26 | 13.58 | 12.15 | 15.39 | 15.58 | 14.04 | 15.56 | 13.84 |
| NW | 4.38 | 4.34 | 3.25 | 3.07 | 2.82 | 5.74 | 3.90 | 5.39 | 4.90 | 6.36 | 6.09 | 5.94 | 6.46 | 5.63 |
| NNW | 1.58 | 1.44 | 1.12 | 1.08 | 1.03 | 1.68 | 1.48 | 1.72 | 1.60 | 1.78 | 2.15 | 1.71 | 1.93 | 1.67 |

*AWF Annual average distribution of wind direction frequency

Contributions of wind aspect to secondary pollution species in $PM_{10}$ are similar. The average contributions of easterly wind are 30.12% for $SO_4^{2-}$, 30.02% for $NO_3^-$ and

31.77% for $NH_4^+$. They are much higher than easterly wind frequency. The average contributions of westerly wind to $SO_4^{2-}$, $NO_3^-$ and $NH_4^+$ are 23.88%, 22.37% and 20.77% respectively. They are much lower than westerly wind frequency. It shows that the sources for secondary pollution species in $PM_{10}$, located in the easterly direction, are much stronger than those in the westerly direction. Secondary pollution species mainly come from long distance transport. The east of Dundee borders the North Sea. The secondary species from the east should come from the North Sea and the European continent. Contributions of wind aspects indicate that European continent is a major source for secondary species because most of the sulphate measured at the station is NSS (non-sea salt sulphate).

Table 5.8 Average contributions of wind aspects on mass and chemical species of TSP (%)

| | AWF* | Mass | $SO_4^{2-}$ | $NO_3^-$ | $NH_4^+$ | $Ca^{2+}$ | $K^+$ | $Cl^-$ | $Na^+$ | $Mg^{2+}$ | Pb | Ni | Zn | Cu |
|---|---|---|---|---|---|---|---|---|---|---|---|---|---|---|
| C | 26.85 | 27.93 | 28.22 | 30.75 | 28.50 | 23.78 | 23.54 | 21.52 | 21.96 | 23.10 | 30.42 | 27.23 | 24.89 | 24.19 |
| N | 0.69 | 0.80 | 0.79 | 0.97 | 0.78 | 0.87 | 0.80 | 0.86 | 0.87 | 0.82 | 0.88 | 0.70 | 0.90 | 0.84 |
| NNE | 1.12 | 1.12 | 1.19 | 0.98 | 1.24 | 0.96 | 1.00 | 0.92 | 0.96 | 0.97 | 1.04 | 1.27 | 0.85 | 0.99 |
| NE | 3.00 | 3.31 | 3.71 | 2.92 | 4.18 | 2.40 | 3.44 | 2.46 | 2.42 | 2.62 | 3.10 | 3.86 | 1.92 | 2.82 |
| ENE | 6.57 | 7.79 | 8.70 | 7.25 | 9.91 | 5.39 | 8.26 | 5.77 | 5.64 | 6.02 | 6.87 | 8.76 | 4.53 | 6.46 |
| E | 8.36 | 9.66 | 10.97 | 8.87 | 12.41 | 6.69 | 9.83 | 6.78 | 6.63 | 7.18 | 7.93 | 10.57 | 5.69 | 7.74 |
| ESE | 5.74 | 7.02 | 7.92 | 6.55 | 9.22 | 4.77 | 7.46 | 4.87 | 4.69 | 5.36 | 5.18 | 7.59 | 3.92 | 5.55 |
| SE | 1.97 | 2.18 | 2.36 | 2.16 | 2.72 | 1.56 | 2.19 | 1.50 | 1.44 | 1.68 | 1.56 | 2.32 | 1.44 | 1.67 |
| SSE | 0.78 | 0.74 | 0.80 | 1.02 | 0.87 | 0.68 | 0.74 | 0.60 | 0.62 | 0.68 | 0.57 | 0.79 | 0.70 | 0.74 |
| S | 0.70 | 0.65 | 0.64 | 0.97 | 0.65 | 0.86 | 0.60 | 0.69 | 0.79 | 0.88 | 0.72 | 0.64 | 0.87 | 1.00 |
| SSW | 1.31 | 1.17 | 1.12 | 1.26 | 0.97 | 1.70 | 1.28 | 1.54 | 1.62 | 1.64 | 1.09 | 1.31 | 1.76 | 1.67 |
| SW | 3.34 | 2.78 | 2.61 | 3.14 | 2.28 | 3.44 | 2.85 | 3.70 | 3.72 | 3.50 | 2.71 | 2.47 | 3.59 | 3.31 |
| WSW | 8.91 | 7.44 | 6.86 | 7.94 | 5.79 | 9.81 | 7.90 | 10.37 | 10.40 | 9.58 | 7.60 | 6.89 | 10.07 | 8.83 |
| W | 13.12 | 11.41 | 10.15 | 11.18 | 8.70 | 14.89 | 12.43 | 15.91 | 15.78 | 14.44 | 12.38 | 10.49 | 15.51 | 13.44 |
| WNW | 11.58 | 10.56 | 9.16 | 9.39 | 7.75 | 14.42 | 11.37 | 14.61 | 14.59 | 14.02 | 11.85 | 10.01 | 15.42 | 13.37 |
| NW | 4.38 | 4.07 | 3.56 | 3.56 | 2.96 | 5.73 | 4.70 | 6.00 | 5.89 | 5.52 | 4.55 | 3.81 | 6.12 | 5.01 |
| NNW | 1.58 | 1.39 | 1.23 | 1.10 | 1.07 | 2.05 | 1.61 | 1.88 | 1.98 | 1.98 | 1.48 | 1.28 | 2.19 | 2.24 |

*AWF Annual average distribution of wind direction frequency

Contributions of wind aspect to two crustal elements in $PM_{10}$ are different. The contribution of easterly wind to $Ca^{2+}$ is 16.63%. It is lower than the wind frequency. The contribution of westerly wind to $Ca^{2+}$ is 38.80%. It is higher than the wind frequency. This implies that the sources for $Ca^{2+}$ located in the westerly direction are stronger than those

located in the easterly direction. In contrast to $Ca^{2+}$, the contribution of easterly wind to $K^+$, with a value of 27.5%, is higher than the wind frequency. The contribution of westerly wind to $K^+$, with a value of 26.52%, is lower than the wind frequency. This means that the sources for $K^+$ located in the easterly direction are stronger than those located in the westerly direction.

Although both of them come from marine source with identical temporal variations, contributions of wind aspect to $Cl^-$ and $Na^+$ for $PM_{10}$ in Dundee are slightly different. The contribution of wind aspect to $Na^+$ is similar to the wind frequency. It means that the sources from all directions are similar for $Na^+$ in Dundee. UK is surrounded by Atlantic Ocean and the North Sea. The sources from all directions are similar for $Na^+$, which suggests that marine aerosols are similar from both Atlantic Ocean and North Sea. The contribution of westerly wind to $Cl^-$ with a value of 38.71% is higher than the wind frequency. The contribution of easterly wind to $Cl^-$ is 17.89%. It is lower than the wind frequency. As mentioned in section 5.3.1, the average equivalent concentration ratio of $Cl^-$ to $Na^+$ for $PM_{10}$ measured in Dundee is 0.55. It is much lower than the value of 1.16 reported for seawater (Wilson, 1975). There is a loss reaction of particulate $Cl^-$ when gaseous acid species react with sea salt aerosol to liberate gaseous HCl, e.g. NaCl (aq) + $HNO_3$ (g) $\rightarrow$ $NaNO_3$ (aq) + HCl (g). The contribution of easterly wind to $Cl^-$ is lower than the wind frequency and the contribution of westerly wind to $Cl^-$ is higher than wind frequency. This may suggest that the loss reaction of particulate $Cl^-$ is stronger for marine aerosol from the easterly direction (or the North Sea) than from the westerly direction (or the Atlantic Ocean). The contribution of easterly wind to $Mg^{2+}$ in $PM_{10}$ is 14.95%. It is much lower than the wind frequency. The contribution of westerly wind to $Mg^{2+}$ is 42.34%. It is much higher than the wind frequency. All these show that the sources for $Mg^{2+}$ in Dundee are much stronger in the westerly direction than in the easterly direction.

Contributions of wind aspect to trace elements in $PM_{10}$ are similar. The contributions of easterly wind to Pb, Ni, Zn and Cu are 15.27%, 14.51%, 12.67% and 16.70%, respectively. They are lower than the wind frequency. The contributions of westerly wind to Pb, Ni, Zn and Cu are 38.30%, 38.25%, 42.02% and 37.84%, respectively. They are higher than the wind frequency. This analysis shows that the sources for trace elements in $PM_{10}$ located in the westerly direction are stronger than those located in the easterly direction.

The average contributions of easterly wind and westerly wind to TSP mass with the values of 24.46% and 29.41% respectively are similar to those for $PM_{10}$ (Table 5.8). They indicate that source aspects for TSP and $PM_{10}$ are similar.

Contributions of wind aspect to secondary species in TSP are generally similar to those in $PM_{10}$. However, there is a difference in intensity, especially for $NO_3^-$. As mentioned above, there may be a system error in sampling and analysis processes for $NO_3^-$ in TSP. The contributions of easterly wind for $SO_4^{2-}$, $NO_3^-$ and $NH_4^+$ are 27.59%, 22.67% and 31.54% respectively while the contributions of westerly wind are 26.17%, 28.51% and 22.24%. It also shows that the European continent is the major source for secondary species in TSP as well.

Contributions of wind aspect to two crustal elements in TSP are also similar to those in $PM_{10}$. The sources for $Ca^{2+}$ in Scotland are stronger than those from the European continent. The sources for $K^+$ from the European continent are stronger than those in Scotland.

In contrast to those in $PM_{10}$, the contributions of wind aspect to $Cl^-$ and $Na^+$ are similar in TSP. The contributions of westerly wind for both of $Cl^-$ and $Na^+$ are higher than wind frequency while the contribution of easterly wind for them are lower than wind frequency. It indicates that the marine aerosol source for TSP from the Atlantic Ocean is stronger than that from the North Sea. The sources for $Mg^{2+}$ in TSP located in westerly direction are also stronger than those located in the easterly direction

Contributions of wind aspect to trace elements in TSP are different. The contributions of wind aspect to Pb and Cu approach the wind frequency. It means that there is no favoured source aspect for these two elements. The sources for Zn located in the westerly direction are stronger than those in the easterly direction. The sources for Ni located in the easterly direction are stronger than those in the westerly direction.

### 5.3.7 Multi variations of masses and chemical species of $PM_{10}$ and TSP with rainfall, temperature, wind speed and wind frequencies

The analysis in sections 5.3.3, 5.3.4 and 5.3.5 indicates that variations of mass and chemical species of $PM_{10}$ and TSP with single weather factor such as rainfall, ambient temperature and wind speed are very complex. Second, third or even fourth order polynomial regressions had to be fitted for these variations. The correlation coefficients are usually low. Contributions of wind aspects to concentrations of masses and chemical

species of $PM_{10}$ and TSP (section 5.3.6) show that aerosol sources for mass and some species may be stronger in certain direction than in other directions. Multi correlations of masses and chemical species of $PM_{10}$ and TSP with the total rainfall, ambient temperature, average wind speed, easterly wind frequency (ENE, E and ESE) and westerly wind frequency (WSW, W and WNW) during the sampling period have been done to derive the equations that can show the effects of multi weather factors on aerosol mass and components.

The multi regression equations at the 95% confidence level that describe relationships among masses of $PM_{10}$ and TSP (ng $m^{-3}$) and rainfall (*RF*, mm), wind speed (*WS*, m $s^{-1}$), easterly and westerly wind frequencies (*EW* and *WW*, %) and ambient temperature (*T*, °C), are shown in equations 5.4-5.5. The traffic volume is not included in these relationships because daily average traffic volume is a constant.

$$PM_{10} = -(1.15 \pm 1.39)*10^2 * RF + (2.07 \pm 2.04)*10^3 * WS + (9.13 \pm 18.46)*10^3 * EW - (8.62 \pm 12.69)*10^3 * WW - (2.55 \pm 2.43)*10^2 * T + (1.25 \pm 0.44)*10^4 \quad (5.4)$$

$$TSP = (5.11 \pm 2.37)*10^2 * RF - (3.48 \pm 3.60)*10^3 * WS + (2.76 \pm 3.25)*10^4 * EW + (2.81 \pm 22.40)*10^3 * WW - (2.65 \pm 4.16)*10^2 * T + (1.95 \pm 0.78)*10^4 \quad (5.5)$$

Equation 5.4 indicates that the mass concentration of $PM_{10}$ decreases with rainfall, westerly wind frequency and ambient temperature and increases with wind speed and easterly wind frequency. The correlation coefficient (*r*) for 59 $PM_{10}$ samples is 0.44. The variations of $PM_{10}$ mass with multi weather factors are similar to those with single weather factors. Mass concentration of $PM_{10}$ decreases with rainfall, which shows the effect of rainfall as a cleaning process. It increases with easterly wind frequency and decreases with westerly wind frequency because $PM_{10}$ sources in easterly direction are stronger than those in the westerly direction. $PM_{10}$ decreases with ambient temperature which is caused by seasonal variation of anthropogenic emission sources. They are high in winter and low in summer. $PM_{10}$ increases with wind speed. The reason for these observations is not immediately apparent. The variation of TSP mass with multi weather factors (equation 5.5) is different with $PM_{10}$. Mass concentration of TSP decreases with wind speed and ambient temperature and increases with rainfall and both of easterly and westerly wind frequencies. The correlation coefficient (*r*) for 60 TSP samples is 0.47. Mass concentration of TSP decreases with wind speed and ambient temperature shows the effects of atmospheric transport and seasonal variation of anthropogenic emission sources. Although, TSP mass increases with both the easterly and westerly wind frequencies, the coefficient for easterly

wind is about one order of magnitude higher than that for the westerly wind. It indicates that TSP sources in the easterly direction are also stronger than those in the westerly direction. TSP increases with rainfall can not be interpreted reasonably.

The multi regression equations at the 95% confidence level that describe relationships among second species in $PM_{10}$ and weather factors are shown in equations 5.6-5.8.

$$SO_{4\,(PM_{10})}^{2-} = -(1.53 \pm 2.59)*10^{2} * RF - (2.11 \pm 3.79)*10^{2} * WS + (7.24 \pm 3.43)*10^{3} * EW + (8.75 \pm 23.60)*10^{2} * WW + (9.56 \pm 4.53)*10^{1} * T + (3.17 \pm 8.20)*10^{2} \quad (5.6)$$

$$NO_{3\,(PM_{10})}^{-} = (1.56 \pm 2.81)*10^{1} * RF - (1.14 \pm 4.13)*10^{2} * WS + (4.05 \pm 3.73)*10^{3} * EW - (3.82 \pm 25.63)*10^{2} * WW - (9.45 \pm 4.92)*10^{1} * T + (1.63 \pm 8.91)*10^{3} \quad (5.7)$$

$$NH_{4\,(PM_{10})}^{+} = (4.56 \pm 11.29)*10^{0} * RF - (6.67 \pm 16.59)*10^{1} * WS + (2.36 \pm 1.45)*10^{3} * EW - (2.67 \pm 10.31)*10^{2} * WW - (2.00 \pm 1.98)*10^{1} * T + (6.84 \pm 3.58)*10^{2} \quad (5.8)$$

$SO_4^{2-}$ in $PM_{10}$ decreases with rainfall and wind speed (equation 5.6). It increases with both the easterly and westerly wind frequencies and ambient temperature. The correlation coefficient ($r$) is significantly high with a value of 0.76. It shows the effects of rainfall cleaning process and atmospheric transport that $SO_4^{2-}$ in $PM_{10}$ decreases with rainfall and wind speed. Although, $SO_4^{2-}$ in $PM_{10}$ increases with both the easterly and westerly wind frequencies, the coefficient for easterly wind is about one order of magnitude higher than that for the westerly wind. It indicates that $SO_4^{2-}$ sources in the easterly direction are stronger than those in the westerly direction. $SO_4^{2-}$ in $PM_{10}$ increases with the ambient temperature. This maybe the result of the effect of ambient temperature on transformation of $SO_2$ to $SO_4^{2-}$. The oxide rate of $SO_2$ is high in high temperature atmosphere. Variation trends of $NO_3^-$ and $NH_4^+$ in $PM_{10}$ with multi weather factors are similar (equations 5.7 and 5.8). They decrease with wind speed, westerly wind frequencies and ambient temperature and increase with rainfall and easterly wind frequency. The correlation coefficients ($r$) are 0.52 for $NO_3^-$ and 0.68 for $NH_4^+$. $NO_3^-$ and $NH_4^+$ concentrations decreasing with wind speed shows the effects of atmospheric transport. Their increases with easterly wind frequency and decrements with westerly wind frequency can be attributed to their sources in east direction being stronger than those in the west direction. $NO_3^-$ and $NH_4^+$ decrease with ambient temperature may show the effect of ambient temperature on evaporation of $NO_3^-$ and $NH_4^+$ in the sampling process. High

temperature may evaporate $NO_3^-$ and $NH_4^+$ from particle sample. It can not be reasonably explained that $NO_3^-$ and $NH_4^+$ in $PM_{10}$ increase with rainfall.

The multi regression equations at the 95% confidence level that describe relationships among second species in TSP and weather factors are shown in equations 5.9-5.11.

$$SO_{4\,(TSP)}^{2-} = (1.85 \pm 0.77)*10^2 * RF - (8.83 \pm 11.65)*10^2 * WS + (1.12 \pm 1.05)*10^4 * EW + (1.14 \pm 7.26)*10^3 * WW - (1.26 \pm 13.49)*10^1 * T + (3.23 \pm 2.52)*10^3 \quad (5.9)$$

$$NO_{3\,(TSP)}^{-} = (6.07 \pm 1.38)*10^1 * RF + (1.50 \pm 2.09)*10^2 * WS - (2.28 \pm 1.89)*10^3 * EW - (2.06 \pm 1.30)*10^3 * WW - (2.75 \pm 2.42)*10^1 * T + (1.16 \pm 0.45)*10^3 \quad (5.10)$$

$$NH_{4\,(TSP)}^{+} = (5.74 \pm 2.22)*10^1 * RF - (2.87 \pm 3.56)*10^2 * WS + (5.29 \pm 3.03)*10^3 * EW + (8.58 \pm 20.90)*10^2 * WW + (2.73 \pm 3.88)*10^1 * T + (1.83 \pm 7.26)*10^2 \quad (5.11)$$

Variations of $SO_4^{2-}$ in TSP with wind speed and wind directions are similar to those in $PM_{10}$. In contrast to those in $PM_{10}$, $SO_4^{2-}$ in TSP increases with rainfall and decreases with ambient temperature. The variations of $SO_4^{2-}$ can not easily be explained. The correlation coefficient ($r$) for equation 5.9 is 0.53. $NO_3^-$ and $NH_4^+$ in TSP with multi weather factors are different. $NO_3^-$ in TSP increases with rainfall and wind speed (equation 5.10). $NO_3^-$ decreases with both the easterly and westerly wind frequencies and the coefficients for both the frequencies are similar. It suggests that sources' direction is not obvious for $NO_3^-$ in TSP. The correlation coefficient ($r$) for equation 5.10 is 0.60. $NH_4^+$ in TSP decreases with wind speed and increases with both the easterly and westerly wind frequencies. The coefficient is one order of magnitude higher for the easterly wind than that for the westerly wind. This observation indicates the effects of atmospheric transport and source directions. $NH_4^+$ in TSP increases with rainfall and ambient temperature. This increment can not easily be explained. The correlation coefficient ($r$) for equation 5.10 is 0.67.

The multi regression equations at the 95% confidence level that describe relationships among crustal elements in $PM_{10}$ and weather factors are shown in equations 5.12-5.13.

$$Ca_{(PM_{10})} = (2.00 \pm 12.27)*10^0 * RF + (3.53 \pm 1.80)*10^2 * WS - (4.12 \pm 1.63)*10^2 * EW - (2.34 \pm 1.12)*10^3 * WW - (1.07 \pm 21.51)*10^0 * T + (1.53 \pm 0.39)*10^3 \quad (5.12)$$

$$K^{+}_{(PM_{10})} = (1.15 \pm 4.48)*10^{0} * RF + (8.56 \pm 6.58)*10^{1} * WS - (3.25 \pm 5.94)*10^{2} * EW - (5.42 \pm 4.09)*10^{2} * WW - (1.14 \pm 0.78)*10^{1} * T + (2.81 \pm 1.42)*10^{2} \quad (5.13)$$

Variation trends of $Ca^{2+}$ and $K^{+}$ in $PM_{10}$ with multi weather factors are similar. Concentrations of the two crustal elements in $PM_{10}$ increase with rainfall and wind speed and decrease with two wind frequencies and ambient temperature. The correlation coefficients ($r$) are 0.44 for $Ca^{2+}$ and 0.38 for $K^{+}$. $Ca^{2+}$ and $K^{+}$ in $PM_{10}$ increase with wind speed because high wind may increase fugitive dust emission source. No reasonable explaination can be put forward for the two crustal elements increasing with rainfall and decreasing with ambient temperature.

The multi regression equations at the 95% confidence level that describe relationships among crustal elements in TSP and weather factors are shown in equations 5.14-5.15.

$$Ca_{(TSP)} = -(9.99 \pm 18.04)*10^{0} * RF + (2.64 \pm 2.73)*10^{2} * WS - (1.34 \pm 2.46)*10^{3} * EW - (6.88 \pm 16.99)*10^{2} * WW - (3.64 \pm 3.16)*10^{1} * T + (1.29 \pm 0.59)*10^{3} \quad (5.14)$$

$$K^{+}_{(TSP)} = -(1.69 \pm 2.12)*10^{1} * RF + (5.05 \pm 3.20)*10^{2} * WS - (4.28 \pm 28.92)*10^{2} * EW - (1.37 \pm 2.00)*10^{3} * WW - (2.47 \pm 37.07)*10^{0} * T + (1.28 \pm 6.93)*10^{2} \quad (5.15)$$

Variation trends of $Ca^{2+}$ and $K^{+}$ in TSP with multi weather factors are also similar. Concentrations of $Ca^{2+}$ and $K^{+}$ in TSP decrease with rainfall, two wind frequencies and ambient temperature. The concentrations increase with wind speed. The correlation coefficients ($r$) are 0.33 for $Ca^{2+}$ and 0.30 for $K^{+}$, respectively. $Ca^{2+}$ and $K^{+}$ in TSP decreasing with rainfall show the effect of rainfall cleaning process. They increase with wind speed because high wind generally increase fugitive dust emission source. It can not be explained reasonably why two crustal elements decrease with ambient temperature.

The multi regression equations at the 95% confidence level that describe relationships among marine aerosol in $PM_{10}$ and weather factors are shown in equations 5.16-5.18.

$$Cl^{-}_{(PM_{10})} = -(1.92 \pm 14.58)*10^{0} * RF + (7.73 \pm 2.14)*10^{1} * WS - (4.67 \pm 1.94)*10^{3} * EW - (3.30 \pm 1.33)*10^{3} * WW - (1.69 \pm 2.55)*10^{1} * T + (1.49 \pm 0.46)*10^{3} \quad (5.16)$$

$$Na^{+}_{(PM_{10})} = -(2.28 \pm 14.46)*10^{0} * RF + (6.41 \pm 2.12)*10^{2} * WS - (2.61 \pm 1.92)*10^{3} * EW - (2.85 \pm 1.32)*10^{3} * WW - (5.10 \pm 2.53)*10^{1} * T + (1.78 \pm 0.46)*10^{3} \quad (5.17)$$

$$Mg_{(PM_{10})} = -(3.19 \pm 2.79)*10^{0} * RF + (5.56 \pm 4.10)*10^{2} * WS - (1.33 \pm 3.70)*10^{2} * EW - (8.36 \pm 25.45)*10^{1} * WW - (1.29 \pm 0.49)*10^{1} * T + (1.94 \pm 0.88)*10^{2} \quad (5.18)$$

Variation trends of $Cl^-$, $Na^+$ and $Mg^{2+}$ in $PM_{10}$ with multi weather factors are similar. Concentrations of $Cl^-$, $Na^+$ and $Mg^{2+}$ in $PM_{10}$ decrease with rainfall, two wind frequencies and ambient temperature. They increase with wind speed. The correlation coefficients ($r$) are 0.54 for $Cl^-$, 0.52 for $Na^+$ and 0.51 for $Mg^{2+}$, respectively. Marine aerosol in $PM_{10}$ decreasing with rainfall shows the effect of rainfall cleaning process. They increase with wind speed because high wind may increase marine source emission by blowing sea water into ambient atmosphere. It can not be explained reasonably why marine aerosol decreases with ambient temperature.

The multi regression equations at the 95% confidence level that describe relationships among marine aerosol in TSP and weather factors are shown in equations 5.19-5.21.

$$Cl^{-}_{(TSP)} = -(2.17 \pm 3.47)*10^{1} * RF + (1.42 \pm 0.52)*10^{3} * WS - (5.04 \pm 4.74)*10^{3} * EW - (3.83 \pm 3.27)*10^{3} * WW - (2.20 \pm 6.07)*10^{1} * T + (1.01 \pm 1.14)*10^{3} \quad (5.19)$$

$$Na^{+}_{(TSP)} = (1.13 \pm 3.00)*10^{1} * RF + (1.27 \pm 0.45)*10^{3} * WS - (6.32 \pm 4.10)*10^{3} * EW - (4.10 \pm 2.83)*10^{3} * WW - (5.34 \pm 52.58)*10^{0} * T + (1.43 \pm 0.98)*10^{3} \quad (5.20)$$

$$Mg_{(TSP)} = (3.00 \pm 2.51)*10^{0} * RF + (4.83 \pm 3.80)*10^{1} * WS - (1.98 \pm 3.42)*10^{2} * EW - (1.26 \pm 2.36)*10^{2} * WW - (1.10 \pm 4.39)*10^{0} * T + (1.08 \pm 0.82)*10^{2} \quad (5.21)$$

Variation trend of $Cl^-$ in TSP with multi weather factors is similar to that in $PM_{10}$. In contrast to those in $PM_{10}$, concentrations of $Na^+$ and $Mg^{2+}$ in TSP increase with rainfall. This can not be reasonably explained. The correlation coefficients ($r$) for equations 5.19, 5.20 and 5.21 are 0.45, 0.47 and 0.32, respectively.

The multi regression equations at the 95% confidence level that describe relationships among trace elements in $PM_{10}$ and weather factors are shown in equations 5.22-5.25.

$$Pb_{(PM_{10})} = -(7.69 \pm 5.28)*10^{-1} * RF - (5.72 \pm 12.75)*10^{0} * WS + (3.69 \pm 11.52)*10^{1} * EW + (1.75 \pm 7.92)*10^{1} * WW - (4.29 \pm 1.52)*10^{0} * T + (6.27 \pm 2.75)*10^{1} \quad (5.22)$$

$$Ni_{(PM_{10})} = -(7.69 \pm 5.28)*10^{-1} * RF + (4.34 \pm 7.76)*10^{0} * WS - (1.06 \pm 0.70)*10^{2} * EW - (6.65 \pm 4.82)*10^{1} * WW - (2.52 \pm 0.93)*10^{0} * T + (8.22 \pm 1.67)*10^{1} \quad (5.23)$$

$$Zn_{(PM_{10})} = -(2.55 \pm 6.58)*10^{-1} * RF + (1.76 \pm 9.67)*10^{0} * WS - (8.46 \pm 8.74)*10^{1} * EW - (3.16 \pm 6.01)*10^{1} * WW - (2.71 \pm 1.15)*10^{0} * T + (7.49 \pm 2.09)*10^{1} \quad (5.24)$$

$$Cu_{(PM_{10})} = -(4.79 \pm 2.77)*10^{-1} * RF - (2.72 \pm 4.07)*10^{0} * WS - (3.43 \pm 36.74)*10^{0} * EW + (4.40 \pm 25.27)*10^{0} * WW - (1.72 \pm 0.49)*10^{0} * T + (4.60 \pm 0.88)*10^{1} \quad (5.25)$$

All four trace elements in $PM_{10}$ decrease with rainfall and temperature, showing the effects of rainfall cleaning process and seasonal variation of anthropogenic emission sources. Decrements of Pb and Cu in $PM_{10}$ (equations 5.22 and 5.24) with wind speed may be explained by high atmospheric transport ability in high wind speed. Ni and Zn in $PM_{10}$ (equation 5.23 and 5.24) increase with wind speed. This can not be explained reasonably. The correlation coefficients ($r$) for equations 5.22, 5.23, 5.24 and 5.25 are 0.42, 0.56, 0.51 and 0.58, respectively

The multi regression equations at the 95% confidence level that describe relationships among trace elements in TSP and weather factors are shown in equations 5.26-5.29.

$$Pb_{(TSP)} = (2.22 \pm 1.29)*10^{0} * RF - (1.08 \pm 1.95)*10^{1} * WS - (1.37 \pm 1.76)*10^{2} * EW - (1.13 \pm 1.21)*10^{2} * WW - (5.32 \pm 2.26)*10^{0} * T + (1.71 \pm 4.22)*10^{2} \quad (5.26)$$

$$Ni_{(TSP)} = -(7.08 \pm 21.26)*10^{-1} * RF + (1.21 \pm 32.14)*10^{0} * WS - (1.71 \pm 29.03)*10^{1} * EW - (8.17 \pm 20.00)*10^{1} * WW - (5.84 \pm 3.72)*10^{0} * T + (5.42 \pm 6.96)*10^{1} \quad (5.27)$$

$$Zn_{(TSP)} = -(3.26 \pm 20.88)*10^{-1} * RF + (1.51 \pm 3.16)*10^{1} * WS - (1.89 \pm 2.85)*10^{2} * EW - (8.41 \pm 19.67)*10^{1} * WW - (7.32 \pm 3.65)*10^{0} * T + (1.84 \pm 0.68)*10^{2} \quad (5.28)$$

$$Cu_{(TSP)} = (2.37 \pm 9.69)*10^{-1} * RF + (8.46 \pm 14.65)*10^{0} * WS - (5.66 \pm 1.32)*10^{1} * EW - (4.50 \pm .13)*10^{1} * WW - (5.28 \pm 16.96)*10^{-1} * T + (3.99 \pm 3.17)*10^{1} \quad (5.29)$$

Pb in TSP increases with rainfall and decreases with other weather factors. The correlation coefficients ($r$) for equations 5.26 is 0.50. Variation trends of Ni and Zn with weather factors are similar. They increase with wind speed and decrease with other weather factors. The correlation coefficients ($r$) for equations 5.27 and 5.28 are 0.35 and 0.41, respectively. Cu in TSP increases with rainfall and wind speed and decreases with wind frequencies and ambient temperature. The correlation coefficients ($r$) for equations 5.29 is low with a value of 0.13. This suggests that there are additional factors other than weather which may affect Cu in TSP.

### 5.3.8 Concluding Remarks

The mass concentrations for $PM_{10}$ and TSP measured at the study station are low. They are lower than most of the values measured at other sites around the world. Temporal

variations and analysis of wind aspect contribution show that $PM_{10}$ and TSP measured at the station come from similar sources. The factors affecting the aerosol mass concentrations are very complex. Analysis of multi regression indicates that $PM_{10}$ increases with the easterly wind frequency and decreases with rainfall and ambient temperature. TSP increases also with easterly wind frequency and decrease with wind speed and ambient temperature. Variations of $PM_{10}$ with wind speed and TSP with rainfall are not as expected.

$SO_4^{2-}$, $NO_3^-$ and $NH_4^+$ are three major components of $PM_{10}$ and TSP. Their concentrations measured at the station, are also low. Their temporal variations are very simular. Most of the sulphate in the particulate are NSS (non-sea salt sulphate). Analysis of wind aspect contribution indicates that the European continent is a major source for secondary pollution species. Variation trends of secondary species in $PM_{10}$ and TSP with multi weather factors are different.

$Ca^{2+}$ and $K^+$ are two important components of $PM_{10}$ and TSP. Their temporal variations are different. Concentrations of $Ca^{2+}$ and $K^+$ in $PM_{10}$ and TSP increase with wind speed. The variations of the two crustal elements in TSP with rainfall are not as expected.

Similar to the results measured at other sites in the UK, the airborne particulates measured at the study station show obvious characteristics of marine aerosol. Concentration of $Cl^-$ and $Na^+$ are relatively high. Their temporal variations are very similar. The analysis of wind aspect contribution indicates the marine aerosol sources from the Atlantic Ocean and from the North Sea are similar. However, the loss reaction of particulate $Cl^-$ in $PM_{10}$ is stronger for marine aerosol from the North Sea than from the Atlantic Ocean. Variation trends of marine aerosol in $PM_{10}$ and TSP with multi weather factors are similar except for those for $Na^+$ and $Mg^{2+}$ in TSP with rainfall.

Although the sources for trace elements are very complex, analysis of multi regression indicates that concentrations of all the trace elements in both $PM_{10}$ and TSP decrease with ambient temperature.

# Chapter 6 Model and software development

A software package on the application of atmospheric dispersion models was developed to simulate the transport of airborne pollutants. The design aim of the software package is to provide a scientific and conventional tool for environmental managers to assess the impact of air pollution sources on ambient air quality and attribute airborne pollutant emission sources to their receptors. This software package can be used by local authorities to conduct air quality review and draw up the action plan to remedy the situation according to the UK National Air Quality Strategy (Department of the Environment, Transport and the Region, 1999). It may also be used as an educational tool by students studying environmental science, engineering and other environment related courses at universities.

The atmospheric dispersion models used in the software package include the up-to-date hybrid plume dispersion models that represent recent advances in the understanding of planetary boundary layer and atmospheric dispersion and the conventional Gaussian plume model that is still generally used. The design allows user to select a different model, according to situation and available parameters. The software package can predict once airborne pollutant concentrations (one hour mean) from multiple point, line and area sources for multiple receptors and various atmospheric dispersion conditions. It can predict a series of one hour mean concentrations, daily mean concentrations and annual mean concentration based on a series of hourly meteorological variables or parameters of the atmospheric boundary structure as well. The daily variation or annual variation for some special sources with temporal emission can be considered by attaching relevant factors. The contributions of various kinds of pollution sources to air pollution can be calculated by grouping the appropriate sources. The software package has very user-friendly interfaces that ensure easy operation even for non-professional users. Microsoft Visual C++ is used to compile the software.

In addition to the above, a receptor model is also used to identify airborne pollutant sources in this work. Positive Matrix Factorization (PMF) model was selected because of the advantages described in section 2.4.3. The software package for the application of PMF was developed by Paatero(1998) and can attribute airborne pollutant emission sources to their receptors. It is not a requirement here that the source profiles should be

comprehensive. Fortran was used to compile the software. This package was purchased from the University of Helsinki, Finland.

## 6.1 Atmospheric Dispersion Models

The atmospheric dispersion models used in the software package, developed by the author, have a general form:

$$C = \frac{QG_yG_z}{u} \tag{6.1}$$

where $Q$ is the source emission rate, $u$ is the wind speed, $G_y$ and $G_z$ are concentration distribution functions in the lateral and vertical directions respectively. As a basic supposition with "steady" plume models, the source and meteorological conditions or planetary boundary layer conditions are assumed to be constant over the average time (one hour).

### 6.1.1 Modified hybrid plume dispersion model

Hybrid plume dispersion model (HPDM) developed by Hanna and Paine (1989) was used to simulate the transport and dispersion of airborne pollutant from an elevated release source. Emphasis in the model is on convective and high-wind conditions. The dispersion estimate for the convective boundary layer were developed from laboratory experiments and field studies. For convective conditions, the vertical concentration distribution is non-Gaussian, but for neutral and stable conditions it is assumed to be Gaussian. In contrast to original HPDM, the author added a function ($P$) that represents the probability that receptor is under the influence of the plume (Wang et al. 1999) to the model. The general form for the modified hybrid plume dispersion model developed by the author, is:

$$C = \frac{QG_yG_z}{u}P \tag{6.2}$$

The lateral concentration distribution is assumed to be Gaussian for all atmospheric stability conditions. If $x$ axis is along the wind direction, $G_y$ is given by:

$$G_y = \frac{1}{\sqrt{2\pi}\,\sigma_y}\exp\left[-0.5\left(\frac{y}{\sigma_y}\right)^2\right] \tag{6.3}$$

where $\sigma_y$ is lateral atmospheric dispersion parameter.

The vertical distribution is assumed to be Gaussian only for stable and neutral conditions because it is non-Gaussian for an unstable condition. In stable and neutral conditions, $G_z$ is given by:

$$G_z = \frac{1}{\sqrt{2\pi}\sigma_z} \exp\left[-0.5\left(\frac{z - h_p}{\sigma_z}\right)^2\right] + \exp\left[-0.5\left(\frac{z + h_p}{\sigma_z}\right)^2\right] \tag{6.4}$$

where $\sigma_z$ is vertical atmospheric dispersion parameter, $h_p$ is the height of the plume centerline above the ground. Total reflection at the surface is accounted for in this equation.

In unstable conditions, a probability density function (p.d.f.) model developed from Weil and Brower (1985) and a convective scaling model described by Hanna and Paine (1987) have been used to describe $G_z$. The p.d.f. model is used for low buoyancy fluxes. Defined by $F_* < 0.1$. $F_*$ is a dimensionless buoyancy flux. It is defined by:

$$F_* = F / u w_*^2 z_i \tag{6.5}$$

with

$$F = w_s R_s^2 (g / T_s)(T_s - T_a) \tag{6.6}$$

where $w_*$ is a convective velocity scale, $w_s$ is initial plume vertical speed, $R_s$ is internal radius of the stack, $g$ is the acceleration due to gravity, $T_s$ is the initial plume temperature and $T_a$ is the ambient temperature. $F(\mathrm{m}^4\ \mathrm{s}^{-3})$ is commonly referred to as the plume buoyancy flux. It is an important parameter when calculating plume rise.

The scaling parameter of $F_*$ is approximately proportional to the ratio of the plume rise to the mixing depth in convective conditions. For $F_* < 0.1$, the upper part of the plume does not touch the top of the mixed layer and the p.d.f. for ground-level concentration is the sum of two Gaussian distributions – one for the updraft and one for the downdraft. If it is assumed that downdrafts occur 60% of the time, then $G_z$ is given by:

$$G_z = \frac{1}{z_i}\left[\left(\frac{0.48}{\sigma^*_{z_1}}\right)\exp\left(-\frac{h_1^{*2}}{2\sigma^{*2}_{z_1}}\right) + \left(\frac{0.32}{\sigma^*_{z_2}}\right)\exp\left(-\frac{h_2^{*2}}{2\sigma^{*2}_{z_2}}\right)\right] \tag{6.7}$$

with

$$\sigma^{*2}_{z_i} = 0.21 F_*^{2/3} X_*^{4/3} + b_i^2 X_*^2 \tag{6.8}$$

and

$$h_i^* = h_s^* + 1.6 F_*^{1/3} X_*^{2/3} + a_i X_* \tag{6.9}$$

where $i$= 1 or 2, $h_s^* = h_s/z_i$, $\sigma_{zi}^* = \sigma_{zi}/z_i$, and $X_* = w_*x/uz_i$. The parameter $h_s$ is the stack height. The constants $a_1$ = -0.35, $a_2$ = 0.4, $b_1$ = 0.24 and $b_2$ = 0.48. Subscripts 1 and 2 refer to the downdrafts and updrafts respectively. $z_i$ is the mixing height.

As the dimensionless buoyancy parameter, $F_*$ approaches 1 from a value less than 1, the plume interacts more and more with the stable air, capping the mixed layer. In this case, a convective scaling model is used. The $G_z$ is given by:

$$G_z = \frac{0.056X^*}{z_i F_*} \qquad \text{for } X_*/F_* \le 10 \qquad (6.10)$$

and

$$G_z = \frac{1}{z_i}\exp\left[-\left(\frac{7F_*}{X_*}\right)^{3/2}\right] \qquad \text{for } X_*/F_* > 10 \qquad (6.11)$$

Another basic supposition with "steady" plume models is that the meteorological conditions are assumed to be constant over the travel time from source to receptor. This supposition is reasonable when the distance between source and receptor is not too large and wind speed is high. It will cause error if the distance is large and wind speed is small. Owen et al. (1999) applied the ADMS-Urban to estimate the concentration of oxides of nitrogen and sulphur dioxide in London. They found that during the winter period the model significantly over-predicted concentrations of $SO_2$ when the wind was blowing from an easterly direction. Analysis of the model prediction showed that these peaks were caused by the large power stations located in the East Thames corridor. These may have led to the errors produced by the neglect of the effect of travel time from the source to the receptor. Wang et al. (1999) noticed this problem and introduced a function that represents the probability that a receptor is under the influence of the plume in their primary aerosol model. It is described as:

$$P = 0 \qquad \text{if } t_T > \tau \qquad (6.12)$$

and

$$P = 1 - t_T/\tau \qquad \text{if } t_T \le \tau \qquad (6.13)$$

where $t_T$ is the plume transport time from source to receptor, $\tau$ is the sample time (one hour).

### 6.1.1.1 Atmospheric dispersion parameters

In neutral and stable conditions, atmospheric dispersion parameters, $\sigma_y$ and $\sigma_z$ are calculated by:

$$\sigma_y = \sigma_v t F_y\left(t/T_{L_y}\right) \tag{6.14}$$

$$\sigma_z = \sigma_w t F_z\left(t/T_{L_z}\right) \tag{6.15}$$

where $\sigma_v$ and $\sigma_w$ are turbulent components, $T_{L_y}$ and $T_{L_z}$ are Lagrangian time scales for dispersion, $F_y$ and $F_z$ are dimensionless functions and given by:

$$F_y = \left[1+0.9\left(t/15000\right)^{1/2}\right]^{-1} \tag{6.16}$$

$$F_z = \left(1+0.5t/T_{L_z}\right)^{-1/2} \tag{6.17}$$

$T_{L_z}$ is given by the formulae:

In stable conditions

$$T_{L_z} = z/\sigma_w \qquad \text{if } z \le L \tag{6.18}$$

and

$$T_{L_z} = 0.27s^{-1/2} \qquad \text{if } L \le 10 \tag{6.19}$$

and

$$T_{L_z} = \frac{\left(z/\sigma_w\right)\left(L-10\right)}{z-10} + \frac{0.27s^{-1/2}\left(z-L\right)}{z-10} \qquad \text{if } 10 < L < z \tag{6.20}$$

where $L$ is Monin-Obukhov length, $s$ is a stability parameter. It is given by:

$$s = (g/T)(d\theta/dz) \tag{6.21}$$

In slightly unstable conditions

$$T_{L_z} = 0.27\frac{z}{\sigma_w}\left(0.55-\frac{0.38z}{|L|}\right) \qquad \text{if } z \le |L| \tag{6.22}$$

and

$$T_{L_z} = 0.3\frac{z_i}{\sigma_w}\left[1-\exp\left(-\frac{5z}{z_i}\right)\right] - 0.0003\exp\left(\frac{8z}{z_i}\right) \qquad \text{if } |L| < z < z_i \tag{6.23}$$

In unstable condition, $\sigma_y$ is given by:

$$\sigma_y = 0.56 z_i X_* /\left(1+0.7X_*\right)^{1/2} \qquad \text{for p.d.f. model} \tag{6.24}$$

and

$$\sigma_y = 0.6 z_i X_* \qquad \text{for convective model} \tag{6.25}$$

### 6.1.1.2 Wind speed profile

In stable conditions, the wind speed profile is given by:

$$u = \frac{u_*}{0.4}\left[\ln\left(\frac{z}{z_0}\right) + 4.7\left(\frac{z}{L}\right)\right] \tag{6.26}$$

In unstable conditions, wind speed profile is given by:

$$u = \frac{u_*}{0.4}\left[\ln\left(\frac{z}{z_0}\right) - \psi_m\right] \tag{6.27}$$

with

$$\psi_m = 2\ln\left[0.5\left(1+\phi_m^{-1}\right)\right] + \ln\left[0.5\left(1+\phi_m^{-2}\right)\right] - 2\arctan\left(\phi_m^{-1}\right) + \pi/2 \tag{6.28}$$

and

$$\phi_m = \left(1 - 15z/L\right)^{-1/4} \tag{6.29}$$

### 6.1.1.3 Plume rise and partial penetration of elevated inversion

Plume rise is a very complex physical process. It does not only depend on smoke characteristics such as the amount, temperature and exit speed of gas, but also depends on ambient temperature, vertical temperature structure and wind speed. In unstable conditions, the p.d.f. model and convective scaling model options contain implicit procedures for treating plume rise. In neutral and stable conditions plume rise, $\Delta h$, is assumed to be given by the minimum of the predictions of the following set of standard equations (Briggs, 1984):

Bent-over stable

$$\Delta h = 2.6\left(F/us\right)^{1/3} \tag{6.30}$$

Calm stable

$$\Delta h = 4F^{1/4}s^{-3/8} \tag{6.31}$$

Final transitional

$$\Delta h = 38.7F^{3/5}u^{-1} \tag{6.32}$$

Unstable break-up

$$\Delta h = 4.3\left(F/u\right)^{3/5}H^{-2/5} \tag{6.33}$$

Neutral break-up

$$\Delta h = 1.3\left(F/uu_*^2\right)\left(1 + h_s/\Delta h\right)^{2/3} \tag{6.34}$$

where $F$ (equation 6.6) is plume buoyancy flux, $H$ ($m^2$ $s^{-3}$) is the surface heat flux, $s$ (equation 6.21) is the stability parameter.

If the plume rise, $\Delta h$ exceeds $0.67(z_i - h_s)$, then the top of the plume impacts the capping inversion, and a partial plume penetration of the inversion is expected. In this case, a new estimate of plume rise, $\Delta h_i$ is made using equation 6.30 and default potential temperature gradient $d\theta/dz$ = 0.5 °C/100 m. The fraction, $F_p$ of plume mass that penetrates the inversion is given using:

$$F_p = 1 \qquad \text{if } (z_i - h_s)/\Delta h_i \leq 0.5 \tag{6.35}$$

and

$$F_p = 1.5 - (z_i - h_s)/\Delta h_i \qquad \text{if } 0.5 < (z_i - h_s)/\Delta h_i < 1.5 \tag{6.36}$$

The effective plume rise of the portion $(1\text{-}F_p)$ of the plume trapped below $z_i$ can be calculated using:

$$\Delta h = (0.62+0.38F_p)(z_i - h_s) \tag{6.37}$$

Hanna and Paine (1989) assessed HPDM model using field data from the Kincaid and Bull Run power plants and a set of selected high-wind data from five power plants. They found that the greatest improvement of HPDM using the conventional Gaussian plume model was seen for high-wind neutral conditions. They recommended that HPDM is better used for the following conditions:

- Buoyant plumes from stacks at least 100 m tall.
- Terrain height less than one-half stack height.
- Cases where building-induced downwash is not important.
- Site where convection is strong or winds are high and the ground surface is grass, agricultural, or forested.

### 6.1.2 Ground-level release dispersion model

A new model developed by Venkatram and Du (1997, 1999) is selected to simulate the transport and dispersion of airborne pollutant from a ground-level release source. This model is based on using simulations of particle motion with a Lagrangian Stochastic model. The data generated from simulation are used to develop a parameterized model. The function ($P$) that represents the probability that receptor is under the influence of the source is not added to the model because the distance that the ground-level emission can

affect is limited. Instead of wind speed, an effective transport velocity $u_e$ is used in the model. The general form for the ground-level release dispersion model is:

$$C = \frac{QG_yG_z}{u_e} \tag{6.38}$$

$G_y$ has the same form to that given in equation 6.3 while $G_z$ is given by:

$$G_z = \frac{1}{\bar{z}}\exp\left[-b\left(\frac{z}{\bar{z}}\right)^{\gamma}\right] \tag{6.39}$$

where $\bar{z}$ is the plume height. It is described as:

$$\bar{z} = 0.04xg(x/|L|) \tag{6.40}$$

where $g$ is a dimensionless function and is given by:

$$g(x/|L|) = (1+0.35x/|L|)^{1/2} \qquad \text{if } L<0 \tag{6.41}$$

and

$$g(x/|L|) = (1+0.24x/|L|)^{-1/2} \qquad \text{if } L>0 \tag{6.42}$$

In unstable conditions, $\gamma = 1.3$ while $b = 0.68$. In stable conditions, $\gamma = 2.0$ while $b = 0.32$. For near-neutral condition (in the narrow range of $-0.01\ m^{-1} < 1/L < 0.01\ m^{-1}$), the linear interpolations for $\gamma$ and $b$ are given by:

$$\gamma = 1.3 + 35(1/L + 0.01) \tag{6.43}$$

$$b = 0.68 - 18(1/L + 0.01) \tag{6.44}$$

Effective transport velocity $u_e$ is described as:

$$u_e = m(x/|L|)u_* x/\bar{z}$$

where $m$ is given by:

$$m(x/|L|) = (1+0.15(x/|L|)^2)^{1/4} \qquad \text{if } L<0$$

and

$$m(x/|L|) = (1+0.26(x/|L|))^{-1/3} \qquad \text{if } L>0$$

No vertical dispersion parameter is used in the ground-level release dispersion model. The lateral dispersion parameter is calculated using the same formulae as those in the modified hybrid plume dispersion model. In stable and neutral conditions, $\sigma_y$ is given by equations 6.14 and 6.16. In unstable conditions, $\sigma_y$ for low buoyancy flux is adopted. It is given by equation 6.24.

The ground-level release dispersion model was assessed by Du and Venkatram (1997) using the data from Project Prairie Grass and the National Reactor Test Station (NRTS) experiment.

### 6.1.3 Conventional Gaussian plume dispersion model

The modified hybrid plume dispersion model and the ground-level release dispersion model represent the application of current advances in the understanding of planetary boundary layer and atmospheric dispersion. The parameters that describe the structure of atmospheric boundary layer such as Monin-Obukhov length $L$, mixing layer height $z_i$, friction velocity $u_*$, convective velocity scale $w_*$, surface roughness $z_0$, surface heat flux $H$, gradient of potential temperature $d\theta/dz$, turbulent components ($\sigma_v$ and $\sigma_w$) are needed as input to these models. However, measured values for these parameters are usually unavailable in routine meteorological observations. Various empirical formulae and suppositions have to be used if one wants estimates of these parameters using routine meteorological observed data.

In case the measured value for the parameters needed as input for the modified hybrid plume dispersion model and ground-level release dispersion model are unavailable or the measured meteorological data can not satisfy the needs for the estimation of these parameters, conventional Gaussian plume dispersion provides another choice for atmospheric dispersion simulation. Conventional Gaussian plume dispersion model has the same form as equation 6.1. $G_y$ is also given by equation 6.3 while $G_z$ is given by:

$$G_z = \frac{1}{\sqrt{2\pi}\sigma_z}\left\{\exp\left[-0.5\left(\frac{z-h_p}{\sigma_z}\right)^2\right]+\exp\left[-0.5\left(\frac{z+h_p}{\sigma_z}\right)^2\right]\right.$$
$$\left.+\sum_{i=1}^{\infty}\left\{\exp\left[-0.5\left(\frac{H_1}{\sigma_z}\right)^2\right]+\exp\left[-0.5\left(\frac{H_2}{\sigma_z}\right)\right]+\exp\left[-0.5\left(\frac{H_3}{\sigma_z}\right)\right]+\exp\left[-0.5\left(\frac{H_4}{\sigma_z}\right)\right]\right\}\right\} \quad (6.45)$$

where $H_1 = z-(2iz_i-h_p)$, $H_2 = z+(2iz_i-h_p)$, $H_3 = z-(2iz_i+h_p)$, $H_4 = z+(2iz_i+h_p)$. The infinite series term in equation 6.45 accounts for the effects of the restriction on vertical plume growth at the top of the mixing layer. The method of image sources is used to account for multiple reflections of the plume from the ground surface and at the top of the mixed layer. If the effective stack height, $h_s$ exceeds the mixing layer height $z_i$, the plume is assumed to fully penetrate the elevated inversion. The plume will not to be brought to ground. Thus, the ground-level concentration is equal to zero.

### 6.1.3.1 Atmospheric dispersion parameters

Two kinds of atmospheric dispersion parameters are used in the conventional Gaussian plume dispersion model to simulate dispersion in rural and urban areas, respectively. In rural areas, Pasquill-Gifford curves (figures 2.2 and 2.3) are used as atmospheric dispersion parameters. The equations used in the Industrial Source Complex (ISC3) dispersion models (EPA, 1995) to approximately fit the curves have been used in the model developed here because they provide the good approaches in a wide range.

$\sigma_y$ and $\sigma_z$ are given by:

$$\sigma_y = 456.11628x\tan[0.017453293(c - d\ln x)] \tag{6.46}$$

$$\sigma_z = ax^b \tag{6.47}$$

where the downwind distance $x$ is in kilometers while $\sigma_y$ and $\sigma_z$ are in meters. The coefficients, $c$ and $d$, are given in Table 6.1. The coefficients of $a$ and $b$ are given in Table 6.2.

Table 6.1 Parameters used to calculate Pasquill-Gifford $\sigma_y$

| Pasquill Stability Category | $c$ | $d$ |
|---|---|---|
| A | 24.1670 | 2.5334 |
| B | 18.3330 | 1.8096 |
| C | 12.5000 | 1.0857 |
| D | 8.3330 | 0.72382 |
| E | 6.2500 | 0.54287 |
| F | 4.1667 | 0.36191 |

In urban areas, Briggs formulae are used to estimate the atmospheric dispersion parameters (Gifford, 1976). The formulae to determine $\sigma_y$ and $\sigma_z$ in an urban area are given in Table 6.3.

Table 6.2 Parameters used to calculate Pasquill-Gifford $\sigma_z$

| Pasquill Stability Category | x (km) | a | b |
|---|---|---|---|
| A* | <.10 | 122.800 | 0.94470 |
| | 0.10 - 0.15 | 158.080 | 1.05420 |
| | 0.16 - 0.20 | 170.220 | 1.09320 |
| | 0.21 - 0.25 | 179.520 | 1.12620 |
| | 0.26 - 0.30 | 217.410 | 1.26440 |
| | 0.31 - 0.40 | 258.890 | 1.40940 |
| | 0.41 - 0.50 | 346.750 | 1.72830 |
| | 0.51 - 3.11 | 453.850 | 2.11660 |
| | >3.11 | ** | ** |
| B* | <.20 | 90.673 | 0.93198 |
| | 0.21 - 0.40 | 98.483 | 0.98332 |
| | >0.40 | 109.300 | 1.09710 |
| C* | All | 61.141 | 0.91465 |
| D | <.30 | 34.459 | 0.86974 |
| | 0.31 - 1.00 | 32.093 | 0.81066 |
| | 1.01 - 3.00 | 32.093 | 0.64403 |
| | 3.01 - 10.00 | 33.504 | 0.60486 |
| | 10.01 – 30.00 | 36.650 | 0.56589 |
| | >30.00 | 44.053 | 0.51179 |
| E | <.10 | 24.260 | 0.83660 |
| | 0.10 - 0.30 | 23.331 | 0.81956 |
| | 0.31 - 1.00 | 21.628 | 0.75660 |
| | 1.01 - 2.00 | 21.628 | 0.63077 |
| | 2.01 - 4.00 | 22.534 | 0.57154 |
| | 4.01 - 10.00 | 24.703 | 0.50527 |
| | 10.01 – 20.00 | 26.970 | 0.46713 |
| | 20.01 – 40.00 | 35.420 | 0.37615 |
| | >40.00 | 47.618 | 0.29592 |

Table 6.2 (continue)

| Pasquill Stability Category | x (km) | a | B |
|---|---|---|---|
| F | <.20 | 15.209 | 0.81558 |
| | 0.21 - 0.70 | 14.457 | 0.78407 |
| | 0.71 - 1.00 | 13.953 | 0.68465 |
| | 1.01 - 2.00 | 13.953 | 0.63227 |
| | 2.01 - 3.00 | 14.823 | 0.54503 |
| | 3.01 - 7.00 | 16.187 | 0.46490 |
| | 7.01 – 15.00 | 17.836 | 0.41507 |
| | 15.01 – 30.00 | 22.651 | 0.32681 |
| | 30.01 – 60.00 | 27.074 | 0.27436 |
| | >60.00 | 34.219 | 0.21716 |

* If the calculated value of $\sigma_z$ exceed 5000 m, $\sigma_z$ is set to 5000 m.

** $\sigma_z$ is equal to 5000 m.

Table 6.3 Briggs formulae used to calculate $\sigma_y$ and $\sigma_z$

| Pasquill Stability Category | $\sigma_y$(m)* | $\sigma_z$(m)* |
|---|---|---|
| A | $0.32\,x\,(1.0 + 0.0004\,x)^{-1/2}$ | $0.24\,x\,(1.0 + 0.001\,x)^{1/2}$ |
| B | $0.32\,x\,(1.0 + 0.0004\,x)^{-1/2}$ | $0.24\,x\,(1.0 + 0.001\,x)^{1/2}$ |
| C | $0.22\,x\,(1.0 + 0.0004\,x)^{-1/2}$ | $0.20\,x$ |
| D | $0.16\,x\,(1.0 + 0.0004\,x)^{-1/2}$ | $0.14\,x\,(1.0 + 0.0003\,x)^{-1/2}$ |
| E | $0.11\,x\,(1.0 + 0.0004\,x)^{-1/2}$ | $0.08\,x\,(1.0 + 0.0015\,x)^{-1/2}$ |
| F | $0.11\,x\,(1.0 + 0.0004\,x)^{-1/2}$ | $0.08\,x\,(1.0 + 0.0015\,x)^{-1/2}$ |

* where x is in meters

### 6.1.3.2 Wind speed profile

The power law is used to adjust the ground wind speed ($u_{10}$) to the wind speed ($u_s$) at stack or release height ($h_s$). The wind speed profile is given by:

$$u_s = u_{10}(h_s/10)^{\alpha} \tag{6.48}$$

where $\alpha$ is the wind profile exponent.

### 6.1.3.3 Plume rise

As mentioned in section 6.1.1.3, plume rise is a very complex physical process. There are two mechanisms, buoyancy and momentum rises, in plume rise process. The buoyancy rise is caused by temperature difference between plume and ambient air. The momentum rise is caused by initial momentum of the stack gas at the stack top. In modified hybrid plume dispersion model, only buoyancy rise is considered in estimating plume rise (equations 6.30 –6.34). Plume rise due to momentum is neglected. The process in between the emission point and the point at which the plume reaches its maximum height is also neglected. A series of formulae for plume rise estimation that consider both buoyancy rise and momentum rise and the plume rise process have been developed by Briggs (1969, 1971, 1974, 1975, 1979). These formulae have been discussed widely and have been adopted by ISC3 model (EPA, 1995). They are used in the conventional Gaussian plume dispersion model to estimate the plume rise. The plume buoyancy and momentum fluxes are two basic parameters used in the plume rise calculation. The plume buoyancy flux, $F$ is given by equation 6.6. The plume momentum flux, $F_m$ ($m^4/s^2$) is given by:

$$F_m = w_s^2 R_s^2 T_a / T_s \tag{6.49}$$

where $w_s$ is stack gas exit velocity, $R_s$ is inside stack top radius, $T_a$ is ambient temperature, $T_s$ is initial plume temperature.

**Stack-tip downwash**

In order to consider stack-tip downwash, modification of the physical stack height is given by:

$$h_s' = h_s + 4R_s w_s / u_s \qquad \text{for } w_s < 1.5u_s \tag{6.50}$$

and

$$h_s' = h_s \qquad \text{for } w_s \geq 1.5u_s \tag{6.51}$$

where $h_s'$ is the modified physical stack height, $h_s$ is physical stack height. This $h_s'$ was used throughout the remainder of the plume height computation. If stack tip downwash is not considered, $h_s' = h_s$ in the following equations (6.52-6.68).

**Unstable and neutral conditions**

Different formulae are used to estimate plume rise for buoyancy or momentum dominating processes. A crossover temperature difference is defined to determine whether the plume rise is dominated by momentum or buoyancy. For cases with stack gas temperature greater than or equal to ambient temperature, the crossover temperature difference, $\Delta T_c$, in unstable and neutral conditions is determined by:

$$\Delta T_c = 0.0297 T_s w_s^{1/3} / (2R_s)^{2/3} \qquad \text{if } F < 55 \tag{6.52}$$

and

$$\Delta T_c = 0.00575 T_s w_s^{2/3} / (2R_s)^{1/3} \qquad \text{if } F \geq 55 \tag{6.53}$$

If the difference between stack gas and ambient temperature, $\Delta T$, exceeds or equals $\Delta T_c$, plume rise is assumed to be buoyancy dominated, otherwise plume rise is assumed to be momentum dominated.

For situations where $\Delta T$ exceeds $\Delta T_c$, the distance to final rise, $x_f$ is calculated by:

$$x_f = 49 F^{5/8} \qquad \text{if } F < 55 \tag{6.54}$$

and

$$x_f = 119 F^{2/5} \qquad \text{if } F \geq 55 \tag{6.55}$$

The final effective plume height, $h_p$ is determined by:

$$h_p = h_s^{'} + 21.425 F^{3/4} / u_s \qquad \text{if } F < 55 \tag{6.56}$$

and

$$h_p = h_s^{'} + 38.71 F^{3/5} / u_s \qquad \text{if } F \geq 55 \tag{6.57}$$

For situations where the stack gas temperature is less than or equal to the ambient air temperature and $\Delta T$ is less than $\Delta T_c$, the assumption is made that the plume rise is dominated by momentum. The plume height is calculated by:

$$h_p = h_s^{'} + 6 R_s w_s / u_s \tag{6.58}$$

**Stable conditions**

For cases with stack gas temperature greater than or equal to ambient temperature, the crossover temperature difference in stable conditions, $\Delta T_c$, is determined by:

$$\Delta T_c = 0.019582 T_s w_s \sqrt{s} \tag{6.59}$$

where $s$ (equation 6.21) is the stability parameter. As a default approximation, the value of $d\theta/dz$ is 0.020 K m$^{-1}$ for stability class E and 0.035 K m$^{-1}$ for stability class F.

For situations where $\Delta T$ exceeds $\Delta T_c$, buoyancy is assumed to dominate. The distance to final rise, $x_f$, is determined using:

$$x_f = 2.0715 u_s / \sqrt{s} \tag{6.60}$$

The plume height is given by:

$$h_p = h_s^{'} + 2.6\left(\frac{F}{u_s s}\right)^{1/3} \tag{6.61}$$

For cases where the stack gas temperature is less than or equal to the ambient air temperature and $\Delta T$ is less than $\Delta T_c$, the assumption is also made that the plume rise is dominated by momentum. In these cases, the plume height is calculated using:

$$h_p = h_s^{'} + 2.6\left(\frac{F_m}{u_s \sqrt{s}}\right)^{1/3} \tag{6.62}$$

The equation for unstable-neutral momentum rise (6.58) is also evaluated. The lower value of these two equations is used as the resulting plume height, since stable plume rise should not exceed unstable-neutral plume rise.

**Plume rise occurring at any distance less than the distance to final rise**

The gradual rise is to be estimated for unstable, neutral, or stable conditions, if the distance downwind from source to receptor, $x$ is less than the distance to final rise. For buoyancy dominated conditions, the plume height is determined using:

$$h_p = h_s^{'} + 1.60\left(F^{1/3} x^{2/3} / u_s\right) \tag{6.63}$$

If the height exceed the final rise for the appropriate condition, the final rise is substituted instead.

For momentum dominated conditions, the following equations are used to calculate a distance dependent momentum plume rise:

$$h_p = h_s^{'} + \left(\frac{3 F_m x}{\beta_j^2 u_s^2}\right)^{1/3} \qquad \text{for unstable conditions} \tag{6.64}$$

where $x$ is the downwind distance with a maximum value defined by $x_{max}$ as follows:

$$x_{max} = \frac{8R_s(w_s + 3u_s)^2}{w_s u_s} \qquad \text{if } F = 0 \qquad (6.65)$$

and

$$x_{max} = 49F^{5/8} \qquad \text{if } 0 < F \leq 55 \qquad (6.66)$$

and

$$x_{max} = 119F^{2/5} \qquad \text{if } F > 55 \qquad (6.67)$$

and

$$h_p = h_s' + \left[\frac{3F_m \sin(x\sqrt{s}/u_s)}{\beta_j^2 u_s \sqrt{s}}\right]^{1/3} \qquad \text{for stable conditions} \qquad (6.68)$$

where $x$ is the downwind distance with a maximum value defined as follows:

$$x_{max} = \frac{0.5\pi u_s}{\sqrt{s}} \qquad (6.69)$$

The jet entrainment coefficient, $\beta_j$ is given by:

$$\beta_j = 1/3 + u_s / w_s \qquad (6.70)$$

As with the buoyant gradual rise, if the distance-dependent momentum rise exceeds the final rise for the appropriate condition, then the final rise is used instead.

## 6.2 Coordinates and their conversion

Two Cartesian coordinate systems, geographic coordinate and dispersion coordinate, are used in the software package developed here. Geographic coordinate is used to describe the locations of sources and receptors. In the geographic coordinate, east and north directions are fixed as positive $x$ and $y$ axes directions respectively while the up-direction is fixed as positive $z$ axis direction. Dispersion coordinate had to be used in simulating atmospheric dispersion because downwind distance is used in the modified hybrid plume dispersion models, ground-level release dispersion model and the conventional Gaussian plume dispersion model. The wind direction varies with time. The origin is the same for the two coordinate systems. The positive direction of the $x'$ axis in the dispersion coordinate system is directly in the downwind direction (Figure 6.1). If the

dispersion. The lateral virtual distance ($x_y$) and vertical virtual distance ($x_z$) had to be added to the actual downwind distance $x$ in simulating atmospheric dispersion.

If there is a squared area emission source with a width of $L$ and an average effective emission height of $H_e$ (Figure 6.2), the initial lateral dimension ($s_l$) and vertical dimension ($s_v$) of the area source can be calculated using:

$$s_l = L/4.3 \tag{6.74}$$

$$s_v = H_e/2.15 \tag{6.75}$$

Then, the lateral virtual distance and the vertical virtual distance are obtained by solving the equations that describe the atmospheric dispersion parameter. A digital iterative algorithm is used to solve non-linear equations.

In cases where large area emission sources with non-squared shape are to be simulated, the area source should be divided into a series of small squared area sources. The virtual point source algorithm is suitable to simulate small area source emission. It is better that the lateral scale of the squared area source is less than 1 km.

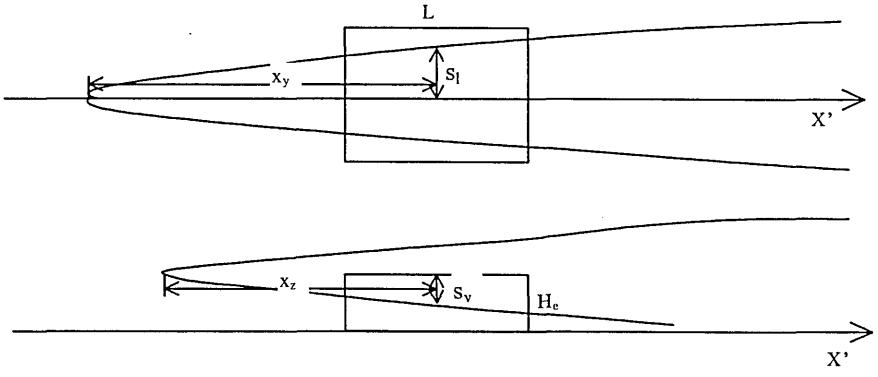


Figure 6.2 The area source emission and lateral and vertical virtual distances

## 6.4 Line emission source

Line emission is another important type of air pollution source that is often considered in air quality management. Road vehicular emission is the most important example of line emission source. For simulating dispersion of a line source, the line emission source is divided into a series of small area emission sources (Figure 6.3). The concentration produced by the line source emission is predicted by accumulating

contributions of series of small area source emissions. If the transverse width of the line source is $w$, a length of $2w$ is used to divide the line source. The initial lateral scale ($l$) of a small area source is the projection of $2w$ on the $y'$ axis of dispersion coordinate.

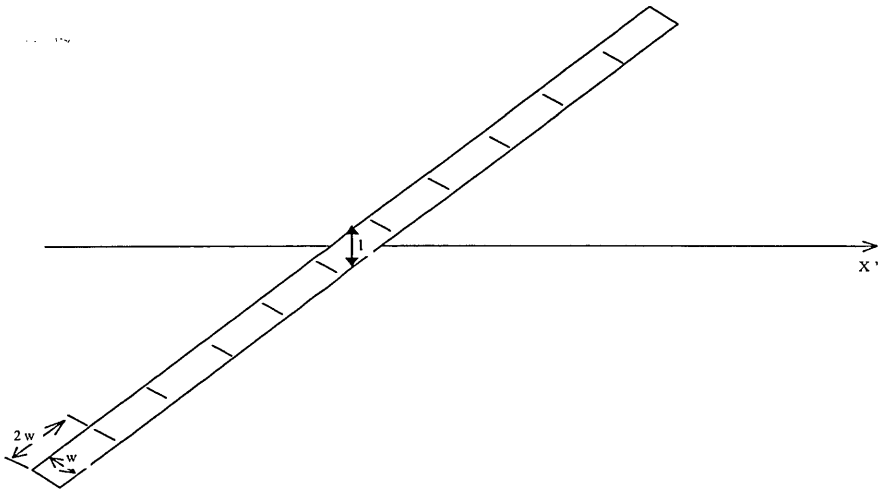


Figure 6.3 Line source emission and split

## 6.5 The software package

The main window of the software package for the atmospheric dispersion models is shown in Figure 6.4. The parameters that describe the characteristics and locations of the three types of airborne pollutant emission sources (point, area and line), receptors, meteorological conditions (for the conventional Gaussian plume model) or planetary boundary layer parameters (for modified hybrid plume dispersion model and ground-level release dispersion model) have to be entered before performing the model simulation. No limits were set for the numbers of three types of sources and receptors that can be modelled. The sources and receptors can be added one by one. They can be revised or deleted conventionally by using their names. The software can treat one year of hourly meteorological parameters or planetary boundary layer parameters. The hourly meteorological parameters or planetary boundary layer parameters can be manually added one by one. Alternatively, the hourly meteorological parameters may be imported from a text file with a fixed format. The hourly meteorological parameters or planetary boundary layer parameters can be revised or deleted conventionally by using the date and time

attached to these parameters. All entered data, parameters and simulated results can be saved in a file via the menu of the file and saved for later application.

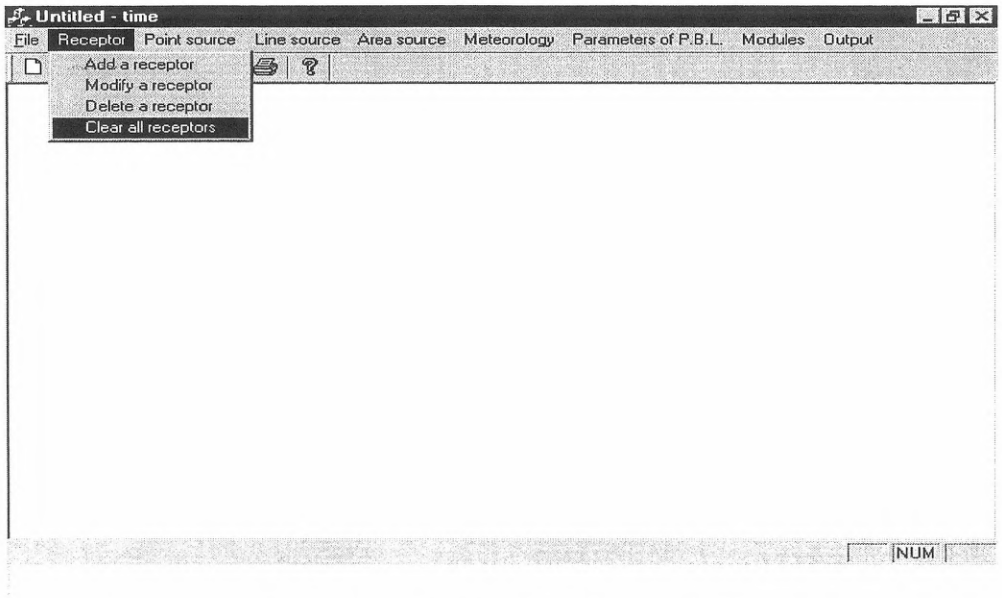


Figure 6.4 Main window of software package

### 6.5.1 Editing of point emission sources

The dialogue for input of a point source emission is shown in Figure 6.5. The name, geographic coordinates ($x$, $y$), emission rate of the airborne pollutant, stack or release height are five of the basic parameters that are used to describe a point source emission. Source name is important from the point of view of the source management. The name has to be entered if one wants to modify or delete a source. The error message will appear if the source with the name entered can not be found. The inner diameter at the top of the stack, smoke temperature and smoke exit velocity are three of the optional parameters needed for calculating the plume rise. The software package automatically set plume rise height to zero if these three parameters are all equal to zero.

"Attach a factor for daily variation", "attach a factor for monthly variation" and "group" are three additional options for input of the airborne pollutant emission sources. Many sources have daily variations. Some industrial and commercial processes only operate during daytime. Road vehicle emission in urban area is much higher at traffic peak time than at other times. The factor that describes the daily variation may be attached to the source. The dialogue for entering daily variation factor (Figure 6.6) will appear if the "attach a factor for daily variation" is selected in the dialogue when inputting the sources.

Some sources have seasonal variation, because several industrial processes have to be stopped for maintenance after a period of operation. In cold districts, the domestic emission is higher in winter than in summer because of the heating required. The factor that describes the monthly variation may be attached to the source. The dialogue for entering monthly variation factor (Figure 6.7) will appear if the "attach a factor for monthly variation" is selected. Attributing airborne pollutant emission sources to their receptors are very important in air quality management. The source may be grouped according to their characteristics or some special interests. Then, the contributions of source groups to air pollution can be calculated by the software package. The dialogue to enter group number (Figure 6.8) appears if the group option is selected. The group number of the sources may take a value of between 1 to 20.

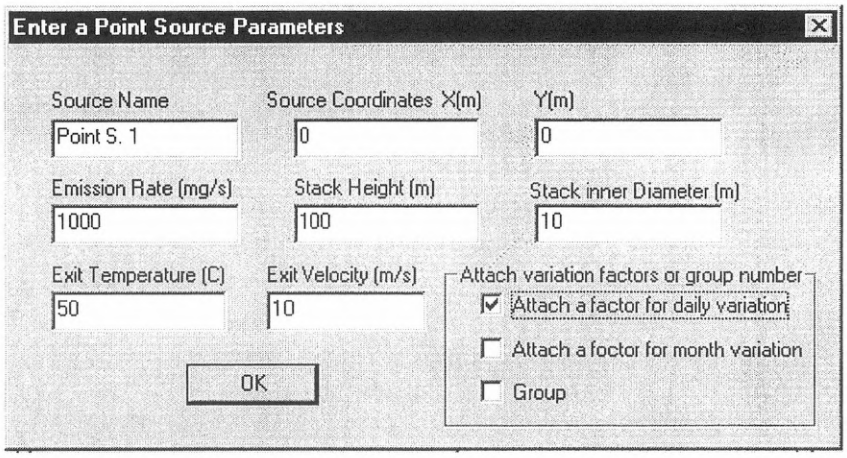


Figure 6.5 The dialogue for input of point emission source

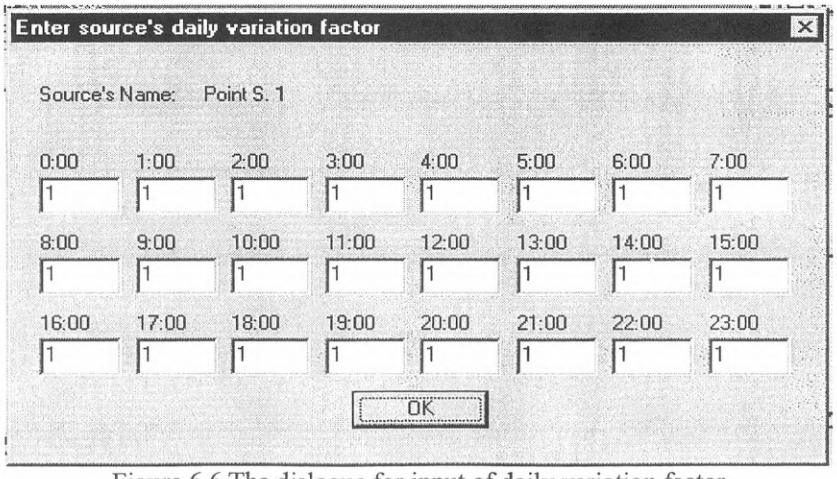


Figure 6.6 The dialogue for input of daily variation factor

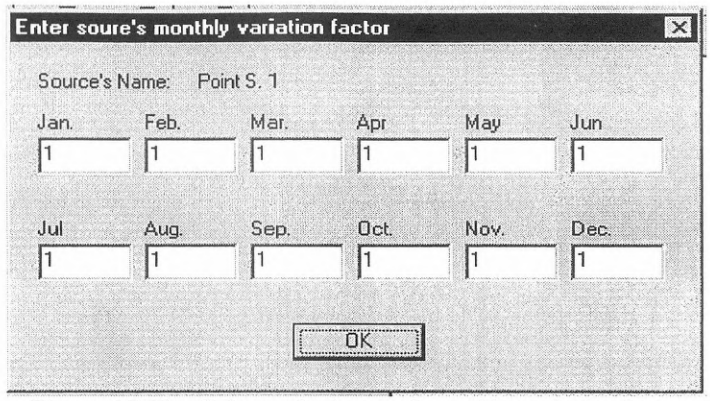


Figure 6.7 The dialogue for input of monthly variation factor

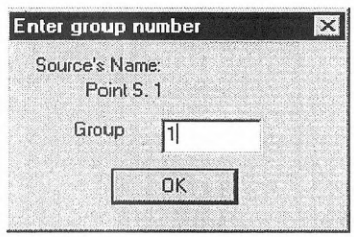


Figure 6.8 The dialogue for input of group number

### 6.5.2 Editing of area emission sources

The dialogue for entering an area source emission is shown in Figure 6.9. The name, central point geographic coordinates ($x$, $y$) of the area source, emission rate of the airborne pollutant, average release height, and lateral scale are six of the basic parameters used to describe an area source emission. For large non-squared area source emission, the source is required to be divided into a series of small squared area sources.

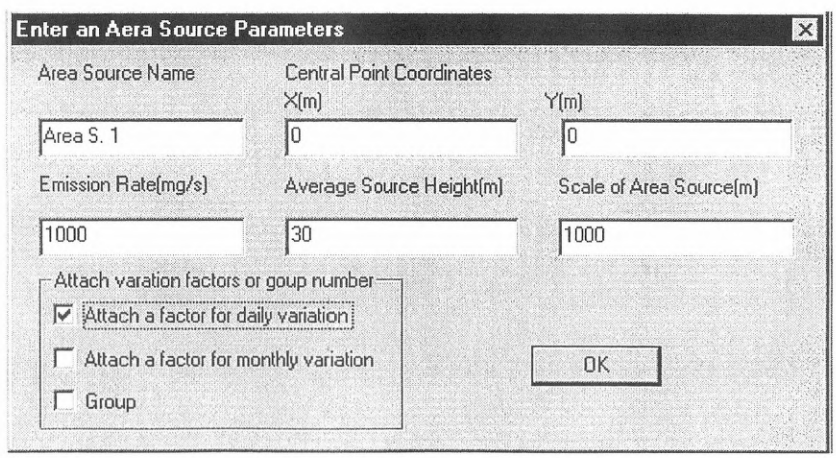


Figure 6.9 The dialogue for input of an area emission source

### 6.5.3 Editing of line emission sources

The dialogue for entering a straight line source emission is shown in Figure 6.10. The name, geographic coordinates ($x_s$, $y_s$) of the start point for the line, geographic coordinates ($x_e$, $y_e$) of the end point for the line, emission rate of the airborne pollutant, release height, and the transverse scale of the line source are eight of the basic parameters used to describe a straight source or a line source. The transverse scale of the road vehicle emission is regarded to be the initial mixing zone. It can be estimated empirically by the total width of all vehicle lanes, adding 3 m to each side (Benson, 1984). The default value of 6 m will be used by the software package if the entered transverse scale for the line source is less than 6 m. For the 'curve' emission source, the curve should first be divided into a series of short straight lines. Then, these straight line sources have to be entered separately.

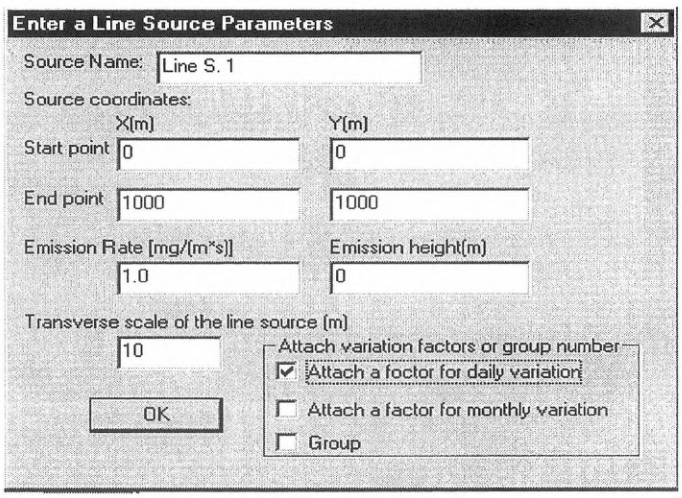


Figure 6.10 The dialogue for input of a line emission source

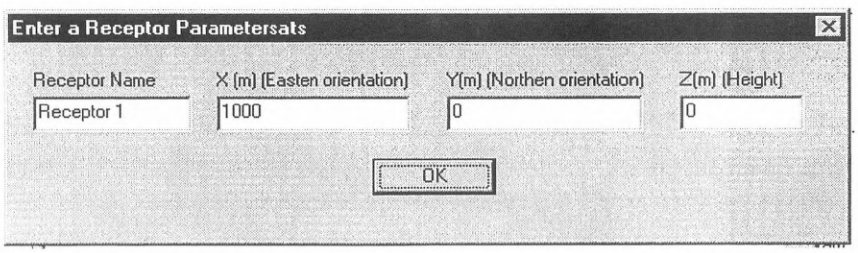


Figure 6.11 The dialogue for input of a receptor

### 6.5.4 Editing of receptors

The dialogue for entering a receptor is shown in Figure 6.11. The name and the geographic coordinates ($x$, $y$, $z$) are four of the basic parameters needed to describe a receptor. The name had to be entered if one wants to modify or delete a receptor. An error message will appear if the receptor with the name entered can not be found.

### 6.5.5 Editing of meteorological parameters

The meteorological parameters have to be entered if a conventional Gaussian plume dispersion model is selected to simulate atmospheric dispersion. The dialogue for entering the hourly meteorological parameters is shown in Figure 6.12. The time (date and hour), ground level wind speed, wind direction, ambient temperature, atmospheric stability, exponent of wind profile are six of the basic meteorological parameters required in the model. Time and date have to be entered if one wants to modify or delete the hourly meteorological parameters. An error message will appear if the hourly meteorological parameters at the time and date entered can not be found.

Wind direction is entered according to the angle that wind is blowing from in degrees and clockwise from north (for example $\theta = 0°$ when wind blows from north, $\theta = 90°$ when wind blows from the east. etc.). Atmospheric stability is selected according to six Pasquill categories, from very unstable (A) to neutral (D) and very stable (F). The value of exponents of wind profile may vary from 0.1 to 0.5. A value of 0.25 is usually used in neutral atmosphere. The mixing height is an optional parameter. The effect of multi reflections by the inverse layer is not considered when mixing height is zero.

The one year hourly meteorological parameters can be treated using the software package. The hourly meteorological parameters can be manually added one by one via the dialogue. Alternatively, they may be imported from a text file with a fixed format. The data format for the text file that stores the series of hourly meteorological parameters has been configured to be "2d2d4d2d5.1f4.1f5.2f6.1f1s6.1f1s7.1f". The first four internal numbers with the formats of "2d" or "4d" represent the day, month, year and hour respectively. These are followed by four floating point numbers with the formats of "5.1f", "4.1f", "5.2f" and "6.1f", representing the ground wind direction, wind speed, exponent of the wind profile and ambient temperature, respectively. Then followed by a character with the format of "1s", which represents the atmospheric stability. The final float number with the format of "7.1f" represents the mixing height.

The different dispersion parameters are used in the conventional Gaussian plume model to simulate atmospheric dispersion in an urban or rural area. The area (urban or rural) has to be selected before using the conventional Gaussian plume model. The dialogue for area selection is shown in Figure 6.13.

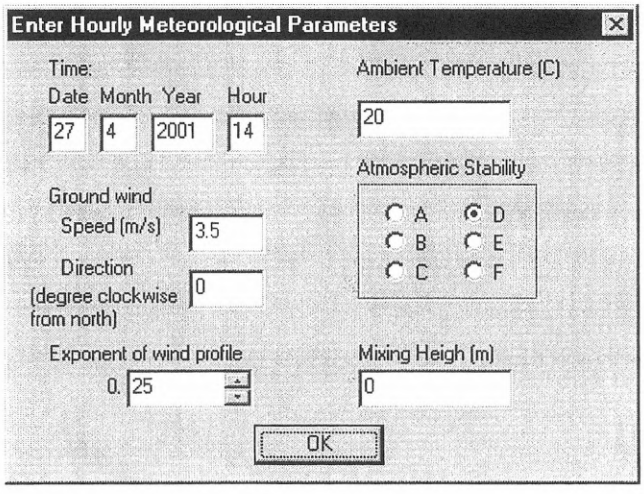


Figure 6.12 The dialogue for input of hourly meteorological parameters

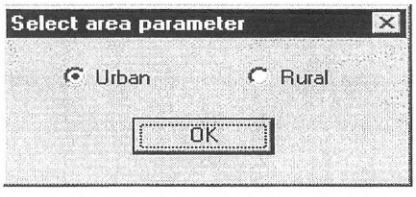


Figure 6.13 The dialogue for area selection

### 6.5.6 Editing of planetary boundary layer parameters

The planetary boundary layer parameters had to be entered if the modified hybrid plume dispersion model and ground-level release dispersion model are selected to simulate atmospheric dispersion. The dialogue for entering the hourly planetary boundary layer parameters is shown in Figure 6.14. The time (date and hour), wind speed, wind direction, turbulent components ($\sigma_v$ and $\sigma_w$), ambient temperature, Monin-Obukhov length ($L$), mixing height ($z_i$), friction velocity ($u_*$), convective velocity scale ($w_*$), surface roughness ($z_0$), surface heat flux ($H$) and gradient of potential temperature ($d\theta/dz$) are twelve of the basic planetary boundary layer parameters to be entered. Time and date also have to be entered if one wants to modify or delete the planetary boundary layer parameters. An error

message appears on the screen if the hourly planetary boundary layer parameters at the time and date entered can not be found.

In contrast to the input of meteorological parameters, the mixing height is very important in describing planetary boundary layer. It is not an optional parameter. A non-zero value must be entered for the mixing height.

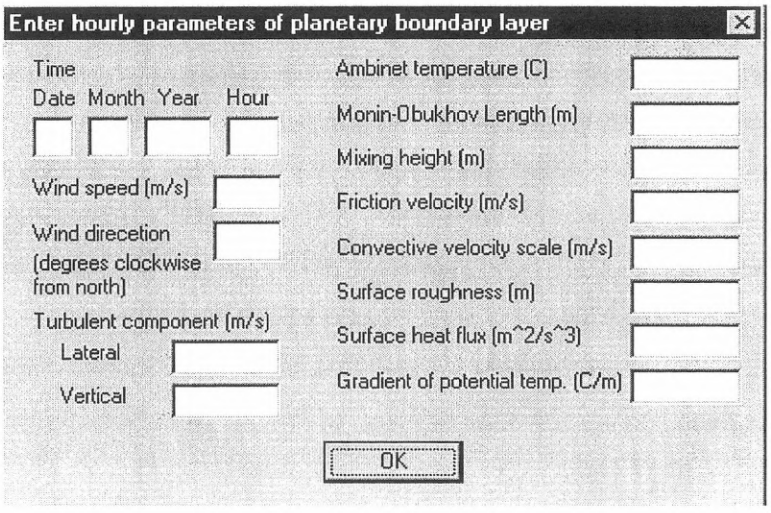


Figure 6.14 The dialogue for input of planetary boundary layer parameters

### 6.5.7 Module selections

The module selection menu of the software package is shown in Figure 6.15. Two kinds of modules, the modified hybrid plume dispersion model (HPDM) and the conventional Gaussian plume model (CGPM), can be selected in the developed software package. In HPDM, the modified hybrid plume dispersion model is used to simulate dispersion of elevated emission sources. The ground-level release dispersion model is used to simulate the dispersion of ground-level emission sources.

The 'once concentration' and the 'series of concentrations' options, can be used for each type of module. The selection of once concentration module can predict one hour mean concentration once for all entered receptors. If the sources are grouped, the contributions of various source groups to the receptors will be calculated as well. The time and date have to be entered when predicting once concentration module. An error message appears if the hourly meteorological parameters at the time and date entered can not be found.

The selection of series of concentrations can predict series of one hour mean concentrations for a receptor based on the series of hourly meteorological parameters or

planetary boundary layer parameters. The daily mean concentrations and total mean concentration can also be calculated. If the sources are grouped, the contributions of various source groups to one hour mean concentrations, daily mean concentrations and total mean concentration will also be calculated as well. The receptor's name has to be entered in order to predict series of concentrations. An error message appears if the receptor with the name entered can not be found.

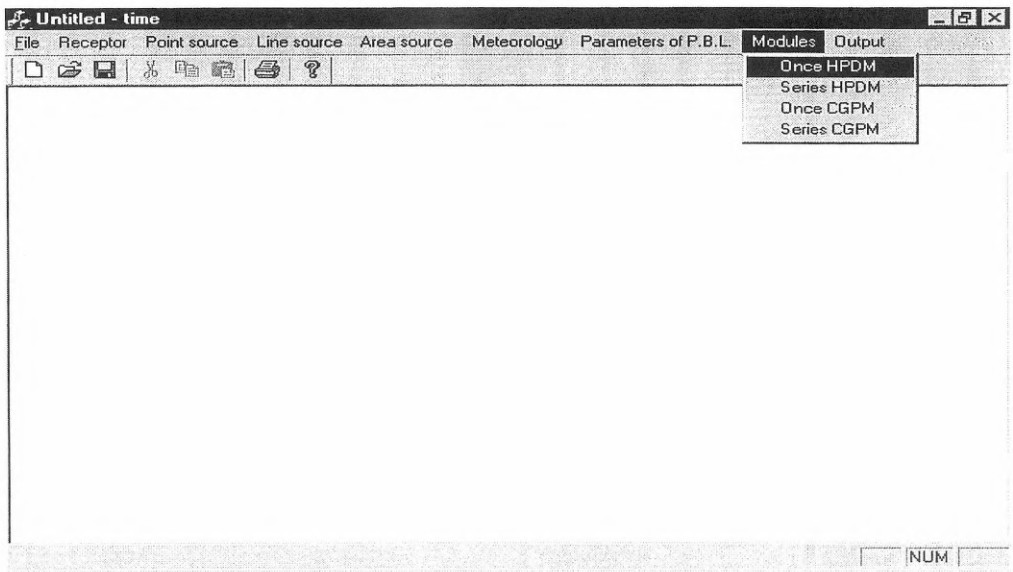


Figure 6.15 The modules selection menu

### 6.5.8 Output from the software package

The output menu of the software package is shown in Figure 6.16. The relevant module's results or entered data and parameters appear on the monitor when an output is chosen. Then the output may be printed out via the menu the 'file' and 'print'. After running the once concentration module, the output of the once concentration results first shows the date, time, meteorological condition and the area (CGPM) or parameters of planetary boundary layer (HPDM). They are followed by the one hour mean once concentrations for all receptors together with the receptors' names and coordinates of their locations. The final output is the maximum concentration at all of the receptor locations. The contributions of various source groups to the receptors will also be shown if the sources are grouped.

After running the 'series of concentrations module', the output of the series of concentrations module results first shows the receptors' name, coordinates of their

locations and the area (CGPM). They are followed by a series of one hour mean concentrations together with the date, time and hourly meteorological parameters (CGPM) or parameters of planetary boundary layer (HPDM). Then, the maxamum 1-h mean concentration is shown. The final output is the average concentration for the whole period. The outputs of daily concentration show daily mean concentrations and the max daily mean concentration for the receptor. If the sources are grouped, the contributions of various source groups to daily mean concentrations are also shown.

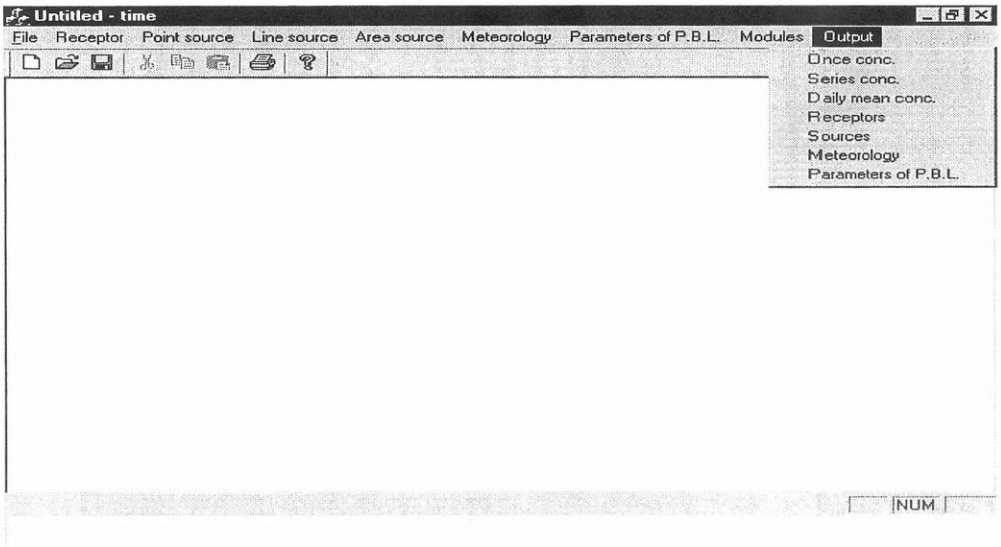


Figure 6.16 The output menu

The output for receptors, sources, meteorology and parameters of the planetary boundary layer shows all data and parameters entered to describe the receptors, point source emissions, line source emissions, area source emissions, hourly meteorological conditions and parameters of the planetary boundary layer. These functions may be used to check the data and parameters entered into the software package.

## 6.6 Comparative test of ground-level release dispersion model and conventional Gaussian plume dispersion model

The up-to-date hybrid plume dispersion model and the ground-level release dispersion model represent recent advances in the understanding of planetary boundary layer and atmospheric dispersion. In contrast to the conventional Gaussian plume dispersion model, the vertical concentration distribution in convective conditions is a non-

Gaussian type for hybrid plume model and ground-level release model. A simple example test has been conducted to compare the ground-level release dispersion model and the conventional Gaussian plume dispersion model.

It is supposed there is a ground level emission point source of pollutants with an emission rate of 1 g $s^{-1}$ located in urban area. Ground-level release model was used to predict ground concentration distribution and vertical concentration distribution in three types of atmospheric dispersion conditions. The planetary boundary layer parameters used to describe these three types of atmospheric dispersion conditions are shown in Table 6.4. Conventional Gaussian plume model was also used to predict ground level concentration distribution and vertical concentration distribution for three types of atmospheric dispersion conditions. The meteorological parameters used to describe these three types of atmospheric dispersion conditions are shown in Table 6.5. The three types of atmospheric stabilities are slightly unstable ($L$ = -150 m or $PS = C$), neutral ($L$ = -2000 m or $PS = D$) and slightly stable ($L$ = 100 m or $PS = E$), respectively.

Table 6.4 Three sets of planetary boundary layer parameters used in the ground-level release model

| $u$ (m $s^{-1}$) | $\sigma_v$ (m $s^{-1}$) | $w^*$ (m $s^{-1}$) | $u^*$ (m $s^{-1}$) | $Z_i$ (m) | $L$ (m) |
|---|---|---|---|---|---|
| 2.5 | | 1.5 | 0.7 | 1500 | -150 |
| 2.5 | 0.6 | | 0.5 | 1000 | -2000 |
| 2.5 | 0.3 | | 0.3 | 700 | 100 |

$u$: ground wind speed; $\sigma_v$: lateral turbulent component
$w^*$: convective velocity scale $u^*$: friction velocity
$Z_i$: mixing height $L$: Monin-Obukhov length

Table 6.5 Three sets of meteorological parameters used in conventional Gaussian plume model

| $u$ (m $s^{-1}$) | *Area* | $\alpha$ | $Z_i$ (m) | *PS* |
|---|---|---|---|---|
| 2.5 | Urban | 0.20 | 1500 | C |
| 2.5 | Urban | 0.25 | 1000 | *D* |
| 2.5 | Urban | 0.30 | 700 | *E* |

*PS*: Pasquill stability class $\alpha$: exponent of wind profile

The ground concentration distributions along downwind axis predicted by the ground-level release model and the conventional Gaussian plume model in three types of atmospheric dispersion conditions are shown in Figure 6.17. For unstable and neutral conditions, the decrement in ground level concentration with the downwind distance

predicted by the ground-level release model is somewhat faster than that predicted by conventional Gaussian plume model. This suggests that vertical mixing in the ground-level release model is stronger than that in the conventional Gaussian plume model. In stable conditions, variation trends of ground level concentration with downwind distance predicted by both of the models are similar.

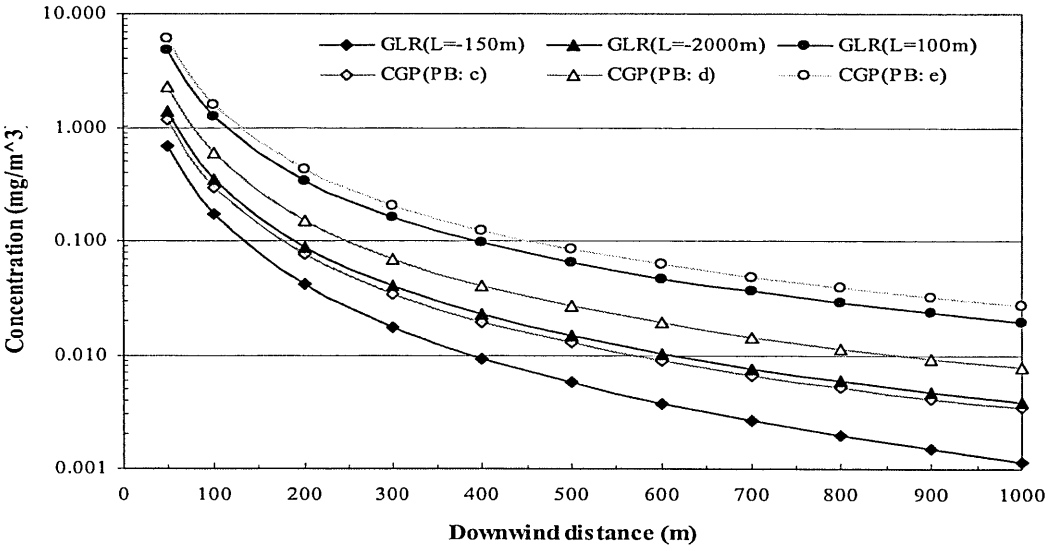


Figure 6.17 Ground level concentration distributions along downwind axis predicted by the ground-level release model and the conventional Gaussian plume model

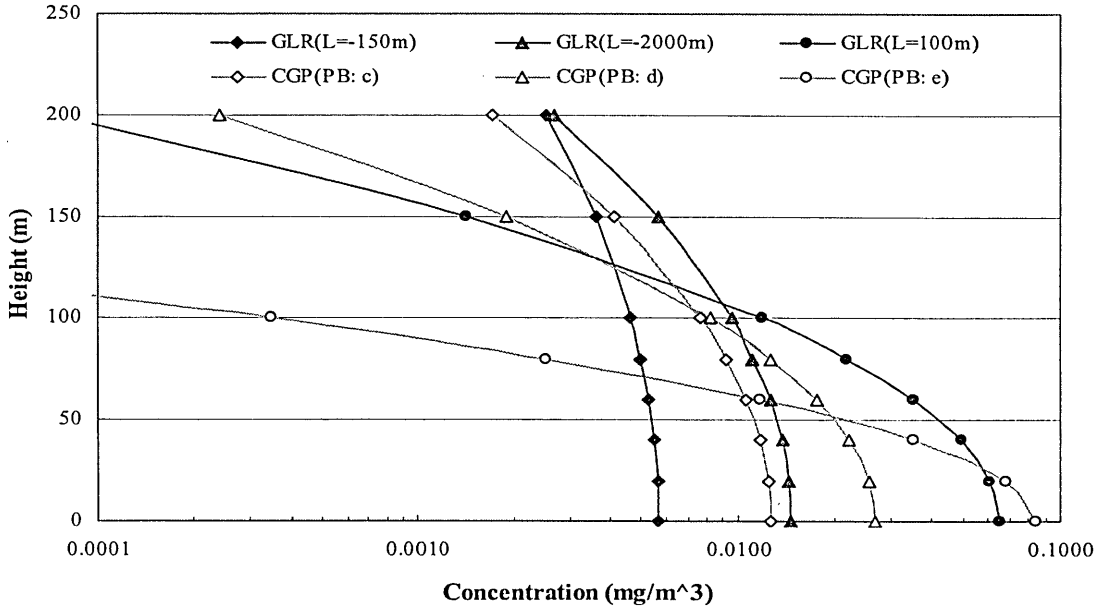


Figure 6.18 Vertical distributions of concentrations at a distance of 500 m predicted by the ground-level release model and the conventional Gaussian plume model

The vertical concentration distributions at a distance of 500 m downwind predicted by the ground-level release model and the conventional Gaussian plume model in three types of atmospheric dispersion conditions are shown in Figure 6.18. In any of the conditions modelled, the decrement of concentration with the height predicted by the conventional Gaussian plume model is much faster than that predicted by the ground-level release model.

Above test results indicate that the major difference between the models that represent recent advances in the understanding of planetary boundary layer and atmospheric dispersion and the conventional Gaussian plume model is in the description of the vertical concentration distribution. There is also some differences in the description of lateral concentration distribution in unstable condition. The tests reported here highlight the difference between the ground-level emission model and the conventional Gaussian plume model.

## 6.7 Positive matrix factorisation model and software package

Positive matrix factorisation (PMF) model and software that were developed by Paatero (1998) have been selected to identify airborne pollutant sources and source contribution because of the individual features in the modelling software. These features have been described in detail by Paatero et al. (1994, 1997). PMF, unlike factor analysis (FA), produces strictly non-negative factor loading and factor. As described in section 5.3, concentrations of chemical components measured in the ambient environment vary widely, especially in the case of some trace elements in aerosols. In the PMF model, the original data can be weighted point-by-point using error estimated. This function is very useful in handling the data with different variation ranges and uncertainties. Furthermore, subjective information, such as the knowledge on air pollution source composition, may be combined with factor analysis in the PMF model trial. The PMF model provides specially enforced rotation techniques to enable the results to approach ideal situations.

There are two types, namely two-way and three-way PMF models. Two-way PMF is a two-dimensional principal component analysis model, in which a two-dimensional matrix is used as input database. A three-way PMF is a straightforward generalisation of a two-way PMF. It is a tri-linear factor analysis model, in which a three-dimensional matrix is used as input database. In this work, two dimensional matrix data of aerosol chemical

composition was used as input database. Thus, a two-way PMF model was used. The two-way PMF model can be written as:

$$X_{ij} = \sum_{h=1}^{p} G_{ih} F_{hj} - E_{ij} \qquad (i=1,\ldots,n; j=1,\ldots,m) \tag{6.76}$$

where $E_{ij} = X_{ij} - \sum_{h=1}^{p} G_{ih} F_{hj}$ is a matrix of residuals. The principle of the two-way PMF model can be presented as:

$$\text{minimize} Q = \sum_{i=1}^{n} \sum_{j=1}^{m} \left( \frac{E_{ij}}{S_{ij}} \right)^2 \quad \text{with } G_{ih} \geq 0, F_{hj} \geq 0 \tag{6.77}$$

where $S_{ij}$ is the point-by-point error estimate of $X_{ij}$. $E_{ij}/S_{ij}$ is the scaled residual.

The explained variance, ***EV***, has been defined in the PMF model. The explained variances for ***F*** are defined as:

$$EV_{kj} = EV_j F_{kj} / \sum_{k=1}^{p} F_{kj} \tag{6.78}$$

where

$$EV_j = 1 - \sum_{i=1}^{n} \left( \frac{E_{ij}}{S_{ij}} \right)^2 / \sum_{i=1}^{n} \left( \frac{X_{ij}}{S_{ij}} \right)^2 \tag{6.79}$$

The explained variances are scaled factors. The explained variances for ***F*** facilitate the answers to two questions: Which are important chemical components in any given factor? And, how important is any given chemical component in the different factors? The explained variances may, in addition, show factor characteristics.

One of the major advantages of a PMF model is that it can handle various elements with different variation ranges and uncertainties by error estimates (Paatero, 1998). The error estimates in a PMF model for the individual data point values are utilised as point-by-point weight by an ***S*** matrix (standard deviation array) for ***X*** matrix (elements array). ***S*** matrix may be calculated using four different methods in a PMF model. Error estimates can be used to treat missing data and data with values under a detection limit.

Another advantage of a PMF model is that it provides different methods to impose expected characteristics for the factors. The subjective information may be used during the factor analysis.

In contrast to previous works (Huang et al., 1999; Xie et al., 1999a), the weightings of data using error estimate and the complementary use of subjective information with the

factor analysis are used in the application of PMF model in this work (Qin and Oduyemi, 2002). Different error estimates were used for different chemical species with different detection limits and precisions. Enforced rotation was applied to modify some factors' mass profiles to approach an ideal pattern.

## 6.8 Concluding remarks

A software package for air quality management has been developed by the author. In contrast to other commercially available software, this software package provides for the choice of different atmospheric models. The atmospheric dispersion models used in the software package include a modified hybrid plume dispersion model and a ground-level release dispersion model that represent recent advances in the understanding of planetary boundary layer and atmospheric dispersion. Also, a conventional Gaussian plume model that is still universally used has been included. The user may select a different model according to the prevailing situation and the available parameters. In the hybrid plume dispersion models, a probability function (p.d.f.) model and a convective scaling model have been used to simulate vertical dispersion in low and high buoyancy fluxes in unstable conditions respectively. The atmospheric dispersion parameters have been described using the parameters that represent the planetary boundary layer conditions and atmospheric dispersion abilities well. In contrast to the original hybrid plume dispersion model developed by Hanna and Paine (1989), a function ($P$) that represents the probability that receptor is under the influence of the pollution plume has been added in the modified hybrid plume dispersion model developed by author. This function is important when the distance between source and receptor is large or wind speed is low. In these situations, neglect of the effect of travel time from source to receptor will over-predict pollutant concentration. In ground-level release dispersion model, a special non Gaussian function that relates to planetary boundary layer parameters has been used to describe the vertical dispersion because vertical distribution is non Gaussian.

Two major advantages of a PMF model, the weightings of data using error estimate and the complementary use of subjective information with the factor analysis are used in application of PMF model. Error estimates allow as many as possible component to compose the element matrix. The complementary use of subjective information can modify some factors' mass profiles to approach the ideal pattern.

# Chapter 7 The methodology for attributing sources of airborne pollutants to their receptors

## 7.1 The methodology for attributing sources of airborne pollutants to their receptors

The atmospheric dispersion model and the receptor model are two major methodologies used to evaluate the contributions of airborne pollutant emission sources to air pollution. The atmospheric dispersion model is a source-oriented methodology (Figure 7.1). It simulates the processes of atmospheric dispersion, transportation and transformation of airborne pollutants from emission sources to receptors. The concentrations of airborne pollutants caused by an emission source or a group of emission sources are predicted by the model. Then the source contributions to the air pollution can be assessed.

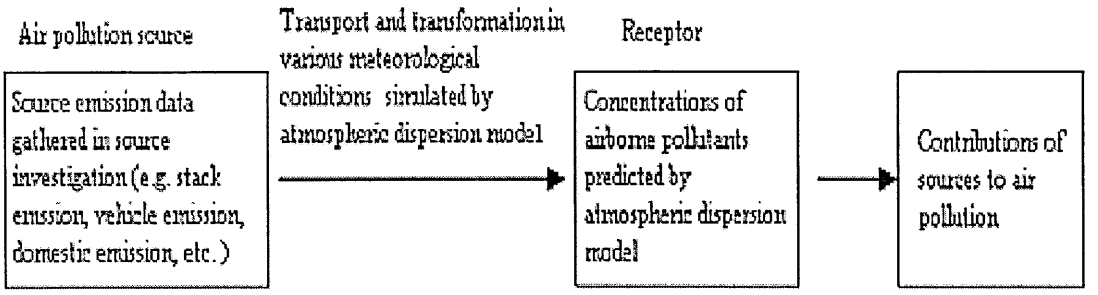


Figure 7.1 The source oriented methodology

On the other hand, a receptor model is a receptor-oriented methodogy (Figure 7.2). The basic idea of a receptor model (factor analysis) is that the chemical species from the same source will be correlated and these correlations can be used to identify the emission source and estimate the source composition. The receptor model can analyse the correlations among the gaseous pollutants, chemical species of aerosol and weather conditions measured at the receptor to identify the air pollution sources and estimate the source composition. Then the source contributions to air pollution are estimated.

In previous research work, it was usual for only one methodology (atmospheric dispersion model or receptor model) to be used to identify airborne pollutant emission

sources and estimate the source contributions. When the source-oriented method is used, the simulating precision of the atmospheric dispersion model directly depends on the precision of the source emission data, excluding the effect of the errors caused by the model itself. The precise source profiles are usually only obtained for a few special sources. There are many fugitive and small sources with widely varying compositions in an urban area. The precise source profiles for these sources are very difficult to obtain. Sometimes, the source profiles may have changed since they were last investigated. Some important special air pollution sources may be over looked when compiling the atmospheric emission inventory, because of lack of information.

In preparing the atmospheric emission inventories in Dundee (Chapter 3), the archive airborne pollutant emission data were only available for four companies. These archive emission data were measured years ago. The source emissions for road traffic had to be estimated, because measured data were unavailable. Since both measured data and fuel (oil and gas) consumption data were unavailable, the emissions from domestic and small industrial and commercial fuel consumption were not covered in the inventory. In general, the atmospheric emission inventories underestimated the air pollution sources, especially $PM_{10}$ sources in Dundee. The errors in the source emission estimates will directly cause errors in the simulation result of the atmospheric dispersion model.

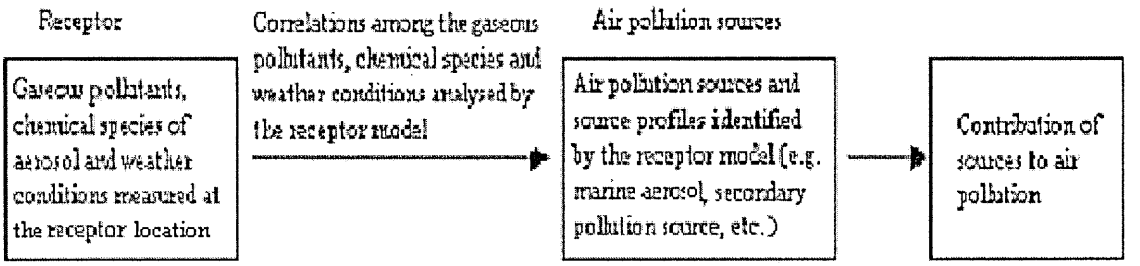


Figure 7.2 The receptor oriented methodology

The receptor model (factor analysis) is based on a series of assumptions: the compositions of source emission are constant over the period of sampling at the receptor; chemical species do not react with each other during transport from the sources to the receptor; the source compositions are linearly independent of each other; measurement of uncertainties for chemical species in the receptor are random, uncorrelated, and normally distributed, etc. These assumptions are fairly restrictive and can never be totally complied with in practice. When a receptor model is used to estimate the source contribution, the

correlations among the gaseous pollutants and chemical species of aerosol measured at the receptor may be the result of the multi effects of meteorology and coincident source locations. The sources and source contributions derived by a receptor model may sometimes be misleading if the correlation among the input species could not present real emission sources.

Both the source-oriented and receptor-oriented methodologies have their advantages and shortcomings. The errors caused by the shortcomings can not be identified and remedied when one methodology is used to attribute airborne pollutant source emissions to their receptor. Seigneur et al. (1999) suggested firstly that source-oriented method and receptor-oriented method should be used to complement each other in PM (particulate matter) 24-hour average modelling although they did not put their suggestions into practice. Chow et al. (1999) tried to apply the Chemical Mass Balance (CMB) source apportionment receptor model and the Industrial Source Complex Short-Term Version 3 dispersion model (ISCST-3) to estimate middle and neighborhood scale variations of source contributions in Las Vegas, Nevada. However, they analysed the model results separately. Their conclusion is that atmospheric dispersion model did not accurately estimate measured $PM_{10}$ because it overestimates the fugitive dust emission while the receptor model produces a reasonable result. They noticed that atmospheric dispersion model provided an insight, with respect to relative contributions from sub sources of fugitive dust. But, they did not try to complement the results derived from the two models

In this work, both the atmospheric dispersion and receptor models are used to identify air pollution sources and estimate the source contributions (Figure 7.3). The errors produced by the models' shortcomings can be corrected by analysing and complementing the results of the two approaches. The performance of the atmospheric dispersion model in predicting concentrations of airborne pollutants was evaluated using measured field data. The errors produced by the atmospheric dispersion model in estimating source emission or neglecting important sources were corrected by the sources identified, using the receptor model. The misleading sources and source contributions produced by the receptor model can be corrected by predicting the results of atmospheric dispersion model. A more precise and reliable result is derived.

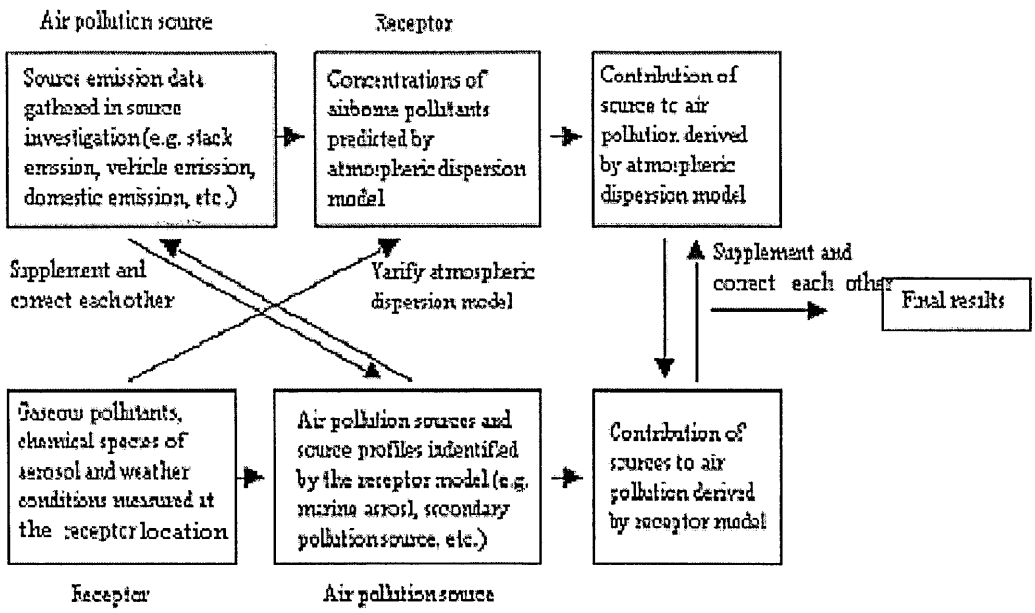


Figure 7.3 The methodology for attributing sources of airborne pollutants to their receptors

## 7.2 Application of atmospheric dispersion model

The atmospheric dispersion models and the software package developed in chapter 6 were used to simulate the transport and dispersion of NOx and $PM_{10}$ and estimate the source contributions in Dundee. The concentration data of NOx and $PM_{10}$ measured at the study monitoring station have been used to evaluate the model performance.

### 7.2.1 Data input for the atmospheric dispersion model

The parameters used to describe airborne pollutant emission sources, receptors and atmospheric dispersion conditions are needed as inputs for the atmospheric dispersion model. A geographical coordinate system has been set up to create the atmospheric emission inventory (Section 3.3). The origin of the coordinate system is located at the library, University of Abertay Dundee. East and north directions are fixed as the positive $x$ and $y$ axes (directions), respectively. The up direction is fixed as positive $z$ axis (direction). This geographical coordinate system has been used in atmospheric dispersion models application. It is shown in Figure 3.5.

The data collected for the atmospheric emission inventories in Dundee (section 3.3) was used as input for source parameters. The data consists of two point emission sources, 13 line emission sources (Table 3.7) and 58 area emission sources (Table 3.9). The daily

variation factors (Tables 3.8 and 3.10) and monthly variation factors are available for different sources. All these data were entered into the atmospheric dispersion model to describe the emission sources of airborne pollutants in Dundee. The airborne particulate matter emitted from the Waste to Energy Plant, Dundee Energy Recycling Limited is taken to be $PM_{10}$. The airborne pollutant emission sources were grouped into point emission, line emission and area emission to calculate the source contributions.

One receptor (the air quality monitoring station at the roof of the library of University of Abertay Dundee) is considered in the simulation of atmospheric dispersion. The parameter used to describe the geographic location of the receptor is: $x = 62$ m, $y = -78$ m and $z = 18$ m.

For meteorological parameters, wind speed, wind direction and ambient temperature were measured at the station. The measured values for the parameters to describe the construction of atmospheric boundary, such as the Monin-Obukhov length ($L$), mixing height ($z_i$), friction velocity ($u_*$), convective velocity scale ($w_*$), surface roughness ($z_0$), surface heat flux ($H$) and gradient of potential temperature ($d\theta/dz$), were unavailable. To satisfy the needs of atmospheric dispersion model, some reasonable empirical assumptions had to be used as input for meteorological parameters. The solar radiation and cloud cover fraction for the estimation of Pasquill stability classes and the data needed to calculate the Monin-Obukhov length ($L$) were not measured at the monitoring station. The Pasquill stability class had to be derived empirically and made to vary with time. It is assumed that atmospheric stability in Dundee is $C$ (slightly unstable) during the period 11:00 – 15:00, $D$ (neutral) during the period 06:00 – 10:00 and 16:00 – 02:00, and, $E$ (slightly stable) during the period 03:00 – 05:00 respectively. According to these assumptions, the frequencies of unstable, neutral and stable atmosphere are 20.8%, 66.7% and 12.5% respectively. The measured wind speed profile and the friction velocity ($u_*$) for the estimation of wind speed profile are unavailable at the station. The power law was used to describe the wind speed profile (equation 6.48). The wind profile exponent ($\alpha$) has been taken to be 0.20 in slightly unstable atmosphere, 0.25 in neutral atmosphere and 0.30 in slightly stable atmosphere. A total of 7470 relevant hourly meteorological parameters and measured hourly mean NOx concentrations at the monitoring station were entered into the atmospheric model.

### 7.2.2 Simulating the dispersion of NOx and $PM_{10}$

The conventional Gaussian plume dispersion model was selected to simulate the transport of airborne pollutants in Dundee. Other more sophisticated models could not be used because the parameters needed for describing the structure of atmospheric boundary were unavailable. Urban atmospheric dispersion condition was selected. The conventional Gaussian plume dispersion model is not suitable for calm conditions. The wind speed was taken to be 0.5 m $s^{-1}$ if the observed wind speed is less than 0.5 m $s^{-1}$. A total of 7470 hourly mean concentrations at the study monitoring station have been predicted for both NOx and $PM_{10}$ by the software package of atmospheric dispersion model, using the data described above. The contributions of point emission, line emission and area emission sources were also calculated.

### 7.2.3 Evaluation of atmospheric dispersion model

The 7470 hourly mean concentrations of NOx and 89 mass concentrations of $PM_{10}$ observed at the monitoring station were used to evaluate the performance of the atmospheric dispersion model. The predicted hourly mean NOx concentrations have been compared with observed hourly mean NOx concentrations directly. The predicted hourly mean $PM_{10}$ concentrations were averaged in accordance with the periods of the 89 observed $PM_{10}$ samples. The averaged concentrations of $PM_{10}$ were compared with observed $PM_{10}$ concentrations.

The following statistics were used to evaluate the performance of the atmospheric dispersion model (Hanna and Paine, 1989):

$$\text{Mean Bias} = \overline{C_p} - \overline{C_0} \tag{7.1}$$

$$\text{Normalised Mean Square Error} = \frac{\overline{(C_p - C_o)^2}}{(\overline{C_p})(\overline{C_o})} \tag{7.2}$$

$$\text{Correlation } r = \frac{\overline{(C_p - \overline{C_p})(C_o - \overline{C_o})}}{\sigma_{C_p}\sigma_{C_o}} \tag{7.3}$$

$$\text{Percentage of } C_p \text{ within a factor of two of } C_o \tag{7.4}$$

where $C_p$ is the predicted concentration and $C_o$ is the observed concentration. In addition, the following attributes of the unpaired concentration distributions were investigated: maximum overall concentration, and the average of top 25 concentrations [$\overline{C}$ (Top 25)] used in evaluating model performance.

### 7.2.3.1 Performance evaluation of the atmospheric dispersion model – NOx prediction

The average concentration of the 7470 predicted NOx concentrations, using conventional Gaussian plume dispersion model, is 0.02871 mg $m^{-3}$. The average concentration for observed concentrations used to assess the model performance is 0.03120 mg $m^{-3}$. Mean Bias is –0.00249 mg $m^{-3}$. On average, the predicted NOx concentrations compare well with the observed concentrations. The average predicted NOx concentration is only about 8.0% lower than the observed average concentration. NOx emission sources entered into the model may be the cause of the slight underestimation of the concentrations, because they do not include all NOx emissions in Dundee.

Normalised Mean Square Error for NOx is significantly low with a value of 0.88. The correlation coefficient, $r$, is 0.59 for a total of 7470 paired concentrations. The predicted NOx concentrations are reasonably well correlated to the observed concentrations. Percentage of $C_p$ within a factor of two of $C_o$ for NOx is 52.3%. The maximum overall predicted NOx concentration is 0.2227 mg $m^{-3}$ while maximum overall observed concentration used to evaluate the model performance is 0.4680 mg $m^{-3}$. The maximum overall predicted NOx concentration is 52.4% less than maximum overall observed concentration. The average of top 25 concentrations [$\overline{C}$ (Top 25)] is 0.0719 mg $m^{-3}$ for the predicted NOx and 0.0663 mg $m^{-3}$ for the observed NOx. The predicted $\overline{C}$ (Top 25) is about 8.4% higher than the observed $\overline{C}$ (Top 25).

The evaluated results show that the performance of the conventional Gaussian plume dispersion model in simulating transport of NOx in Dundee is reasonably good. The predicted results are reliable.

For the evaluation of the model performance with the observed concentrations, the ratios of predicted concentration to observed concentration ($C_p/C_o$) for the 7470 paired NOx concentrations were grouped into 10 sets, using the same number in accordance with the observed concentration ranges from low to high. Average concentrations and standard deviations for these ratios and their variations with the observed concentration are shown in Figure 7.4.

In general, the conventional Gaussian plume dispersion model overpredicts NOx concentration when observed concentration is lower than its average value (0.03120 mg $m^{-3}$). The model underpredicts NOx concentrations when observed concentration is higher than its average value. The deviation of the ratio of $C_p/C_o$ for NOx is large when observed

concentration is low. It suggests that the percentage of $C_p$ within a factor of two of $C_o$ is low and the model performance is poor when observed concentration is low. The deviation of the ratio of $C_p/C_o$ for NOx is relatively small when observed concentration is high, which implies that the percentage of $C_p$ within a factor of two of $C_o$ is high and the model performance is good when observed concentration is high.

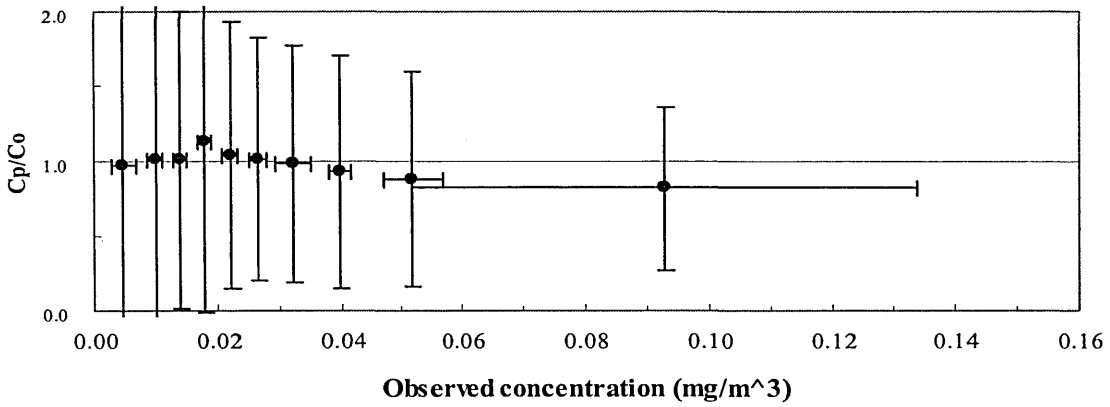


Figure 7.4 Variation of $C_p/C_o$ with observed concentrations for NOx

Variation of ratios of $C_p/C_o$ for NOx with the observed concentration is reasonable. The Gaussian model presents a statistical average status for various types of atmospheric dispersion conditions. Its performance would be better when atmospheric dispersion conditions approach normal situations (observed concentration approach average concentration). Its performance should be poor when atmospheric dispersion conditions approach that for extreme situations (observed concentration is very low or very high).

For evaluating model performance with the observed wind speed, the ratios of the predicted concentration to the observed concentration ($C_p/C_o$) for the 7470 paired NOx concentrations are grouped into 10 sets, as discussed previously. Average concentrations and standard deviations for the ratios of these 10 and their variations with observed wind speed are shown in Figure 7.5.

The performance of the conventional Gaussian plume dispersion model in predicting NOx concentration is good when observed wind speed varies between 1.3 and 3.0 m $s^{-1}$, although the concentrations show slight under estimations. The deviation of the ratio of $C_p/C_o$ for the NOx data is small, which suggests that the percentage of $C_p$ within a factor of two of $C_o$ is high. The model underpredicted NOx concentration when wind is

very high. The conventional Gaussian plume dispersion model is not suitable for simulating atmospheric dispersion in calm and 'low' wind conditions, because the dispersion along the wind direction is neglected. It is not strange that the model overpredicts NOx concentration when wind speed is less 1.0 m $s^{-1}$. Here, the average ratio of $C_p/C_o$ approaches 1 when wind speed approaches zero, because a value of 0.5 m $s^{-1}$ was used in the model to simulate the dispersion process when observed wind speed is less than 0.5 m $s^{-1}$.

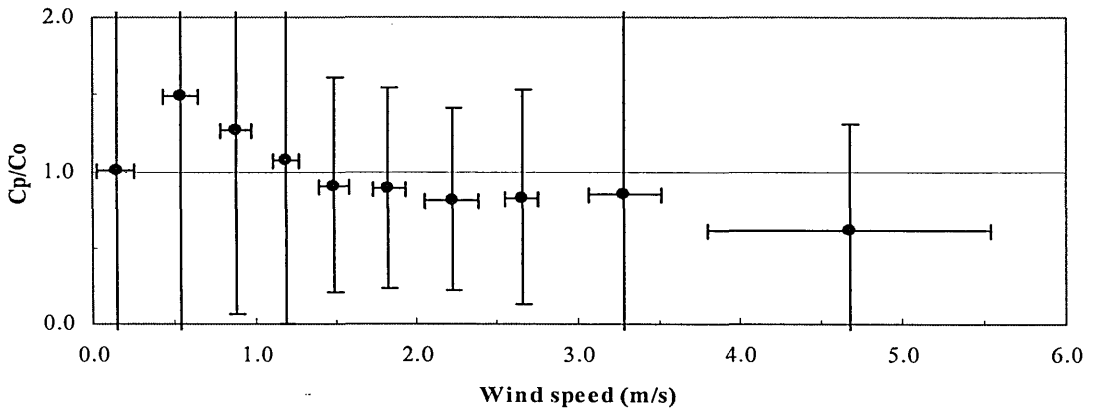


Figure 7.5 Variation of $C_p/C_o$ with observed wind speed

For evaluating model performance with observed wind direction, the ratios of predicted concentration to observed concentration ($C_p/C_o$) for the 7470 paired NOx concentrations were grouped using 16 wind aspects. Average concentrations and standard deviations for these 16 sets and their variations with the observed wind aspect are shown in Figure 7.6.

When wind comes from E, ESE and NW, the model performance in terms of predicting NOx concentration is reasonably good. The average ratios of $C_p/C_o$ approach 1 and the deviations of the ratio are relatively small. When wind comes from NE, ENE and WNW, the average ratios of $C_p/C_o$ also approach 1. However, the deviations of the ratio are large. When wind comes from SW, WSW and W, the model performance, with small deviations of ratios of $C_p/C_o$, is reasonably good, although the model underestimates NOx concentration. When wind comes form N, NNE, SE, SSE, S, SSW and NNW, the model performance is poor because the model overpredicts the NOx concentrations and the deviations of ratios of $C_p/C_o$ are large. If the model overpredicts NOx concentration when

wind comes from an aspect, it implies that the source data that represents the source emission rates located on this aspect may be higher than the actual emission rates. On the other hand, the source data that represents the source emission rates located in an aspect may be lower than the actual emissions rates if the model underpredicts NOx concentration when wind comes from this aspect.

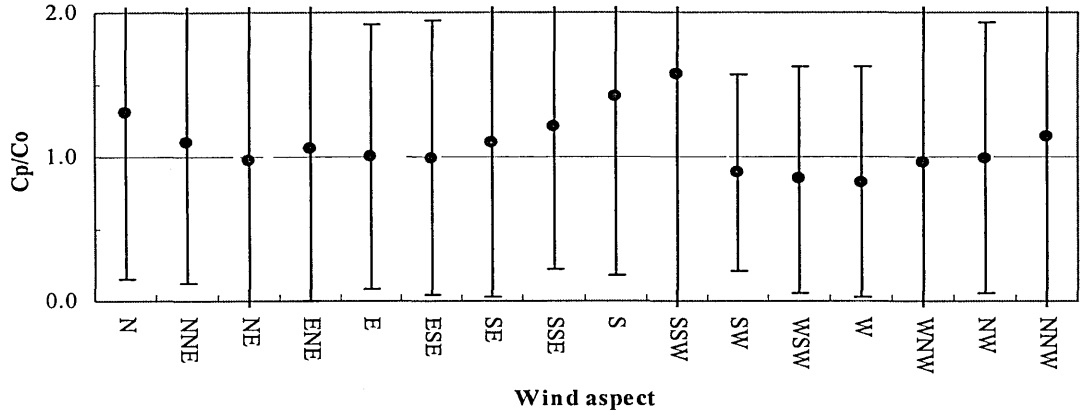


Figure 7.6 Variation of $C_p/C_o$ with observed wind aspect

### 7.2.3.2 Performance evaluation of the atmospheric dispersion model -- $PM_{10}$ prediction

The average value for the 89 predicted $PM_{10}$ concentrations using the conventional Gaussian plume dispersion model is 0.00115 mg $m^{-3}$. The average value for 89 observed $PM_{10}$ concentrations used to assess the model performance is 0.01210 mg $m^{-3}$. Mean Bias is –0.01095 mg $m^{-3}$. The conventional Gaussian plume dispersion model significantly underpredicted the $PM_{10}$ concentration measured at the study station. On average, only about 9.5% of observed $PM_{10}$ concentration is predicted by the model. This can be attributed to the $PM_{10}$ emission sources entered into the model. As mentioned in chapter 3, only one point emission source and road vehicle emission sources are covered in the atmospheric emission inventories for $PM_{10}$. The data for many important natural $PM_{10}$ emission sources such as marine aerosol, dust and secondary pollution aerosol are unavailable for Dundee.

Normalised Mean Square Error (NMSE) for $PM_{10}$ is 11.12. The correlation $r$ is –0.01 for a total of 89 paired concentrations. The highest ratio of $C_p/C_o$ is 0.23. The

percentage of $C_p$ within a factor of two of $C_o$ for $PM_{10}$ is 0. The maximum overall predicted $PM_{10}$ concentration is 0.00232 mg $m^{-3}$ while maximum overall observed concentrations used to evaluate the model performance is 0.03749 mg $m^{-3}$. The maximum overall predicted $PM_{10}$ concentration is only about 6.2% of maximum overall observed concentration. The average of top 25 concentrations [$\overline{C}$ (Top 25)] is 0.00164 mg $m^{-3}$ for the predicted $PM_{10}$ concentrations and 0.01994 mg $m^{-3}$ for the observed $PM_{10}$ concentrations. The predicted $\overline{C}$ (Top 25) is only about 8.2% of the observed $\overline{C}$ (Top 25).

The evaluated results show that the results from the conventional Gaussian plume dispersion model for simulating the transport of $PM_{10}$ in Dundee compare poorly with the observed data, because some important natural sources for $PM_{10}$ have not been included in the atmospheric inventories.

### 7.2.4 Results from the application of the atmospheric dispersion model

Predicted NOx one hour mean concentrations using the conventional Gaussian plume dispersion model have been compared and evaluated using observed concentrations. The assessment results show that the model can simulate the transport of NOx in Dundee reasonably well. The predicted results are reliable. The emission sources have been grouped into point emission, line emission and area emission for the model simulation process. The simulation results indicate that the average contributions of point emission, line emission and area emission sources to NOx concentration predicted at the study monitoring station are 1.2%, 6.2% and 92.6%, respectively. Area emission is the most important source that affects NOx concentration at the study station. Both area emission and line emission come from road vehicle emissions in the atmospheric emission inventories in Dundee. Thus, the road vehicle emission is the most important source that affects NOx concentration at the station. The contribution of road vehicle emission to NOx concentration predicted at the station is 98.8%.

The comparision between the results of the atmospheric dispersion model and the $PM_{10}$ concentrations measured at the study station is poor. The cause is that some important natural sources for $PM_{10}$ were not included in the atmospheric inventories in Dundee. However, reliability of the conventional Gaussian plume dispersion model in simulating atmospheric transport and dispersion has been proved to be reasonably good when predicting the NOx concentrations. Thus, the predicted results are directly linked to data input. On average, the contribution of the $PM_{10}$ emission sources gathered in the

atmospheric emission inventories is about 9.5%. The simulation results indicate that the average contributions of point emission, line emission and area emission to $PM_{10}$ concentration predicted at the study monitoring station are 1.6%, 5.5% and 92.9%, respectively. Among the available sources, the road vehicle emission is the most important source that affects predicted $PM_{10}$ concentration at the station. The contribution of road vehicle emission to $PM_{10}$ concentrations predicted at the station is 98.4%. However, the poor prediction of $PM_{10}$ is associated with not accounting for other $PM_{10}$ sources.

## 7.3 Application of receptor model

As described above, the atmospheric dispersion model underpredicts $PM_{10}$ concentrations measured at the study station. The major cause is that the source information for $PM_{10}$ is not comprehensive. The data for some important $PM_{10}$ sources are unavailable and have not been included in the atmospheric inventories in Dundee. In this case, receptor model provides a means to identify $PM_{10}$ sources and attribute sources to their receptors. The software package for positive matrix factorization model (Paatero, 1998) has been used to identify emission sources and attribute sources to $PM_{10}$ measured at the study station.

### 7.3.1 The element matrix for positive matrix factorization model (PMF) analysis

PMF model was applied to analyse $PM_{10}$ data measured at the study monitoring station. The concentrations of all 12 analysed chemical components of $PM_{10}$ ($SO_4^{2-}$, $NO_3^-$, $NH_4^+$, $Ca^{2+}$, $K^+$, $Cl^-$, $Na^+$, $Mg^{2+}$, Pb, Ni, Zn and Cu), average concentration of NOx, easterly wind frequency (ENE, E and ESE), westerly wind frequency (WSW, W and WNW) and average wind speed during the sampling time were selected to compose the input element matrix. The gaseous pollutant, NOx was selected because it may serve as a marker for the road vehicle emission. As mentioned above, 98.8% of NOx measured at the study station comes from vehicle emission. The wind direction frequencies and average wind speed were adopted as components of the element matrix because they can show source direction and the relationship with the wind speed. The final input element matrix includes concentrations of chemical species for 59 $PM_{10}$ samples and average NOx concentrations and wind condition during the sample time. The input element matrix with dimensions of 59 x 16 adopted for the PMF model analysis are shown in Table 7.1.

Table 7.1 Element matrix for PMF model analysis (ng $m^{-3}$)

| $SO_4^{2-}$ | $NO_3^-$ | $NH_4^+$ | $Ca^{2+}$ | $K^+$ | $Cl^-$ | $Na^+$ | $Mg^{2+}$ | Pb | Ni | Zn | Cu | NOx | E* (%) | W** (%) | WS*** (m $s^{-1}$) |
|---|---|---|---|---|---|---|---|---|---|---|---|---|---|---|---|
| 688 | 971 | 254 | 875 | 97 | 1047 | 1140 | 434 | 0 | 24 | 51 | 45 | 30536 | 20.6 | 34.8 | 2.0 |
| 505 | 208 | 80 | 545 | 53 | 1134 | 970 | 147 | 133 | 30 | 53 | 37 | 24955 | 0.6 | 65.5 | 3.1 |
| 589 | 0 | 167 | 718 | 12 | 845 | 1152 | 442 | 101 | 63 | 97 | 62 | 43579 | 0.5 | 48.6 | 1.3 |
| 2457 | 3287 | 1701 | 917 | 207 | 1741 | 1725 | 436 | 101 | 63 | 71 | 62 | 116963 | 21.2 | 23.7 | 1.5 |
| 703 | 1160 | 281 | 1319 | 111 | 1135 | 1451 | 263 | 0 | 58 | 71 | 53 | 20181 | 0.5 | 66.4 | 3.3 |
| 1610 | 2057 | 683 | 242 | 63 | 882 | 1164 | 165 | 71 | 25 | 44 | 49 | 46861 | 2.9 | 56.9 | 1.7 |
| 431 | 0 | 202 | 971 | 0 | 240 | 495 | 385 | 51 | 72 | 22 | 41 | 40828 | 4.1 | 46.0 | 1.5 |
| 550 | 681 | 134 | 556 | 39 | 333 | 505 | 307 | 87 | 48 | 63 | 42 | 49462 | 0.5 | 54.5 | 1.8 |
| 624 | 0 | 83 | 654 | 3 | 485 | 653 | 91 | 132 | 86 | 168 | 37 | 60832 | 3.2 | 45.9 | 1.4 |
| 592 | 1202 | 468 | 339 | 142 | 343 | 438 | 83 | 49 | 93 | 33 | 25 | 57796 | 0.0 | 48.1 | 1.8 |
| 604 | 215 | 153 | 1373 | 100 | 1126 | 1284 | 560 | 78 | 16 | 54 | 20 | 35757 | 0.2 | 60.7 | 3.2 |
| 1068 | 453 | 351 | 1758 | 281 | 902 | 1336 | 331 | 0 | 0 | 53 | 18 | 26891 | 4.7 | 65.6 | 3.0 |
| 3338 | 929 | 728 | 2284 | 56 | 1803 | 1614 | 328 | 0 | 0 | 68 | 45 | 28248 | 0.0 | 67.7 | 2.9 |
| 1139 | 0 | 125 | 727 | 111 | 2888 | 2484 | 402 | 0 | 47 | 25 | 14 | 23905 | 1.8 | 70.3 | 3.8 |
| 422 | 322 | 164 | 1809 | 35 | 1373 | 1305 | 158 | 0 | 50 | 50 | 25 | 28572 | 0.7 | 57.7 | 2.7 |
| 644 | 1089 | 490 | 1059 | 66 | 1515 | 1424 | 87 | 0 | 0 | 51 | 28 | 49992 | 6.6 | 53.1 | 1.8 |
| 1455 | 1993 | 960 | 564 | 214 | 1477 | 1317 | 100 | 48 | 21 | 29 | 45 | 50726 | 11.8 | 14.5 | 0.9 |
| 1386 | 1485 | 588 | 743 | 108 | 1949 | 1798 | 92 | 0 | 20 | 26 | 27 | 50650 | 4.0 | 44.6 | 1.8 |
| 1105 | 962 | 308 | 581 | 156 | 1461 | 1519 | 75 | 0 | 30 | 16 | 30 | 24030 | 1.0 | 73.3 | 3.4 |
| 1766 | 632 | 182 | 218 | 61 | 1541 | 1411 | 35 | 0 | 51 | 0 | 13 | 29771 | 1.0 | 65.3 | 2.5 |
| 781 | 917 | 342 | 772 | 24 | 903 | 926 | 35 | 0 | 0 | 10 | 25 | 19573 | 0.5 | 63.3 | 2.6 |
| 1006 | 433 | 244 | 800 | 108 | 1136 | 1135 | 56 | 0 | 32 | 8 | 17 | 21978 | 8.7 | 58.0 | 3.2 |
| 797 | 0 | 185 | 976 | 44 | 1490 | 1255 | 29 | 0 | 11 | 4 | 25 | 16103 | 1.2 | 73.0 | 3.0 |
| 1348 | 411 | 181 | 577 | 94 | 868 | 910 | 64 | 0 | 25 | 12 | 14 | 20446 | 0.5 | 66.8 | 2.3 |
| 1220 | 649 | 304 | 1947 | 51 | 1212 | 1514 | 122 | 0 | 45 | 36 | 19 | 33333 | 15.0 | 18.3 | 1.2 |
| 3391 | 3059 | 1648 | 1367 | 90 | 1552 | 1530 | 140 | 0 | 25 | 60 | 30 | 35822 | 35.7 | 21.0 | 2.3 |
| 2388 | 2205 | 902 | 2310 | 139 | 1250 | 1515 | 87 | 0 | 28 | 42 | 20 | 30903 | 14.4 | 13.6 | 0.9 |
| 2907 | 2875 | 1128 | 577 | 105 | 1933 | 2020 | 125 | 0 | 29 | 20 | 17 | 37641 | 28.2 | 2.3 | 1.0 |
| 2630 | 2220 | 1681 | 857 | 1432 | 622 | 3915 | 46 | 0 | 19 | 14 | 19 | 27156 | 49.6 | 2.4 | 1.9 |
| 1293 | 292 | 207 | 1301 | 159 | 962 | 1154 | 44 | 0 | 60 | 8 | 14 | 32097 | 14.2 | 35.0 | 1.8 |
| 2619 | 2074 | 962 | 709 | 147 | 916 | 1260 | 76 | 0 | 0 | 17 | 12 | 28184 | 15.3 | 32.7 | 1.2 |
| 2579 | 0 | 683 | 730 | 107 | 1088 | 1427 | 63 | 0 | 0 | 14 | 15 | 29622 | 26.3 | 25.3 | 1.7 |
| 2729 | 1919 | 1014 | 768 | 94 | 910 | 1464 | 58 | 0 | 27 | 11 | 17 | 24183 | 29.6 | 17.1 | 1.3 |
| 2640 | 1726 | 1111 | 867 | 90 | 284 | 531 | 39 | 51 | 19 | 33 | 15 | 28657 | 69.3 | 0.5 | 3.1 |

Table 7.1 (Continue)

| $SO_4^{2-}$ | $NO_3^-$ | $NH_4^+$ | $Ca^{2+}$ | $K^+$ | $Cl^-$ | $Na^+$ | $Mg^{2+}$ | Pb | Ni | Zn | Cu | NOx | E* (%) | W** (%) | WS*** ($m\ s^{-1}$) |
|---|---|---|---|---|---|---|---|---|---|---|---|---|---|---|---|
| 3169 | 2126 | 1546 | 1008 | 58 | 217 | 376 | 27 | 88 | 50 | 16 | 6 | 30536 | 20.6 | 34.8 | 2.0 |
| 3534 | 1472 | 905 | 36 | 80 | 291 | 731 | 90 | 55 | 0 | 7 | 21 | 29351 | 43.9 | 4.5 | 1.6 |
| 3994 | 2193 | 1791 | 234 | 49 | 342 | 572 | 58 | 52 | 0 | 0 | 15 | 37814 | 55.4 | 0.7 | 1.7 |
| 4204 | 1784 | 945 | 223 | 184 | 1322 | 1361 | 202 | 0 | 0 | 9 | 8 | 36150 | 58.1 | 1.2 | 2.4 |
| 7455 | 7692 | 3121 | 243 | 70 | 876 | 1609 | 222 | 89 | 15 | 0 | 20 | 35078 | 52.6 | 2.2 | 1.9 |
| 2122 | 0 | 286 | 89 | 0 | 444 | 575 | 44 | 59 | 0 | 0 | 20 | 28097 | 6.9 | 47.7 | 1.7 |
| 2915 | 1374 | 572 | 495 | 74 | 382 | 790 | 46 | 0 | 0 | 12 | 10 | 22252 | 34.6 | 19.1 | 1.6 |
| 661 | 725 | 272 | 317 | 34 | 280 | 388 | 32 | 0 | 0 | 4 | 0 | 19801 | 9.1 | 51.2 | 2.0 |
| 1375 | 625 | 313 | 256 | 71 | 2750 | 2080 | 48 | 0 | 33 | 0 | 15 | 21217 | 64.8 | 0.0 | 2.6 |
| 3107 | 1517 | 601 | 391 | 86 | 1406 | 1783 | 69 | 0 | 38 | 6 | 12 | 32811 | 29.5 | 27.1 | 1.6 |
| 2879 | 317 | 391 | 1169 | 20 | 922 | 965 | 38 | 0 | 0 | 18 | 24 | 15331 | 1.7 | 64.3 | 2.3 |
| 1767 | 216 | 218 | 368 | 58 | 2759 | 2209 | 114 | 0 | 0 | 22 | 16 | 14578 | 16.7 | 56.7 | 3.0 |
| 7359 | 3610 | 2183 | 736 | 127 | 475 | 1893 | 137 | 0 | 0 | 17 | 15 | 35042 | 46.7 | 10.4 | 1.9 |
| 3214 | 673 | 550 | 793 | 27 | 179 | 434 | 60 | 0 | 28 | 11 | 11 | 26550 | 22.6 | 43.0 | 2.1 |
| 526 | 0 | 238 | 830 | 0 | 894 | 679 | 37 | 0 | 64 | 21 | 28 | 13154 | 18.9 | 25.6 | 1.5 |
| 2723 | 651 | 689 | 795 | 71 | 670 | 975 | 40 | 0 | 0 | 22 | 26 | 21109 | 45.8 | 5.7 | 1.5 |
| 2429 | 310 | 850 | 577 | 84 | 186 | 453 | 24 | 0 | 19 | 7 | 19 | 16053 | 54.9 | 0.0 | 1.6 |
| 3025 | 452 | 522 | 1362 | 9 | 140 | 332 | 62 | 0 | 0 | 32 | 14 | 22666 | 50.6 | 9.6 | 1.6 |
| 2467 | 638 | 556 | 423 | 133 | 276 | 296 | 0 | 0 | 0 | 0 | 13 | 15760 | 24.3 | 32.4 | 1.6 |
| 489 | 0 | 181 | 1171 | 42 | 504 | 605 | 31 | 0 | 0 | 33 | 10 | 12073 | 8.7 | 51.2 | 1.9 |
| 2692 | 327 | 301 | 1083 | 223 | 1928 | 1641 | 51 | 0 | 29 | 67 | 20 | 13927 | 24.5 | 20.3 | 1.3 |
| 2444 | 222 | 418 | 280 | 205 | 542 | 754 | 67 | 0 | 0 | 10 | 12 | 20251 | 23.6 | 31.4 | 1.7 |
| 3932 | 950 | 886 | 0 | 96 | 401 | 1073 | 28 | 0 | 30 | 0 | 20 | 12017 | 40.6 | 0.3 | 1.5 |
| 3163 | 361 | 839 | 285 | 102 | 231 | 294 | 27 | 0 | 0 | 10 | 22 | 24591 | 23.9 | 20.4 | 1.2 |
| 5417 | 650 | 1677 | 0 | 1 | 79 | 70 | 21 | 0 | 47 | 0 | 41 | 19190 | 39.8 | 2.4 | 1.3 |

* : Easterly wind frequency (ENE, E and ESE)
**: Westerly wind frequency (WSW, W and WNW)
***: Wind speed

### 7.3.2 Error estimates

Chemical components measured in the ambient environment vary widely, especially for some trace elements in aerosols. Huang et al. (1999) thought that the choice of elements might affect the results of factor analysis because some elements could degrade the resolution of factor analysis by varying randomly in response to analytical uncertainties or by being below detection limits.

One of the major advantages of a PMF model is that it can handle various elements with different variation ranges and uncertainties by error estimates (Paatero, 1998). The error estimates in a PMF model for the individual data point values are utilised as point-by-point weight by a $\boldsymbol{S}$ matrix (standard deviation array) for $\boldsymbol{X}$ matrix (elements array). $\boldsymbol{S}$ matrix may be calculated using four different methods in a PMF model. Error estimates can be used to treat missing data and data with values under a detection limit. These error estimates are very important and may affect the results of the analysis of a PMF model. The error estimate $S_{ij}$ is calculated using the following formula in the application of a PMF model:

$$S_{ij} = T_j + U_j\sqrt{\max(|X_{ij}|,|Y_{ij}|)} + V_j \max(|X_{ij}|,|Y_{ij}|) \quad (7.5)$$

where $Y_{ij}$ is the fitted value by the PMF model for $X_{ij}$. The first item will dominate the error estimates when the value of $X_{ij}$ or $Y_{ij}$ is low. The last two items will dominate the error estimates when the value of $X_{ij}$ or $Y_{ij}$ is high. There is no simple rule for selecting coefficients. The optimal way for selecting coefficients depends on a basic understanding of the data and 'trial and error'. The chemical components with less precision may create anomalous single element factors that can not be interpreted physically. Large values should be used as coefficients for these components. Different coefficients should be used to calculate the error estimates for different chemical components with different random errors.

For the chemical species such as $Ca^{2+}$, $Mg^{2+}$, Cu, Pb, Ni, Zn and NOx and wind speed, for which detection limits are available (Chapter 4), $T_j$ in equation 7.5 was assigned the value of a detection limit. For the ions and wind direction frequencies for which detection limits are unavailable, an artificial value (based on the value in the element matrix) was assigned to $T_j$. The values of $T_j$ used in equation 7.5 for 16 of the components in the element matrix are shown in Table 7.2.

The analysis precision is used as the initial value of $V_j$ for chemical species of $PM_{10}$, NOx and wind speed (chapter 4). An artificial value is used for wind direction frequencies. The initial values of $V_j$ used in the error estimate are also shown in Table 7.2. Then, the values of $V_j$ were modified by 'trial and error', basically according to standard deviation of scaled residuals ($E_{ij}/S_{ij}$). A small deviation of scaled residuals for a component in the element matrix means that PMF model provides a good fitted value for this component. On the other hand, it may suggest that random error is small for this

component. Thus, a small value of $V_j$ may be used in this situation. A large deviation of scaled residuals for a component means that PMF model provides a poorly fitted value for this component. It may be interpreted that random error is large for this component. A large value of $V_j$ should be used in this situation. For example, 0.24 is the initial value of $V_j$ for $SO_4^{2-}$. The value of $V_j$ for $SO_4^{2-}$ was subsequently reduced in model trial because the standard deviation of its scaled residuals is small. The initial value of $V_j$ for $NH_4^+$ is 0.05. The value of $V_j$ was increased in the model trial because the standard deviation of its scaled residuals is large. The final values of $V_j$ used in error estimate for 16 of the components are also shown in Table 7.2.

Table 7.2 The values of $T_j$ and $V_j$ used

| | $SO_4^{2-}$ | $NO_3^-$ | $NH_4^+$ | $Ca^{2+}$ | $K^+$ | $Cl^-$ | $Na^+$ | $Mg^{2+}$ | Pb | Ni | Zn | Cu | NOx | E | W | WS |
|---|---|---|---|---|---|---|---|---|---|---|---|---|---|---|---|---|
| $T_j$ | 20 | 20 | 20 | 20 | 10 | 20 | 20 | 0.9 | 41.7 | 8.9 | 2.1 | 4.8 | 1000 | 2 | 2 | 0.1 |
| $V_j^*$ | 0.24 | 0.14 | 0.05 | 0.01 | 0.09 | 0.11 | 0.05 | 0.01 | 0.08 | 0.14 | 0.02 | 0.19 | 0.01 | 0.1 | 0.1 | 0.01 |
| $V_j^{**}$ | 0.2 | 0.15 | 0.15 | 0.05 | 0.3 | 0.1 | 0.1 | 0.2 | 0.05 | 0.2 | 0.2 | 0.2 | 0.2 | 0.3 | 0.2 | 0.2 |

*: Initial values

**: Final values

### 7.3.3 Model trial

According to the analysis of $PM_{10}$ chemical composition (section 5.3), $PM_{10}$ measured at the study station comes from at least three sources (secondary aerosol, marine aerosol and local emission). The element matrix shown in Table 7.1 was first analysed using a PMF model with a factorisation rank of 3. Then the factorisation rank was increased one by one to find an appropriate number of factors (sources). The most suitable results from the physical interpretation point view have been used as the principle for judging the appropriate number of factors. There are as yet no exact rules to assess the performance of PMF model. A research group headed by Hopke (Polissar et al., 1996; Alexandr et al., 1998; Xie et al., 1999) have tried to use $Q$ value (sum of total scaled residuals, Equation 6.77), frequency distribution of scaled residuals and multiple linear regression to assess the performance of PMF model. The theoretical value of $Q$ is approximately equal to the number of degrees of freedom of the input element matrix. It is 944 (59x16) in this case. The standard deviations of scaled residuals (SDOSR) and percentages of scaled residuals with absolute value less than 2 (POSR) are used to describe the frequency distribution of scaled residuals in this work. The values of $Q$, correlation

coefficient ($r$) between measured values ($X_{ij}$) and model fitted values ($Y_{ij}$), SDOSR and POSR in the PMF model trial, with a factorisation rank from 3 to 6, are shown in Table 7.3.

Table 7.3 Assessment of PMF model performance

| | 3 factors ($Q$ = 1630) | | | 4 factors ($Q$ = 1255) | | | 5 factors ($Q$ = 943) | | | 6 factors ($Q$ = 719) | | |
|---|---|---|---|---|---|---|---|---|---|---|---|---|
| | $r$ | SDOSR | POSR | $r$ | SDOSR | POSR | $r$ | SDOSR | POSR | $r$ | SDOSR | POSR |
| $SO_4^{2-}$ | 0.76 | 1.72 | 74.6% | 0.92 | 0.99 | 94.9% | 0.91 | 1.01 | 94.9% | 0.90 | 1.03 | 96.6% |
| $NO_3^-$ | 0.94 | 1.76 | 83.1% | 0.99 | 0.45 | 100.0% | 1.00 | 0.41 | 100.0% | 1.00 | 0.37 | 100.0% |
| $NH_4^+$ | 0.92 | 1.44 | 93.2% | 0.97 | 1.00 | 94.9% | 0.96 | 1.00 | 96.6% | 0.96 | 1.04 | 96.6% |
| $Ca^{2+}$ | 1.00 | 0.39 | 100.0% | 1.00 | 0.38 | 100.0% | 1.00 | 0.17 | 100.0% | 1.00 | 0.16 | 100.0% |
| $K^+$ | 0.21 | 1.11 | 96.6% | 0.18 | 1.13 | 93.2% | 0.19 | 1.13 | 94.9% | 0.19 | 1.13 | 94.9% |
| $Cl^-$ | 0.98 | 0.90 | 98.3% | 0.98 | 0.90 | 98.3% | 0.99 | 0.66 | 100.0% | 0.99 | 0.66 | 100.0% |
| $Na^+$ | 0.77 | 1.46 | 93.2% | 0.76 | 1.51 | 93.2% | 0.77 | 1.48 | 93.2% | 0.77 | 1.46 | 93.2% |
| $Mg^{2+}$ | 0.30 | 2.13 | 57.6% | 0.30 | 2.09 | 62.7% | 0.84 | 1.29 | 88.1% | 0.87 | 1.07 | 89.8% |
| Pb | 0.07 | 0.83 | 78.0% | 0.15 | 0.82 | 94.9% | 0.58 | 0.68 | 98.3% | 0.55 | 0.69 | 96.6% |
| Ni | 0.08 | 1.35 | 83.1% | 0.07 | 1.35 | 84.7% | 0.40 | 1.26 | 88.1% | 0.38 | 1.25 | 88.1% |
| Zn | 0.44 | 1.71 | 74.6% | 0.44 | 1.71 | 72.9% | 0.74 | 1.23 | 89.8% | 0.69 | 1.19 | 91.5% |
| Cu | 0.13 | 1.18 | 89.8% | 0.07 | 1.16 | 88.1% | 0.75 | 0.82 | 98.3% | 0.75 | 0.82 | 98.3% |
| NOx | 0.66 | 1.52 | 84.7% | 0.64 | 1.47 | 78.0% | 0.78 | 1.23 | 83.1% | 0.77 | 1.18 | 89.8% |
| E | 0.61 | 1.78 | 66.1% | 0.84 | 1.14 | 93.2% | 0.85 | 1.11 | 93.2% | 0.89 | 0.95 | 96.6% |
| W | 0.46 | 1.49 | 81.4% | 0.47 | 1.48 | 81.4% | 0.49 | 1.38 | 81.4% | 0.98 | 0.29 | 100.0% |
| WS | 0.28 | 1.44 | 83.1% | 0.35 | 1.28 | 86.4% | 0.31 | 1.25 | 84.7% | 0.80 | 0.72 | 96.6% |

### 7.3.3.1 PMF model trial results with a factorisation rank of three

The results of a PMF model can be illustrated qualitatively by the scaled factor compositions (Explained Variances, equation 6.78). The scaled factor compositions derived using a PMF model with a factorisation rank of three are shown in Figure 7.7. The characteristics of three factors are clear and may easily be interpreted physically. Factor 1 has a high loading for chemical species $Cl^-$ and $Na^+$ and a loading for $K^+$ and $Mg^{2+}$. $Cl^-$, $Na^+$ and $Mg^{2+}$ are major components of marine aerosol. Thus, this factor represents a marine aerosol source. There is a loading for westerly wind frequency in this factor as well. The analysis of the contribution of wind aspect to chemical species of $PM_{10}$ (section 5.36) shows that the contribution of westerly wind to $Cl^-$ is higher than westerly wind

frequency while the contribution of easterly wind to $Cl^-$ is lower than the easterly wind frequency. A loading for westerly wind in this factor suggests that the source for $Cl^-$ from the Atlantic Ocean is stronger than that from the North Sea.

Factor 2 has a high loading for $Ca^{2+}$ and Zn. $Ca^{2+}$ is usually used as markers for soil and construction dust.

Factor 3 has a high loading for chemical components $NO_3^+$ and $NH_4^+$ and a loading for $SO_4^{2-}$. $NO_3^+$, $NH_4^+$ and $SO_4^{2-}$ are secondary pollutants formed from gases of $NO_x$ and $SO_2$. This factor represents a secondary aerosol source. Factor 3 has a loading for easterly wind frequency. The analysis of contribution of wind aspect to chemical species of $PM_{10}$ (section 5.36) shows that the average contributions of easterly wind for $SO_4^{2-}$, $NO_3^-$ and $NH_4^+$ are much higher than easterly wind frequency while the average contributions of westerly wind to them are much lower than westerly wind frequency. A loading for easterly wind suggests that the European continent is a major source for the secondary species of $PM_{10}$.

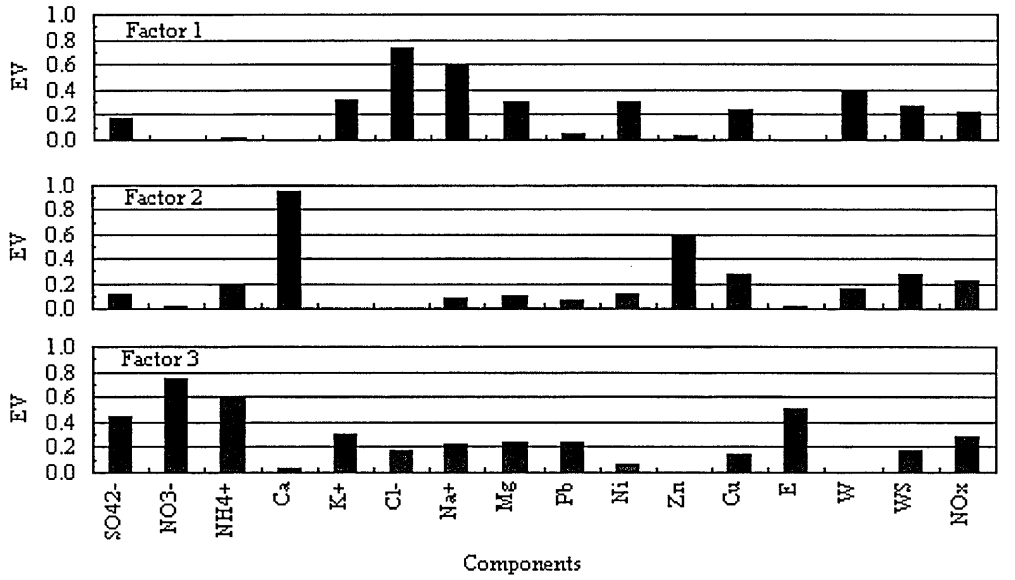


Figure 7.7 Scaled factor compositions of 3 factors derived using PMF model

The value of $Q$ for the PMF model trial with a factorisation rank 3, is 1630 (Table 7.3). It is much larger than the theoretical value (944, the number of degrees of freedom of the input element matrix). The 'best-fit' result of the PMF model is that of $Ca^{2+}$, with the highest correlation coefficient (1.00) and percentages of scaled residual with absolute value less than 2 (100.0%) and the lowest standard deviation of scaled residuals (0.39). Correlation between measured values and model fitted values is very good for $NO_3^-$, $NH_4^+$,

$Cl^-$, with the correlation coefficient values higher than 0.9. On the other hand, it is poor for $K^+$, $Mg^{2+}$, Pb, Ni, Cu and WS (wind speed) with the correlation coefficient values lower than 0.3. The standard deviation of scaled residual is relatively low for $K^+$, $Cl^-$ and Pb with a value less than 1.0. It is high for other elements. Percentage of scaled residuals with absolute value less than 2 is high for $NH_4^+$, $K^+$, $Cl^-$ and $Na^+$ with a value higher than 90.0%. It is lower for other elements. The performance of the PMF model with a factorisation rank of three is not as good as one would expect.

### 7.3.3.2 PMF model trial results with a factorisation rank of four

The scaled factor compositions derived using the PMF model with a factorisation rank of four are shown in Figure 7.8. Comparison with the results for the factorisation rank of three shows that the characteristics of factors 1 and 2 have not changed. They represent the marine aerosol source and soil and construction dust source. A new factor (factor 4) with a high loading for easterly wind frequency and a loading for $SO_4^{2-}$ and $NH_4^+$ is separated from the former factor 3. Now, factor 3 has a high loading for $NO_3^+$ and a loading for $NH_4^+$. It represents the secondary aerosol source of ammonium nitrate. Factor 4 with a loading for $SO_4^{2-}$ and $NH_4^+$ represents the secondary aerosol source of ammonium sulphate. Factor 4 has a high loading for easterly wind frequency. It implies that the European continent is a major source for secondary aerosol of ammonium sulphate.

The value of $Q$ for the PMF model trial with a factorisation rank 4 is 1255 (Table 7.3). It is also larger than the theoretical value. The best fitted result of the PMF model is that of Ca. Correlation between measured values and model fitted values has been improved for most of the elements, especially for $SO_4^{2-}$ and easterly wind frequency. The correlation for $SO_4^{2-}$ with a correlation coefficient of 0.92 is very good now. At the same time, the standard deviations of scaled residuals have reduced and the percentages of scaled residual with absolute value less than 2 have increased for most elements, as expected. The values of standard deviation of scaled residual for $SO_4^{2-}$ and easterly wind frequency approach 1.0, while the percentages of scaled residual with absolute value less than 2 are higher than 90.0%. The performance of PMF model has been improved in the model trial with a factorisation rank of four, evidenced by the discussion above.

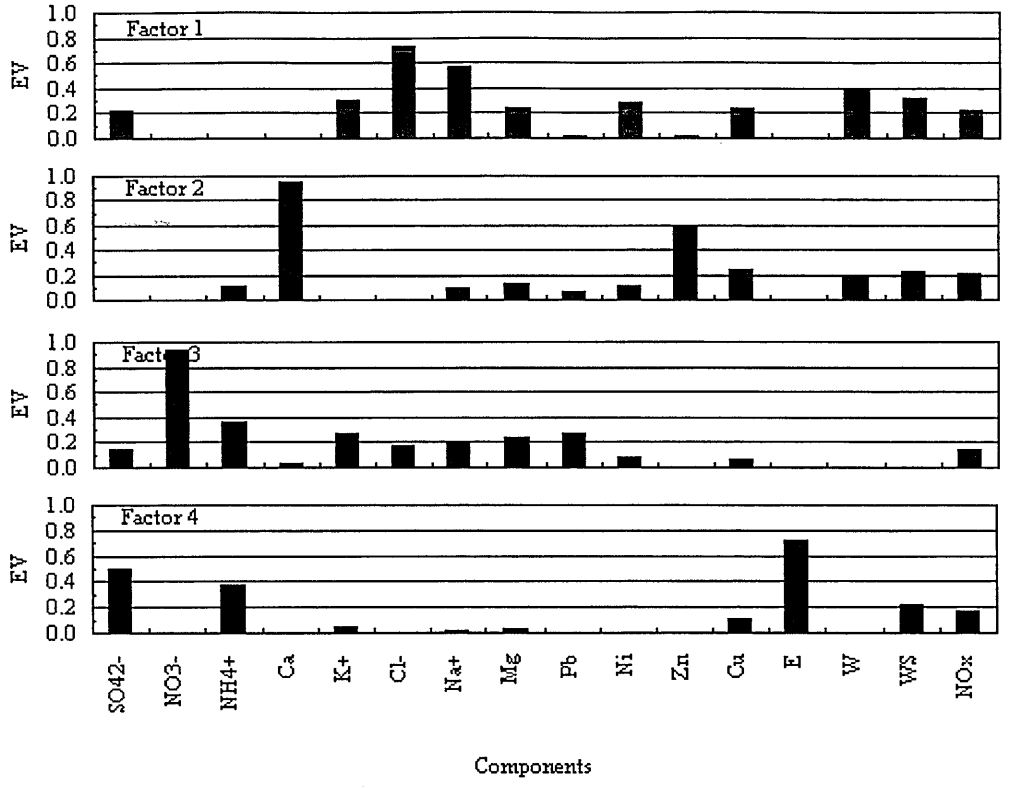


Figure 7.8 Scaled factor compositions of 4 factors derived using PMF model

### 7.3.3.3 PMF model trial results with a factorisation rank of five

The scaled factor compositions derived using the PMF model with a factorisation rank of five are shown in Figure 7.9. In comparison with the result of factorisation rank of four, the characteristics of factors 1, 2, 3 and 4 have not changed. They also represent the marine aerosol source, soil and construction dust source, the secondary aerosol source of ammonium nitrate and the secondary aerosol source of ammonium sulphate, respectively. A new factor (factor 5) with a loading for heavy metals ($Mg^{2+}$, Pb, Ni, Zn and Cu) and westerly wind frequency has been separated. Factor 5 can be interpreted as a source coming from incinerator and fuel oil burning.

The value of $Q$ for PMF model trial with a factorisation rank 5 is 943 (Table 7.3). It is almost equal to the theoretical value. The best fitted results of the PMF model are that of $Ca^{2+}$ and $NO_3^+$ with a correlation coefficient of 1.00 and percentage of scaled residual with absolute values less than 2 of 100.0%. The correlation between measured values and model fitted values has been improved for the heavy metals ($Mg^{2+}$, Pb, Ni, Zn and Cu). The standard deviations of scaled residual for most elements are less than 1. The percentages of

scaled residual with absolute value less than 2 for most elements are higher than 90%. In conclusion, the performance of the PMF model is good in the model trial with a factorisation rank of five.

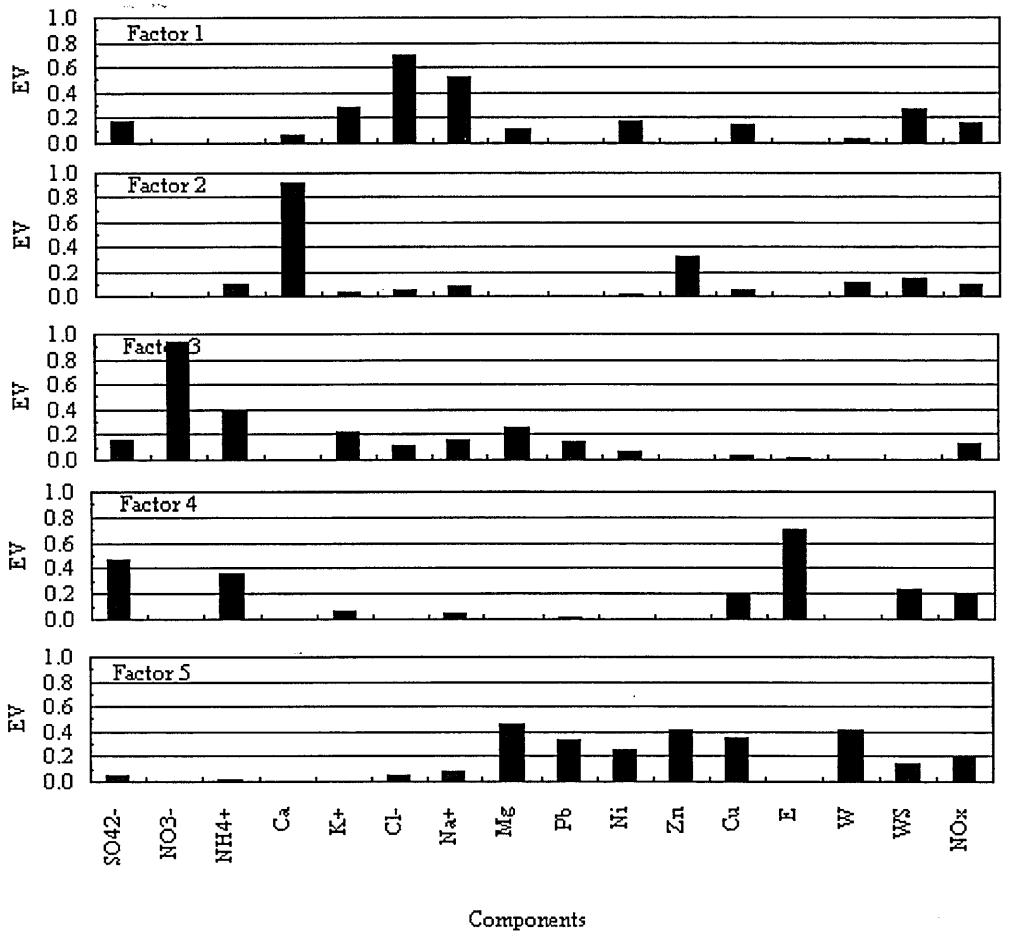


Figure 7.9 Scaled factor compositions of 5 factors derived using PMF model

### 7.3.3.4 PMF model trial results with a factorisation rank of six

The scaled factor compositions produced using the PMF model with a factorisation rank of six are shown in Figure 7.10. In comparison with the results of factorisation rank of five, the characteristics of factors 1, 2, 3, 4 and 5 have not changed. They represent the marine aerosol source, soil and construction dust source, the secondary aerosol source of ammonium nitrate, the secondary aerosol source of ammonium sulphate and incinerator and fuel oil burning source as well. A new factor (factor 6) with a high loading for westerly

wind frequency and a loading for wind speed has been separated. It is difficult to interpret factor 6 physically because there is no high loading for any chemical species of $PM_{10}$.

The value of $Q$ for the PMF model trial with a factorisation rank 6 is 719 (Table 7.3). It is less than the theoretical value. The 'best fit' results of PMF model are also that of $Ca^{2+}$ and $NO_3^+$. The fitted result of the PMF model has been improved for westerly wind frequency and wind speed. However, the fitted result of the PMF model is similar for other elements.

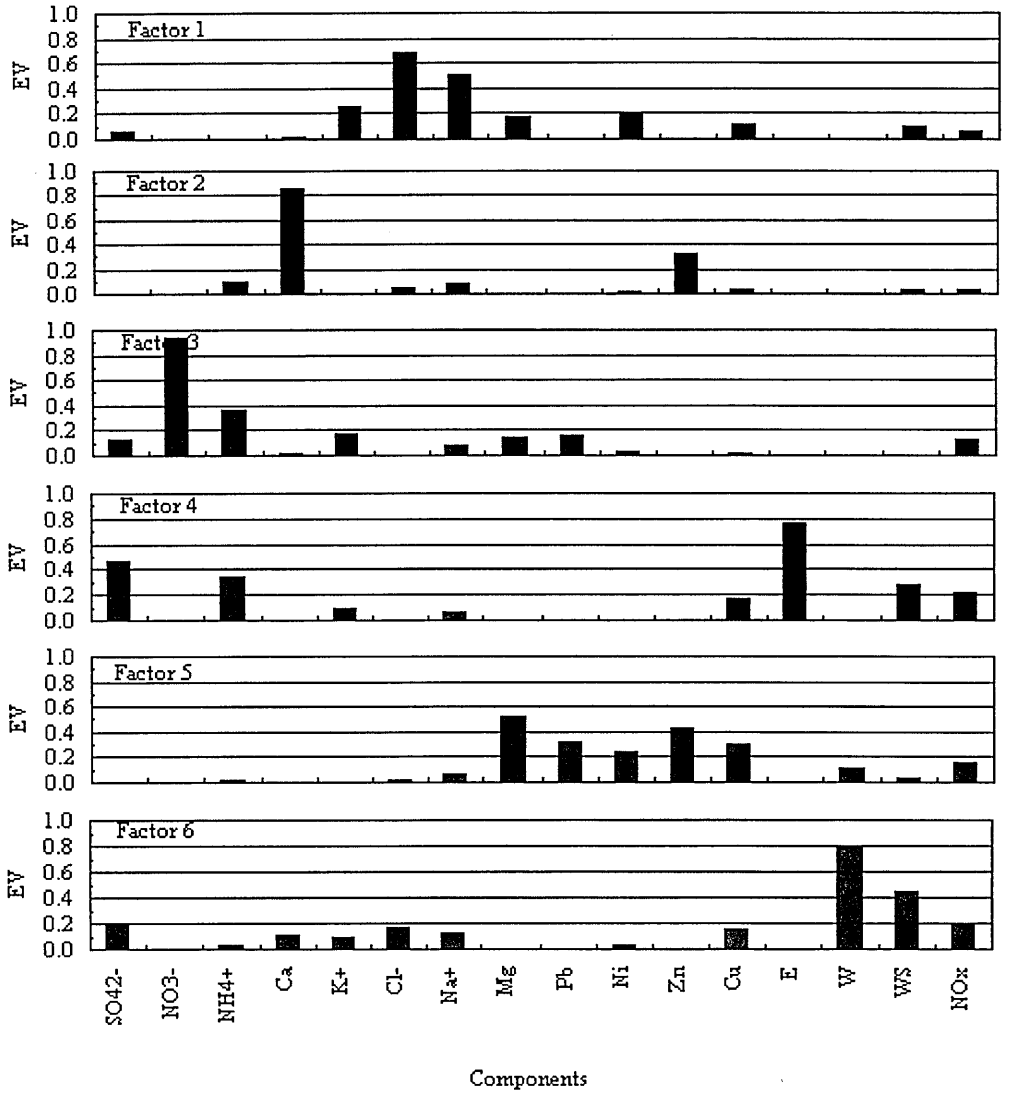


Figure 7.10 Scaled factor compositions of 6 factors derived using PMF model

The results of the PMF model trial with a factorisation rank from 3 to 6 show that the results of 5 factors are the most suitable results that can be interpreted physically while the performance of the model is good as expected.

### 7.3.4 Factor mass profiles

As mentioned above, the result of 5 factors derived using the PMF model are the most suitable result that can be interpreted physically while the performance of the model is good. The percentages of measured chemical species in $PM_{10}$ that can be attributed to these 5 factors are 85.0%, 94.1%, 84.7%, 99.2%, 61.8%, 92.9%, 89.2%, 81.7%, 49.1%, 51.2%, 73.7% and 76.2% for $SO_4^{2-}$, $NO_3^-$, $NH_4^+$, $Ca^{2+}$, $K^+$, $Cl^-$, $Na^+$, $Mg^{2+}$, Pb, Ni, Zn and Cu respectively. The factor characteristics can be illustrated quantitatively by the scaled factors. The mass profiles of the factors provide further means to confirm source characteristics quantitatively. The 5 factor mass profiles (12 chemical species) derived by the PMF model are shown in Table 7.4.

Table 7.4 Mass profiles of 5 factors derived using PMF model

| | Factor 1 | Factor 2 | Factor 3 | Factor 4 | Factor 5 |
|---|---|---|---|---|---|
| $SO_4^{2-}$ | 13.73% | 0.01% | 17.20% | 80.75% | 16.98% |
| $NO_3^-$ | 0.01% | 0.07% | 53.03% | 0.04% | 0.03% |
| $NH_4^+$ | 0.03% | 4.52% | 14.38% | 16.41% | 2.19% |
| $Ca^{2+}$ | 2.20% | 79.91% | 0.01% | 0.00% | 1.00% |
| $K^+$ | 1.61% | 0.32% | 1.27% | 0.41% | 0.03% |
| $Cl^-$ | 43.10% | 4.08% | 4.16% | 0.00% | 13.67% |
| $Na^+$ | 38.28% | 9.96% | 8.49% | 2.06% | 27.16% |
| $Mg^{2+}$ | 0.51% | 0.00% | 1.03% | 0.00% | 22.37% |
| Pb | 0.00% | 0.00% | 0.30% | 0.05% | 5.01% |
| Ni | 0.32% | 0.05% | 0.09% | 0.01% | 2.98% |
| Zn | 0.00% | 0.94% | 0.00% | 0.00% | 4.90% |
| Cu | 0.22% | 0.14% | 0.04% | 0.27% | 3.68% |
| Equivalent Anion/Cation | 0.88 | 0.17 | 1.11 | 1.66 | 0.57 |

The best way to assess the result of factor analysis is to compare the derived factor mass profiles with the real source profiles of $PM_{10}$. Unfortunately, measured $PM_{10}$ profiles for the local Dundee airborne pollutant emission sources are unavailable. The factor mass profiles had to be assessed by analysing source characteristics and comparing them with some artificial ideal source profiles used in SCAQS (Southern California Air Quality Study) $PM_{2.5}$ and $PM_{10}$ receptor modelling (Watson et al., 1994). Some real source profiles such as secondary pollution sources and fresh marine source should be very similar to the

ideal source profiles. However, contamination in the environment could make real primary source profiles depart slightly from the ideal patterns.

The mass profile of factor 1 has high percentages for $Cl^-$, $Na^+$ and $SO_4^{2-}$. The percentages for $Cl^-$, $Na^+$, $SO_4^{2-}$, $Ca^{2+}$ and $K^+$ are 43.10%, 38.28%, 13.73%, 2.20% and 1.61% respectively. The ionic balance in this factor is reasonably good with an equivalent anion/cation ratio of 0.88. In ideal fresh pure marine aerosol source profile used by Watson et al. (1994), the percentages for $Cl^-$, $Na^+$, $SO_4^{2-}$, $Ca^{2+}$ and $K^+$ are 57.40%, 32.00%, 8.00%, 1.22% and 1.18%, respectively. The equivalent anion/cation ratio is 1.26. Percentage of $Cl^-$ in factor 1 derived using PMF is lower than the value in the ideal fresh pure marine aerosol profile, while percentages of $Na^+$ and $SO_4^{2-}$ are higher than the ideal values. There is a loss reaction of particulate $Cl^-$ in the ambient environment when gaseous acid species react with sea salt aerosols to liberate gaseous HCl. The mass profile of factor 1 indicates that this factor should represent an aged marine aerosol source with some $Cl^-$ replaced by $SO_4^{2-}$.

The mass profile of factor 2 has a high percentage for $Ca^{2+}$ (79.91%). $Na^+$, $NH_4^+$ and $Cl^-$ are three components with relatively high percentages among the remaining species. The ions are not the major components in this factor and so the ionic balance is poor with the value of 0.17 for equivalent anion/cation ratio. The mass profile also shows that factor 2 should represent the source from soil and construction dust. However, it is difficult to assess factor 2 quantitatively, because a reasonable source profile that can describe local soil and construction dust is unavailable.

The scaled factor composition of factor 3 shows that it represents the secondary aerosol source of ammonium nitrate. There are only two chemical components (77.5% $NO_3^-$ and 22.6% $NH_4^+$; $NO_3^-/NH_4^+$ = 3.43) in the artificial ideal source profile of ammonium nitrate (Watson et al., 1994). The anion and cation are fully balanced. The mass profile of factor 3 has high percentages for $NO_3^-$, $SO_4^{2-}$ and $NH_4^+$. $NO_3^-$ and $NH_4^+$ hold about 67.41% of the source mass. The ratio 3.69 for $NO_3^-/NH_4^+$ in factor 3 approaches the ideal value. The anion and cation can be matched in this factor. The ratio of equivalent anion/cation is 1.11. However, the mass loading of $SO_4^{2-}$ in factor 3 is relatively high (17.20 %). The mass profile of factor 3 indicates that factor 3 should represent the secondary aerosol source with both ammonium nitrate and ammonium sulphate.

The mass profile of factor 4 has high percentages for $SO_4^{2-}$ and $NH_4^+$. There are only two chemical components (27.3% $NH_4^+$ and 72.7% $SO_4^{2-}$; $SO_4^{2-}/NH_4^+$ = 2.66) in the artificial ideal source profile of ammonium sulphate (Watson et al., 1994). The anion and

cation are fully balanced. In factor 4, $SO_4^{2-}$ and $NH_4^+$ hold about 97.16% of the source mass. The ratio of 5.35 for $SO_4^{2-}/NH_4^+$ is about double the ideal value. The loading of $NO_3^-$ is very low (0.04%). The ratio of equivalent anion/cation is 1.66. It indicates that a fraction of $SO_4^{2-}$ has not been associated with $NH_4^+$. The mass profile shows that factor 4 probably represents a secondary aerosol source of ammonium sulphate, although its structure is not exactly the same as the ideal one.

The scaled factor composition of factor 5 shows that it represents incinerator and fuel oil burning source, because it has a loading for metal elements. The mass profile of factor 5 is different to the scaled factor composition. It has a relatively high percentage for $Na^+$, $Mg^{2+}$, $SO_4^{2-}$ and $Cl^-$. The mass profile of factor 5 can not be interpreted reasonably as a source coming from incinerator and fuel oil burning because there are high percentages for the loading of $Na^+$ and $Cl^-$. $Na^+$ and $Cl^-$ are usually regarded as coming from a marine source.

### 7.3.5 Rotation

An evaluation of factor mass profiles shows there are some differences between the characteristics represented by scale factor components and mass profile for factors 3 and 5. 17.20% of $SO_4^{2-}$ in the mass profile of factor 3 shows that it is different from the ideal pattern of a pure secondary aerosol source of ammonium of nitrate. The high percentages of $Na^+$ and $Cl^-$ in the mass profile of factor 5 has meant that it can not be interpreted reasonably as a source coming from incinerator and fuel oil burning emission. The author has enough reasons to believe the $SO_4^{2-}$ should approach zero in a pure secondary aerosol source of ammonium nitrate. $Cl^-$ and $Na^+$ come mainly from marine aerosol. They should approach zero in the factor that represent incinerator and fuel oil burning emission source.

PMF model provides four methods to impose expected characteristics for the factors. Of these the method of pulling individual factor elements toward zero (Paatero, 1998) was chosen to pull $SO_4^{2-}$ in factor 3 and $Cl^-$ and $Na^+$ in factors 5 toward zero. The pulling down operation is controlled by the "Fkey" matrix. This matrix of integer value is of the same size as that of factor matrix ***F***. Each element of Fkey controls the behaviour of the corresponding element in ***F***. One element in factor matrix ***F*** that represents $SO_4^{2-}$ in factors 3 and two elements in the matrix that represents $Cl^-$ and $Na^+$ in factor 5 were identified. A Fkey matrix was constructed with zero for all elements except the elements that control the behaviour of $SO_4^{2-}$ in factor 3 and $Cl^-$ and $Na^+$ in factor 5 in the ***F*** matrix. 9

was used as the value for these three control elements (a "medium-strong" pulling). ***F*** and ***G*** matrices resulting from the previous model trial without enforced rotation were used as the initial values for the matrices. With the same element matrix and error estimates, the $SO_4^{2-}$ in factor 3 and $Cl^-$ and $Na^+$ in factor 5 have been successfully pulled toward zero by the Fkey matrix.

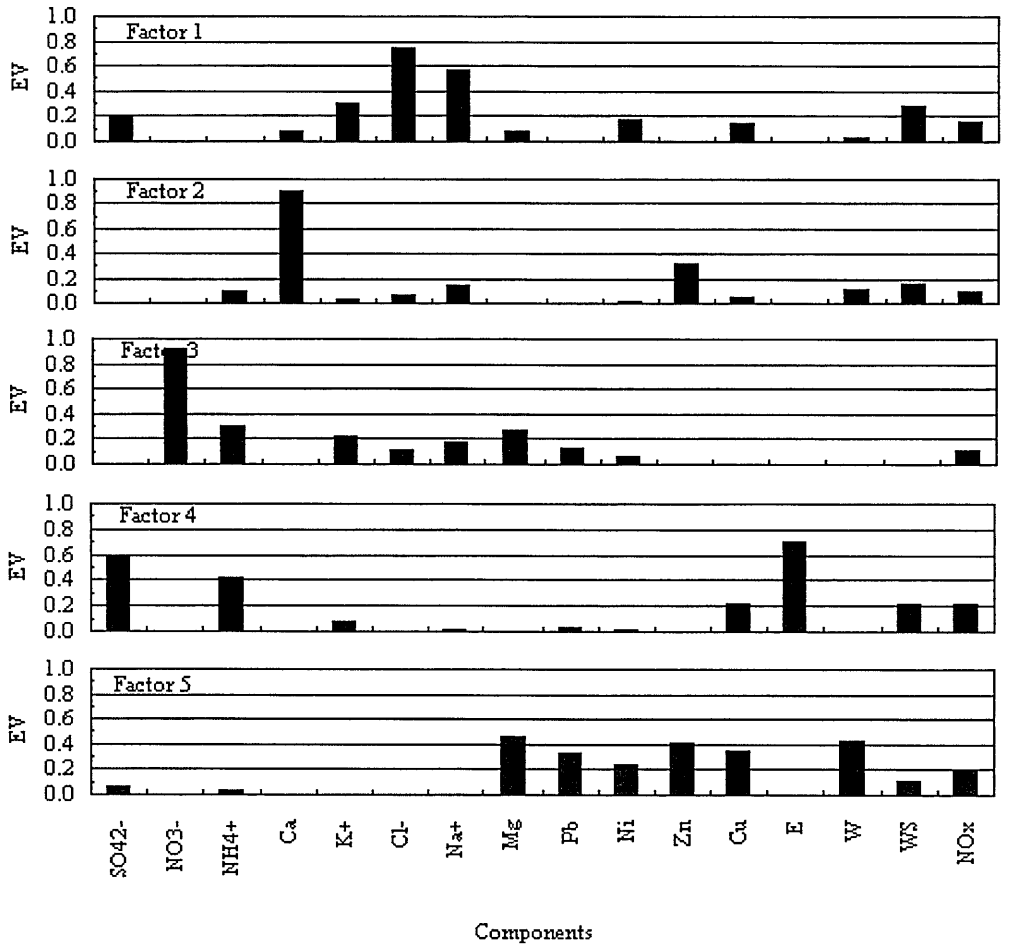


Figure 7.11 Scaled factor compositions of 5 factors derived using PMF model with enforced rotation

The scaled compositions of five factors derived using PMF model with enforced rotation are shown in Figure 7.11. They are very similar to those in Figure 7.9 except that the component of $SO_4^{2-}$ in factor 3 and components of $Cl^-$ and $Na^+$ in factor 5 are zero. The characteristics of all five factors shown by scaled factors have not changed. They represent the aged marine aerosol source, soil and construction dust source, the secondary aerosol source of ammonium nitrate, the secondary aerosol source of ammonium sulphate and incinerator and fuel oil burning source, respectively.

There is no obvious difference in the performance of the PMF model without rotation and that with enforced rotation. The calculated $Q$ value with enforced rotation is 966. It is only about 2.4% higher than the value without enforced rotation. The correlation coefficients of the measured and fitted values, standard deviations of scaled residuals and percentages of scaled residuals with absolute value less than 2, for cases without rotation and with enforced rotation, are almost the same.

The mass profiles of 5 factors derived by PMF model with enforced rotation are shown in Table 7.5. In comparison with values in Table 7.4, the smallest of changes are in factors 1, 2 and 4 while mass percentages of $SO_4^{2-}$ in factor 3 and $Cl^-$ and $Na^+$ in factor 5 reduce to zero. The mass profile of factor 3 has high percentages for $NO_3^-$ and $NH_4^+$. $NO_3^-$ and $NH_4^+$ hold about 79.99% of the source mass. The anion and cation can also be matched. The ratio of equivalent anion/cation is 0.88. Although, the ratio 4.41 for $NO_3^-$ /$NH_4^+$ is larger than the ideal value, the mass profile of factor 3 can represent the secondary aerosol source of ammonium nitrate well.

Table 7.5 Mass profiles of 5 factors derived from a PMF model with enforced rotation

| | Factor 1 | Factor 2 | Factor 3 | Factor 4 | Factor 5 |
|---|---|---|---|---|---|
| $SO_4^{2-}$ | 15.45% | 0.02% | 0.00% | 82.49% | 32.16% |
| $NO_3^-$ | 0.00% | 0.03% | 65.04% | 0.18% | 0.04% |
| $NH_4^+$ | 0.11% | 4.29% | 14.75% | 16.23% | 5.01% |
| $Ca^{2+}$ | 2.54% | 74.58% | 0.00% | 0.00% | 0.04% |
| $K^+$ | 1.53% | 0.24% | 1.54% | 0.36% | 0.00% |
| $Cl^-$ | 41.69% | 4.75% | 5.17% | 0.01% | 0.00% |
| $Na^+$ | 37.84% | 15.01% | 11.57% | 0.38% | 0.00% |
| $Mg^{2+}$ | 0.34% | 0.00% | 1.46% | 0.00% | 36.19% |
| Pb | 0.00% | 0.00% | 0.34% | 0.07% | 8.15% |
| Ni | 0.29% | 0.06% | 0.11% | 0.02% | 4.67% |
| Zn | 0.00% | 0.90% | 0.00% | 0.00% | 7.76% |
| Cu | 0.20% | 0.13% | 0.01% | 0.26% | 5.98% |
| Equivalent Anion/Cation | 0.89 | 0.15 | 0.88 | 1.86 | 2.41 |

The mass profile of factor 5 in Table 7.5 has a relatively high percentage for heavy metals and secondary aerosol components of $SO_4^{2-}$ and $NH_4^+$. It can be interpreted reasonably as a source coming from incinerator and fuel oil burning emission. However, it

is difficult to assess factor 5 quantitatively because reasonable source profile that can describe local incinerator and fuel oil burning emission is unavailable.

### 7.3.6 Factor mass contributions

The average mass contributions of 5 factors to $PM_{10}$, derived by PMF model, are shown in Table 7.6 in both mass and percentage formats. On average, the total chemical species mass contribution of 5 factors to $PM_{10}$, measured at the study monitoring station is 6856 ng $m^{-3}$. About 58.1% of $PM_{10}$ mass may be attributed to 5 sources represented by these factors. Factors 1 and 4 with average percentages of 17.8% and 16.9%, respectively, are two relatively high and stable mass contributors to $PM_{10}$. Factor 1 relates to aged marine aerosol with some chlorine replaced by sulphate. Factor 4 relates to the second aerosol source of ammonium sulphate. Factors 3 and 2, with average percentages of 12.1% and 9.5% respectively, follows. They relate to secondary aerosol source of ammonium nitrate and soil and construction dust. Factor 5 is the smallest contributor with an average percentage of 1.8% only. It represents local emission sources from incinerator and oil burning.

Among these five aerosol sources identified by PMF model, only the smallest contributor that represents local emission sources from incinerator and oil burning has been used in atmospheric dispersion model for $PM_{10}$ prediction. The performance of atmospheric dispersion model was poor in simulating $PM_{10}$ transportation because four important sources were not included as source input.

Table 7.6 Average contributions of 5 factors to $PM_{10}$ derived from a PMF model

| | Factor 1 | Factor 2 | Factor 3 | Factor 4 | Factor 5 | Sum |
|---|---|---|---|---|---|---|
| Mass(ng $m^{-3}$) | 1974±1462 | 977±695 | 1700±1996 | 2016±1849 | 189±212 | 6856±3056 |
| Percentage (%) | 17.8 ±12.7 | 9.5±7.2 | 12.1±9.6 | 16.9±15.1 | 1.8±2.4 | 58.1±14.3 |

The temporal variations of mass contributions of 5 factors to $PM_{10}$ are shown in Figure 7.12. In general, the temporal variation of each factor is similar to the variation of major species in the correspondent factor (Figure 5.10). Factor 1 represents the aged marine aerosol with some chlorine replaced by sulphate. Its contribution to $PM_{10}$ is reasonably high during the period 7 February 2000 to 27 Mach 2000. It is relatively low and fluctuating during the summer. Factor 2 is related to soil and construction dust source. Its contribution to $PM_{10}$ is relatively low during the period 24 April 2000 to 8 June 2000.

Factor 3 represents the secondary aerosol source of ammonium nitrate. Its contribution to $PM_{10}$ is generally high in the spring and low in the summer, although it fluctuates, as expected. Factor 4 represents the secondary aerosol source of ammonium sulphate. Its contribution to $PM_{10}$ is reasonably high in the spring and summer and low in the winter. Factor 5 is interpreted as a source from the incinerator and fuel oil burning emission. Its contribution is relatively higher in winter and lower in spring and summer with less fluctuation. It probably shows the impact of seasonal variation of anthropogenic emission source (for example, house heating emission) on $PM_{10}$.

For the $PM_{10}$ sample with the highest concentration (12 May 2000), about 52.5% of $PM_{10}$ mass may be attributed to these five factors. The secondary aerosol source of ammonium nitrate is the largest contributor with a percentage of 31.8%. The secondary aerosol source of ammonium sulphate is second with a percentage of 18.4%. The contributions of aged marine aerosol source, soil and construction dust source and incinerator and oil burning emission source are small with a percentage of 1.6%, 0.8% and 0.0%, respectively.

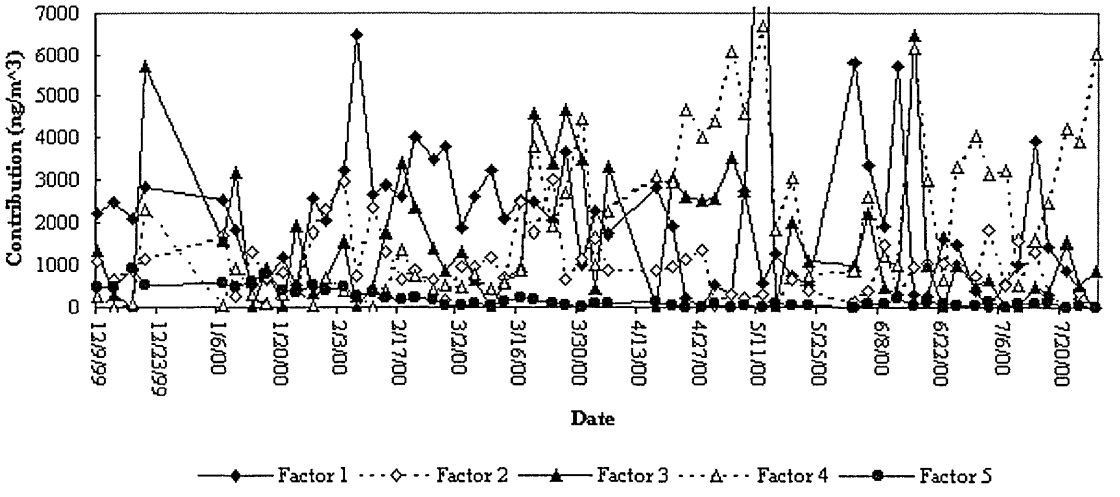


Figure 7.12 Temporal variations of contributions from 5 factors

## 7.4 Discussion of results

As mentioned in section 7.1, source-oriented and receptor-oriented methodologies have their advantages and shortcomings. The errors caused by the shortcomings can not be

identified and remedied when one methodology is used to attribute airborne pollutant source emissions to their receptor. In this thesis, a new methodology described in Figure 7.3 has been applied to attribute sources of airborne pollutant to their receptors. Both the atmospheric dispersion and receptor models were used to identify air pollution sources and estimate the source contributions. The errors produced by the models' shortcoming can be corrected by analysing and complementing the results of the two approaches. The performance of the atmospheric dispersion model in predicting concentrations of airborne pollutants was evaluated using measured field data. The errors produced by atmospheric dispersion model in estimating source emission or neglecting important sources were corrected by the sources identified using the receptor model. On the other hand, atmospheric dispersion model could estimate some source contributions that a receptor model could not. A more precise and reliable result is derived using both approaches.

The conventional Gaussian plume dispersion model has been used to simulate the transport of NOx and $PM_{10}$ in Dundee. The results of the model performance show that the model can predict the NOx concentrations measured at the study monitoring station well because NOx emission sources are comprehensive. Contributions of point emission, line emission and area emission sources to NOx measured at the station have been derived. They are 1.2%, 6.2% and 92.6% respectively. Both area emission and line emission are associated with the road vehicle emission in the atmospheric emission inventories in Dundee. Thus, the road vehicle emission is the most important source that affects NOx concentration at the station. The contribution of road vehicle emission to NOx concentration predicted at the station is 98.8%. There is no need to use receptor model to identify missing sources and estimate mission source contributions in this case.

The performance of the atmospheric dispersion model in predicting $PM_{10}$ concentrations measured at the station is poor, because only some anthropogenic emission sources (road vehicle emission and a point emission source, Waste to Energy Plant, Dundee Energy Recycling Limited) are included in the atmospheric inventories in Dundee. Some important natural sources for $PM_{10}$ such as secondary aerosols, marine aerosols and dust were not investigated in the inventories. The atmospheric dispersion model can not identify missing sources and estimate missing source contributions.

The aerosol sources are not comprehensive in Dundee. The factor analysis had to be done to identify aerosol sources. Positive matrix factorization (PMF) model has been used to identify $PM_{10}$ sources and estimate the source contributions in Dundee. All analysed

chemical species were selected to compose the input elements. Different error estimates were used for different chemical species with different detection and precision limits. Enforced rotation was applied to modify some factors' mass profiles in order to approach an ideal pattern. Five distinct factors have been identified by the PMF model successfully. The source characteristics have been shown in the scaled factors qualitatively. They have been further confirmed and verified quantitatively by analysing source mass profiles. These 5 factors represent five $PM_{10}$ sources that affect the $PM_{10}$ measured at the station. They are aged marine aerosol with some chlorine replaced by sulphate, soil and construction dust, secondary aerosol of ammonium nitrate, secondary ammonium sulphate, and incinerator and oil burning emission sources, respectively.

The average mass contribution of the five sources to $PM_{10}$ mass measured at the study monitoring station is about 58.1%. The aged marine aerosol with some chlorine replaced by sulphate and secondary aerosol of ammonium sulphate are two relatively high and stable $PM_{10}$ sources in Dundee. Their contributions to $PM_{10}$ at the station are 17.8% and 16.9% respectively. Secondary aerosol of ammonium nitrate and soil and construction dust are the other two important sources. Their contributions to $PM_{10}$ at the station are 12.1% and 9.5% respectively. Incinerator and oil burning emission is a minor source for $PM_{10}$ in Dundee. Its contribution to $PM_{10}$ at the station is about 1.8%.

Although, NOx is included in the input element matrix to serve as a marker of road vehicle emission, the PMF model can not separate a factor that represent road vehicle emission source in Dundee. This may be attributed to the fact that important chemical species in particulates emitted by vehicle, such as carbon, have not been analysed in this work. However, atmospheric inventories in Dundee indicate that that road vehicle emission is an important $PM_{10}$ source. The contribution of road vehicle emission to aerosol can be estimated using the results of the conventional Gaussian plume dispersion model in simulating $PM_{10}$ transport. The contribution of road traffic emission to $PM_{10}$ measured at the monitoring station is about 9.5%.

In complementing the results of atmospheric dispersion with those of the receptor models when attributing $PM_{10}$ sources, a total six sources can be identified for $PM_{10}$ sources in Dundee. They are aged marine aerosol with some chlorine replaced by sulphate, soil and construction dust, secondary aerosol of ammonium nitrate, secondary ammonium sulphate, incinerator and oil burning emission and road vehicle emission sources, respectively. The average mass contribution of the six sources to $PM_{10}$ mass measured at

the study monitoring station is about 67.6%. These complementary results can interpret $PM_{10}$ sources and describe source contributions more comprehensively than if either of the two approaches had been used.

# Chapter 8 Conclusions and proposals for future research work

## 8.1 Conclusions

One of the major aims of this research project was to develop a comprehensive air quality database in Dundee. This database has now been developed and it consists of concentrations of gaseous pollutants and particulates, chemical compositions of particulates, weather conditions and atmospheric emission inventories. The database enhances the information needed by Dundee City Council in the management of local air quality. This database extends the existing knowledge on air pollution in the UK. It can be used to evaluate the performance of the atmospheric dispersion and receptor models and to develop new methodologies for air quality management.

Atmospheric emission inventories are the primary information needed in air quality management. Based upon already available and this research project data, atmospheric emission inventories in Dundee were categorised into point, line and area emission sources. The source characteristics are described in detail to satisfy the requirement of input to atmospheric dispersion model. The inventories covered two significant point emission sources for NOx. The total annual emission of NOx from these two point sources in Dundee is 258.77 tonnes. Most of it comes from the Baldovie Waste to Energy Plant. There is only one significant point emission source for the particulate matter. The total annual emission of particulate matter from this point source is 20.62 tonnes. There are 13 line emission sources covered by the inventories. The total annual emissions from line emission sources are 227.41 tonnes for NOx and 7.25 tonnes for $PM_{10}$. There are 58 area emission sources covered by the inventories. The total annual emissions from area emission sources are 850.83 tonnes for NOx and 32.17 tonnes for $PM_{10}$.

The total annual emissions covered by the atmospheric emission inventories compiled in this research project are 1337.01 tonnes for NOx and 60.04 tonnes for airborne particulate matter. These figures underestimate source emissions in Dundee, especially for $PM_{10}$. NOx is produced from various combustion processes and comes mainly from anthropogenic sources. The NOx comes from industrial and commercial combustion processes, domestic gas consuming emissions and road traffic. Road traffic on many minor roads have not been included in the inventories. The sources of $PM_{10}$ are very complex.

They come from various anthropogenic activities as well as natural and fugitive emissions. The $PM_{10}$ emissions from natural and fugitive sources have not been included in the inventories.

Urban background air quality and atmospheric dispersion conditions in Dundee were monitored using an automatic monitoring station set up on the roof of the University of Abertay Dundee library. The concentrations of NO, $NO_2$ and NOx as well as wind speed, wind direction, ambient temperature and the amount of rainfall were measured continually at the station. $PM_{10}$ and TSP were sampled on weekdays and at weekends. The station was operated from December 1999 to December 2000. One year of systematic data for air quality and atmospheric dispersion conditions were gathered. 94 $PM_{10}$ samples and 95 TSP samples were collected. Chemical compositions of $PM_{10}$ and TSP samples were analysed in the laboratory, using wet chemical analysis. The metal elements ($Ca^{2+}$, $Mg^{2+}$, Zn, Cu, Ni and Pb) were analysed using Atomic Absorption Spectrophotometer (AAS). The ions ($SO_4^{2-}$, $NO_3^-$, $Cl^-$, $NH_4^+$, $Na^+$ and $K^+$) were analysed using High Performance Liquid Chromatography (HPLC). The wet chemical analysis was conducted for 59 $PM_{10}$ samples and 60 TSP samples.

In the year 2000, the annual average ambient temperature measured at the study station was 10.1 °C. The highest temperature was 24.5 °C while the lowest temperature was –1.0 °C. The hottest month was August. The coldest month was December. The total rainfall was 674 mm. The rainfall in Dundee varied with season, as expected. Autumn 2000 was the wettest season and it held about 45.3% of annual total rainfall. Summer 2000 was the driest season, which held only about 14.6% of annual total rainfall.

The major prevailing wind direction in 2000 was westerly. The yearly average frequency for westerly wind (WSW, W and WNW) was 33.61%. The next prevailing wind direction in 2000 was easterly. The yearly average frequency for easterly wind (ENE, E and ESE) was 20.66%. The frequency for calm conditions in 2000 was high, with a yearly average value of 26.85%. There was some seasonal variation for wind direction. In February 2000, the dominated wind was westerly. The frequency for calm condition was significantly low during the period. In May 2000, the easterly wind was more prevalent than the westerly wind. In August 2000, the westerly wind dominated again and the frequency for calm condition was high. In November 2000, the westerly wind was more prevalent than the easterly wind and the frequency for calm condition was high.

The average wind speed in 2000 was 1.9 m $s^{-1}$ and the maximum wind speed was 8.0 m $s^{-1}$. The strongest wind was in February, with an average speed of 2.6 m $s^{-1}$. The weakest wind was in July, with an average speed of 1.5 m $s^{-1}$. Measured wind speed was high during the daytime and low at night. Although it is not as obvious as wind speed, the distributions of wind direction also show some regular daily variation. The frequency of easterly wind in 2000 increased in the afternoon and at early night. It decreased late at night and in the morning. The daily variations of wind speed and wind direction show the effect of sea-land boundary layer on the local wind field.

In 2000, the variation range of one hour mean concentration for NO, $NO_2$ and NOx measured at the study station were 0.000 to 0.323 ppm, 0.000 to 0.049 ppm and 0.000 to 0.372 ppm, respectively. The annual mean concentrations of NO, $NO_2$ and NOx were 0.006 ppm, 0.012 ppm and 0.017 ppm, respectively. The highest one hour mean concentration and annual average concentration for $NO_2$ have not breached the values stipulated in the UK air quality strategy objectives for 2005 (Department of the Environment, Transport and the Regions, 1999). The monthly variations of concentrations of NO, $NO_2$ and NOx are indirectly proportional to the ambient temperature. The higher concentrations appeared in November, December and January, corresponding to lower ambient temperatures. The lower concentrations appeared in June, July and August, corresponding to higher ambient temperatures. The daily variations of concentrations for NO, $NO_2$ and NOx on weekdays and at weekends have good correlation with the daily variations of traffic flow on arterial and feed roads in Dundee. This suggests that road vehicle emission is a major source of NOx pollution. Because most of the fresh vehicular NOx emission is NO, with $NO_2$ being the product of NO oxidised in ambient atmosphere, the daily variations of $NO_2$ is much flatter than those of NO and NOx. Analysis of multi regression indicates that concentrations of NO, $NO_2$ and NOx measured at the study station increase with traffic flow on the arterial road and decrease with wind speed and ambient temperature.

The mass concentrations for $PM_{10}$ and TSP measured at the study station, with an average value of 12200 ng $m^{-3}$ and 17600 ng $m^{-3}$, respectively, are low. They are lower than most of the values measured at other sites around the world. The maximum concentration of $PM_{10}$ and average concentration of Pb measured at the station are less than the limits stipulated in the UK air quality strategy objectives for 2005 (Department of the Environment, Transport and the Regions, 1999). However, the maximum concentration

of $PM_{10}$ in this study was averaged over 3 days. The maximum 24 hours mean concentration of $PM_{10}$ at the station may be larger than the values presented. Temporal variations and analysis of wind aspect contribution show that $PM_{10}$ and TSP come from similar sources. Rainfall is one of the major deposition processes of aerosol. Multi regression analysis shows that mass concentration of $PM_{10}$ decreases with the total rainfall during the sample time. However, the effect of rainfall on the mass concentrations of TSP is not as expected.

$SO_4^{2-}$, $NO_3^-$ and $NH_4^+$ are three major components for $PM_{10}$ and TSP. They hold about 31.4% of $PM_{10}$ mass and 32.5% TSP mass. The temporal variations of $SO_4^{2-}$, $NO_3^-$ and $NH_4^+$ are generally well correlated. Most of the sulphate in the particulate is non-sea salt sulphate (NSS). Analysis of wind aspect contributions indicates that the European continent is a major source for secondary pollution species. Variation trends of secondary species in $PM_{10}$ and TSP with multi weather factors are different.

$Ca^{2+}$ and $K^+$ are two important components of $PM_{10}$ and TSP. They hold about 8.5% of $PM_{10}$ mass and 14.9% TSP mass. Concentrations of $Ca^{2+}$ and $K^+$ in $PM_{10}$ and TSP increase with wind speed. However, the temporal variations of $Ca^{2+}$ and $K^+$ and analysis of wind aspect contributions indicated that $Ca^{2+}$ and $K^+$ measured at the station come from different sources.

Concentration of $Cl^-$, $Na^+$ and $Mg^{2+}$ are relatively high. They hold about 19.8% of $PM_{10}$ mass and 21.0% of TSP mass. The temporal variations of $Cl^-$ and $Na^+$ are very well correlated. The analysis of wind aspect contribution indicates the marine aerosol sources from the Atlantic Ocean and from the North Sea are similar. However, the loss reaction of particulate $Cl^-$ in $PM_{10}$ is stronger for marine aerosol from the North Sea than from the Atlantic Ocean. Variation trends of marine aerosol in $PM_{10}$ and TSP with multi weather factors are similar except with those for $Na^+$ and $Mg^{2+}$ in TSP with rainfall.

Pb, Ni, Zn and Cu hold about 0.9% of $PM_{10}$ mass and 1.6% of TSP mass. The temporal variations of trace elements fluctuated, but they are not correlated with each other. It suggests that the sources for trace elements are very complex. The concentrations of trace elements in $PM_{10}$ measured at the station decrease with ambient temperature

Another major aim of this research project was to develop and test a new methodology that complements the advantages of atmospheric dispersion model and receptor model to overcome shortcomings of the two models when attributing sources of airborne pollutant to their receptors. In this methodology, both the atmospheric dispersion

and receptor models have been used to identify air pollution sources and estimate the source contributions. The errors produced by the models' shortcomings can be corrected by analysing and complementing the results of the two approaches. The performance of the atmospheric dispersion model in predicting concentrations of airborne pollutants has been evaluated, using the field monitoring results. The errors produced by the atmospheric dispersion model in estimating source emissions or by neglecting important sources have been corrected by using the sources identified by the receptor model. The misleading sources and source contributions produced by the receptor model can be corrected by predicting results of the atmospheric dispersion model. A sound, precise and reliable result has been derived using this methodology.

A software package that embodies the atmospheric dispersion models has been developed using C++. The design aim of the software package is to provide a scientific and convenient tool for environmental managers to assess the impact of air pollution sources on ambient air quality and to attribute airborne pollutant emission sources to their receptors. This software package can be used by local authorities to conduct an air quality review and to draw up the action plan for local air quality management according to requirements of the UK National Air Quality Strategy. It can also be used as an educational tool for students studying environmental science, engineering and other environmental related courses at university.

In contrast to other commercially available software for air quality management, the software package developed by the author provides for the choice of different atmospheric models. The user may select a model according to the prevailing situation and the available parameters. The atmospheric dispersion models used in the software package included a modified hybrid plume dispersion model and a ground-level release dispersion model that represent recent advances in the understanding of planetary boundary layer and atmospheric dispersion. Also, a conventional Gaussian plume model that is still universally used has been included. The modified hybrid plume dispersion model should be used to simulate the transport and dispersion of airborne pollutant from an elevated release source. Emphasis in the model is on convective and high-wind conditions. For convective conditions, the vertical concentration distribution is non-Gaussian, but for neutral and stable conditions it is assumed to be Gaussian. In contrast to the original hybrid plume dispersion model developed by Hanna and Paine (1989), a function ($P$) that represents the probability that receptor is under the influence of the plume has been added to our

modified hybrid plume dispersion model. This function is important when the distance between source and receptor is large or wind speed is less. In situations where distance between source and receptor is large or wind speed is low, neglect of travel time from source to receptor will over predict the pollutant concentration on the receptor. A newly developed model is used to simulate the transport and dispersion of airborne pollutant from a ground-level release source. In cases where the measured value for the parameters needed as input for the modified hybrid plume dispersion model and the ground-level release dispersion model are unavailable or the measured meteorological data can not satisfy the needs for estimating these parameters, conventional Gaussian plume dispersion provides another choice for atmospheric dispersion simulation.

The software package can predict 'once' airborne pollutant concentrations (one hour mean) from multiple point, line and area sources for multiple receptors and various atmospheric dispersion conditions. It can also predict series of one hour mean concentrations, daily mean concentrations and annual mean concentration based on a series of hourly meteorological parameters or parameters of atmospheric boundary structure. The daily variation or annual variation for some special sources with temporal emission can be considered by attaching relevant factors. The contributions of various kinds of pollution sources to air pollution can be calculated by grouping the sources. The software package is designed to have very user-friendly interfaces that ensure easy operation even for non-professional users.

For simulating the dispersion of area source emission using the models for the point source, the virtual point source algorithm is used. This is an imaginary or virtual point source that is located at a certain distance upwind of the area source (the virtual distance) to account for the initial size of the area source plume. The concentration distribution of airborne pollutant produced by area source emission is predicted by simulating this virtual point source dispersion. For simulating dispersion of line source, the line emission source is divided into series of small area emission sources. The concentration produced by the line source emission is predicted by accumulating contributions of series of small area source emissions.

The developed software package has been used to simulate the transport of NOx and $PM_{10}$ in Dundee. The performance of the software package has been evaluated by using the comprehensive database gathered in this project. The results show that the developed software performs very well in simulating the transport of NOx in Dundee. The

predicted results are reliable. The results indicate that the average contributions of point emission, line emission and area emission sourecs to NOx concentration predicted at the monitoring station are 1.2%, 6.2% and 92.6%, respectively. This suggests that area emission is the most important source that affects NOx concentration at the station. Both area and line emissions are associated with road vehicle emission in the atmospheric emission inventories made up for Dundee. Thus, road vehicle emission is the most important source that affects NOx concentration at the station. The contribution of road vehicle emission to NOx concentration predicted at the station is 98.8%.

The comparison between the predicted results from the atmospheric dispersion model and the $PM_{10}$ concentrations measured at the station is poor. The major cause of the poor comparison is that some important natural sources for $PM_{10}$ have not been included in the atmospheric inventories in Dundee. However, the reliability of the conventional Gaussian plume dispersion model in simulating atmospheric transport and dispersion is not in question, and has been proved to be satisfactory in predicting the NOx concentrations. Thus, the predicted results are consistent with the input of the sources. On average, the contribution of the $PM_{10}$ emission sources gathered in the atmospheric emission inventories to $PM_{10}$ measured at the monitoring station is about 9.5%. Almost all of these contributions come from road traffic emissions (98.4%).

In order to complement the dispersion model work, positive matrix factorization (PMF) model has been used to identify $PM_{10}$ sources and to estimate the source contributions. All analysed chemical species were selected to compose the input element matrix. Different error estimates were used for different chemical species with different detection limits and precision. Enforced rotation was applied to modify some factors' mass profiles to approach ideal pattern. Five distinct factors have been identified successfully by the PMF model. These five factors represent five $PM_{10}$ sources that affect the $PM_{10}$ measured at the study station. The source characteristics of five factors are shown in the scaled factors qualitatively. They are further confirmed and verified quantitatively by analysing source mass profiles. These five sources are aged marine aerosol with some chlorine replaced by sulphate, soil and construction dust, secondary aerosol of ammonium nitrate, secondary ammonium sulphate, and incinerator and oil burning emission source respectively.

The average mass contribution of the five sources to the $PM_{10}$ mass measured at the monitoring station is about 58.1%. The aged marine aerosol with some chlorine replaced

by sulphate and secondary aerosol of ammonium sulphate are the two relatively high and stable $PM_{10}$ sources in Dundee. Their contributions to $PM_{10}$ at the station are 17.8% and 16.9% respectively. Secondary aerosol of ammonium nitrate and soil and construction dust are the other two important sources. Their contributions to $PM_{10}$ at the station are 12.1% and 9.5%. Incinerator and oil burning emission is a minor source for $PM_{10}$ in Dundee. Its contribution to $PM_{10}$ at the station is about 1.8%.

Although NOx is included in the input element matrix to serve as a marker for road vehicle emission, the PMF model was not able to separate a factor that represents the road vehicle emission source for $PM_{10}$ in Dundee. This may be attributed to the fact that important chemical species in particulates emitted by vehicle, such as carbon, have not been analysed in this work. However, the result of the software package for atmospheric dispersion models in simulating $PM_{10}$ transport indicates that road vehicle emission is another important $PM_{10}$ source in Dundee. Its contribution to $PM_{10}$ measured at the monitoring station is about 9.5%.

Complementary results of the atmospheric dispersion and receptor models in attributing $PM_{10}$ sources have shown that a total of six sources can be identified for $PM_{10}$ sources in Dundee. They are aged marine aerosol with some chlorine replaced by sulphate, soil and construction dust, secondary aerosol of ammonium nitrate, secondary ammonium sulphate, incinerator and oil burning emission and road vehicle emission sources, respectively. The average mass contribution of the six sources to $PM_{10}$ mass measured at the study monitoring station is about 67.6%. These complementary results can interpret $PM_{10}$ sources and describe source contributions more comprehensively than if either the receptor or dispersion model approach had been used on its own.

## 8.2 Proposal for future research work

The atmospheric emission inventories gathered in this research project have underestimated source emissions in Dundee, especially for $PM_{10}$. The survey of airborne pollutant emission sources in Dundee should be continued in order to further improve the emission inventories. NOx is produced from various combustion processes. More attentions should be put on small industrial and commercial combustion processes, domestic gas consumption and road traffic on many minor roads when conducting a survey of NOx in future. The survey for $PM_{10}$ sources should focus on natural and fugitive

emission sources such as marine aerosol, soil, road and construction dust and secondary pollution aerosol from long distance transport.

There are 40 $PM_{10}$ and 40 TSP samples collected at the study station whose chemical compositions were not analyzed in the laboratory because of time constraints. The chemical analysis should be conducted for these particulate samples to get a complete one year air quality data that describes the chemical composition of airborne particulates in Dundee. If one wants to identify particulate sources and estimate source contributions precisely, C, the most important component of aerosol, Al and Si, two important crustral elements, As and V, two important trace elements for coal combustion and oil combustion emission sources should be analysed.

The conventional Gaussian plume dispersion model in the software package developed by the author has been evaluated using the measured data at the study station. However, the modified hybrid plume dispersion model and the ground-level release dispersion model in the modelling package could not be assessed because the necessary planetary boundary layer parameters were unavailable. These two models should be evaluated using a database with detailed information for meteorological conditions and construction of a planetary boundary layer. The differences between these two models and the conventional Gaussian plume dispersion model should be analysed.

There are available empirical formulae and suppositions to estimate the parameters of the atmospheric boundary layer using routine meteorological observed data. These empirical formulae and suppositions should be included in the software package.

The methodology for attributing sources of airborne pollutants to their receptors developed in this project should be used for other cities to further evaluate and improve the methodology. When the inventories of airborne pollution sources are comprehensive, the atmospheric dispersion model can be used to estimate the source contributions. When the inventories of airborne pollution sources are not comprehensive, both atmospheric dispersion and receptor model have to be used to attribute airborne pollutants to their sources. The possible air pollution sources and source contributions may then be interpreted by combining the results of these two models.

# References:

AEA Technology (1995) Air Pollution in the UK: 1993/94. The National Environmental Technology Centre, Oxfordshire

Allen G, Sioutas C, Koutrakis P, Reiss R, Lurmann FW, Roberts PT (1997) Evaluation of the TEOM method for measurement of ambient particulate mass in urban areas. Journal of the Air & Waste Management Association, 47(6): 682-689

Alexandr V, Polissar A V, Hopke P K, Paatero P (1998) Atmospheric aerosol over Alaska - 2. Elemental composition and sources. Journal of Geophysical Research-Atmospheres 103:D15, 19045-19057

American Meteorological Society workshop on stability classification schemes and sigma curves – summary of recommendations (1977) Bull. Am. Meteorol. Soc. 58: 1305-1309

Artaxo P, Oyola P, Martinez R (1999) Aerosol composition and source apportionment in Santiago de Chile. Nuclear Instruments & Methods in Physics Resarch Section B-Beam Interactions with Materials and Atoms. 150(1~4): 409- 416

Barratt B, Beevers S, Buckingham C, Carslaw D, Fuller G, Hedley S, Hutchinson D, Rice J (1997) The AIM project and air quality in London 1996. The South East Institute of Public Health, Tunbridge Wells, Kent. UK

Benson P E (1984) CLINE4 — A dispersion model for predicting air pollutant concentrations near roadways. FHWA/CA/TL-84/15

Bergin M S, Noblet G S, Petrini K, Dhieux J R, Milford J B, Harley R A (1999) Formal uncertainty analysis of a Langrangian photochemical air pollution model. Environ. Sci. Technol. 33(7): 1116-1126

Bowers J F, Bjorklund J R and Cheney C S (1979) Industrial Source Complex (ISC) Dispersion Model User's Guide. Volume I, EPA-450/4-79-030, U.S. Environmental Protection Agency, Research Triangle Park, North Carolina 27711

Bowers J F, Bjorklund J R and Cheney C S (1979) Industrial Source Complex (ISC) Dispersion Model User's Guide. Volume II, EPA-450/4-79-031, U.S. Environmental Protection Agency, Research Triangle Park, North Carolina 27711

Briggs G A (1969) Plume rise. USAEC critical review series, TID-25075, National Technical Information Service, Springfield, Virginia 22161

Briggs G A (1973) Diffusion estimation for small emissions in environment research labs. USAEC Report ATDL-106, Nat. Oceanic and Atmos. Asmin. 83-147

Briggs G A (1974) Diffusion Estimation for Small Emissions. In ERL, ARL USAEC Report ATDL-106, U.S. Atomic Energy Commission, Oak Ridge, Tennessee

Briggs G A (1975) Plume rise predictions. In lectures on air pollution and environmental impact analysis, American Meteorological Society, Boston, Massachusetts

Briggs G A (1979) Some recent analyses of plume rise observations. In Proceedings of the second international clean air congress, Academic Press, New York

Briggs G A (1984) Plume rise and buoyancy effects. Atmospheric Science and Power Production, D.Randerson, Ed., DOE/TIC-27601: 327-366

Brook J R, Dann T F, Bonvalot Y (1999) Observation and interpretation from Canadian fine particle monitoring Program. Journal of the Air & Waste Management Association. 49: PM-35-44

Businger J A, Ayra S P S (1974) Height of the mixed layer in the stably stratified planetary boundary layer. Adv. Geophys. 18A: 73-92

Carmichael G R, Hong M S, Ueda H, Chen L L, Murano K, Park J K, Lee H G, Kim Y, Kang C, Shim S (1997) Aerosol composition at Cheju Island, Korea. Journal of Geophysical Research-Atmospheres. 102(D5): 6047-6061

Carruthers D J, Weng W S, Hunt J C R, Holroyd R J, McHugh C A, Dyster S J (2000) Plume/puff spread and mean concentration module specifications. ADMS 3, P10/01Q/00 & P12/01Q/00, http//www.cerc.co.uk

Chan Y C, Simpson R W, Mctainsh G H, Vowles P D, Cohen D D, Bailey G M (1997) Characterisation of chemical species in PM2.5 and PM10 aerosols in Brisbane, Australia. Atmospheric Environment. 31(22): 3773-3785

Charron A, Plaisance H, Sauvage S, Coddeville P, Galloo JC, Guillermo R (2000) A study of the source-receptor relationships influenceing the acidity of precpitation collected at a rural site in France. Atmospheric Environment. 34: 3665-3674

Chen W C, Wang C S, Wei C C (1997) An assessment of source contributions to ambient aerosols in Central Taiwan. Journal of the Air & Waste Management Association. 47(4):501-509

Chester R, Nimmo M, Fones GR, Keyse S, Zhang Z (2000) Trace metal chemistry of particulate aerosols from the UK mainland coastal rim of the NE Irish sea. Atmospheric Environment. 34: 949-958

Chow J C, Watson J G, Lowenthal D H, Solomon P A, Magllano K L, Ziman S D, Richards L W (1992) PM10 source apportionment in California San-Joaquin valley. Atmospheric Environment Part A-General Topics. 26(18): 3335-3354

Chow J C, Watson J G, Lowenthal D H, Solomon P A, Maglliano K L, Ziman S D, Richards L W (1993) PM10 and PM2.5 composition in California San Joaquin valley. Aerosol Science and Technology. 18(2): 105-128

Chow J C, Watson J G, Green M C, Lowenthal D H, DuBois D W, Kohl S D, Egami R T, Gillies J, Rogers C F, Frazier C A (1999) Middle- and neighbourhood-scale variation of $PM_{10}$ source contributions in Las Vegas Nevada. Journal of the Air & Waste Management Association. 49: 641-654

Clarke R H (1979) A model for short and medium range dispersion of radionuclides released to the atmospheric. First report of a working group on atmospheric dispersion. National Radiological Protection Board report, NRPB R-91.

Collett R S and Oduyemi K (1997) Air quality modelling: a technical review of mathematical approaches. Meteorol. Appl. 4: 235-246.

Collett R S, Oduyemi K and Davidson B (1997) An investigation into ambient levels of traffic-related pollutants in urban centres: a case study of the Seagate, Dundee, United Kingdom. Journal of Environmental Management. 51: 289-304.

Dabberdt W F and Hoydysh W G (1991) Street canyon dispersion: sensitivity to block shape and entrainment. Atmospheric Environment. 25A(7): 1143-1153.

Deardorff J W, Willis G E (1975) A parameterisation of diffusion into the mixed layer. J. Appl. Meteorol. 14: 1451-1458.

Department of the Environment, Transport and the Regions (1998a) Preparation and use of atmospheric emissions inventories. LAQM.TG2(98) . The Publications Centre

Department of the Environment, Transport and the Regions (1998b) Selection and use of dispersion models. LAQM.TG3(98) . The Publications Centre

Department of the Environment, Transport and the Regions (1998c) Pollutant specific guidance: Consultation Draft DETR, London

Department of the Environment, Transport and the Regions (1999) Review of the United Kingdom national air quality strategy. Product Code 98EP0541/A.

DePaul F T and Sheih C M (1985) Tracer study of dispersion in an urban street canyon. Atmospheric Environment. 19(4): 555-559.

Draxler R R (1976) Determination of atmospheric diffusion parameters. Atmospheric Environment, 10: 99-105.

Du S, Venkatram A (1997) A Parameterisation of vertical dispersion of ground-level releases. Journal of Applied Meteorology. 36: 1004-1015.

Dundee Energy Resources Ltd. (1994) Baldovie waste to energy plant: proposed redevelopment of existing facility. Document No. 4906000/ES/94/7003.

Dye A L, Rhead M M, Trier CJ (2000) The quantitative morphology of roadside and background urban aerosol in Plymouth, UK, Atmospheric Environment 34: 3139-3148

Eldering A and Cass GR (1996) Source-oriented model for air pollutant effects on visibility. Journal of Geophysical Research-Atmospheres. 101(D14): 19343-19369

ELE International (1993) Dialog and MM900 user manual.

EPA (1988) Air emission species manual. Volumes I and II. Research Triangle Park, NC.

EPA (1989) Receptor model technical series, Vol. III. CMB7 user's manual. Research Triangle Park, NC. EPA-450/4-90-004.

EPA (1994) Guidelines for PM10 sampling and analysis applicable to receptor modeling. EPA-452/R-94-009.

EPA (1995) User's guide for the industrial source complex (ISC3) dispersion model, volume II – description of model algorithms. EPA-454/B-95-003a.

EPA(1998a) AP-42, fifth edition: Compilation of air pollutant emission factors. Volume I, stationary point and area sources. http://www.epa.gov/ttnchiel/ap43.html

EPA(1998b) AP-42, fifth edition: Compilation of air pollutant emission factors. Volume II, mobile sources. http://www.epa.gov//ttnchiel/ap43.html

Everitt BS (1993) Cluster analysis, Halsted Press, an imprint of John Wiely & Sons Inc., New York.

Fang G C, Chang C N, Wu Y S, Fu P P C, Yang D G, Chu C C (1999) Characterization of chemical species in PM2.5 and PM10 aerosols in suburban and rural sites of central Taiwan. Science of the Total Environment. 234(1~3): 203- 212

Farrow I K, Kisenyi J M, Dimmonds A C, Savage C A and Cudworth R S (1993a) Legislated emissions from the seven diesel vehicles from large scale survey. Report No LR 931, Warren Spring Laboratory, Stevenage

Farrow I K, Kisenyi J M, Dimmonds A C, Savage C A and Cudworth R S (1993b) Regulated emissions from the forty gasoline vehicles without catalysts from large a scale survey. Report No LR 933, Warren Spring Laboratory, Stevenage

Farrow I K, Kisenyi J M, Dimmonds A C, Savage C A and Cudworth R S (1993c) Regulated emissions from the three gasoline vehicles with catalysts from large scale survey. Report No LR 932, Warren Spring Laboratory, Stevenage

Fraser M P, Cass G R, Simoneit B R T (1998) Gas-phase and particle-phase organic compounds emitted from motor vehicle traffic in a Los Angeles roadway tunnel. Environmental Science & Technology. 32(14): 2051-2060

Ganor E, Levin Z, VanGrieken R (1998) Composition of individual aerosol particles above the Israelian Mediterranean Coast during the summer time Atmospheric Environment. 32:1631-1642

Gifford F A (1961) Use of routine meteorological observations for estimating atmospheric dispersion. Nucl. Safety. 2: 47-51

Gifford F A (1976a) Turbulent Diffusion - Typing Schemes: A Review. Nucl. Saf., 17, 68-86

Gifford F A (1976b) Consequences of effluent release. J. Nuclear Safety. 17: 68-86

Gray H A, Cass G R (1998) Source contributions to atmospheric fine carbon particle concentrations. Atmospheric Environment. 32(22): 3805-3825

Hanna S R, Paine R (1989) Hybrid plume dispersion model (HPDM) development and evaluation. Journal of Applied Meteorology. 28: 206-224.

Harris J M and Kahl J D W (1994) An analysis of 10-day isentropic flow patterns for Barrow, Alaska: 1985-1992. Journal of Geophysical Research 99(D12): 25845-25855.

Harrison R M and Jones M (1995) The chemical composition of air born particles in the UK atmosphere. The Science of the Total Environment. 168:195-214.

Henry R C (1991) Data Handling in Science and Technology, Volume 7: Receptor modeling for air quality management (Hopke P K ed.). Elsevier Science Publishers B. V., pp. 117-148.

Henry R C (1997) History and fundamentals of multivariate air quality receptor models. Chemometrics and Intelligent Laboratory Systems. 37:37-42

HORIBA, Ltd. (1996) Instruction manual, APNA-360 Ambient NOx Monitor

Hopke P K (1991a) An introduction to receptor modelling. Chemometric and Intelligent Laboratory Systems. 10: 21-43

Hopke P K (1991b) Data Handling in Science and technology, Volume 7: Receptor modeling for air quality management (Hopke P K ed.). Elsevier Science Publishers B. V., pp.149-212

Hopke P K, Paatero P, Jia H, Ross R T, Harshman R A (1998) Three-way (PARAFAC) factor analysis: examination and comparison of alternative computational methods as applied to ill-conditioned data. Chemometrics and Intelligent Laboratory Systems. 43:25-42

Hoydysh W G and Dabberdt W F (1988) Kinematics and dispersion in an urban street canyon. Atmospheric Environment. 22(12): 2677-2689

Huang S L, Rahn K A, Arimoto R (1999) Testing and optimizing two factor-analysis techniques on aerosol at Narragansett, Rhode Island. Atmospheric Environment. 33(14): 2169-2185

Irwin J S (1979) Scheme for estimating dispersion parameters as a function of release height. EPA-600/4-79-062.

Johnson W B (1973) Diffusion simulation model for carbon monoxide. JAPCA. 23(6): 490-498.

Kahl J D, Harris J M, Herbert G A, Olson M P (1989) Inter comparison of three long-range trajectory models applied to Arctic haze. Tellus. 41B: 524-536.

Kaneyasu N, Ohta S, Murao N (1995) Seasonal-variation in the chemical-composition of atmospheric aerosols and gaseous species in Sapporo, Japan. Atmospheric Environment. 29(13):1559-1568

Kim Y P, Lee J H, Baik N J, Kim J Y, Shim S G, Kang C H (1998) Summertime characteristics of aerosol composition at Cheju Island, Korea. Atmospheric Environment. 32(22): 3905-3915

Kitto A N and Harrison R M (1992) Processes affecting concentrations of aerosol strong acidity at sites in eastern England. Atmospheric Environment. 26A(13): 2389-2399

Kleeman M J, Cass G R, Eldering A (1997) Modelling the airborne particle complex as a source-oriented external mixture Journal of Geophysical Research-Atmospheres. 102(D17): 21355-21372

Kleeman M J and Cass G R (1998) Source contributions to the size and compositon distribution of urban particulate air pollution. Atmospheric Environment. 32(16): 2803-2816

Kleeman MJ, Hughes LS, Allen JO, Cass GR (1999) Source contributions to the size and composition distribution of atmospheric particels: southern California in September 1996. Environmental Science & Technology 33:4331-4341

Kublay N, Saydam A C (1995) Trace-elements in atmospheric particulates over the eastern Mediterranean - concentrations, sources, and temporal variability. Atmospheric Environment. 29(17): 2289-2300

Kulshrestha U C, Kumar N, Saxena A, Kumari K M, Srivastava S S (1995) Identification of the nature and source of atmospheric aerosols near the Taj-Mahal (India). Environmental Monitoring and Assessment. 34(1): 1-11

Lamb R G, Neiburgur M (1971) An interim version of a generalised urban air pollution model. Atmospheric Environment. 5: 239-264

Lamb R G (1973) Note on the application of K theory to turbulent diffusion problem involving chemical reactions. Atmospheric. Environment. 7:235

Lamb R G, Seinfeld J H (1973) Mathematical modeling of urban air pollution – general theory. Environmental Science & Technology. 7:253-261

Lamb R G, Chen W H, Seinfeld J H (1975) Numerical-empirical analyses of atmospheric diffusion theories. Journal of Atmospheric Science. 32: 1794-1807

Lamb R G, Duran D R (1977) Eddy diffusivities derived from a numerical model of convective boundary layer. Nuovo. Cimento, 1C: 1-17

Lawson D R (1990) Emission from in-use motor vehicles in Los Angeles: a pilot study of remote sensing and the inspection and maintenance program. Journal of the Air & Waste Management Association. 40(8): 1096-1105

Lee D S, Garland J A and Fox A A (1994) Atmospheric concentrations of trace elements in urban aresa of the United Kingdom. Atmospheric Environment. 28(16):2691-2173

Liousse C, Penner J E, Chuang C, Walton J J, Eddleman H, Cachier H (1996) A global three-dimensional model study of carbonaceous aerosols. Journal of Geophysical Research-Atmospheres. 101(D14): 19411-19432

Lindsay S (1992) High performance liquid chromatography. John Wiley & Sons Ltd., West Sussex, England. pp. 1-16

London Research Centre (1998) Atmospheric emission inventories. http//www.london-research.gov.uk/emission/webhtm.htm

Lurmann F W, Wexler A S, Pandis S N, Musarra S, Kumar N, Seinfeld J H (1997) Modelling urban and regional aerosols .2. Application to California's South Coast Air Basin. Atmospheric Environment. 31(17): 2695-2715

Maenhaut W, Ducastel G, Leck C, Nilsson E D, Heintzenberg J (1996) Multi-elemental composition and sources of the high Arctic atmospheric aerosol during summer and autumn. Tellus Series B-Chemical and Physical Meteorology. 48(2): 300-321

Martin D, Mithieux G, Strauss B (1987) On the use of the synoptic vertical wind component in a transport trajectory model. Atmospheric Environment. 21: 45-52.

McHugh CA, Carruthers DJ, Edmunds HA (1997) ADMS-Urban: an air quality management system for traffic, domestic and industrial pollution. International Journal of Environment and Pollution. 8(3-6): 666-674

Metcalfe SE, Whyatt JD, Derwent RG (1995) A comparison of model and observed network estimates of sulphur deposition across Great Britain for 1990 and its likely source attribution Q. J. R. Meteorol. Soc. 121: 1387-1441

Morales J A, Pirela D, Durban J (1996) Determination of the levels of Na, K, Ca, Mg, Fe, Zn and Cu in aerosols of the western Venezuelan savannah region. The Science of the Total Environment. 180(2): 155-164

Motallebi N (1999) Wintertime PM2.5 and PM10 source apportionment at Sacramento, California. Journal of the Air & Waste Management Association. 49:PM-25-34

Mukai H, Ambe Y, Shibata K, Muku T, Takeshita K, Fukuma T, Takahashi J, Mizota S (1990) Long-term variation of chemical composition of atmospheric aerosol on the Oki Islands in the Sea of Japan. Atmospheric Environment. 24A(6): 1379-1390

Nieuwstadt F T M, Van Duuren H (1980) Dispersion experiments with SF6 from the 213 high meteorological mast at Cabau in the Netherlands. Proceeding of the fourth symposium on turbulence, Diffusion and air pollution, Reno, Nevada, American Meteorological Society, Boston, Mass. 34-40

Oduyemi K and Davidson B (1998) The impacts of road traffic management on urban air quality. the Science of Total Environment. 218: 59-66.

Olendrzynski K, Jonson JE, Bartnicki J, Jakobsen HA, Berge E (2000) EMEP Eulerian model for acid deposition over Europe. International Journal of Environment and Pollution. 4: (1-6) 391-399

Olendrzynski K, Berge E, Bartnicki J (2000) EMEP Eulerian acid deposition model and its applications. European Journal of Operational Research. 122: (2) 426-439.

Olson M P, Oikawa K K, Macafee A W (1978) A trajectory model applied to the long-range transport of air pollutants. Atmospheric Environmental Services. Canada.

Orlic I, Wen X, Ng TH, Tang SM (1999) Two years of aerosol pollution monitoring in Singapore. a review. Nuclear Instruments & Methods in Physics Research Section B-Beam Interaction with Material and Atoms. 150(1—4): 457- 464

Owen B, Edmunds HA, Carruthers DJ, Raper DW (1999) Use of a new generation urban scale dispersion model to estimate the concentration of oxides of nitrogen and sulphur dioxide in a large urban area. The Science of Total Environment, 235: 277-291

Owen B, Edmunds HA, Carruthers DJ, Singles RJ (2000) Prediction of total oxides of nitrogen and nitrogen dioxide concentrations in a large urban area using a new generation urban scale dispersion model with integral chemical model. Atmospheric Environment, 34: 379-406

Paatero P, Tapper U (1994) Positive matrix factorisation: a non-negative factor model with optimal utilisation of error estimates of data values. Environmetrics 5, 111-126

Paatero P (1997) Least squares formulation of robust non-negative factor analysis, Chemometrics and Intelligent Laboratory systems. 38, 223-242

Paatero P (1998) User's guide for positive matrix factorisation programs PMF2 and PMF3. University of Helsinki

Pandey P K, Patel K S, Subrt P (1998) Trace elemental composition of atmospheric particulate at Bhilai in central-east India. the Science of the Total Environment. 215 (1—2): 123-134

Pasquill F (1971) Atmospheric diffusion of pollution. Q. J. Roy. Meteorol. Soc. 97: 369-395.

Pasquill F, Smith F B (1983) Atmospheric diffusion 3rd edn. New York, John Wiley & Sons.

Patashnich H, Rupprecht E G (1991) Continuous PM-10 measurement using the Tapered Element Oscillating MicroBalance. Journal of the Air & Waste Management Association. 41: 1079-1083

Perkin Elmer (1989) Model 1100 B Atomic absorption spectrometer operator's manual

Pinto J P, Stevens R K, Willis R D, Kellogg R, Mamane Y, Novak J, Santroch J, Benes I, Lenicek J, Bures V (1998) Czech air quality monitoring and receptor modeling study. Environmental Science & Technology. 32(7): 843-854

Pio, C.A., Santos, I. M., Anaclet, T.D., Nunes, T.V. 1(991) Particulate and gaseous air pollutants levels at the Portuguese west coast. Atmospheric Environment 25A, 669-680

Polissar A V, Hopke P K, Malm W C, Sisler F (1996)The ratio of aerosol optical absorption coefficients to sulfur concentrations, as an indicator of smoke from forest fires when sampling in polar regions. Atmospheric Environment 30, 1147-1157

Polissar A V, Hopke P K, Malm W C, Sisler J F(1998) Atmospheric aerosol over Alaska - 1. Spatial and seasonal variability Journal of Geophysical Research-Atmospheres. 103(D15): 19035-19044

Polissar A V, Hopke P K, Paatero P, Kaufmann Y J, Hall D K, Bodhaine B A, Dutton E G, Harris J M (1999) The aerosol at Barrow, Alaska: long-term trends and source locations. Atmospheric Environment. 33(16): 2441-2458

Pryor S C, Barthelmie R J, Hoff R M, Sakiyama S, Simpson R, Steyn D (1997) REVEAL: Characterizing fine aerosols in the Fraser Valley, BC. Atmosphere-Ocean. 35 (2):209-227

Qin Y and Kot S C (1993). Dispersion of vehicular emission in street canyon, Guangzhou City, South China (PRC). Atmospheric Environment, 27B(3): 283-291.

Qin Y, Chan C K, Chan L Y (1997) Characteristics of chemical compositions of atmospheric aerosols in Hong Kong: spatial and seasonal distributions. The Science of the Total Environment 206, 25-27.

Qin Y, Chan C K and Chan L Y (1998). Compositions and characteristics of atmospheric aerosols in Hong Kong. Chinese Environmental Science. 18(6): 450-459 (in Chinese).

Qin Y (1999) Research degree project proposal and plan of work. Approval of a research degree project proposal & plan for Research Degrees Committee, University of Abertay Dundee.

Qin Y, Oduyemi K, Chan L Y (2002) Comparative testing of PMF and CFA models. Chemometrics and Intelligent Laboratory Systems. 61: 75 - 87

Rahn K A (1999) A graphical technique for determining major components in a mixed aerosol. I. Descriptive aspects. Atmospheric Environment. 33(9):1441-1455

Ramadan Z, Song X H, Hopke P K (2000) Identification of sources of Phoenix aerosol by positive matrix factorization Journal of the Air & Waste Management Association. 50: 1308-1320

Rupprecht & Patashnich Co., Inc. (1996) Operating manual, Partisol model 2000 air sampler.

Seigneur C, Pai P, Hopke P K, Grosjeen D (1999) Modelling atmospheric particulate matter. Environmental Science & Technology. 33(2): NEWS 80A-86A

Seinfeld J H, Pandis S N (1997) Atmospheric chemistry and physics, from air pollution to climate change. John Wiley & Sons, Inc.

Sherman C A (1978) A mass-consistent model for wind fields over complex terrain. Journal of Applied Meteorology. 17(3): 312-319

Spectra-Physics (1988a) IsoChrom isocratic pump users guide.

Spectra-Physics (1988b) SP4400 Integrator users guide.

Stephhens R D, Cadle S H (1991) Remote sensing measurements of carbon monoxide emission from on-road vehicles. Journal of Air & Waste Management Association. 41(1): 39-46

Taylor F I (1921) Diffusion by continuous movements. Proc. London Math. Soc. Ser. 2 (20): 196.

The Quality of Urban Air Review Croup (1996) Airborne Particulate Matter in the United Kingdom. Third Report of the Quality of Urban Air Review Group, Birmingham.

The Quality of Urban Air Review Group (1993) Diesel vehicle emission and urban air quality. Second report of the Quality of Urban Air Review Group, Birmingham.

The Secretary of State for the Environment, the Secretary of State for Wales and the Secretary of State for Scotland (1997) The United Kingdom National Air Quality Strategy. The Publications Centre

Turner D B (1970) Workbook of atmospheric dispersion estimates. AP 26 (NTIS PB 191-482), Research Triangle Park, NCU.S.EPA

Turner, D B, 1970: Workbook of Atmospheric Dispersion Estimates. PHS Publication No. 999-AP-26. U.S. Department of Health, Education and Welfare, National Air Pollution Control Administration, Cincinnati, Ohio

VanMalderen H, VanGrieken R, Khodzher T, Obolkin V, Potemkin V (1996) Composition of individual aerosol particles above Lake Baikal, Siberia. Atmospheric Environment. 30(9): 1453-1465

Vega E, Garcia I, Apam D, Ruiz M E, Barbiaux M (1997) Application of a chemical mass balance receptor model to respirable particulate matter in Mexico City. Journal of the Air & Waste Management Association. 47(4): 524-529

Veltkamp P R, Hansen K J, Barkley R M, Sievers R E (1996) Principal component analysis of summertime organic aerosols at Niwot Ridge, Colorado. Journal of Geophysical Research-Atmospheres. 101(D14): 19495-19504

Venkatram A (1996) An examination of the Pasquill-Gifford-Turner dispersion scheme. Atmospheric Environment. 30(8), 1283-1290

Wakamatsu, S., Utsunomiya, A., Han, J S., Mori, A., Uno, I., Uehara, K (1996) Seasonal variation in atmospheric aerosols concentration covering northern Kyushu, Japan and Seoul, Korea. Atmospheric Environment 30, 2343-2354

Wang I T, Chico T, Huang Y H, Farber RJ (1999) Development, evaluation and application of a primary aerosol model. Journal of Air & Waste Management Association. 49: PM-57-68

Watson J G, Chow J C, Lu Z, Fujuta E M, Lowenthal D H and Lawson D R (1994) Chemical mass balance source apportionment of PM10 during the southern California air quality study. Aerosol Science and Technology. 21:1-3

Watson J G, Chow J C (1991) Data Handling in Science and technology, Volume 7: Receptor modeling for air quality management (Hopke P K ed.). Elsevier Science Publishers B. V., pp. 83-116

Watson J G, Chow J C (1993) Ambient air sampling, In 'Aerosol measurement: principles, techniques and applications'. Willeke K, Baron P, (Eds.) Van Nostrand Reinhold, New York :622-639

Weil J C, Sykes R I and Venkatram A (1992) Evaluating air-quality models: review and outlook. Journal of Applied Meteorology. 31(10):1121-1145

Welz B (1986) Atomic absorption spectrometry. Second, completely revised edition, VCH Publishers, New York, NY, USA.

Wexler A S Lurmann F W and Seinfeld J H (1994) Modelling urban and regional aerosols --I. model development. Atmospheric Environment. 28(3): 531-546

Wilson T R S (1975) Salinity and major elements of sea water. In: Skirrow J P. editors. Chemical Oceanography, Vol. 1. 2nd ed: 365-413

Wongphatarakul V, Friedlander S K, Pinto J P (1998) A comparative study of PM2.5 ambient aerosol chemical databases. Aerosol Science and Technology. 32 (24): 3926-3934.

Xie Y L, Hopke P K, Paatero P (1998) Positive matrix factorization applied to a curve resolution problem. Journal of Chemometrics. 12(6): 357-36

Xie Y L, Hopke P K, Paatero P, Barrie L A, Li S M (1999a) Identification of source nature and seasonal variations of arctic aerosol by positive matrix factorization. Journal of the Atmospheric Science 56, 249- 260

Xie Y L, Hopke P K, Paatero P, Barrie L A, Li S M (1999b) Locations and preferred pathways of possible sources of Arctic aerosol. Atmospheric Environment. 33(14): 2229-2239

Xie Y L, Hopke P K, Paatero P, Barrie L A, Li S M (1999c) Identification of source nature and seasonal variations of Arctic aerosol by the multilinear engine. Atmospheric Environment. 33(16):2549-2562

Yaaqub R R, Davies, T D, Jickells T D, Miller J M (1991) Trace elements in daily collected aerosols at a site in southeast England. Atmospheric Environment. 25A: 985-996

# Appendix Journal papers based on PhD research project

Qin Y, Oduyemi K, Chan LY (2002) Comparative testing of PMF and CFA models. Chemometrics and Intelligent Laboratory Systems. 61: 75 - 87

Y Qin, K Oduyemi (2002) Atmospheric aerosol in Dundee, UK: 1. chemical compositions and their variations. Submitted to Atmospheric Environment.

Y Qin, K Oduyemi (2002) Atmospheric aerosol in Dundee, UK: 2. source identification and contribution estimation. In preparation.

Y Qin, K Oduyemi (2002) A software package for atmospheric dispersion models. In preparation.